Carbon Dioxide and Coccolithophore Physiology in Ancient Oceans

Harry-Luke Oliver McClelland

St Edmund Hall
University of Oxford

A thesis submitted for the degree of
Doctor of Philosophy

Trinity 2015

Coccolithophores form an important and dynamically evolving component of the carbon cycle. These ubiquitous single-celled marine calcifying phytoplankton are responsible for half of the calcium carbonate production in the modern surface ocean, and their adorning calcite plates (coccoliths), produced intracellularly, have contributed to sedimentary carbonate for over 200 million years. They constitute a significant control on the partitioning of carbon between the atmosphere, ocean and sedimentary reservoirs on timescales from the instantaneous to the geological. Coccolithophores are also uniquely placed to record aspects of the carbonate chemistry of the surface ocean, because the carbon isotopic composition of the organic matter ($\delta^{13}C_{org}$) and calcite ($\delta^{13}C_{cal}$) that they produce is a function of many parameters, including ambient aqueous carbon dioxide concentration [CO_2].

This thesis addresses the bidirectional interaction between coccolithophores and the carbon cycle in the geological past, by asking how cellular carbon fluxes relate to physical evidence that is preserved throughout geological time. First, I present and calibrate a novel rationale for size-normalising coccolith mass, and show that over two glacial-interglacial cycles, coccolithophores appear to calcify more under high [CO_2] conditions; a result that is manifest on evolutionary timescales, and is necessarily elusive to experiments. Second, I investigate the parameters controlling $\delta^{13}C_{cal}$ and $\delta^{13}C_{org}$ in coccolithophores through *in vivo* experimentation, and development of a model of cellular isotopic fluxes. I show that so called "vital effects" in coccolithophores arise as a result of differences in calcification to photosynthesis ratios. Third, using a combination of novel and established protocols for extraction and isotopic analysis of specific organic molecules from fossils taxonomically separated by size, I show the very first size-specific geologic time series of coccolith-associated $\delta^{13}C_{org}$, and the first time-series of size-separated coccolith $\delta^{13}C_{cal}$ over a glacial cycle. A novel means of inferring past carbon dioxide concentrations, based on an iterative inverse modelling approach, is presented and tested.

Carbon Dioxide and Coccolithophore Physiology in Ancient Oceans

Harry-Luke Oliver McClelland

St Edmund Hall

University of Oxford

A thesis submitted for the degree of

Doctor of Philosophy

Trinity 2015

Mac and Marian

Here's to you - happy days

Acknowledgements

I would like to thank NERC, the UKOARP and EAG for funding, and the Oxford Earth Sciences department for hosting me and providing such a fantastic environment to do four years of research. Thank you to my supervisor, Ros Rickaby, for the enthusiastic discussions, the opportunities I have been given over the past four years, and for the extensive freedom to pursue whichever avenues took my interest. Thank you to Michaël Hermoso, for discussions about coccolithophores and isotopes, and for all your guidance in the lab, from growing coccolithophores to analysing fossils in sediment. Thank you to Jorn Bruggeman for showing me that modelling isn't scary, for your patience, and generosity with your time. Thanks to Luc Beaufort, Nico Barbarin and Yves Gally for accommodating my many trips to Aix, and your help with SYRACO. Thank you to Renee Lee for teaching me biochemical techniques. Thanks to Mervyn Greaves and Patricia Ferretti for sharing your foram Mg/Ca data. Thank you to Chris Day and Norman Charnley for being so helpful and for running the light stable isotopes always so efficiently. Thank you to Pete Ditchfield for analysing organic carbon isotopes. Thank you to Ann Pearson for hosting me in Harvard, and showing me your lab. Thank you to Ian Probert for providing strains of coccolithophores. Thank you to Ian Hall for your time and patience working in Cardiff. Thanks to Sam Hirst, and Ian Chan for being great students. Thanks to OceanBug, Mahdi Bendif and Jeremy Hoffman for enthusiastic and inspiring discussions about coccolithophores and paleoclimate. Thank you to Gideon Henderson and Dieter Wolf-Gladrow for examining this thesis, and for a thoroughly enjoyable viva.

Thank you to Tom Browning, Will Hutchison, Duane Smythe, Tracy Aze, Liam Marriott and Joe Larkin for the daily conversations about life, the universe and everything, for the beers we've shared and keeping me sane. Thank you Ana for your huge part in making my time in Oxford so enriching and fun. Thanks to Trev, Helena and Helene for being great housemates, and for bullying me into thinking about things differently. Thank you to David Acaster for inspiring me to pursue science... Thank you to Amrit Gherra for making me realise that science isn't everything... and to David Neave for helping me to remember how much I love it. Thank you to Roger and Judy, Ann and Richard, the rest of my family - the Waltons, the Wards, the Jacksons and the Gherras for your constant love and support.

Lastly and most especially, thank you Mum and Dad for your encouragement, for your unwavering belief and for helping me to keep everything in perspective.

Abstract

Coccolithophores form an important and dynamically evolving component of the carbon cycle. These ubiquitous single-celled marine calcifying phytoplankton are responsible for half of the calcium carbonate production in the modern surface ocean, and their adorning calcite plates (coccoliths), produced intracellularly, have contributed to sedimentary carbonate for over 200 million years. They constitute a significant control on the partitioning of carbon between the atmosphere, ocean and sedimentary reservoirs on timescales from the instantaneous to the geological. Coccolithophores are also uniquely placed to record aspects of the carbonate chemistry of the surface ocean, because the carbon isotopic composition of the organic matter ($\delta^{13}C_{org}$) and calcite ($\delta^{13}C_{cal}$) that they produce is a function of many parameters, including ambient aqueous carbon dioxide concentration [CO_2].

This thesis addresses the bidirectional interaction between coccolithophores and the carbon cycle in the geological past, by asking how cellular carbon fluxes relate to physical evidence that is preserved throughout geological time. First, I present and calibrate a novel rationale for size-normalising coccolith mass, and show that over two glacial-interglacial cycles, coccolithophores appear to calcify more under high [CO_2] conditions; a result that is manifest on evolutionary timescales, and is necessarily elusive to experiments. Second, I investigate the parameters controlling $\delta^{13}C_{cal}$ and $\delta^{13}C_{org}$ in coccolithophores through *in vivo* experimentation, and development of a model of cellular isotopic fluxes. I show that so called "vital effects" in coccolithophores arise as a result of differences in calcification to photosynthesis ratios. Third, using a combination of novel and established protocols for extraction and isotopic analysis of specific organic molecules from fossils taxonomically separated by size, I show the very first size-specific geologic time series of coccolith-associated $\delta^{13}C_{org}$, and the first time-series of size-separated coccolith $\delta^{13}C_{cal}$ over a glacial cycle. A novel means of inferring past carbon dioxide concentrations, based on an iterative inverse modelling approach, is presented and tested.

Extended Abstract

Coccolithophores are single-celled photoautotrophic algae that produce microscopic plates of calcite called coccoliths. They are ubiquitous in modern oceans and have contributed to the calcite fraction of pelagic sediments since the Triassic. Coccoliths can be seen from space when they turn vast swathes of the ocean milky white during blooms, they are essential biostratigraphic tools thanks to their high preservation potential and rapid evolutionary turnover, and they are what chalk is made from. From a geological and carbon cycle perspective, as paleoclimatologists we have a dual interest in coccolithophores: Firstly as actors, they both consume carbon dioxide via photosynthetic carbon fixation, and they calcify: coccoliths constitute half of the calcite that is produced in the surface ocean. Calcification, and the export of calcite from the surface ocean to depth, and to sediments, alters the buffering capacity of the ocean for CO_2, but also has implications for the export of organic matter from the surface ocean through ballasting. Coccolithophores have a significant influence on the partitioning of carbon between the atmosphere, surface ocean, deep ocean and sediments, on instantaneous to geological timescales. Secondly, as recorders, the chemical and isotopic composition of coccolithophore biomass is a function of the conditions in which they lived. Despite great efforts over the past three decades to understand the physiology of these charismatic microflora however, relatively little attention has been paid to understanding the factors that control their composition, and what insight might be gained from studying it. The broad aim of this thesis is to unpick the clues hidden in fossil coccoliths; to see what we can learn about how their dynamic role in the carbon cycle has changed over geological time, and how aspects of seawater carbonate chemistry are recorded in their biomass.

Chapter 2

Calcite production decreases the surface ocean's capacity to buffer changes in the partial pressure of carbon dioxide in the atmosphere (pCO_2). Results from culture manipulation experiments mimicking the effects of climate change in the laboratory suggest that coccolithophores calcify less when pCO_2 is higher, constituting a negative feedback to changes in pCO_2. However, the extent to which these results are representative of natural populations, and of the response over more than a few hundred generations, is unclear. Here I describe a novel rationale for size-normalization of coccolith mass, for the most abundant family of coccolithophores, the Noëlaerhabdaceae. I use this approach to investigate the calcification response of ancient populations over a few million generations, subjected to natural environmental change. Coupled gradual increases in temperature and the CO_2 concentration of the surface water ($[CO_2]$) cause an increase in coccolithophore community calcification, but the response is species-specific. Selection appears to favour the more heavily calcified forms under increasing $[CO_2]$ and temperature, which to first order, implies a positive climatic feedback. Selection is manifest in natural populations over millennial timescales, so this temporal dimension has necessarily eluded laboratory experiments.

Chapter 3

For half a century, the isotopic analysis of calcite microfossils, and associated organic matter, has been used to study past climates. Sourcing carbon directly from solution in seawater, and thus avoiding the isotopic complications of heterotrophy, coccolithophores are uniquely placed to record the isotopic composition of surface seawater, and preserve this signal throughout geological time. However, coccolith calcite is precipitated inside the cell in a chemical and isotopic microenvironment, which can substantially differ to the ambient seawater. The enigmatic nature of the departure from expected isotopic compositions, termed *vital effects*, has severely limited the use

of coccoliths in paleoceanographic and paleoclimatic proxies. Here, with new data from laboratory culture manipulations, vital effects in the carbon isotopic composition of coccolithophore organic and inorganic matter are shown to be greatest when cellular carbon utilisation is high, and to disappear when utilisation is low. Further, interspecific differences can be reconciled with a single isotopic flux model. The so-called heavy and light groups exist as a result of cells exhibiting respectively high and low calcification to photosynthesis ratios, but cell size, growth rate, [DIC] and pH are all moderating factors. The model presented here is consistent with recent molecular and experimental studies, and is consistent with vital effects in oxygen.

Chapter 4

Carbon dioxide is the greenhouse gas that to a large extent dictates the climatic state of the Earth on long timescales, and yet we know very little for certain about how its atmospheric abundance varied in the geological past. Prior to 800ka, which is the temporal extent of pCO_{2atm} records from bubbles trapped in ice, proxies based on the isotopic composition of organic matter from phytoplankton have dominated Cenozoic pCO_{2atm} reconstructions. The basis of these proxies is the well-documented effect of the variation in passive CO_2 supply to the cell at different CO_2 concentrations on the apparent magnitude of isotopic fractionation of carbon into organic matter. However, although additional factors contribute to this apparent fractionation, these are universally treated as a black box. Here I use a novel protocol for the extraction and isotopic analysis of a specific type of organic macromolecule, preserved within sedimentary coccolith calcite, to reconstruct, for the first time, organic and inorganic carbon isotopes from ancient cells of known size and taxonomic affiliation. Through analysis of sediments spanning a glacial cycle, a real-world proof of concept of this novel approach is undertaken, revealing that the carbon isotopic composition of organic and inorganic matter is sensitive to changes in $[CO_2]$ even over the subtle range

of [CO_2] change that typifies a glacial cycle. The model derived and calibrated in the previous chapter is used to capitalise on this unprecedented degree of linked information to simultaneously constrain cellular utilisation (which includes [CO_2]) and calcification to photosynthesis ratios.

Contents

List of Figures

Chapter 1

Introduction

Carbon is the molecular backbone of life on Earth. By mass, you are one fifth carbon. The most common oxide of carbon, carbon dioxide, is the form in which carbon makes the transition from the inorganic world of rocks and gas into the organic world, usually via photosynthesis, and back again, via respiration or combustion. Carbon dioxide (CO_2) allows plants to grow, puts bubbles in beer, makes bread rise, and in its role as a greenhouse gas is largely responsible for the surface of the Earth being a habitable temperature.

In the geological past, the CO_2 concentration of the atmosphere has largely dictated Earth's climatic state (Falkowski *et al.*, 2000; Gattuso *et al.*, 2015; IPCC, 2014; Ridgwell & Zeebe, 2005). For at least a million years, CO_2 has been at the centre of positive feedback mechanisms enabling the manifestation of tiny changes in solar forcing as large climatic changes, while negative feedbacks stop the system from spinning out of control (Lüthi *et al.*, 2008). The largest reservoir of carbon on Earth is in rocks, but the timescale on which carbon is naturally exchanged between this reservoir and the more volatile systems; the ocean, atmosphere and biosphere, is on the order of millions of years (Berner *et al.*, 1983).

By burning fossil fuels, humans have artificially accelerated carbon exchange with the rock reservoir. The unprecedented rate of release of carbon into the atmosphere over the past two centuries has no natural equivalent reversal process effective on timescales less than a few million years (Falkowski *et al.*, 2000). This asymmetry has

knocked the climate system out of balance, exponentially increasing the concentration of CO_2 in the atmosphere, and with empirical and modelling evidence pointing towards a resultant increase in temperature (Broecker, 1975; IPCC, 2014; Joos *et al.*, 1999). A third of this anthropogenic CO_2 has dissolved in the oceans however (Sabine *et al.*, 2004), and at this point the CO_2 problem bifurcates; global warming, driven by increasing pCO_{2atm} is buffered by CO_2 dissolution in the ocean, but the effect on seawater chemistry is carbonation and acidification, processes which have as yet unknown consequences for organisms (Riebesell *et al.*, 2009). The increased appreciation of the scale of the problem over the past few decades has lead to an urgent need to understand all components of the carbon cycle in greater detail. One such aspect of the carbon cycle that has received much recent interest is how calcifying organisms in the surface ocean respond to a changing climate, due to their influence on the partitioning of carbon between the atmosphere, surface ocean, deep ocean and sediments (Orr *et al.*, 2005).

Holding a unique role, and particularly of interest in recent times are the coccolithophores (Beaufort *et al.*, 2011; Gibbs *et al.*, 2013; Iglesias-Rodriguez *et al.*, 2008; O'Dea *et al.*, 2014; Orr *et al.*, 2005; Ridgwell *et al.*, 2009; Ridgwell & Schmidt, 2010; Riebesell *et al.*, 2000b): a group of single-celled calcifying phytoplankton, ubiquitous in modern oceans, and responsible for up to half of the calcite production in the surface ocean (Milliman, 1993). They produce plates of calcium carbonate, called coccoliths, which have formed a significant component of the sedimentary and nannofossil record for over 200 million years (Bown, 1998). The production, export from the surface ocean, and sedimentation of these plates exerts a significant influence on exchange between reservoirs of carbon over timescales spanning from the instantaneous to the geological (Barker *et al.*, 2003b). In producing biogenic material directly from seawater that has a high preservation potential, coccolithophores are also uniquely positioned to record aspects of past climates, and form an archive conserving this information across geological time (Hermoso, 2014; Pagani, 2002; Stoll & Ziveri, 2004).

1.1 Coccolithophores as organisms

Photosynthetic carbon fixation in the ocean generates almost half of the oxygen that we breathe (Falkowski & Raven, 2013). Despite numerical inferiority to the cyanobacteria, three groups of eukaryotic algae; the diatoms, the dinoflagellates and the coccolithophores, dominate the net primary production in the surface ocean, including export and sequestration of organic carbon in the deep ocean, and the flux of organic carbon and nutrients to higher trophic levels (Falkowski *et al.*, 2004). The evolution of oxygenic photosynthesis in eukaryotes occurred only once in the history of life on Earth (Falkowski *et al.*, 2004). This significant event involved the capture and endosymbiosis of a photosynthetic prokaryote (related to modern cyanobacteria) by a heterotrophic eukaryote that already possessed a mitochondrion (Gould *et al.*, 2008). Pigment specialisation resulted in early divergence between "green" and "red" algal clades, named on the basis of differing light absorbance frequencies.

Secondary endosymbiotic events appear to have been more common: The haptophytes (Haptophyta) are one of four extant clades, the others being the heterokonts (including the diatoms), cryptophytes, and the alveolates (including the dinoflagellates) (Gould *et al.*, 2008; Sanchez-Puerta & Delwiche, 2008), whose plastids are derived from a primary red alga, having, at some stage, undergone a secondary endosymbiosis. The phylogenetic relationships between haptophytes and the other three extant "red lineage" clades is a topic of current controversy; these four clades may share a single common ancestor (Cavalier-Smith, 1999); the haptophytes may have descended from one of multiple secondary endosymbiotic events (Burki *et al.*, 2012), or may be the end result of a lineage including multiple nested endosymbioses (Stiller *et al.*, 2014). Gene-loss and dependence on the host cell of the enslaved red algal endosymbiont, has resulted in the highly specialised, and multiple-membrane bound plastid organelles of modern haptophytes. Thanks to a poor fossil record prior to the evolution of calcitic scales, and the uncertainties associated with molecular clock

analyses, the age of the origin of non-calcifying haptophytes is highly debated. Estimates range from the latest Neoproterozoic at 580Ma (Cavalier-Smith, 2002) to 1.2 Ga (Falkowski *et al.*, 2004; Yoon *et al.*, 2004) and even as much as 1.9 Ga (de Vargas & Aubry, 2007). Coccolithophores, defined as haptophytes that produce calcified scales, first appeared in the fossil record in the Late Triassic (Bown, 1998).

Coccolithophores are eukaryotic photosynthesisers, and as such possess a nucleus, mitochondria and at least one chlorophyll c containing ("red") plastid (Fig. 1.1). They are also calcifiers, but unusually for eukaryotes, calcite production occurs intracellularly. They therefore possess a compartment derived from the Golgi body called the coccolith vesicle (CV), in which their characteristic coccoliths are precipitated one at a time, before being exocytosed and incorporated into a tessellated exoskeleton called the coccosphere (Taylor *et al.*, 2007a; Young *et al.*, 1999, Fig. 1.2). Taxonomically, coccolithophores are calcifying members of the class Prymnesiophyceae (Haptophyta). As members of the division Haptophyta, they possess an active or vestigial haptonema, which is an organelle with an enigmatic function; known to coil and uncoil when stressed, it may be for anchorage, object sensing or even extracellular coccolith arrangement (Young *et al.*, 2009).

1.1.1 Life-cycle

Coccolithophores are capable of sexual reproduction, but their biflagellate motile haploid (gametic) and non-motile diploid forms are independently capable of reproducing asexually (de Vargas & Aubry, 2007). In nature, coccolithophores adopt a dimorphic lifecycle, transitioning between these two forms by meiosis and syngamy (Young & Henriksen, 2003), although in culture, meiosis and syngamy have never been observed in coccolithophores (Collins, 2010); instead they reproduce asexually indefinitely by mitotic binary fission. Recent work has suggested that sexual reproduction may even be a trait that is selected against, and lost in modern populations, due to it's high

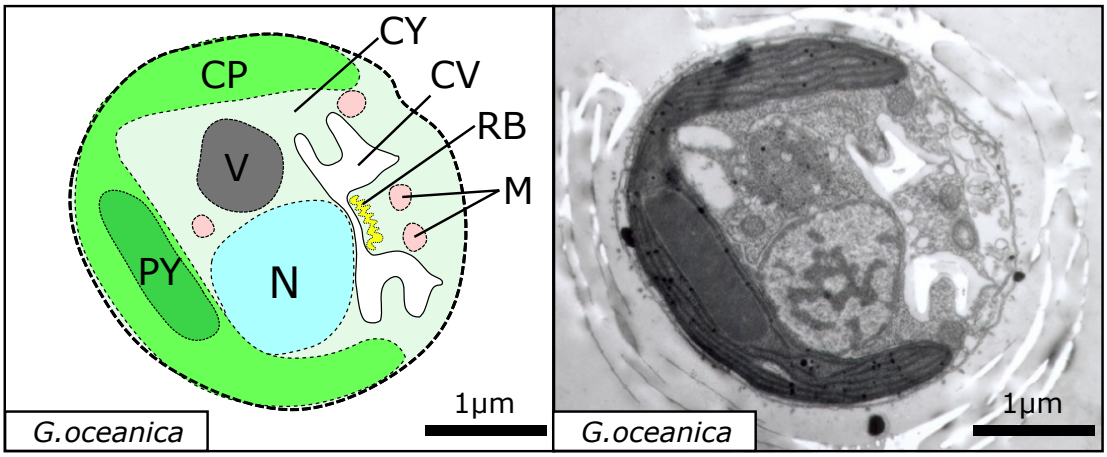

Figure 1.1: Cellular anatomy of *Gephyrocapsa oceanica*. **Left:** Simplified diagram of the cell, with important components and organelles highlighted and labelled. **Right:** Transmission electron micrograph image courtesy of Mahdi Bendif, used with permission. The cell consists of the following components: **CP:** Chloroplast, **N:** Nucleus, **CV:** Coccolith vesicle, **RB:** Reticular body, **M:** Mitochondria, **V:** Vacuole, **PY:** Pyrenoid and **CY:** Cytosol. Note also in the right image coccoliths in cross-section surrounding the perimeter of the cell, having been exocytosed and incorporated into the coccosphere.

energetic cost and the long term nature of its benefit, leading to evolutionary "dead ends"(von Dassow *et al.*, 2014). Others suggest that the haploid stage not only allows phenotypic novelty to arise through new combinations of alleles following recombination, but that it also provides an essential escape strategy from viruses to which the diploid phase is uniquely susceptible (Frada *et al.*, 2008).

1.1.2 Coccolithogenesis

Coccoliths form one at a time, initially by precipitation of calcite onto the periphery of a precursor organic scale, which is first synthesised inside the CV, forming a proto-coccolith ring (der Wal & Jong, 1983; Young & Henriksen, 2003). Further calcification is controlled by the presence and incorporation of acidic polysaccharides (Marsh, 1994; Marsh *et al.*, 1992, 2002a), and possibly within a protein matrix (Corstjens *et al.*, 1998). The entire process occurs within the CV, but in close association with a bundle of anastomosing tubes, known as the reticular body, which forms a

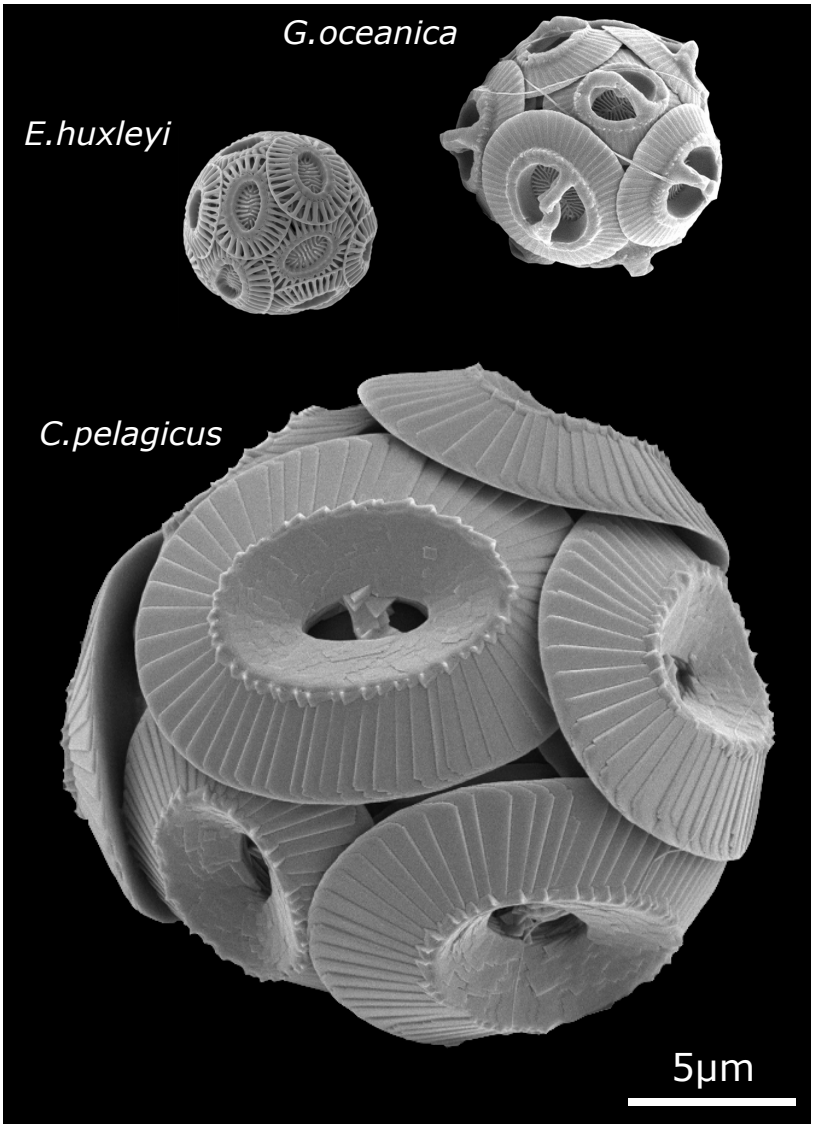

Figure 1.2: Coccospheres of *Emiliania huxleyi*, *Gephyrocapsa oceanica* and *Coccolithus pelagicus*; the three main species of coccolithophore that form the basis of this thesis. SEM images are from `http://ina.tmsoc.org/Nannotax3`

.

structural complex with the CV. Early coccolith growth occurs with the CV abutting the nucleus, and when coccolith growth is complete, exocytosis occurs via fusion of the CV membrane with the cellular membrane (Young & Henriksen, 2003).

1.1.3 Coccoliths

Of the coccolithophores that once lived in the surface ocean, coccoliths in ocean sediments are usually the only evidence to survive geological time. Despite their beautifully elaborate construction, the functional role of coccoliths is still unknown. It has been hypothesised that they are used for defence against viruses or predators, for channelling light (Young, 1994), adjusting ambient nutrient concentration via changing buoyancy (Baumann *et al.*, 1978) or simply as a wastebin for excess alkalinity in the cell (Riebesell, 2004). It has even been suggested that they are vestigial structures, originally used to channel organic matter towards the cell when ancestral forms were partially heterotrophic (pers. comm. Marie-Pierre Aubry). Coccolithophores produce different coccoliths during each stage of their lifecycle. Heterococcoliths are extremely common, routinely used for biostratigraphy, and are associated with the diploid phase (Bown, 1998; Houdan *et al.*, 2004). Holococcoliths are rarer in sediments, blocky and less ornate in construction, are thought to be formed extracellularly (Young *et al.*, 1999), and are associated with the haploid phase (Houdan *et al.*, 2004). This thesis is concerned with heterococcoliths. Heterococcoliths are formed of two coaxial shields, consisting of radially arranged monocrysts of calcite, with alternating crystallographic axes (Fig. 1.3). The so-called R and V units are named on the basis of their radially (in the plane of the coccolith) and vertically (perpendicular to the plane of the coccolith) oriented crystal axes respectively (Young *et al.*, 1999). As coccoliths in sediment are usually viewed with a cross-polarised light microscope, the orientation of the crystallographic axes have profound implications for visibility and apparent thickness of the coccolith (Beaufort, 2005; Beaufort *et al.*, 2014; Bollmann, 2014). In the Noëlaerhabdaceae, both the proximal and the distal (to the cell) shields

are formed of the R unit, and so both are visible under cross-polarised light. Other coccolithophore species, such as the genera *Coccolithus* and *Calcidiscus* for example, produce coccoliths where the proximal shield is formed of the R unit, but the distal shield is formed of the V unit, and so is close to invisible under crossed polarised light (Fig. 1.3).

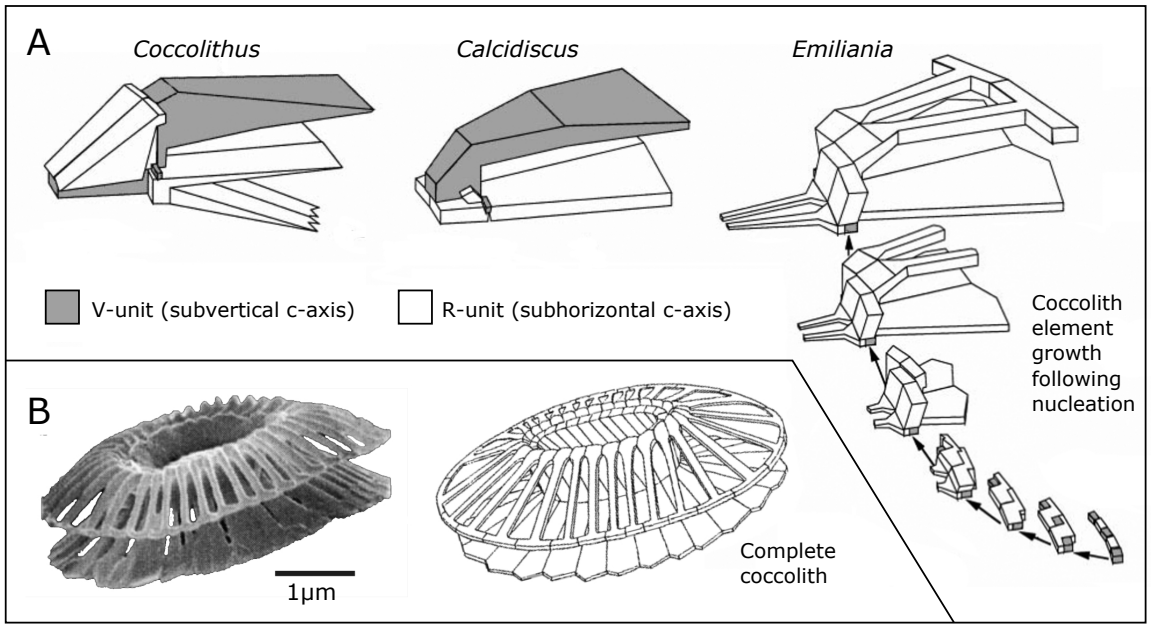

Figure 1.3: Summary of coccolith ultrastructure. **A:**V/R model of coccolith growth. Right: From nucleation points constituting the proto-coccolith ring to fully formed elements in *Emiliania huxleyi* - note both proximal and distal shields are formed of the R-unit. Left: Example genera with alternate V/R configuration of proximal and distal shields. **B:** SEM image and drawing of complete coccoliths of *E.huxleyi*. Drawings and SEM image samples from Young *et al.* (1992, 1999).

1.2 Carbon

1.2.1 The CO_2 problem

CO_2 is the world's most important greenhouse gas, second only to water vapour in terms of its total contribution to the greenhouse effect (Trenberth, 1998). CO_2 has

driven natural climatic change for at least the last million years, and the effect of its anthropogenically increased concentration in the modern atmosphere is beginning to be realised (Broecker, 1975; Hönisch *et al.*, 2009; IPCC, 2014; Lüthi *et al.*, 2008). In contrast to water vapour, which has an atmospheric residence time of only a few days, and simply constitutes a fast climate feedback mechanism, the concentration of CO_2 in the atmosphere is controlled by natural biological, oceanographic and human induced processes operational on timescales of months to hundreds of millions of years (IPCC, 2014).

For almost a million years prior to the industrial revolution in the late 18th century, the mixing ratio of CO_2 in the atmosphere (pCO_{2atm}) oscillated between ∼180 and ∼280 ppm with a period of ∼100 ky (Hönisch *et al.*, 2009; Lüthi *et al.*, 2008), tipping the Earth's climate into and out of glacial states. Ocean temperatures and relative global ice volume have been inferred from the isotopic and trace metal composition of carbonate shells of organisms that lived in the ocean (e.g. Elderfield & Ganssen, 2000; Elderfield *et al.*, 2012; Zachos *et al.*, 2001), atmospheric temperature from the hydrogen and oxygen isotopic composition of contemporaneous ice (Jouzel *et al.*, 2007), and pCO_{2atm} is recorded in gas bubbles trapped in this same ice (Lüthi *et al.*, 2008). Before 800 ka, the glacial/interglacial oscillation frequency, as inferred from benthic carbonate records increases, but we have no direct records of pCO_{2atm} for this time (Elderfield *et al.*, 2012; Lisiecki & Raymo, 2005; Lüthi *et al.*, 2008). These oscillations between relative warmth and relative cool are a result of a plethora of feedback mechanisms initiated by the amount and distribution of solar energy to the surface of the Earth, with a regularity enforced by the gravitational perturbations by other planets in the solar system, dominantly Jupiter and Saturn (Berger, 1988; Loutre, 2003; Milanković, 1930). In the two centuries since the industrial revolution, approximately 550 billion tonnes of carbon, in the form of gaseous CO_2, has been injected into the atmosphere through the burning of fossil fuels, cement production and deforestation (IPCC, 2014), leading to a departure from the natural

balance and causing annual average pCO_{2atm}, to finally surpass 400 ppm in March 2015 (`www.esrl.noaa.gov/gmd/ccgg/trends/`). The last time in geological history that pCO_{2atm} was this high is hotly debated, although it is certainly a few million years (Beerling & Royer, 2011; Seki *et al.*, 2010), and perhaps as many as 25 million years since the atmosphere consistently contained more than 400 ppm CO_2 (Beerling & Royer, 2011; Pagani *et al.*, 2011; Pearson & Palmer, 2000; Pearson *et al.*, 2009). Around a third of the anthropogenic CO_2 emitted thus far has been sequestered in the ocean (IPCC, 2014; Siegenthaler & Sarmiento, 1993), with more already in the pipeline over the next few hundred years (Archer *et al.*, 1997). CO_2 dissolution in seawater results in a decrease in pH (ocean acidification), but an increase in total carbon concentration (ocean carbonation); a possible tradeoff with unknown consequences for calcifying organisms (Doney *et al.*, 2009; Ridgwell *et al.*, 2009).

1.2.2 CO_2 in seawater

The dynamic chemical system resulting from the dissolution of CO_2 in seawater is central to all aspects of this work. When CO_2 dissolves in seawater it reacts to form carbonic acid, which rapidly dissociates to its constituent ions, carbonate (CO_3^{2-}), bicarbonate (HCO_3^-) and protons (H^+), leaving a negligible fraction of carbon in the form of molecular carbonic acid (Zeebe & Wolf-Gladrow, 2001). A chemical equilibrium exists between carbonic acid, CO_2 (aq), HCO_3^- and CO_3^{2-}: the position of equilibrium is a function of pH [1] (and vice versa), but also of the 1st and 2nd dissociation constants of carbonic acid, which are functions of temperature, salinity and pressure (Fig. 1.4). The summed concentrations of these carbon species constitutes the concentration of dissolved inorganic carbon (DIC). At very high pH, CO_3^{2-} is the most abundant carbon species, and at low pH, CO_2 is the most abundant. In the modern ocean, which has a pH of around 8.2, HCO_3^-, CO_3^{2-} and CO_2 exist in a ratio

[1] Although the system is usefully described in terms of pH, changes in seawater carbonate chemistry in the ocean are generally through inputs and output of TA and DIC, which alter pH, rather than through direct addition or subtraction of protons.

of approximately 100:10:1. Exchange between the ocean and atmosphere is solely through dissolution and outgassing of CO_2, with the Henry's law constant between CO_2 (aq) and CO_2 (g) a function of temperature and salinity (Zeebe & Wolf-Gladrow, 2001). Around a hundred times more carbon is stored in seawater that is in equilibrium with the atmosphere than if CO_2 were a gas like O_2 or N_2 that does not react with water, because the vast majority of carbon exists as CO_3^{2-} and HCO_3^- ions. At low pH therefore, relatively less carbon can be dissolved in seawater for a given atmospheric composition.

Most carbon system perturbations can be considered in terms of the effect on a system in equilibrium. For this, it is useful to introduce the concept of total alkalinity, defined by Dickson (1981) as, "the number of moles of hydrogen equivalent to the excess of proton acceptors over proton donors in 1 kg sample". This definition quantitatively describes the acid-titrating capacity of seawater, but in the context in which we are considering the DIC system in seawater, total alkalinity (TA) is essentially a measure of the buffering capacity of sea water for CO_2, because the higher the TA, the higher the proportion of carbon that can be stored as HCO_3^- or CO_3^{2-}. Any perturbation to a DIC system approximately in equilibrium is usefully considered in terms of the relative effect of the perturbation on DIC and on TA. For example, the precipitation of 1 mole of calcite from seawater removes one mole of DIC and two moles of TA. This has a relatively greater effect on TA than on DIC, and so counterintuitively drives [CO_2 (aq)] towards higher values (Fig. 1.5). For reestablishment of equilibrium with an atmosphere that is large relative to the perturbation, this constitutes an outgassing of CO_2. The latter part of this thesis is concerned with isotopes in the DIC system of seawater. Kinetics and isotopes are addressed in detail in Chapter 3, so they will not be discussed here.

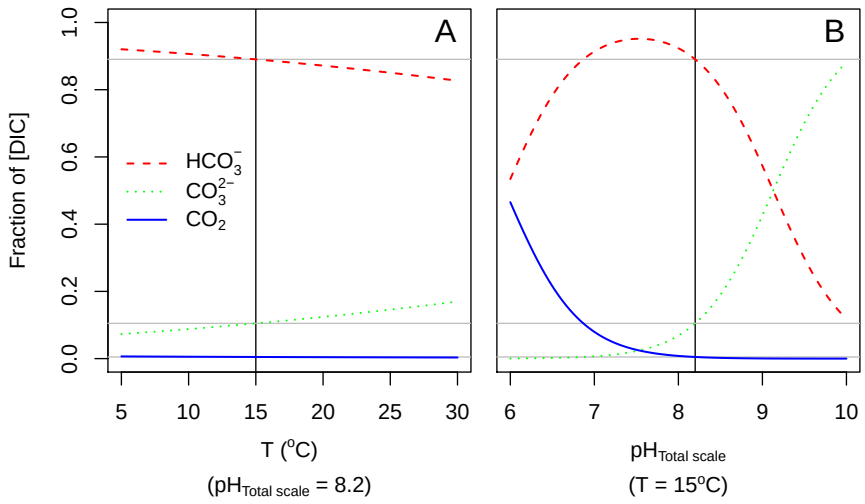

Figure 1.4: The DIC system in seawater as a function of temperature (A) and pH (B).

1.3 Coccolithophores as Actors

Half of the primary productivity on Earth occurs in the surface ocean (Falkowski *et al.*, 2004). Estimates of the fractional contribution of coccolithophores to marine primary productivity range from 1% (Jin *et al.*, 2006) to 17% (Gregg & Casey, 2007). Coccolithophores, as the most abundant calcifying phytoplankton in the oceans (O'Brien *et al.*, 2013), are also purportedly responsible for up to half of the calcification in the surface of the open ocean (Milliman, 1993). These estimates have large uncertainties, but nevertheless - poorly defined as they are - what do these numbers actually mean from a biogeochemical point of view? The pre-anthropogenic carbon cycle involves fluxes of carbon between the atmosphere, oceans, biosphere and rocks, with multiple internal feedbacks over a vast range of timescales (Archer *et al.*, 1997). On geologically long timescales (Fig. 1.6; 10^6 y+) coccolithophore calcite and organic matter burial in pelagic sediments, and eventual subduction and sequestration in the mantle, constitutes a net sink of carbon from the ocean/atmosphere system (Ridgwell & Zeebe, 2005). The following discussion is concerned with shorter timescales than this.

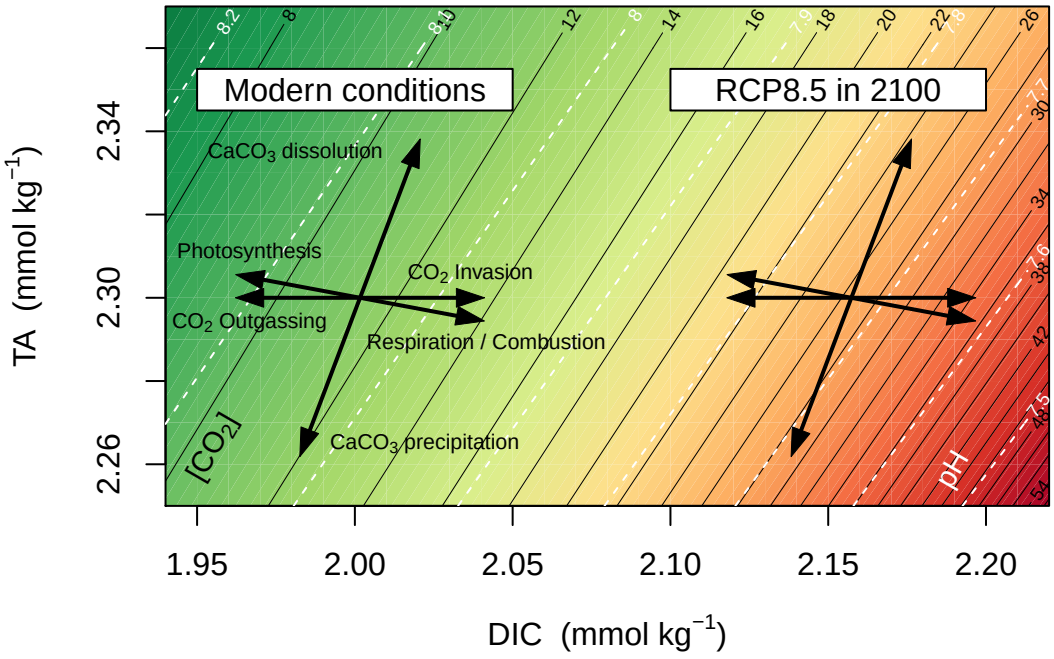

Figure 1.5: The sensitivity of the dissolved inorganic carbon (DIC) system to various perturbations, under typical modern ocean conditions (pCO_{2atm} = 400 ppm), and under conditions in 2100 if the IPCC's "worst case scenario", RCP8.5, comes to fruition (pCO_{2atm} = 936 ppm), assuming a temperature of 25°C, salinity of 35, and total alkalinity (TA) of 2.30 mmol kg^{-1}. Note how the effect of adding CO_2 to seawater (e.g. dissolution of CO_2 following burning of fossil fuels) has a relatively larger effect on the pH and [CO_2] when DIC is higher at a given TA - this is in effect a reduction in the buffering capacity of the water for CO_2. Contours represent [CO_2] and pH at chemical equilibrium. Diagram inspired by Zeebe & Wolf-Gladrow (2001) and Zondervan *et al.* (2001).

The ocean contains almost 40,000 PgC (1 PgC = 10^{15} grams or 1 billion metric tonnes, of carbon) in the form of DIC (Sigman & Boyle, 2000). Only about 2% of this carbon exists in the surface ocean, which equilibrates with the similarly-sized atmospheric reservoir on a timescale of years (Revelle & Suess, 1957). Processes in the surface ocean act as biogeochemical "pumps", driving the sequestration of carbon and nutrients into the deep ocean: the largest reservoir of carbon on Earth with a residence time of less than few thousand years. To a large extent, the role of coccolithophores in the carbon cycle is through their impact on these pumps (Riebesell *et al.*, 2009).

1.3.1 Organic carbon

Although the standing stock of organic matter in the surface ocean constitutes a small reservoir of carbon relative to the terrestrial biosphere (Sarmiento & Bender, 1994), and although much of the particulate organic matter is continuously cycled through respiration and remineralisation in the surface ocean, some sinks under the act of gravity, ballasted by heavy minerals, and is exported from the surface ocean to be sequestered at depth (Klaas & Archer, 2002). This mechanism, by which carbon from the atmosphere is pumped into the deep ocean, is called the organic carbon pump (Omta *et al.*, 2009; Sigman & Haug, 2003). Much of this organic matter is respired and remineralised at depth and is effectively sequestered in the deep ocean where the residence time of DIC is over a thousand years (Sigman & Boyle, 2000). The small fraction remaining that survives respiration in the surface or deep oceans may be buried in sediment, and, if the oxygen concentration is low enough to inhibit respiration, may enter into the rock reservoir where the residence time is three orders of magnitude greater than the deep ocean (Sigman & Boyle, 2000).

1.3.2 Inorganic carbon

On short timescales, calcification in the surface ocean decreases the capacity of the surface ocean to dissolve CO_2, due to the relatively larger effect on TA than on

DIC (Fig. 1.5). These changes are "locked in" following export of calcite from the surface ocean to the deep ocean, where approximately 80% of the calcite dissolves (Milliman *et al.*, 1999; Ridgwell & Zeebe, 2005). On longer timescales, the burial rate of alkalinity in the form of calcite controls whole ocean alkalinity, and therefore the capacity of the far larger deep ocean to dissolve CO_2 (Omta *et al.*, 2013). An important feedback concerning carbonate sediments becomes relevant on timescales longer than a few thousand years (Fig. 1.6 10^3-10^5 y): The depth of the lysocline (the depth below which $CaCO_3$ is unstable and dissolves) responds to changes in the calcite saturation state ($\Omega_{calcite}$) of the deep ocean, which is a function of DIC and of TA (Zeebe & Wolf-Gladrow, 2001). Enhancement of the organic carbon pump in the absence of a change in calcite export increases deep ocean DIC without a corresponding increase in deep ocean TA. This decreases $\Omega_{calcite}$ of the deep ocean causing dissolution of carbonate sediments and a temporary shoaling of the lysocline. The resultant increase in whole ocean alkalinity causes the lysocline return to its original depth, with more DIC in total stored in the ocean than before. On the other hand, although an increase in calcite export from the surface ocean may temporarily cause a slight increase in deep ocean alkalinity, on long timescales the depth of the lysocline migrates with the effect of causing the rate of alkalinity burial to equal that from riverine input (Sigman & Boyle, 2000).

1.3.3 Rain ratio

The ratio of inorganic to organic carbon produced in the surface ocean (production ratio), the same ratio exported from the surface ocean (export ratio), and that transitioning the water/sediment interface at depth (rain ratio), have been considered to be critical parameters in carbon cycle dynamics (Barker *et al.*, 2003b; Hutchins, 2011; Richaud *et al.*, 2007). The production ratio is far lower than the export ratio, because internal cycling in the surface ocean through respiration and remineralisation of organic matter is greater than dissolution of calcite (Duarte & Cebrian, 1996; Milliman

& Droxler, 1996). As the standing stock of biomass is small, the export ratio determines the effect of biological activity on the buffering capacity of the surface ocean for CO_2, and thus influences pCO_{2atm} on timescales of greater than the equilibration time between the surface ocean and the atmosphere (years), but less than the mixing time of the whole ocean ($\sim$ 1000 years). The rain ratio hypothesis however, is manifest as a change in pCO_{2atm} on a longer timescale. It states that a decrease in the rain ratio, and corresponding increase in dissolution of carbonate sediments through localised acidification of porewater due to respiration and remineralisation of organic matter, would liberate alkalinity and thus increase $[CO_3^{2-}]$ and $\Omega_{calcite}$ of the deep ocean, resulting in a drawdown of atmospheric CO_2 (Archer & Maier-Reimer, 1994; Archer, 1991). The "silicate switch" proposed by Ridgwell *et al.* (2002) could, according to the rain ratio hypothesis, help explain the magnitude of pCO_{2atm} change observed between glacial and interglacial times, through a subtle shift in ecosystem composition driven by silicious diatoms being able to further outcompete the coccolithophores.

Organic matter is a similar density to water, and must be ballasted by heavy minerals in order to be efficiently exported from the surface ocean, usually in the form of faecal pellets or aggregates (McCave, 1975). $CaCO_3$ may be responsible for in the region of 80% of this ballasting, with implications for the export and rain ratios (Klaas & Archer, 2002). On glacial-interglacial timescales, the tight coupling between $CaCO_3$ production and the efficiency of organic carbon export due to ballasting implies that the rain ratio is insensitive to changes in the calcification in the surface ocean (Barker *et al.*, 2003b; Ridgwell, 2003). On timescales of tens to hundreds of years however, it is unclear whether an increase in calcification in the surface ocean has a greater effect on sequestration of alkalinity (Zondervan *et al.*, 2001), or on the export efficiency of organic matter (Ziveri *et al.*, 2007). This topic is currently an active area of research, and the magnitude and sign of the net sum of these effects currently unknown (Riebesell *et al.*, 2009), although it appears to be spatially heterogeneous in the global ocean (Munhoven, 2007; Wilson *et al.*, 2012).

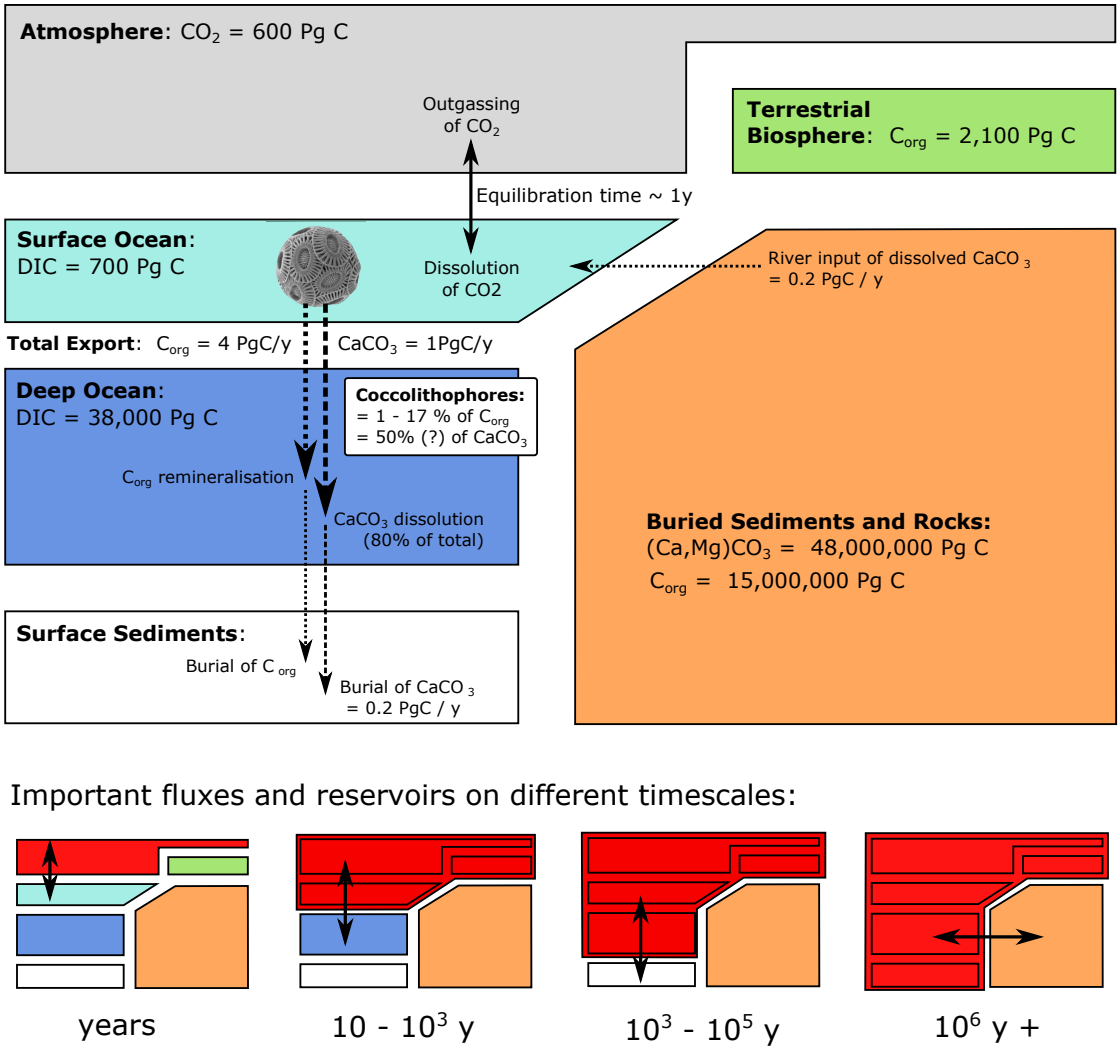

Important fluxes and reservoirs on different timescales:

Figure 1.6: Reservoirs of Carbon. Redrawn after Sigman & Boyle (2000)

1.4 Coccolithophores as recorders

As the only organisms in the surface ocean to use dissolved inorganic carbon to produce both organic matter and calcite, and having populated surface ocean waters since the Triassic (Bown, 1998), coccolithophores are uniquely positioned to record aspects of surface ocean carbonate chemistry through geological time. The isotopic composition of organic matter and of calcite is determined by the contrasting processes responsible for their formation, and also the composition of ambient seawater (Hermoso, 2014). Both the isotopic composition of seawater, and the magnitude of isotopic fractionation into biogenic matter, are functions of environmental parameters of interest (Bolton & Stoll, 2013; Pagani, 2002; Stoll & Ziveri, 2004; Zachos *et al.*, 2001).

The oxygen isotopic composition of seawater reflects global ice volume (Zachos *et al.*, 2001), whilst the carbon isotopic composition of DIC largely reflects surface ocean primary productivity (Sarnthein & Winn, 1988), or provides insight into ocean circulation changes (Piotrowski & Goldstein, 2005). In order to reconstruct light stable isotope ratios in ancient waters, the calcite remains of contemporaneous microfossils are analysed isotopically, and a calibrated "vital effect" correction is applied (Spero & Lea, 1996). Upon incorporation into calcite, oxygen is additionally subject to a strong temperature-dependent isotopic fractionation (Urey, 1947), which itself can be exploited as a temperature proxy (Watkins *et al.*, 2014), but which must be factored into any reconstruction of seawater isotopic compositions (Elderfield & Ganssen, 2000; Lea *et al.*, 2002). In foraminifera, carbon and oxygen vital effects are generally assumed to be approximately constant (Spero & Lea, 1996), but in coccolithophores, calcite is precipitated intracellularly and these offsets are species-specific functions of many parameters including physiological parameters such as growth rate, and environmental parameters such as DIC, pH and temperature (Bolton & Stoll, 2013; Rickaby *et al.*, 2010b). Although the taxonomically delimited heavy and light

groups are well established in the nannofossil community (Ziveri *et al.*, 2003), the nature of vital effects in coccolithophores has remained enigmatic. As a result, since the pioneering work of Emiliani and Broecker in the 1960s (Broecker, 1966; Emiliani, 1966), coccolithophores have remained subordinate to their calcifying zooplankton counterparts, the foraminifera, in terms of their contribution to paleoceanographic and paleoclimatic reconstruction. Recently, attention has turned to the vital effects themselves as providing information about past climates (Bolton & Stoll, 2013), but this avenue of research is in its infancy.

Alkenones are long chain (C_{37}-C_{39}) ethyl and methyl ketones, that are produced by a single known family of coccolithophores, the Noëlaerhabdaceae, and are readily preserved in sediment due to their resistance to degradation (Prahl *et al.*, 1989). An aspect of their organic structure, the undersaturation ratio ($U_{37}{}^{k}$), systematically varies with temperature, and so geochemical analysis of alkenones preserved in sediment has been widely used to reconstruct past sea surface temperatures (SSTs; Conte *et al.*, 2006; Herbert, 2003; Sikes *et al.*, 1991). These highly preserved organic molecules have also been used to reconstruct ancient pCO_{2atm} through carbon isotopic analysis (Pagani, 2002; Pagani *et al.*, 2005). The isotopic composition of bulk organic carbon can be calculated from that of alkenones, and its systematic relationship to ambient [CO_2] has been well documented (Laws *et al.*, 2001). This relationship arises due to the effect of [CO_2] on the passive diffusional flux of carbon into the cell and the implications for intracellular Rayleigh fractionation driven by the large kinetic fractionation of carbon isotopes that occurs during photosynthetic carbon fixation (Farquhar *et al.*, 1982; Laws *et al.*, 1995; Popp *et al.*, 1998; Rau, 1996).

The potential for coccolithophore biogenic material preserved in sediments to form the basis of isotopic paleoclimate proxies is substantial. However, a holistic understanding of how environmental and physiological parameters simultaneously control isotopic vital effects, and the fractionation of carbon into organic matter, is currently lacking.

1.5 Thesis objectives

This thesis aims to develop new ways of extracting information pertinent to the carbon cycle from coccolithophores preserved in sediment. Coccolithophores play an active role in carbon cycle dynamics, and they also passively record aspects of seawater carbonate chemistry. The questions that this thesis addresses are therefore:

1. What physiological information is recorded in fossil coccoliths? Can the geological record be used as a laboratory to study physiological changes on timescales not possible with *in vivo* experimentation?

2. What controls the isotopic composition of calcite and organic matter in coccolithophores? Can coccolithophore [CO_2] proxies be improved?

To answer these questions, I have used a range of approaches including *in vivo* experimentation, isotopic and morphometric analysis of fossil coccoliths preserved in sediment, and of material grown in culture, and numerical modelling. By chapter, the work described in this thesis is as follows:

Chapter 2 : A laboratory-calibrated novel approach for size-normalising coccolith mass in the most abundant family of coccolithophores, the Noëlaerhabdaceae. This approach is used with sedimentary material to infer calcification changes in the Noëlaerhabdaceae through a glacial cycle.

Chapter 3 : A new cellular carbon isotopic flux model for coccolithophores, calibrated using new data from cultures, uncovers the sources of vital effects in coccolith calcite and organic matter.

Chapter 4 : A novel technique for extraction and analysis of organic carbon from within single taxon fossil coccolith samples is combined with the model from Chapter 3 to develop a new approach for studying past [CO_2]. This new approach is tested on Late-Pleistocene samples.

Chapter 2

Calcification response of a key phytoplankton family to millennial-scale environmental change

2.1 Introduction

Coccolithophores are the modern ocean's dominant calcifying phytoplankton and coccoliths, the distinctive calcite plates that they produce, have populated the fossil record for over 200 million years (Bown, 1998; Milliman, 1993). Biogenic calcification is an important climatic feedback (Boyd & Doney, 2003; Rost & Riebesell, 2004), and in most organisms is thought to be strongly affected by changes in the carbonate chemistry of seawater. In coccolithophores, calcite precipitation occurs inside the cell, so the site of calcite precipitation is buffered from the external environment and is subject to an unusually high degree of biological control. The most abundant modern species of coccolithophore are *Emiliania huxleyi* and *Gephyrocapsa oceanica*; bloom-forming members of the family Noëlaerhabdaceae (Haptophyta: Coccolithophyceae: Isochrysidales: Noëlaerhabdaceae). Laboratory culture experiments have shown that these two species tend to calcify less when carbon dioxide concentrations are higher (Riebesell *et al.*, 2000a; Sett *et al.*, 2014; Zondervan *et al.*, 2001), although the trade off between dissolved inorganic carbon (DIC) availability and pH appears

to be critical (Bach *et al.*, 2015). Yet these observed responses each characterize a single genome, adapted to the modern environment and exposed to artificially manipulated conditions in the laboratory in the absence of genetic change (phenotypic plasticity). In nature, communities are genetically and phenotypically heterogeneous, and selective pressures lead to competition. Environments are dynamic, and changes in average conditions are subtle and prolonged. Sexual reproduction, which has never been observed in the laboratory in coccolithophores, genetically homogenizes a population within a biological species, whilst accelerating adaptation through propagation of the most beneficial combinations of alleles and removal of deleterious mutations via natural selection. To elucidate the role of these phytoplanktonic marine calcifiers in nature across geological history, their response must be studied on timescales of tens to tens of thousands of years, within natural populations, where evolutionarily relevant processes such as meiosis and syngamy may occur (Bendif *et al.*, 2014; von Dassow *et al.*, 2014), and where the rate and amplitude of environmental change is representative of the real world. Indeed a theoretical model has suggested that on such timescales the selective pressure of increasing [CO_2(aq)] may have favoured the more heavily calcified forms of coccolithophore (Irie *et al.*, 2010).

An apparent dichotomy exists between the consensus view of phenotypic plasticity as observed in short-term experiments and the theoretical result of long-term evolutionary adaptation. However, experiments lasting hundreds of generations have shown that asexual coccolithophore populations have the potential to adapt in culture (Lohbeck *et al.*, 2012; Schlüter *et al.*, 2014) and large-scale surveys have revealed significant spatial heterogeneity in nature (Beaufort *et al.*, 2011; Horigome *et al.*, 2014). The fossil record, by contrast, is an archive of information about ancient natural coccolithophore communities that responded to environmental changes over geological timescales. The challenge is to extract meaningful information from this resource. Isolated coccoliths in deep-sea sediment are often the only remnants of ancient coccolithophores to survive geological time, so inferences about the physiology of coccolithophores that lived in the past must come from this evidence alone.

Studies to date have yielded contradictory results regarding the response of calcification to changes in seawater carbonate chemistry on geological timescales (Beaufort *et al.*, 2011; Iglesias-Rodriguez *et al.*, 2008), but this disagreement is, at least in part, a result of the lack of consistency between the parameter measured, and how this is inferred to represent *calcification intensity*. Coccolith mass has been used extensively to infer calcification ability (Beaufort *et al.*, 2011; Halloran *et al.*, 2008; Horigome *et al.*, 2014; Iglesias-Rodriguez *et al.*, 2008; Meier *et al.*, 2014a,b), but as it is not independent of coccolith size, size-normalization is highly nontrivial and it remains a biologically abstract quantity. To solve this problem, I have developed a procedure for size-normalising coccolith mass, by correlating an index based on coccolith morphometry with the molar ratio of particulate inorganic to particulate organic carbon (PIC:POC) ratio composing biogenic matter. The PIC:POC ratio is a direct record of the ratio of integrated rates of calcification to photosynthesis (Rost & Riebesell, 2004), and therefore describes an energetic and carbon budget trade off between calcification and biological (metabolic) activity that makes more sense biologically than coccolith mass in the context of physiology and adaptation, and is independent of coccolithophore cell size. Through size-normalising mass by consideration of a dimensionless but biologically meaningful parameter, problems associated with allometry are circumvented.

To explore the calcification response of natural coccolithophore populations to changes in seawater carbonate chemistry and temperature in the form of a down-core experiment, I used this novel approach to analyze sediment-core material from two glacial terminations, which are of contrasting magnitude. The larger of these terminations sees an increase in pCO_2 similar in magnitude to that since the industrial revolution, albeit two orders of magnitude slower. This approach constitutes a real world experiment in which the response of natural populations to the environmental changes of a glacial cycle can be explored.

2.2 Materials and Methods

2.2.1 *In vivo* calibration

2.2.1.1 Culture experiments

Duplicate monoclonal batch cultures of four strains of coccolithophore belonging to the family Noëlaerhabdaceae were grown in sterile filtered (0.2μm) artificial seawater prepared according to ESAW (Berges *et al.*, 2001) adapted for a range of DIC concentrations ([DIC] = 1.380 mM, 2.147 mM, 3.067 mM and 6.135 mM) at constant pH (8.2) by varying sodium bicarbonate addition and titration with HCl and with nitrate (442 μM), phosphate (5.00 μM), vitamins, trace metals and EDTA according to K/2 (as defined by Keller *et al.*, 1987). Carbonate chemistry manipulation at constant pH is more analogous to changes expected in the surface ocean on a glacial-interglacial timescale than holding alkalinity constant, due to buffering by carbonate sediments. Cultures were maintained at 15°C with an incident photon flux of 250 μE and a 12 hr / 12 hr light / dark cycle. Cells were acclimated for >20 generations in dilute batch culture for each experimental condition prior to inoculation. Cells were inoculated in 2.4 l polycarbonate flasks, with no headspace and sealed off to the air with teflon lined caps. Removal of small aliquots of medium during the experiment was unavoidable due to the need to count and measure cells, and resulted in a maximum headspace of 20 cm^3 at harvest. To minimise the drift in culture conditions throughout the course of the experiment, cells were harvested at ∼1-2% (and never greater than 4%) of maximum cell density, which was determined for each experimental condition and strain combination via preliminary experimentation. Strains were AC478 (RCC1211 *Gephyrocapsa oceanica* from Portuguese coast in Atlantic Ocean), AC472 (RCC1216 *Emiliania huxleyi*, from Tasman Sea in Pacific Ocean), AC448 (RCC1256 *Emiliania huxleyi*, Icelandic coast in Atlantic Ocean) and AC279 (RCC1314 *Gephyrocapsa oceanica*, French coast in Atlantic Ocean) from the Roscoff culture collection (RCC). Particulate material was harvested by dry filtration onto pre-weighed membranes

with 0.2 μm pore-size, and rinsed of salt with a minimal amount of deionised water (adjusted to pH 7). Coccolithophore size and concentration were obtained using a Beckman Z2 Coulter Counter (see *www.beckmancoulter.com* for description of Coulter principle). Coccosphere and cell size were measured three times each respectively pre- and post-decalcification both morning and evening on the harvest day and the preceding day. Cells were decalcified by reducing the pH of the suspension with HCl addition to 5.0 with for around 20 minutes. The Coulter counter was calibrated to use ESAW + K/2 medium as an electrolyte, and for use with the acidified electrolyte, to accommodate for the difference in ionic strength. Cell division is synchronized under the light/dark cycle and cell size was assumed to increase linearly throughout the day (Müller *et al.*, 2008). By measuring cell and coccosphere size morning and evening, the bias introduced due to the time of day of measurement can be removed by interpolation to the same time of day. This also removes the daily variation in the slope of Eq. 2.3 which is a function of cell size (Müller *et al.*, 2008) and number of coccoliths per cell. Culture health was monitored by cell counts and microscope inspection on alternate days. Molar PIC and POC were measured with a *Rock Eval analyser*, which is preferable to making assumptions about carbon density of biogenic material. An aliquot of culture residue was bleached with dilute sodium hyperchlorite solution (4% available chlorine for 20 minutes) to remove the organic matter, and washed three times in deionised water to remove the bleach. The resultant "pseudo-sediment" was subsequently analysed using the computational software, SYRACO (Beaufort & Dollfus, 2004; Beaufort, 2005; Beaufort *et al.*, 2014).

2.2.1.2 Size-normalization of coccolith mass

The concept for size-normalising coccolith mass is based on the following arguments:

(i) The molar PIC:POC ratio of coccolithophore biomass is proportional to the ratio of spherical volumes of calcite to organic matter (Fig.2.2B).

(ii) Coccolith length, estimated by the square root of coccolith area ($\sqrt{A_L}$), is proportional to coccosphere radius (R_s): $R_s \propto \sqrt{A_L}$ (Fig.2.2C).

(iii) The coccosphere is a spherical shell of calcite, and coccolith thickness (T_L) is proportional to the difference between the internal and external radii of the coccosphere ($T_s = R_s - R_c$): $T_s \propto T_L$ (Fig.2.2D).

(iv) Given (i), (ii) and (iii), a combination of coccolith mass and area can be related back to coccolithophore PIC:POC, via cell and coccosphere dimensions, thus providing a rationale for size-normalisation of mass (Fig.2.2E).

Each assumption was tested, and the mass-normalisation concept was calibrated using the cultured coccolithophores for a purely geometric validation. (i) was established via *in vivo* measurement of coccosphere and cell volumes, and direct measurement of the molar PIC:POC ratio of the biomass:

$$\ln\left(PIC : POC_{volume}\right) \propto \ln\left(\frac{V_s - V_c}{V_c}\right) = \ln\left(\left(\frac{R_s}{R_c}\right)^3 - 1\right), \tag{2.1}$$

where V_s and V_c are respectively the volumes of the coccosphere and the cell, and R_s and R_c are respectively the radii of the coccosphere and the cell (as labelled in Fig.2.2A).

To generate isolated coccoliths as are found in sediment, the filtered culture residue was bleached to remove organic matter whilst preserving the calcite intact, emulating the effect of decomposition. This synthetic coccolith-sediment was analysed using SYRACO (Beaufort *et al.*, 2014); an automated image analysis tool, which measures coccolith area and mass. The relationship between the ratio of volumes of calcite to that of the cell and PIC:POC (Eq.2.1) can be simplified by approximating the cell and coccosphere as having the same radius (R_s). The volume of organic material is then the volume of a sphere of radius, R_s, and the volume of calcite in the coccosphere is that of a thin shell of thickness T_s and radius R_s. Using assumptions (ii) and (iii) gives:

$$\ln\left(PIC : POC_{coccolith}\right) \propto \ln\left(\frac{R_s^2 \times T_s}{R_s^3}\right) = \ln\left(\frac{T_s}{R_s}\right)$$
$$\propto \ln\left(\frac{T_L}{\sqrt{A_L}}\right) = \ln\left(\frac{M_L}{A_L^{\frac{3}{2}}}\right), \tag{2.2}$$

where M_L = coccolith mass, and A_L = coccolith area are the direct output from the SYRACO analysis, and $M_L/A_L = T_L$.

2.2.2 Down-core experiment

2.2.2.1 Site

SYRACO analysis was performed on sediment from ODP site 1123 (Expedition 181), on Chatham rise, east of New Zealand in the southernmost Pacific (41°47.2'S, 171°29.9'W, 3290 m water depth). Depths span the penultimate and 6th most recent glacial-interglacial cycles (MIS 7-5:∼200-100ka and MIS 15-13:∼600-500 ka, respectively), and sample resolution is higher (∼1000 year) over the terminations (TII:∼140-125 ka and TVI:∼540-520 ka). Dissolution proxies (Crundwell *et al.*, 2008) and SEM observations of coccoliths show good preservation at this site throughout the periods of interest. ODP site 1123 exists at the northern edge of the sub tropical front (STF) in the southernmost Pacific Ocean, and may see an increased influence of sub antarctic water during glacials and subtropical water during interglacials (Crundwell *et al.*, 2008). The sediment age model for side ODP site 1123 is based on a correlation with the orbitally tuned benthic oxygen isotope stack of LR04 (Elderfield *et al.*, 2012; Lisiecki & Raymo, 2005). An *in situ* proxy reconstruction of sea surface temperature (SST) was employed, based on Mg/Ca ratios of planktic forams using species-specific published calibration throughout the periods of interest. [CO_2(aq)] was calculated from published pCO_2 records from ice cores (see methods) and from reconstructed SSTs, assuming equilibrium between the atmosphere and surface waters. [CO_2(aq)] and temperature increased during each glacial termination (Fig.2.1). pH and [DIC] were unconstrained, but on these timescales, the decrease in pH due to invasion of

CO_2 may be partially buffered by dissolution of carbonate sediments. For this reason, $[CO_2(aq)]$ is used to describe the carbonate system, as this is the most well constrained component. $[CO_2(aq)]$ is estimated from global pCO_2 of an assumed well mixed atmosphere from Vostok (Fig.2.1, *left*) and Dome C (Fig.2.1, *right*) Antarctic ice cores (compiled by (Lüthi *et al.*, 2008)), with dissolution assumed to be controlled only by SST at a constant salinity of 35. EDC3 gas age was converted to LR04 using a published conversion (Parrenin *et al.*, 2007). Carbon isotopic composition of planktic forams were used as a rough proxy for relative nutrient ($\sim$ phosphate) availability corrected for the effect of temperature via: $[\text{Nutrients}] = 1.1(\delta^{13}\text{C} - 0.1\,\text{SST})$(Lynch–Stieglitz *et al.*, 1995). Relative nutrient concentrations appear to show no systematic variation across the glacial terminations (Fig.2.1).

2.2.2.2 Temperature reconstruction

Temperatures across the MIS 7-5 interval were inferred from the *G.bulloides* 250-300 μm and 300-355 μm size fractions using the equation: $\text{Mg/Ca} = 0.47 \exp 1.08T$, and those across MIS 15-13 were inferred from *Globigerina inflata* using the equation: $\text{Mg/Ca} = 0.299 \exp 0.090T$. Species specific calibrations are from Anand *et al.* (2003). Paired stable isotope ($\delta^{18}O$ and $\delta^{13}C$) and Mg/Ca analyses were performed on typically 60 individual shells of *Globigerina inflata* (MIS 15-13) and *Globigerina bulloides* (MIS 7-5), picked from the 300-355 μm size fraction. In Fig.2.3 and Fig.2.1, the alternative filled points are temperatures inferred from the 250-300 μ size fraction, which captures the glacial termination more clearly than the larger fraction. The difference in temperature as inferred from the different size fractions however has little effect on $[CO_2(aq)]$. Prior to isotopic analyses, samples were crushed, cleaned in 3% hydrogen peroxide solution to remove any possible organic contaminants, rinsed with acetone and dried overnight in an oven at 60°C. Measurements of the isotopic composition of carbon dioxide, released from the foraminiferal carbonate using a MULTIPREP system, were performed on a VG SIRA mass spectrometer at the Univ. Cambridge.

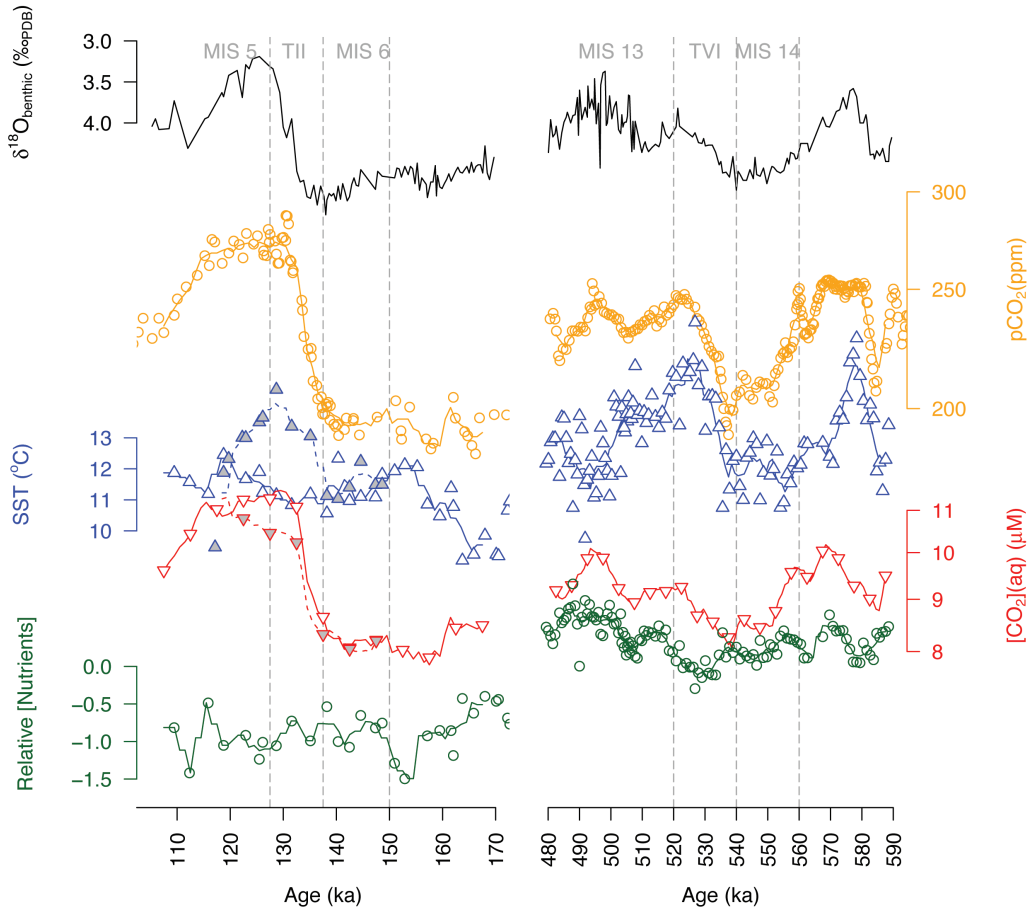

Figure 2.1: Time series of proxy-reconstructed climatic parameters at ODP site 1123. Benthic Oxygen isotopes from foraminifera (Elderfield *et al.*, 2012) allow for temporal alignment with other records. Reconstructed sea surface temperature (SST) estimates are based on Mg/Ca ratios of planktic foraminifera. $[CO_2]$ is estimated from global pCO_2 of an assumed well mixed atmosphere from Vostok (*left*) and Dome C (*right*) Antarctic ice cores (compiled by (Lüthi *et al.*, 2008)), with dissolution assumed to be controlled only by SST at a constant salinity of 35. EDC3 gas age was converted to LR04 using a published conversion (Parrenin *et al.*, 2007). Carbon isotopic composition of planktic foraminifera were used as a rough proxy for relative nutrient availability corrected for the effect of temperature (as in Lynch–Stieglitz *et al.*, 1995).

Calibration to the Vienna Peedee Belemnite standard was through the NBS19 standard (Coplen, 1995), and the analytical precision was better than 0.08 ‰ for $\delta^{18}O$ and 0.06 ‰ for $\delta^{13}C$ (1σ). For Mg/Ca measurements, samples were prepared following the cleaning procedure described by Barker *et al.* (2003a). Analyses were performed on a Varian Vista Pro Inductively Coupled Plasma Optical Emission Spectrometer (ICP-OES) and a Perkin Elmer Elan DRCII quadrupole based Inductively Coupled Plasma - Mass Spectrometer (ICP-MS) at the Univ. Cambridge, following established procedures (de Villiers *et al.*, 2002; Yu & Day, 2005). Precision for measured Mg/Ca ratios determined from replicate runs of a standard solution containing Mg/Ca = 1.3 mmol / mol was 0.46%. Accuracy of Mg/Ca determinations was confirmed by interlaboratory studies of foraminifera and carbonate reference materials (Greaves & Caillon, 2008; Rosenthal *et al.*, 2004).

2.2.3 SYRACO Analysis

SYRACO analysis (Beaufort *et al.*, 2014) measures the mass and area of each coccolith belonging to the family Noëlaerhabdaceae in the analysed samples. Additionally, each coccolith is assigned to a morphotaxonomic group on the basis of shape. These groupings approximate species-level taxonomic classifications and provide insight into subsets of the population. Smear slides were prepared using a trial and error approach to attain the optimum coccolith density. SYRACO analysis was carried out in CEREGE.

2.3 Results

2.3.1 *In vivo* calibration

The *in vivo* experiments reveal linear relationships between 1-dimensional coccolith size ($\sqrt{A_L}$), and cell radius, and between coccolith thickness and coccosphere thickness, across the species studied (Fig.2.2C and Fig.2.2D respectively). The relationship

between coccolith size and cell size agrees with the well established relationship between coccolith size and cell size in the Noëlaerhabdaceae (Henderiks, 2008), which is derived from fossils (red dashed line Fig.2.2C). That all strains lie on the same line as fossil Noëlaerhabdaceae supports an assumption that this family of coccolithophores can be treated as a continuum of forms (Beaufort *et al.*, 2011).

The ratio of calcite to cellular volume is here shown to be an excellent indicator of the molar PIC:POC ratio (Fig.2.2B; Eq.2.1), suggesting that volumetric measurements using a coulter counter can constitute a fast, inexpensive means of estimating PIC:POC. Volume-predicted PIC:POC has a highly significant relationship with measured PIC:POC ($p < 0.001$, F-statistic = 123 on 1 and 28 DF), and an excellent linear fit ($R^2_{adj} = 0.81$). The coccolith aspect ratio (AR = coccolith thickness / coccolith length) is also a highly significant predictor of PIC:POC (Fig.2.2E; Eq.2.2; $p < 0.001$, F-statistic = 79 on 1 and 30 DF) and has good linear fit ($R^2_{adj} = 0.71$).

The relationship between coccolith aspect ratio and PIC:POC is of the form of Eq.2.2, and quantitatively is found using an ordinary least squares linear regression incorporating an estimate of the uncertainty in PIC:POC based on the 1σ prediction interval giving:

$$\begin{aligned} PIC : POC_{coccolith} &= e^{3.5\pm0.2} AR_L^{1.12}, \\ &= 33.1^{+7.3}_{-6.0}\, AR_L^{1.12}, \end{aligned} \tag{2.3}$$

where $AR_L = \frac{T_L}{\sqrt{A_L}} = M_L/A_L^{\frac{3}{2}}$ is the lateral cross-sectional aspect ratio of a coccolith (AR_L).

Regressions are y-on-x ordinary least squares regressions on the mean of a fitted gaussian on log-transformed data. An ordinary least squares regression was chosen because the uncertainty in the y-axis variable far exceeds that of the x-axis variable. Frequency histograms, each with a fitted gaussian curve, are given in the supplementary material. Equation 2.3, derived from first principles, describes the relationship

between coccolith aspect ratio and PIC:POC, and is supported empirically (Fig.2.2E). AR_L is taken to be the most sensible way of size-normalising coccolith mass, which alone is biologically meaningless. Caveats associated with directly translating AR_L to PIC:POC using Eq.2.3 are discussed later.

The relationship between coccolith length (L_c) and coccosphere diameter ($D_s = 2R_s$) in the reticulofenestrids is established (Henderiks, 2008), and given as follows:

$$D_s = 1.02 + 1.42L_c, \tag{2.4}$$

where all lengths are in μm. Given that,

$$A_c = \pi \left(\frac{L_c C}{2} \right)^2, \tag{2.5}$$

where A_c = coccolith area, W_c and L_c = respectively the semi minor and major axes of the elliptical coccolith and $C = \sqrt{W_c/L_c}$ = "circularity", Eq 2.4 becomes:

$$R_s = 0.51 + \frac{1.42}{\sqrt{\pi}C}\sqrt{A_c}. \tag{2.6}$$

When a value of $C = 0.9$ is used, which is typical (Henderiks, 2008), the relationship between the square root of coccolith area and coccosphere radius presented here (Figure 2.2 C) is in very close agreement with Eq 2.6. A more recently published relationship between coccolith length and coccosphere diameter, has a different gradient (Müller *et al.*, 2010), but the measurements of length are based on coccolith volume, related to distal shield length via an equation from the literature (Young & Ziveri, 2000) - not from direct measurements of area or length.

Box 2.1: Relationship between coccolith length and coccosphere diameter

2.3.2 Down-core experiment

Here I show morphotaxon-specific records for the groups dominated by large *Gephyrocapsa* spp. and by *E. huxleyi* (MG_{Geo} and MG_{Emi} respectively). These species are numerically the most abundant coccolithophore species in the modern ocean and throughout most of the Quaternary, they are the most thoroughly studied in the

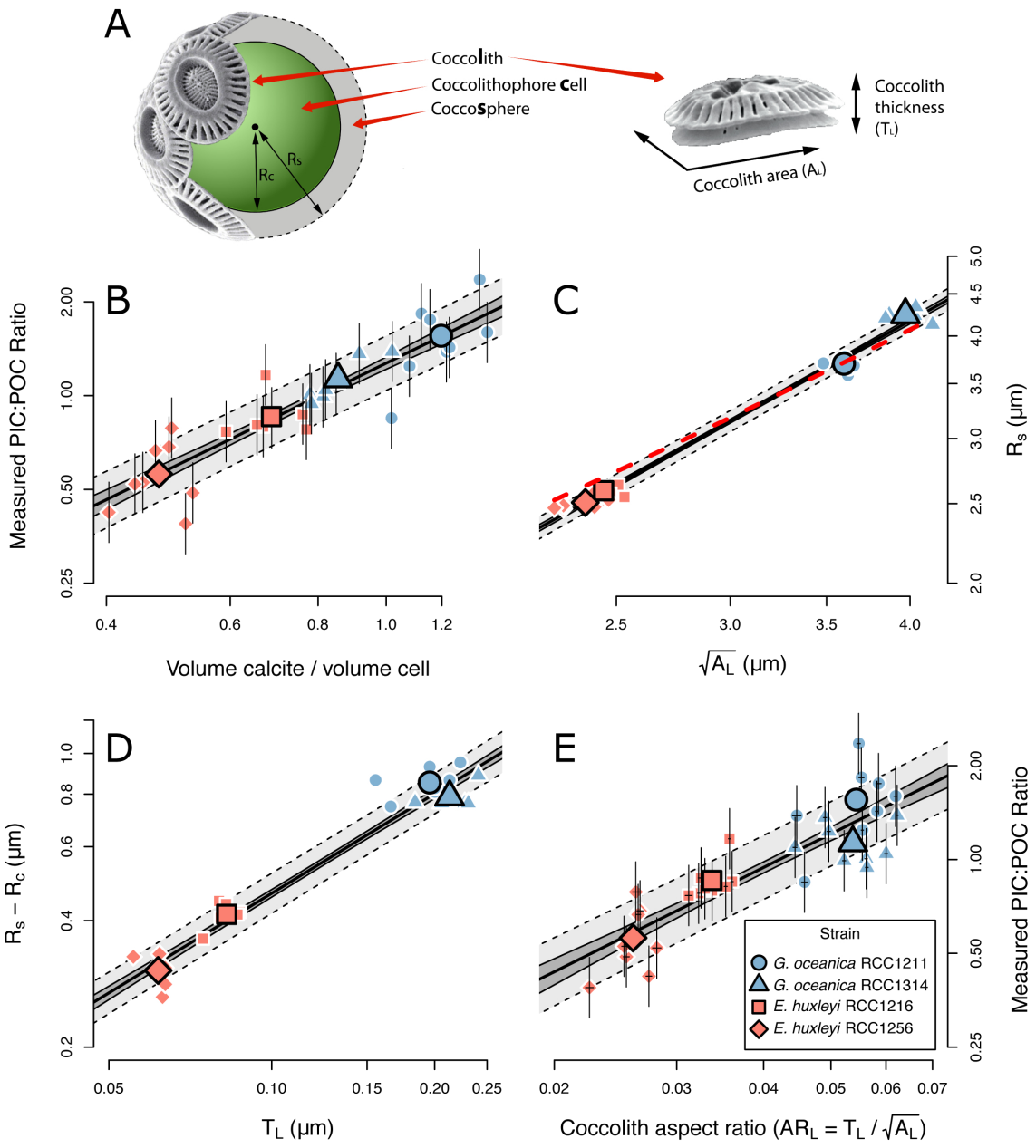

Figure 2.2: Size-normalisation of coccolith mass. A, Schematic representation of coccolithophore cell, with variables defined. **B,** Regression of molar PIC:POC ratio against volumetric ratios of calcite to organic material (Eq. 2.1). **C,** Regression of coccosphere radius against the square root of coccolith area. The red dashed line represents an independently derived relationship between coccolith size and coccosphere size (Henderiks, 2008) - see also Box 2.1. **D,** Regression of coccosphere thickness against coccolith thickness. **E,** Regression of molar PIC:POC ratio against coccolith aspect ratio ($AR_L = T_L/\sqrt{A_L}$; Eq. 2.3). The dark region around each regression line represents the 1σ confidence interval of the regression, whilst the lighter region with the dashed border represents the 1σ prediction interval of the regression. Error bars on individual points represent the 1σ confidence interval of each measurement. SEM images courtesy of Jeremy Young, reproduced with permission.

laboratory, and their ultrastructure is suited to SYRACO analysis. Over TII, mean Noëlaerhabdaceae coccolith mass and area increase transiently across the termination. This is accompanied by an increase in the mean-independent variance (arithmetic coefficient of variation; ACV) in both of these variables (Fig.2.3), implying a non-uniform response within the population. Specifically, the mass and area of MG_{Geo} transiently increase in parallel (almost doubling) over the termination, but (MG_{Emi}) shows a subtle decrease. Over TVI, prior to the first appearance of *E.huxleyi* coccoliths in the fossil record at around 290ka (Young, 1998), the absolute magnitude and ACV of Noëlaerhabdaceae coccolith mass is very stable, though with a large decrease in ACV during the MIS14 glacial inception. The absolute magnitude of coccolith area, however, peaks during MIS14 glacial maximum and decreases during TVI, but with little change in the area ACV. The time series of population mean AR_L (size-normalised mass) exhibits an increase across both terminations. This effect is paralleled but larger in the AR_L of MG_{Geo}, which increases by $\sim 30\%$ across both TII and TVI. By contrast, the AR_L response of MG_{Emi} across TII is of a slight decrease. The absence of *E. huxleyi* explains the higher population mean AR_L over TVI than over TII, and its presence and opposing response to *G. oceanica*, as inferred from the morphotaxa, explains the increased variance observed over TII. The parameter AR_L reconciles the differing response of mass and area of MG_{Geo} to increasing [CO_2(aq)] and temperature across these two terminations.

2.4 Discussion

2.4.1 Biological implications

The AR_L time series shows that coccoliths become more calcified in Noëlaerhabdaceae, and especially *G.oceanica*, with increasing [CO_2(aq)] and temperature at site 1123 in natural populations over a timescale of thousands of years. This increase contrasts with results from the literature that describe the capacity for phenotypic

plasticity in these organisms. In the laboratory, single strains of *G. oceanica* calcify relatively less with increasing CO_2 concentration (Rickaby *et al.*, 2010b; Riebesell *et al.*, 2000a; Sett *et al.*, 2014; Zondervan *et al.*, 2001), and there is no discernible effect of temperature (Sett *et al.*, 2014). *E. huxleyi*'s plastic response to increasing CO_2 concentration over the reconstructed [CO_2(aq)] range is of decreasing calcification when [DIC] or alkalinity (ALK) is held constant (Bach *et al.*, 2011; Müller *et al.*, 2010; Riebesell *et al.*, 2000a; Sett *et al.*, 2014; Zondervan *et al.*, 2001) but the opposite at constant pH (Bach *et al.*, 2011). In *E. huxleyi* the plastic effect of temperature in the laboratory is large, but non-linear and poorly constrained (Sett *et al.*, 2014).

2.4.2 Coccolith morphometry as a proxy for PIC:POC

So far, the proposed method for size-normalising coccolith mass has used the PIC:POC ratio simply to justify the theoretical rationale with real biological data. It is however, possible to use this relationship as a proxy for PIC:POC, using the coccolith aspect ratio as an input. The predictive power of Eq.2.3 as a proxy for Noëlaerhabdaceae PIC:POC is dictated by the spread of the residuals about the regression line: the prediction interval - not only by the confidence interval, which describes the uncertainty in the relationship (McClelland *et al.*, 2014). With a formal consideration of the associated uncertainty, Eq.2.3 can be used as a proxy to directly infer

Figure 2.3 (following page): Calcification response of the Noëlaerhabdaceae to environmental changes over two glacial-interglacial cycles. A, benthic $\delta^{18}O$ (Elderfield *et al.*, 2012), and 5kyr interval average sea-surface temperature (from Mg/Ca ratios in planktic foraminifera; filled triangles over TII represent an alternative size fraction - see methods) and [CO_2] (calculated from CO_2atm (Lüthi *et al.*, 2008) and SST) at ODP site 1123 in the southern Pacific Ocean. **B-D,** Coccolith morphometrics: (**B**) Mass, (**C**) Area and (**D**) Aspect ratio. Raw data are displayed as frequency-density contour plots. Points represent 5 kyr averages. *Emiliania huxley*-affiliated morphotaxa (MG_{Emi}) are hollow squares, *Gephyrocapsa* spp.-affiliated morphotaxa (MG_{Geo}) are hollow diamonds and filled circles (population mean) represent the mean of the Noëlaerhabdaceae-affiliated morphotaxa in each sample. Arithmetic coefficient of variation (CV) is a measure of the mean-independent variance of log-normal data, and is shown in grey.

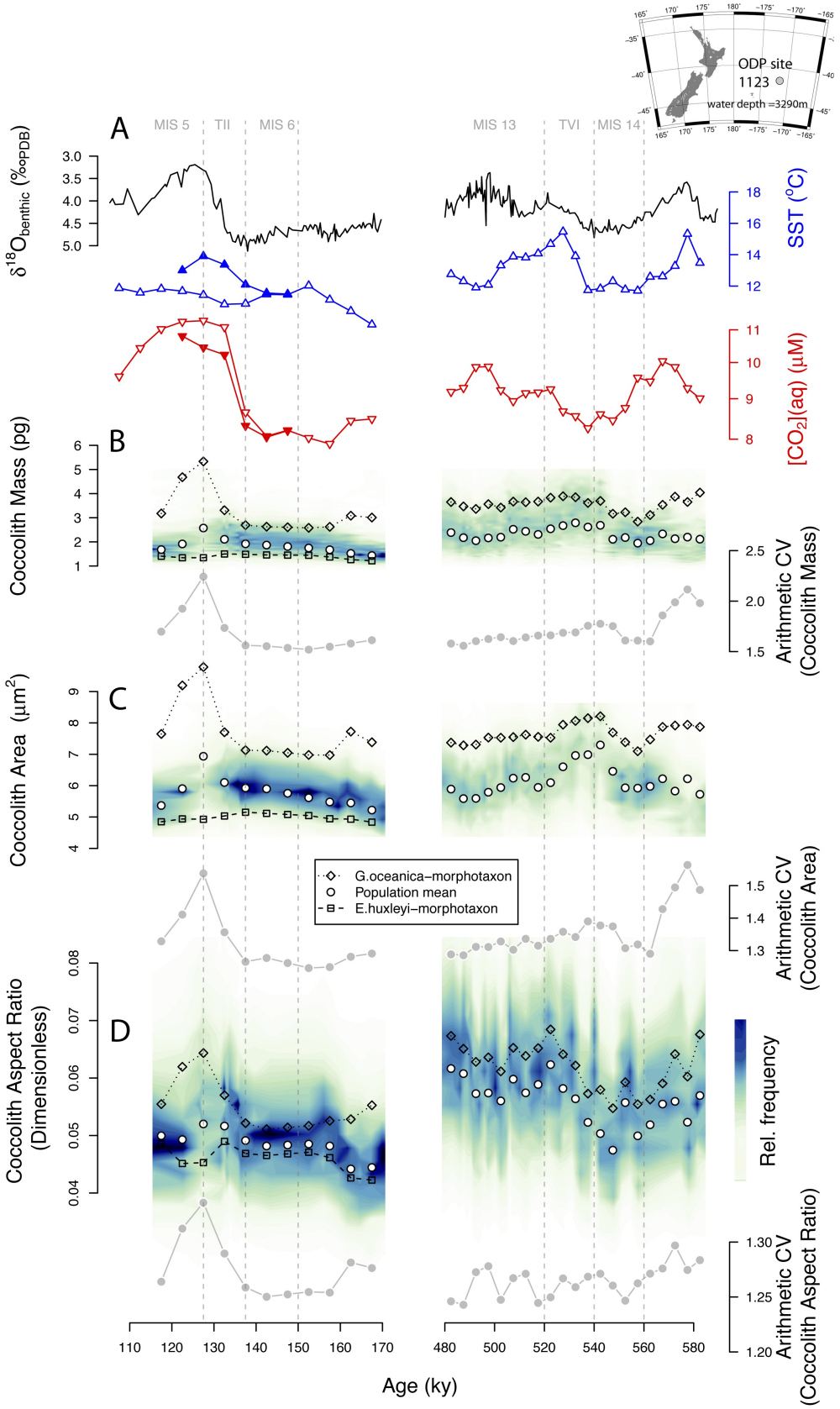
A
MIS 5
TII
MIS 6
MIS 13
TVI
MIS 14
ODP site
1123
water depth =3290m
δ18Obenthic (‰PDB)
SST (°C)
[CO2](aq) (μM)
B
Coccolith Mass (pg)
Arithmetic CV (Coccolith Mass)
C
Coccolith Area (μm2)
Arithmetic CV (Coccolith Area)
G.oceanica–morphotaxon
Population mean
E.huxleyi–morphotaxon
D
Coccolith Aspect Ratio (Dimensionless)
Rel. frequency
Arithmetic CV (Coccolith Aspect Ratio)
Age (ky)

PIC:POC from Noëlaerhabdaceae coccolith morphometry (Fig.2.2E). If the constant of proportionality between coccolith size and cell size is systematically influenced by the environment or differences between species, this will be reflected in the estimate of PIC:POC. In this calibration, hundreds of thousands of cells, and thousands of individual coccoliths were measured for each sample, which has the effect of averaging over the potential variation in the slope of Eq.2.3 due to variations in the number of coccoliths per cell, or the degree of overlap of coccoliths. Indeed, the established relationship between coccolith size and cell size in heterogeneous natural fossil populations (Henderiks, 2008) agrees with the data presented here very well (Fig.2.2C), lending support to the constant relationship between cell size and coccolith size, and application to the whole Noëlaerhabdaceae family. Coccolith over-production in *E.huxleyi* where multiple coccolith layers are produced, and many more individual coccoliths are lost, will cause coccolith morphometry to underestimate net PIC:POC, and this is unavoidable. In the rare deposits where preservation is exceptional and coccospheres are intact, such as in the Lagerstätte deposits of Tanzania (Gibbs *et al.*, 2013; O'Dea *et al.*, 2014), Eq.2.1 may be used to estimate PIC:POC directly. This approach would bypass the assumptions necessary to infer PIC:POC directly from isolated coccoliths.

I have compiled PIC:POC values from the literature and compared them with results inferred from the down-core record (Fig.2.4 and Fig.2.5). The PIC:POC of both the Noëlaerhabdaceae mean, and of MG_{Geo}, increases in response to $[CO_2(aq)]$ and temperature. This is opposite to results from the laboratory (Fig.2.5). Any change in PIC:POC inferred from AR_L of MG_{Emi} coccoliths are well within the range of uncertainty however. Although the uncertainties in these estimates are large, these results are necessarily elusive to laboratory experiments due to the timescales involved.

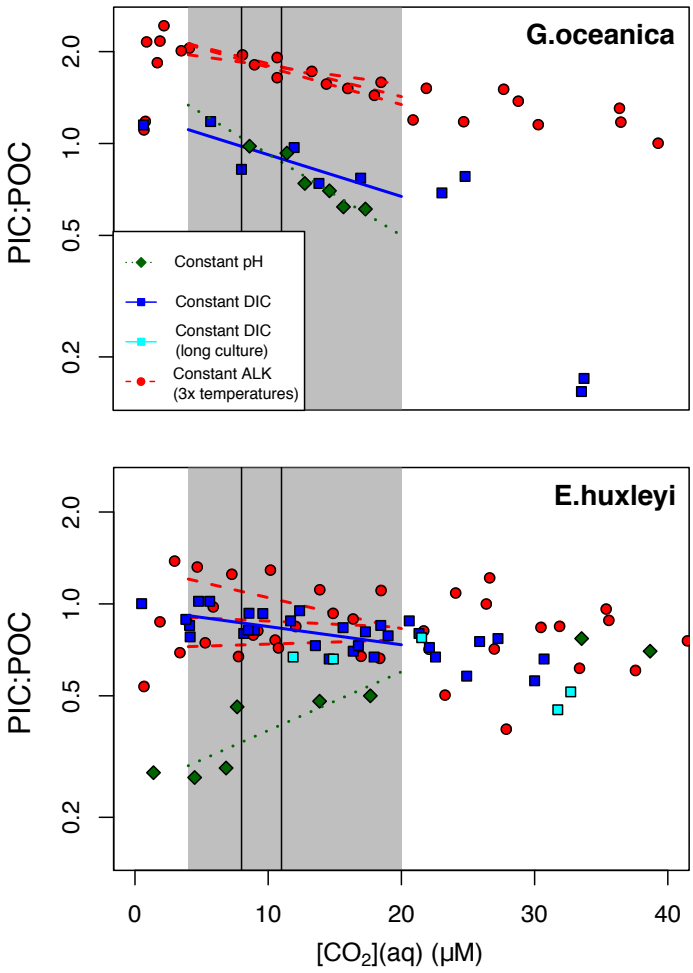

Figure 2.4: Plastic response of E. huxleyi and G. oceanica from the literature. Least-squares linear regressions for each method of carbon manipulation are shown, over a representative range of $[CO_2]$ (grey shaded region). The solid vertical lines delimit the range of $[CO_2]$ experienced at ODP site 1123 over the glacial terminations. Three separate regressions are given within the const.TA experiments, for three experiments undertaken at different temperatures. Slopes are based on the ∼4-20 μM rage of $[CO_2]$, to capture the linear part of the response, representative of the $[CO_2]$ range ∼8-11 μM. *E. huxleyi* data from (Bach *et al.*, 2011; Iglesias-Rodriguez *et al.*, 2008; Langer *et al.*, 2009; Müller *et al.*, 2010; Sett *et al.*, 2014; Zondervan *et al.*, 2001) and (Riebesell *et al.*, 2000a), and *G. oceanica* data taken from (Rickaby *et al.*, 2010b; Sett *et al.*, 2014; Zondervan *et al.*, 2001) and (Riebesell *et al.*, 2000a)). Nb: The constant alkalinity *E. huxleyi* (15°C) data from (Bach *et al.*, 2011) is the same as that of (Sett *et al.*, 2014) so has been omitted.

Acclimation, adaptation or shifts in relative abundance

Phenotypic plasticity, as observed in laboratory experiments to date, cannot explain coccoliths becoming more calcified with [CO_2(aq)] and temperature. The downcore observations therefore suggest either a component of selection for more heavily calcifying forms, or that the parameter space, and thus phenotypic plasticity, has not been thoroughly explored in the laboratory. Selection may drive evolution of the population internally through differential suitability of forms to the environment, or through differential susceptibility to grazers or viral attacks (Raven & Crawfurd, 2012), or via propagation of differentially adapted forms introduced from elsewhere along gradients of nutrients, pH, salinity or temperature. Alternatively the apparent increase in size-normalised coccolith mass, within MG_{Geo} in particular, may be due to a transient increase in the relative abundance of established more highly calcifying pseudo-cryptic sub lineages (Beaufort *et al.*, 2011; de Vargas *et al.*, 2004). The increased mean-independent variance in size-normalised coccolith mass across TII may be the result of selection for different growth strategies, and/or differences in phenotypic plasticity across the population. As a substrate, low CO_2 concentrations may limit growth rate (Riebesell *et al.*, 1993), so increasing its concentration may allow for faster growth; but elevated CO_2 at constant alkalinity decreases the saturation state of calcite making it more energetically costly to calcify. Increases in pCO_2 also drive increases in temperature. To explain the increased variance over TII by the differential effect of phenotypic plasticity within the population superimposed on a

Figure 2.5 (following page): Fractional change in PIC:POC of natural heterogeneous populations over glacial terminations (left), compared with that of monoclonal strains subject to an equivalent CO_2 change in culture (right). A, The response of MG_{Emi} in nature is within the range of uncertainty and of plasticity of *E. huxleyi* observed in the laboratory. **B&C**, The PIC:POC of MG_{Geo} in nature increases across both terminations, which is opposite to the equivalent plastic response as inferred from culture manipulations in *G. oceanica*. Error bars represent the 1σ uncertainty, which for the down-core response, is calculated using the prediction interval of Eq.2.3. For culture results, details of the regressions are given in the supplementary material.

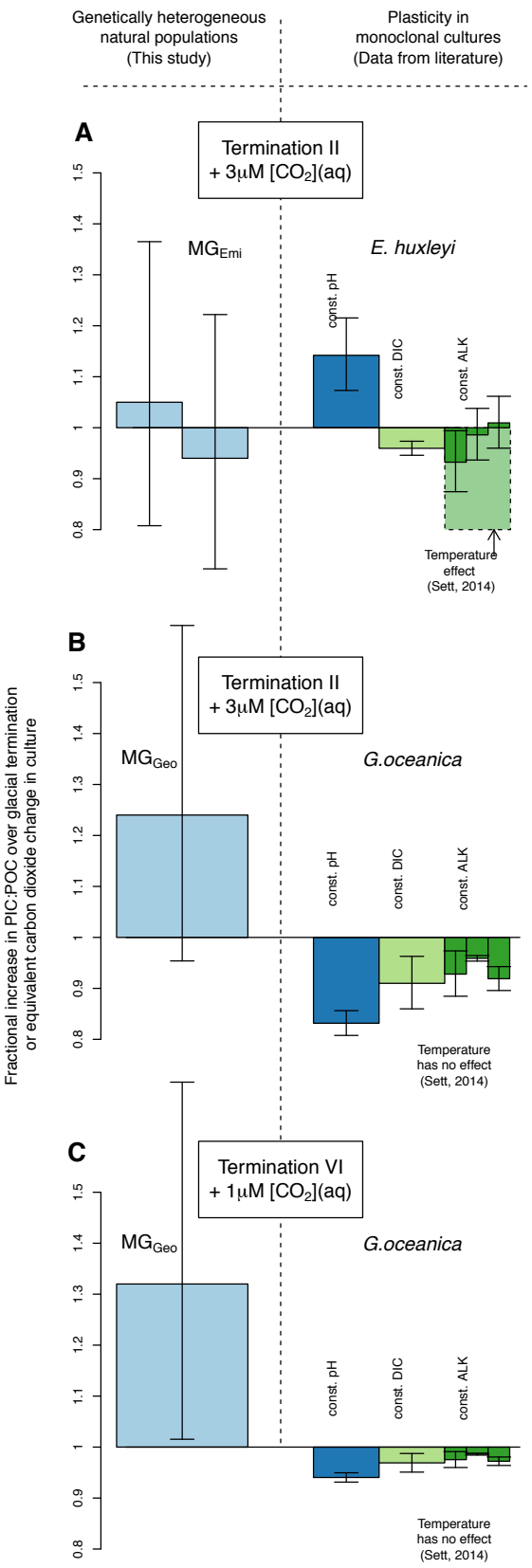
Genetically heterogeneous natural populations (This study)
Plasticity in monoclonal cultures (Data from literature)
A
Termination II
+ 3μM [CO2](aq)
MGEmi
E. huxleyi
const. pH
const. DIC
const. ALK
Temperature effect (Sett, 2014)
B
Termination II
+ 3μM [CO2](aq)
MGGeo
G.oceanica
const. pH
const. DIC
const. ALK
Temperature has no effect (Sett, 2014)
C
Termination VI
+ 1μM [CO2](aq)
MGGeo
G.oceanica
const. pH
const. DIC
const. ALK
Temperature has no effect (Sett, 2014)
Fractional increase in PIC:POC over glacial termination or equivalent carbon dioxide change in culture
0.8
0.9
1
1.1
1.2
1.3
1.4
1.5

general selection for more highly calcified forms, the more lightly calcifying forms would need to be more susceptible to a decreasing saturation state, but this is not observed in culture. If anything, the relatively heavily calcifying *G. oceanica* appears to exhibit a greater plastic decrease in size-normalised coccolith mass with increasing CO_2 than the relatively lightly calcifying *E. huxleyi*. Alternatively, increasing [CO_2(aq)] could conceivably create diverging niches; lightly calcifying forms could be selected on the basis of more efficient utilization of the CO_2 substrate, and highly calcifying forms could be selected on the basis of greater integrity of their calcitic (presumably defensive) structure. Whatever the mechanism, it is interesting to note that the size-normalised coccolith mass of the population is driven to a very narrow range during glacial times (Fig.2.3). If this observation does indeed reflect a narrow range of PIC:POC values, it may indicate that it is universally energetically favourable, at low temperature and [CO_2(aq)], to minimise the effect of biomass production on intracellular carbonate chemistry by maintaining a balance between the relative rate of photosynthesis to calcification (Fig.2.6).

2.4.3 Biogeochemical implications

From a biogeochemical viewpoint, calcification and photosynthesis alter the buffering capacity of water for CO_2 in opposing ways through their respective effects on [DIC] and [ALK]. These effects are relevant on scales ranging from the sub-cellular environment in coccolithophores to global biogeochemical cycles. In the sub-cellular environment, the ratio of calcification to photosynthesis determines the steady state drift in pH, that would otherwise occur if it were not counteracted by the active pumping of protons into or out of the cell (Fig.2.6). During blooms, coccolithophores constitute an instantaneous net sink or source of CO_2, or drive a change in pH, depending on their PIC:POC ratio (Fig.2.6). Under typical modern conditions, formation of biomass in the surface ocean with a PIC:POC of higher or lower than $\sim$1.86 constitutes respectively an instantaneous source or sink of CO_2 (Fig.2.6), with

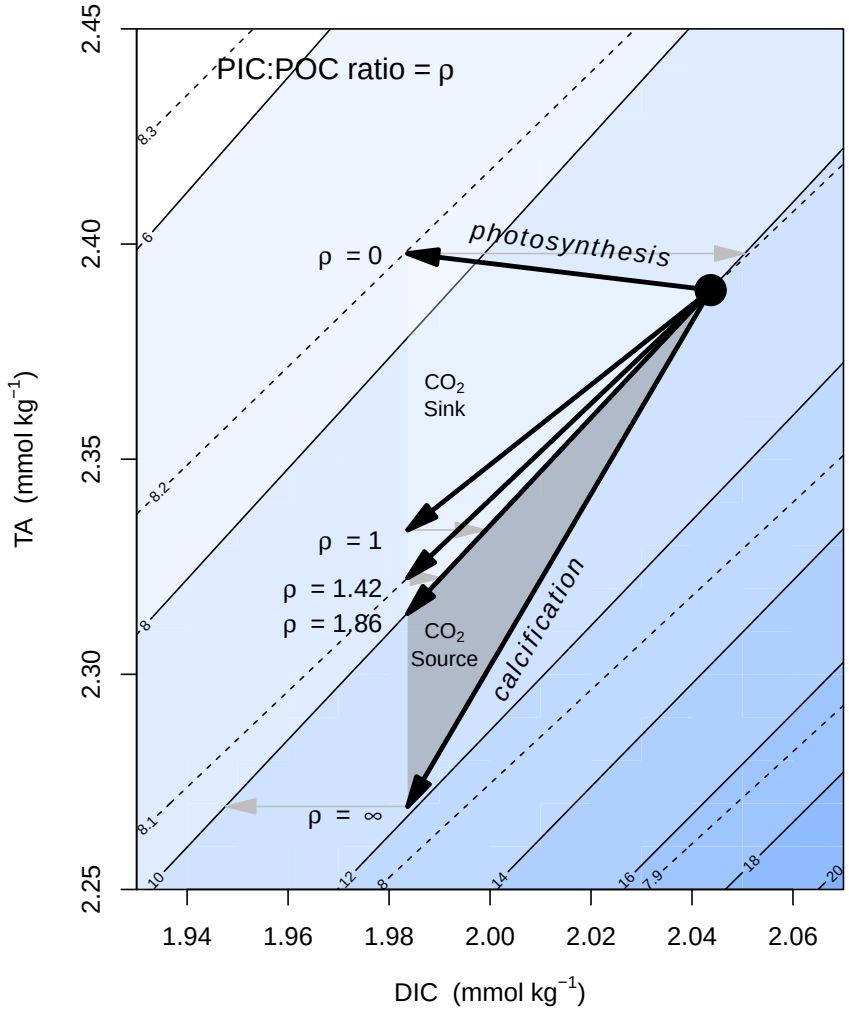

Figure 2.6: Instantaneous effect of biomass production on seawater carbonate chemistry as a function of PIC:POC (ρ). Solid line isocontours represent [CO_2] (μmol/kg), and dashed isocontours represent pH. Solid arrows represent the instantaneous effect of biogenic matter formation, and shaded arrows CO_2 exchange with an atmospheric carbon pool that is large relative to the perturbed sample of seawater. Depending on its ρ, biogenic material may form an instantaneous sink or source of CO_2. For conditions typical of the modern ocean, when ρ is $<$ or $>$ 1.42, pH initially increases or decreases respectively, and when ρ is $<$ or $>$ 1.86 [CO_2] initially decreases or increases respectively. These critical values depend on the carbonate chemistry of the surface ocean (Frankignoulle *et al.*, 1994). Photosynthesis (net photosynthesis = photosynthesis - respiration) removes one mole of DIC from surface ocean seawater and adds 15/106 moles of alkalinity (Zeebe & Wolf-Gladrow, 2001)) for each mole of POC produced. Calcification removes 1 mole of DIC and 2 moles of alkalinity for each mole of PIC produced. [TA] relative to [DIC] dictates the buffering capacity of the surface ocean for CO_2. [CO_2] and pH were calculated across DIC and TA values at salinity = 35, temperature = 25°C, assuming zero concentration of phosphate and silicate and zero hydrostatic pressure, and published values for the first and second dissociation constants of carbonic acid (Lueker *et al.*, 2000).

this critical value varying with the carbonate chemistry of the water. This effect is not permanent however; the effect of biomass production on surface ocean seawater chemistry is often transient due to respiration and remineralisation of organic matter, and dissolution of calcite causing cycling within the surface ocean. Carbon fluxes between the atmosphere and ocean are dominantly influenced by export of organic matter and calcite from the surface ocean. Export has a prolonged effect on surface ocean/atmosphere partitioning of CO_2 because DIC and ALK are sequestered in the deep ocean or sediments, which have residence times of respectively hundreds, and tens of thousands of years. In constituting up to half of the calcification in the surface ocean (Milliman, 1993), of which members of the family Noëlaerhabdaceae typically contributing on the order of half (Ziveri *et al.*, 2007), it is through their role in pumping calcite to depth that coccolithophores constitute a significant lever on the global climate system.

In the modern ocean, phytoplankton stock is a function of light, nutrients, grazing and viral lysis (Sarmiento & Gruber, 2013). The effect of predators and viruses cannot explain the current distribution of primary production in the surface ocean, which is dominated by nutrient availability (Moore *et al.*, 2013). In coccolithophores, the PIC:POC ratio describes the amount of calcite produced per unit organic matter. As organic matter production is finite and limited by the availability of biologically accessible nitrogen and iron, the PIC:POC ratio directly corresponds to the amount of calcite produced for a given standing stock or flux of ultimately limiting nutrients. In the absence of other changes, an increase in the PIC:POC ratio of coccolithophores in the surface ocean leads to an increase in ALK export, and thus a decrease in the buffering capacity of the surface ocean for CO_2. A confounding effect arises because cells are approximately the same density as water, and must be ballasted by heavy minerals, dominantly calcite, in the form of aggregates or faecal pellets in order to be efficiently exported from the surface ocean. In terms of the net effect on seawater carbonate chemistry in the surface ocean, export of calcite therefore constitutes a

trade-off between direct removal of calcite, and the effect this has on the efficiency of export of organic matter (Loubere *et al.*, 2007).

In the down-core record presented here, the size-normalised mass of coccoliths from coccolithophores belonging to the family Noëlaerhabdaceae, on average, calcify more under increasing $[CO_2](aq)$ and temperature. As shown through *in vivo* experimental results, this can be interpreted as a likely increase in coccolithophore PIC:POC. Although it is impossible to decouple the effects of temperature, $[CO_2(aq)]$, salinity and nutrient availability down-core, these parameters have varied together throughout geological time. On glacial-interglacial timescales therefore, to first order, coccolithophores may actually export relatively more ALK from the surface ocean and therefore decrease the surface ocean's buffering capacity for CO_2 when pCO_2 is high, thus constituting a positive feedback to increasing atmospheric CO_2 on millennial timescales.

2.5 Conclusions

I have shown that natural coccolithophore populations appear to adapt to rising $[CO_2]$ and temperature on a millennial timescale, dominantly via selection for an increased tendency to calcify. Thus, this work introduces a temporal dimension to the prevailing view based on the results of culture manipulation experiments. The theoretical model predicting this outcome describes a trade-off between fast growth and calcification (Irie *et al.*, 2010), confounding the implications for the total rate of calcite production in the surface ocean. I anticipate these results to be of use to biogeochemical modellers, but a more thorough understanding of the fate of biogenic material produced in the surface ocean is essential before the full implications of this work are realised.

Chapter 3

Towards an understanding of light stable isotopes in coccolithophores

3.1 Introduction

The scientific literature concerned with how single celled phytoplankton isotopically fractionate carbon during photosynthetic fixation into organic matter is rich and contentious. Recent years have seen a plethora of models pursuing a quantitative understanding of these processes (see Table. 3.1). The motivation for these models is in quantifying the relationship with the external carbon dioxide concentration, to find a proxy for pCO_{2atm} (Badger *et al.*, 2013a; Heureux & Rickaby, 2015; Hollander & McKenzie, 1991; Pagani, 2002; Pagani *et al.*, 2005, 2011; Seki *et al.*, 2010). And yet coccolithophores, which are responsible for producing alkenones - the most widely used organic molecule for estimating pCO_{2atm} via isotopic analysis - also use carbon for calcification; a process that has been almost completely ignored in isotopic flux models. In coccolithophores, photosynthetic carbon fixation and calcification are inextricably linked via intracellular fluxes (Buitenhuis *et al.*, 1999; Paasche, 1963; Sekino & Shiraiwa, 1994), with inevitable consequences for the isotopic composition of both organic matter and calcite. There has been a single attempt to address the isotopic implications of simultaneous intracellular calcite and organic matter formation in the form of a model (Bolton & Stoll, 2013). The work presented in this chapter uses laboratory culture manipulations and modelling to understand the interacting

isotopic effects of intracellular processes in coccolithophores. To establish the state of the literature it is most straightforward to start with models of organic carbon before extending the discussion to inorganic carbon, and then to an extensive consideration of how coccolithophores acquire carbon.

3.1.1 Carbon isotopes in organic matter

Ribulose-1,5-bisphosphate carboxylase/oxygenase (RuBisCO) is the enzyme responsible for catalysing the rate-limiting step of photosynthetic carbon fixation (Badger & Andrews, 1998). It has long been known that RuBisCO strongly discriminates against the heavy isotope of carbon (^{13}C), resulting in organic matter that is significantly lighter isotopically than the dissolved inorganic carbon substrate (Guy *et al.*, 1993; Tcherkez *et al.*, 2006). As more data becomes available, the magnitude of this fractionation appears to be much more variable across species than once thought (Boller *et al.*, 2015, 2011). The isotopic fractionation between the extracellular carbon source and the resultant organic matter (ϵ_p) is not simply the enzymatic fractionation associated with carbon fixation catalysed by RuBisCO (ϵ_f), because a number of parameters affect the isotopic composition of the carbon pool immediately in the vicinity of the enzyme (Laws *et al.*, 2001). Thirty years ago, the concept of "leakiness" (f) was introduced, defined as the fraction of carbon taken up by the cell that is lost back into the surrounding medium (Sharkey & Berry, 1985). When f is low, a large proportion of the carbon that enters the cell is ultimately fixed, and due to the strong isotopic fractionation by RuBisCO, the intracellular carbon pool, and thus also organic matter, becomes isotopically heavy (Farquhar, 1983; Farquhar *et al.*, 1982; Rau, 1996; Sharkey & Berry, 1985). If carbon is assumed to enter the cell in the form of CO_2 alone, the relationship between ϵ_p and f is linear (Francois *et al.*, 1993). Furthermore, if this carbon is assumed to move via passive diffusion into and out of the cell, there is a linear relationship between ϵ_p and the ratio of growth rate to [CO_2] ($\frac{\mu}{[CO_2]}$; Laws *et al.*, 1995; Rau, 1997). The gradient of this relationship is set by the cellular carbon

content and membrane permeability (Laws *et al.*, 2001) and the volume to surface area ratio (Popp *et al.*, 1998), all assumed to be constant. Following the realisation that the relationship between ϵ_p and $\frac{\mu}{[CO_2]}$ is not linear, came the inference of active CO_2 (Laws *et al.*, 1997) or active HCO_3^- (Keller & Morel, 1999) uptake at low [CO_2] or high growth rate. Since this early work, models have increasingly highlighted the importance of intracellular compartmentation (Cassar *et al.*, 2006; Hopkinson *et al.*, 2011; Schulz *et al.*, 2007), but only very recently have models explicitly included the compartment where calcification occurs in coccolithophores (Bolton & Stoll, 2013; Holtz *et al.*, 2014, 2015).

3.1.2 Carbon isotopes in coccolith calcite

The isotopic offset between biogenic calcite and inorganically precipitated calcite is termed the vital effect. Here we focus on carbon isotopes of calcite, but oxygen is discussed later (Section 3.3.7). There have been relatively few studies of carbon isotopes in coccolith calcite (see Hermoso, 2014, for a review), fewer still where experiments have been carried out *in vivo* under closely monitored conditions, and a single attempt to model the effect of external parameters quantitatively (Bolton & Stoll, 2013). Nevertheless, the taxonomically delimited "light" and "heavy" groups which precipitate calcite with a carbon isotopic composition that is respectively lighter and heavier than expected for inorganically precipitated calcite, are well established (Hermoso, 2014; Hermoso *et al.*, 2014; Ziveri *et al.*, 2003). The direction and magnitude of the vital effect correlates strongly with size (Bolton *et al.*, 2012), growth rate, and calcification to photosynthesis ratio (Hermoso, 2014). These parameters are covarying across species however, and so cannot be decoupled without an explicit mechanistic understanding and a quantitative model. *C. pelagicus* and *C. leptoporus*, are large, heavily calcifying, have a relatively slow division rate and belong to the light group. Contrastingly, *E. huxleyi* is very small, lightly calcifying, has a rapid division rate and belongs to the heavy group. *G. oceanica* which exhibits intermediate parameter

values, precipitates calcite with approximately the same isotopic composition as abiogenic calcite (Hermoso, 2014; Rickaby *et al.*, 2010a; Ziveri *et al.*, 2003). In nature, large coccoliths (reflecting large cells; Henderiks, 2008) are consistently isotopically lighter in carbon than small coccoliths in modern ocean sediments (Fink *et al.*, 2010) and in fossils (e.g. Bolton & Stoll, 2013; Bolton *et al.*, 2012). The magnitude of the vital effect decreases with increasing [DIC] (Rickaby *et al.*, 2010a), and also with increasing $\delta^{18}O_{medium}$ (Hermoso *et al.*, 2014). Bolton & Stoll (2013) modelled carbon isotopic fluxes in coccolithophores based on published data (Rickaby *et al.*, 2010a), concluding that HCO_3^- is pumped into the chloroplast at low CO_2 at the expense of moving HCO_3^- to the coccolith vesicle, leaving the cytosolic pool isotopically light in carbon. This effect was shown to be greater in large cells, due to a greater carbon requirement in the chloroplast, thereby providing an explanation of the vital effect, although why *E. huxleyi* is heavier than expected is not discussed. Hermoso (2014) by contrast suggested that photosynthetic carbon fixation leaves the intracellular pool isotopically heavy in carbon, resulting in forms that photosynthesise more producing heavier calcite. Despite historically frustrating paleoceanographers, the fact that the vital effect in coccolith calcite is a function of multiple external parameters, does in fact present a unique opportunity for proxy development (e.g. Bolton & Stoll, 2013; Bolton *et al.*, 2012).

3.1.3 CCMs in coccolithophores

RuBisCO has a low affinity, catalytic turnover and specificity, for its substrate, CO_2 (Badger & Andrews, 1998; Tcherkez *et al.*, 2006). In the modern ocean, the uncatalysed reacto-diffusive supply rate of CO_2 alone to the surface of algal cells larger than a few microns is not high enough to account for the observed rates of photosynthesis (Falkowski & Raven, 2013; Riebesell *et al.*, 1993). Modern algae have evolved to cope with decreasing CO_2 concentrations, both through adaptations manifest at the level of the RuBisCO enzyme itself (Tcherkez *et al.*, 2006; Young *et al.*, 2012), and through

Table 3.1: Significant recent works modelling isotopes in phytoplankton

Study	Model set-up and assumptions	Conclusions
Holtz *et al.*, 2014, 2015 (*E. huxleyi*)	– 4 compartments (PY, CP, CV, CY)[1] – Carbonate chemistry consists of HCO_3^-, CO_3^{2-}, CO_2 and H^+. – Hypothesised Ca^{2+}/HCO_3^- CY-to-CV transporter coupled to an H^+ATPase, with no leakage of HCO_3^- from CV. – Hypothesised up regulation of HCO_3^- down-gradient flux into cell with decreased [CO_2] in PY. – Passive CO_2 and HCO_3^- fluxes. No HCO_3^- flux from CP to PY. – CA assumed in CP and PY but not in CY and CV – Isotope model consists of 2 compartments (CY and CP) and does not consider isotopes of calcite. – Membrane permeabilities to CO_2 and HCO_3^- assumed, but highly heterogeneous; different for all compartments.	– HCO_3^- is used at low [CO_2] – Intracellular pH gradients allow concentration of CO_2 around RuBisCO without up-gradient movement of carbon. – pHs: PY = 5.0, CY = 7.0, CP = 8.0, CV = 8.3-8.6 – A net efflux of CO_2 is not necessary to remove δ^{13}C from cell
Bolton & Stoll, 2013 (Coccolithophores)	– 3 compartments (CP, CV, CY) – Carbonate chemistry consists of HCO_3^- and CO_2. – HCO_3^- fluxes are all active and independent of [HCO_3^-] – Passive CO_2 fluxes. – Membrane permeabilities and CA activities assumed (from Hopkinson *et al.*, 2011). – ϵ_f assumed (-27‰).	– HCO_3^- active transport to CP increases at low [CO_2], at the expense of HCO_3^- transport to CV – This effect is greatest in large cells. – Difference in vital effects ($\delta^{13}C_{cal}$-$\delta^{13}C_{\ medium}$) between small and large cells greatest at low [CO_2]
Hopkinson *et al.*, 2011 (Diatoms)	– 1, 2, & 3 compartments (PY, CP, CY) – Carbonate chemistry consists of HCO_3^- and CO_2. – Used ^{18}O labelled DIC to track temporal evolution of carbonate system. – Passive CO_2 fluxes. – Passive and active HCO_3^- fluxes. – ϵ_f assumed (-29‰).	– Membranes are highly permeable to CO_2 (1.5×10^{-4} - 5.6×10^{-4} m/s) – Membranes are highly impermeable to HCO_3^- (2.5×10^{-8} - 2.9×10^{-7} m/s) – $\delta^{13}C_{org}$ is a function of passive diffusion of CO_2, active movement of HCO_3^-, kinetic fractionation factors associated with CA-catalysed hydration and dehydration, and the kinetic isotopic fractionation associated with RuBisCO.
Schulz *et al.*, 2007 (*E. huxleyi*)	– 2 compartments (CP, CY) – Carbonate chemistry consists of HCO_3^- and CO_2. – Active uptake of HCO_3^- and CO_2 independent of concentration – Passive CO_2 fluxes (membrane permeability to CO_2 = 1.8×10^{-5} (from Sültemeyer & Rinast, 1996, - green algae)) – No efflux of HCO_3^- – ϵ_f assumed (-29‰).	– CCM relies upon active (ATP driven) uptake of CO_2 and HCO_3^- – Reduction in ϵ_p with increased HCO_3^- uptake into CP – ϵ_p is larger when there is a greater degree of intracellular carbon leakage from the chloroplast.
Cassar *et al.*, 2006 (Diatom - *Phaeodactylum tricornutum*)	– 2 compartments – Active and diffusive uptake of CO_2 – No HCO_3^- uptake – ϵ_f assumed (-27‰). – Inferred fluxes based on an energy minimisation approach.	– ϵ_p is not a unique function of $\frac{\mu}{CO_2}$ – ϵ_p depends on leakiness of CP
Keller & Morel, 1999 (General phytoplankton)	– 1 compartment – No HCO_3^- diffusion or efflux – Active HCO_3^- uptake scales with growth rate – ϵ_f assumed.	– Downward curvature of ϵ_p against $\frac{\mu}{CO_2}$ is consistent with active HCO_3^- uptake (contrary to Laws *et al.*, 1997) – ϵ_p is a poor indicator of carbon substrate

evolving carbon concentrating mechanisms (CCMs) for elevating the concentration of CO_2 in the vicinity of RuBisCO (Badger & Andrews, 1998). In general, CCMs can involve any mechanism for artificially concentrating carbon around RuBisCO in order to favour carboxylation over oxygenation, which includes, but is not exclusive to: bicarbonate transport proteins, carbonic anhydrases and proton pumps. Bicarbonate transport proteins facilitate, or drive, the down-gradient transport of bicarbonate ions across otherwise impermeable membranes. Carbonic anhydrases (CAs) are metalloenzymes that catalyse the hydration and dehydration of CO_2 and HCO_3^- respectively, decreasing the time required to reach equilibrium by many orders of magnitude, but not affecting the position of equilibrium. Proton pumps maintain optimum pH, or create pH gradients inside the cell, thus changing the equilibrium ratios of dissolved carbon species and inducing controlled passive diffusion. Another means of increasing photosynthetic rate at a given external CO_2 concentration, though not strictly a CCM, is an up regulation of RuBisCO production (Raven *et al.*, 2014). In most of the early models, passive diffusion of CO_2 has been assumed to be the sole external source of carbon to unicellular photosynthesising algae, but this assumption needs updating for coccolithophores in light of the recent literature.

Carbon dioxide is a small and neutral molecule, and moves passively across membranes by aquaporin-based diffusion. Estimates of membrane permeabilities for diatoms and other closely related unicellular algae suggest they constitute a minimal barrier to CO_2 diffusion (Hopkinson *et al.*, 2011), although membrane permeabilities to CO_2 have not been measured directly in coccolithophores. Due to the low permeability of cellular membranes to charged chemical species, appreciable bicarbonate uptake requires facilitation by transporter proteins. The most likely proteins responsible for bicarbonate uptake in coccolithophores are the solute carrier 4 (SLC4) family of proteins, which facilitate down-gradient Cl^- / HCO_3^- exchange, or Na^+ / HCO_3^- cotransport. In *E. huxleyi*, there is strong evidence to suggest that an SLC4 anion exchange protein facilitates transmembrane passage of HCO_3^- ions, as evidenced

through the effect of an inhibitor on DIC uptake (Herfort *et al.*, 2002), and through the presence of an SLC4 homologue in the transcriptome of *E. huxleyi* (Mackinder *et al.*, 2011; von Dassow *et al.*, 2009). In coccolithophore isotope flux models, the evolving consensus is that HCO_3^- forms a larger fraction of the carbon entering the cell at low [CO_2] (Bolton & Stoll, 2013; Holtz *et al.*, 2014, 2015; Schulz *et al.*, 2007), a conclusion supported by a transcriptional up-regulation of a putative anion exchanger protein at low [DIC] in *E. huxleyi* (Bach *et al.*, 2013), and directly measured CO_2 and HCO_3^- uptake rates in *E. huxleyi* (Kottmeier *et al.*, 2014; Rost *et al.*, 2003, 2002). These conclusions are also consistent with earlier work showing that in *G. oceanica* and *C. pelagicus*, DIC uptake is dramatically decreased in the presence of an inhibitor of anion exchange mechanisms (Nimer *et al.*, 1997). I am aware of no genomic, transcriptomic or proteomic evidence to date of putative transmembrane ATP-driven bicarbonate transporters in this group of organisms. The presence of extra-cellular CA (CA_e) activity is less clear (Mackinder *et al.*, 2010). Despite early reports that *E. huxleyi* lacks CA_e (Rost *et al.*, 2003), recent work is in favour of the presence (Richier *et al.*, 2009) and possibly upregulation of CA_e at low [CO_2] (Bach *et al.*, 2013; Richier *et al.*, 2011). Nimer *et al.* (1997) showed that CA_e was not detected in either *G. oceanica* nor *C. pelagicus*, even when cells were carbon limited, but this view may similarly change as more experimental and molecular work is conducted on coccolithophore species other than *E. huxleyi*. Calcite precipitation from DIC causes a decrease in pH (see Chapter 2), which in the coccolith vesicle must be counteracted by the removal or consumption of protons, or of CO_2, to maintain optimum conditions for calcification to occur (Mackinder *et al.*, 2010). It has been proposed that this CO_2 surplus may form a CCM and contribute a physiological benefit to the cell (Buitenhuis *et al.*, 1999; Paasche, 1963), however rates of calcification and photosynthesis appear not to be linked (Leonardos *et al.*, 2009; Trimborn *et al.*, 2007). In many organisms, H^+ATPases actively pump protons between organnelles, and across the cellular membrane (Taylor *et al.*, 2012). It appears that coccolithophores have

acquired a novel voltage-gated H^+ channel, which allows intracellular pH homeostasis to be maintained when the H+ electrochemical gradient is sufficient (Taylor *et al.*, 2011).

3.2 Culture manipulation experiments

In this study, the aim is to glean greater insight into what isotopes preserved in fossil material can tell us about the geological past. To this end I used culture manipulation experiments to probe the physiological response and implications for the isotopic composition of biogenic material in three species of coccolithophore. Across all experiments, pH was held constant whilst DIC was varied. These experimental conditions are somewhat analogous to seawater chemistry changes on geological timescales, whereby changes in pH are largely buffered by interaction with carbonate sediments (Ridgwell & Zeebe, 2005). This is in contrast to the ocean's response to CO_2 invasion on anthropogenic timescales, whereby the invasion is too fast to be buffered, and the result is a decrease in pH following an increase in DIC at approximately constant alkalinity (Fig.3.1). For these experiments, strains were provided by Ian Probert from the culture collection of the Station Biologique de Roscoff.

3.2.1 Methods

Three sets of experiments investigating the isotopic consequences of varying [DIC] at constant pH contributed to the dataset presented here. Datasets are designated a code according to the person who conducted the experiments. HM: Harry McClelland - two strains of *E. huxleyi* and two strains of *G. oceanica*, grown at 4 different DIC concentrations; MH: Michaël Hermoso - one strain of *G. oceanica*, grown at 14 different DIC concentrations; IC: Ian Chan[2] - one strain of *E. huxleyi* and one strain of *C. pelagicus* each grown at 6 different DIC concentrations. The protocols followed

[2]Ian Chan was a 4th year undergraduate masters student cosupervised by MH and HM in academic year 2013/2014

Carbon isotopic composition is quoted as a per mil (‰) deviation from a standard:

$$\delta^{13}C_{sample} = 1000 \times \frac{R_{sample} - R_{standard}}{R_{standard}}, \tag{3.1}$$

where $\delta^{13}C_{sample}$ is referred to as the isotopic composition of the sample, and

$$R = \frac{[^{13}C]}{[^{12}C]}, \tag{3.2}$$

where $[^{13}C]$ = the concentration of the rarer heavy isotope of carbon, and of mass 13, $[^{12}C]$ = the concentration of the common isotope of carbon, and of mass 12.
Similarly, $\delta^{18}O$ is a standardised means of describing the ratio of the heavy, rare isotope, ^{18}O to the lighter common isotope, ^{16}O. Unless otherwise noted, both carbon and oxygen isotopic compositions are quoted relative to the Vienna Pee Dee Belemnite standard (VPDB).
Differences in stable isotopic ratios of sources (S) and products (P) are given by the absolute fractionation factor (α_{P-S}):

$$\alpha_{P-S} = \frac{R_P}{R_S} = \frac{1000 + \delta^{13}C_P}{1000 + \delta^{13}C_S}. \tag{3.3}$$

At values close to unity, as is usual, α_{P-S} more helpfully represented by the per mil fractionation (ϵ_{P-S}):

$$\epsilon_{P-S} = (\alpha_{P-S} - 1) \times 1000 \approx \delta^{13}C_P - \delta^{13}C_S = \Delta_{P-S}, \tag{3.4}$$

where Δ is an approximation for ϵ, valid when α is close to unity. As the fractionation factors dealt with in the thesis are very small, Δ and ϵ will be interchangeably used to refer to the permil fractionation.

Box 3.1: Notation used for isotopes

for manipulation experiments in culture are described in Chapter 2, with the single exception that the experiments conducted by MH and IC used aged natural seawater (from the Marine Biological Association, Plymouth) rather than artificial seawater.

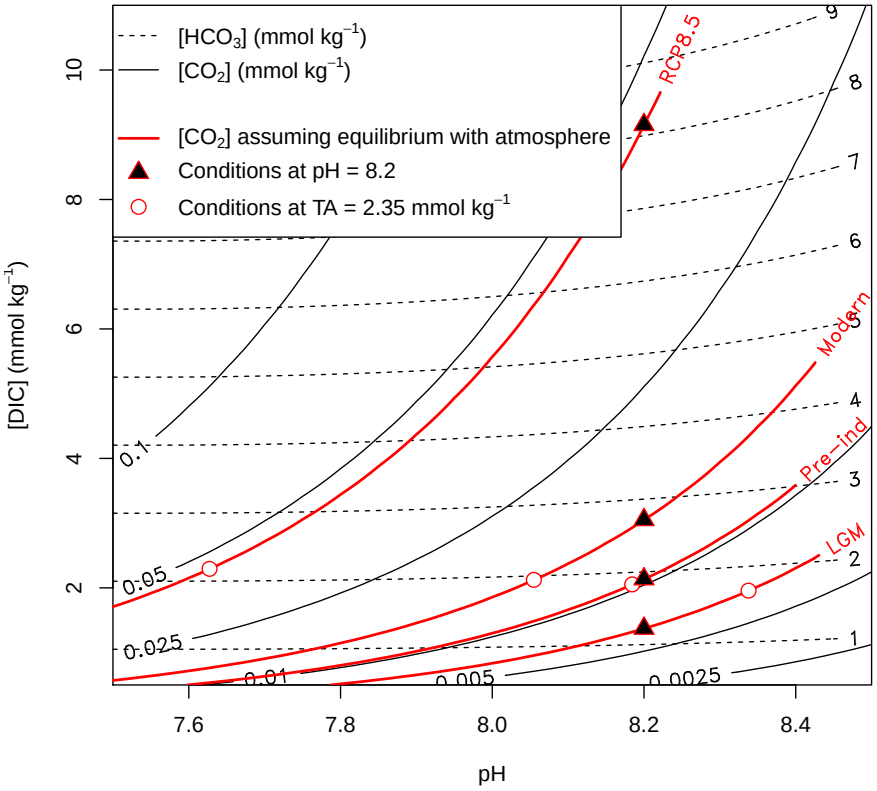

Figure 3.1: Carbonate chemistry conditions across experiments. Red lines represent equilibrium with the atmosphere at pCO_{2atm} values typical of glacial (LGM), interglacial (Pre-Ind) and modern atmospheres, and an extreme future emissions scenario (RCP8.5) IPCC (2014). In these experiments, DIC was varied at a constant pH of 8.2 (black triangles). The carbonate chemistry variation for the same four [CO_2] levels, but assuming constant alkalinity (TA) is also highlighted (white dots). In reality, the carbonate chemistry of the surface ocean in equilibrium with each of these pCO_{2atm} values would lie on the red line between the black triangle and the white dot, with the position determined by the rate of change and extent of interaction with carbonate sediments

Carbon and oxygen isotopic compositions of calcite were measured in Oxford using a VG Isogas Prism II mass spectrometer with an on-line VG Isocarb common acid bath preparation system. Samples were first rinsed with neutralised deionised water

to remove any salt. Samples were then dosed with acetone and dried at 60°C for at least 30 minutes. In the instrument they were reacted with purified phosphoric acid at 90°C. Calibration to PDB standard was via the international standard NBS-19 using the Oxford in-house (NOCZ) Carrara marble standard. Reproducibility of replicated standards was better than 0.1‰ (1σ) for δ^{13}C and δ^{18}O expressed relative to the V-PDB standard. Carbon isotopic composition of organic material was measured on an automated carbon and nitrogen elemental analyzer (Carlo Erba EA1108) at the Research Laboratory for Archaeology and the History of Art at the University of Oxford. Samples were decalcified with HCl, and rinsed with MilliQ water at least 3 times before being weighed into tin capsules. The internal alanine standard reproducibility is approximately 0.16‰ expressed relative to the V-PDB standard.

3.2.2 Results

The culture results show that the variation in vital effects, and the fractionation of carbon into organic matter, is species specific and is a function of [DIC], with the most extreme differences at low [DIC], and interspecific differences at a minimum at high [DIC] (Fig. 3.2). *E. huxleyi*, is the smallest species studied with coccospheres $\sim$ 2.5-3 μm in radius, *G. oceanica* the second smallest with coccospheres $\sim$ 4 μm in radius and *C. pelagicus* is the largest with coccosphere radii of $\sim$ 8-10 μm. Growth rates (μ; divisions per day) in *E. huxleyi* and *G. oceanica* are all around 1 division per day with little change over different [DIC] concentrations. The division rate of *C. pelagicus* meanwhile was found to decrease strongly from $\sim$0.8 to $\sim$ 0.3 divisions per day with increasing [DIC].

Isotopically, *E. huxleyi* produces calcite with the heaviest δ^{13}C at low DIC ($\sim$ 2‰ heavier than DIC), which becomes lighter with increasing DIC. *C.pelagicus* precipitates calcite with the lightest δ^{13}C at low DIC ($\sim$ 1.5‰ lighter than DIC), which becomes heavier with increasing DIC. The calcite produced by *G. oceanica* is closer to that of DIC than both *E. huxleyi* and *C. pelagicus* over most of the DIC range,

but tails off to very light values at very low DIC. *E. huxleyi* and *C. pelagicus* were not grown at such low DIC concentrations. At high DIC, the calcite produced by all three species tends towards a value of $\sim \delta^{13}\mathrm{C}_{DIC} + 1‰$, which is approximately the composition expected if the calcite were precipitated inorganically (Zeebe & Wolf-Gladrow, 2001). The calcite carbon isotopes show a similar species-specific direction and magnitude of offset from equilibrium as found by other authors for *G. oceanica* and *C. pelagicus* (Rickaby *et al.*, 2010a; Ziveri *et al.*, 2003), but this is the first time that this [DIC]-dependent trend from heavy values in *E. huxleyi* has been observed. $\delta^{13}\mathrm{C}_{org}$ in all three species is lightest when DIC is high, and becomes around 2 - 3 ‰ heavier at low DIC (Fig. 3.2). The effect of decreasing DIC is greatest, and $\delta^{13}\mathrm{C}_{org}$ is heaviest, in the larger cells. The trend of *G. oceanica* from the present study is in disagreement with that of Rickaby *et al.* (2010a), but is consistent with almost all results from the literature, in coccolithophores and across other single celled algae (e.g. Laws *et al.*, 1995; Popp *et al.*, 1998).

Figure 3.2 (following page): Results from culture manipulation experiments, testing the physiological and isotopic response of coccolithophores to varying [DIC] at constant pH, temperature, nutrients and light intensity. **A:** Carbon isotopic composition of coccolith calcite relative to DIC,**B:** Carbon isotopic composition of organic matter relative to DIC, **C:** Growth rate (μ), defined as average number of cellular binary divisions per day, **D:** Oxygen isotopic composition of coccolith calcite relative to DIC, **E:** Coccosphere radius.

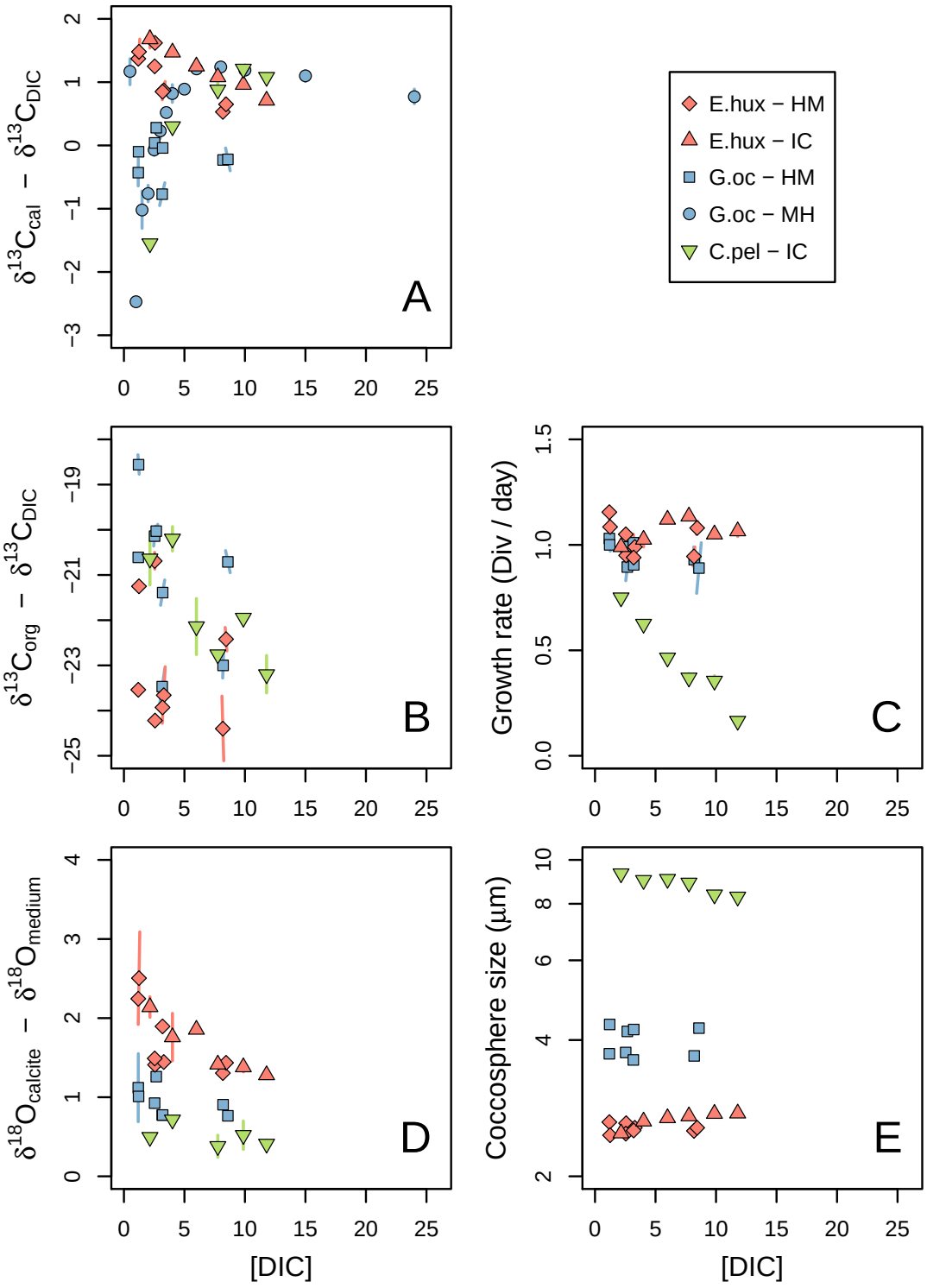
E.hux − HM
E.hux − IC
G.oc − HM
G.oc − MH
C.pel − IC
A
B
C
D
E
δ13Ccal − δ13CDIC
δ13Corg − δ13CDIC
Growth rate (Div / day)
δ18Ocalcite − δ18Omedium
Coccosphere size (µm)
[DIC]
[DIC]

3.3 Model[3]

To understand the dependence of vital effects, and the isotopic fractionation of carbon into organic matter, on [DIC], pH, growth rate, cell size, and various other parameters, I have constructed an isotope flux model. For isotope notation used see Box.3.1 on p.53.

3.3.1 Set-up

The coccolithophore cell is assumed to consist of three compartments: the chloroplast, where carbon fixation occurs in the presence of the enzymatic catalyst, RuBisCO, the coccolith vesicle, where calcification occurs, and the cytosol. The chloroplast and the coccolith vesicle are each in contact with the cytosol alone, and the cytosol is in contact with the external medium (Fig. 3.3). DIC species are taken up into the cell in different proportions, as a function of chemical-species-specific membrane permeabilities, cellular surface area, [DIC], pH and the state of chemical disequilibrium. The isotopic composition of biogenic matter in coccolithophores is controlled by a number of inter-dependent factors including the equilibrium and kinetic characteristics of the DIC system (Section 1.2.2; Fig. 3.4). Kinetic isotopic fractionation factors of internal reactions of the carbonate system dictate the equilibrium isotopic fractionation between DIC species, and reaction rate constants the equilibration time of the system, in each compartment. The rate of interconversion of DIC species is a strong function of pH, and the presence of the enzyme carbonic anhydrase (see Fig. 3.4). Carbon dioxide (CO_2) is the substrate for photosynthesis, and bicarbonate (HCO_3^-) is assumed to be the substrate for calcification, which is justified at the rates considered here (Zeebe & Wolf-Gladrow, 2001). Each of these processes have an associated isotopic fractionation factor. As carbonate ions (CO_3^{2-}) are assumed to not traverse membranes, and HCO_3^- is the only sink or source of CO_3^{2-}, the assumption of steady state

[3]Modelling was undertaken partially in collaboration with Jorn Bruggeman of the Plymouth Marine Laboratory.

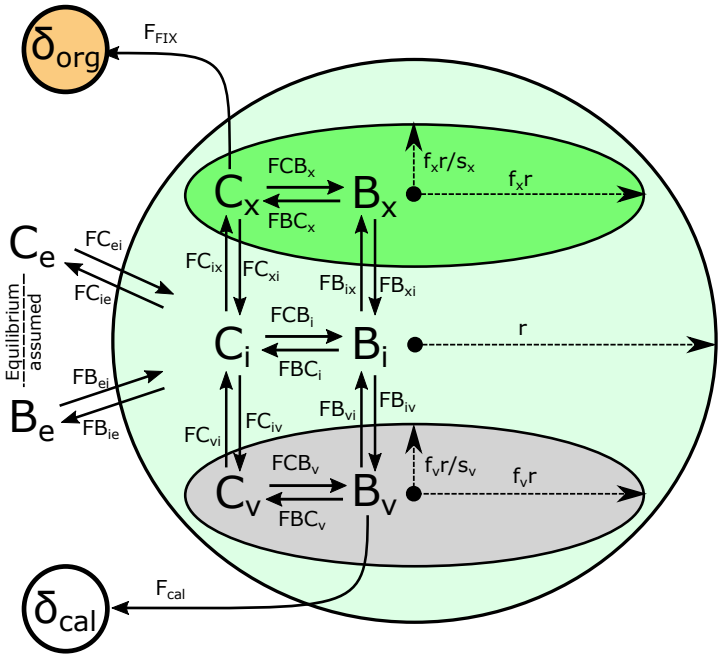

Figure 3.3: Cellular compartmental configuration and fluxes as modelled. See Table 3.2 for nomenclature. Chemical and isotopic equilibrium is assumed in the external medium, but neither is assumed inside the cell. NB: subscript *cell* refers to outer cell membrane, whilst subscript *i* refers to cytosol. $V_i = V_{cell} - V_x - V_v$

Table 3.2: General nomenclature

Symbol	Description	Units
C, B	Carbon species: Carbon dioxide (CO_2) and Bicarbonate (HCO_3^-)	NA
e, i, x and v	Compartments: External, cytosol, choroplast and coccolith vesicle respectively	NA
$F\Theta_{ab}$	Flux of carbon species, Θ, from compartment a to compartment b	$molC\,s^{-1}$
$F\Theta\Phi_a$	Rate of conversion of carbon species, Θ, to carbon species, Φ, in compartment a	$molC\,s^{-1}$
Θ_a	Concentration of carbon species, Θ, in compartment a	$mol\,m^{-3}$
$P_{\Theta a}$	Permeability of compartment a membrane to carbon species Θ	$m\,s^{-1}$
V_a, SA_a	Volume and Surface Area of compartment, a	m^3, m^2
f_a, s_a	Scale and shape factor of compartment a, for inferring V_a and SA_a (see section 3.3.3.3)	$[Dimensionless]$

means that CO_3^{2-} does not feature in the following calculations. This model employs values taken from the literature, but leaves a few universal parameters (membrane permeability, and enzymatic isotopic fractionation by RuBisCO) which are otherwise poorly constrained in coccolithophores, to be fitted to the data across all species. In the absence of of species-specific empirical measurements of membrane permeability, a single value is used across all species.

Figure 3.4 (following page): Carbonate chemistry and isotopes Effects of pH on: **A:** Equilibrium concentrations of CO_2 and HCO_3^- (as a fraction of total DIC), **B:** Equilibrium isotopic compositions of CO_2 and HCO_3^- (Relative to DIC), **C:** Reaction rates within DIC system. Hydration, hydroxylation and CA-catalysed hydration in blue (dashed), red and grey respectively, and total rate of conversion of CO_2 to HCO_3^- in black (dashed), at different CA concentrations. **D:** Net pH-dependent kinetic fractionation factors for conversion of CO_2 to HCO_3^- (CB; red) and of HCO_3^- to CO_2 (BC; blue, dashed), at the same CA concentrations as (C). Plotted for context, Hopkinson *et al.* (2011) deduced intracellular CA activities which correspond to a concentration of $\sim$ 0.1 mM assuming a specific activity of CA of 2.7×10^7 s^{-1} (Uchikawa & Zeebe, 2012). Hydration and hydroxylation reactions are unimportant when CA concentrations are greater than $\sim$ 1 μM. Above this, as long as the substrate concentration is well below the half saturation concentration of CA, the rate of CA-catalysed hydration/dehydration scales linearly with the concentration of CA (see section 3.3.3.4).

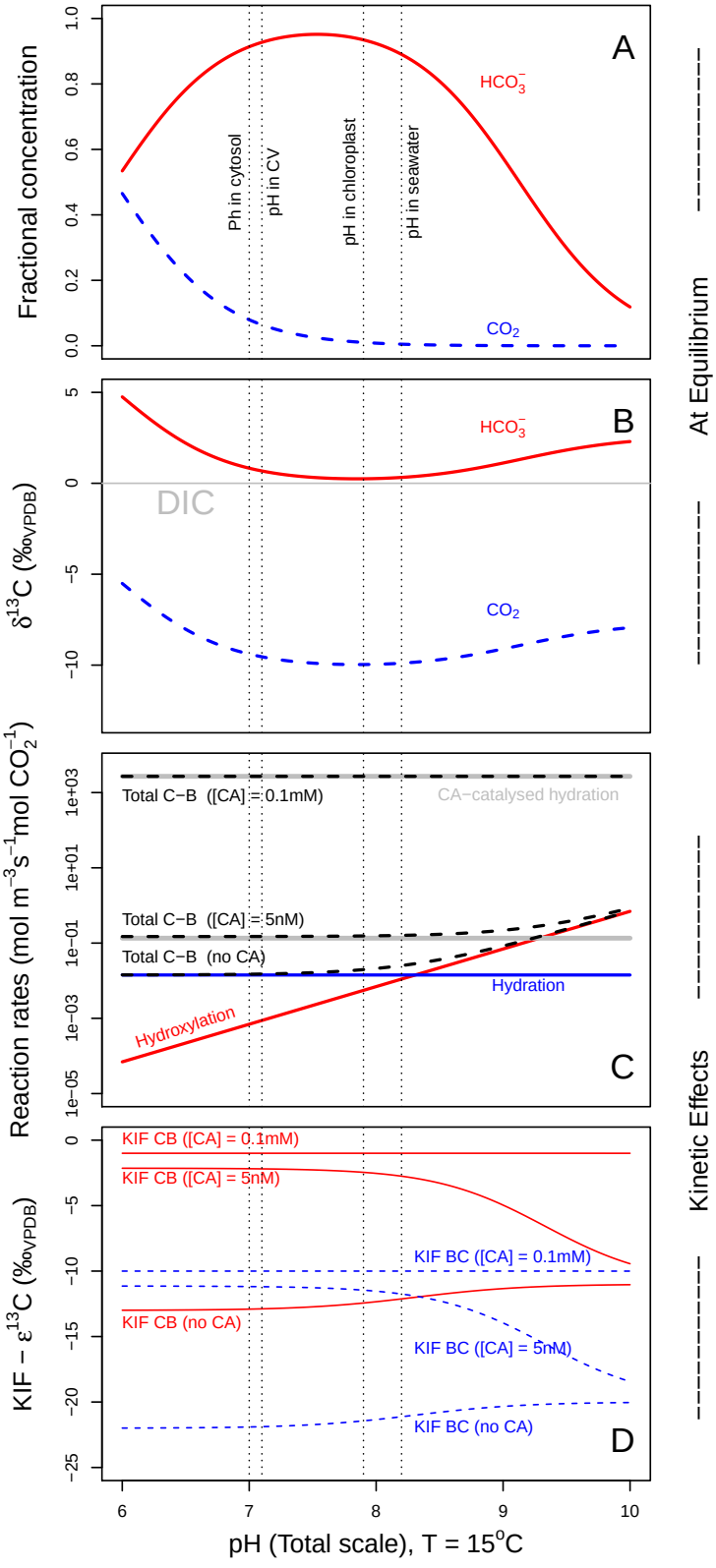
A
B
C
D
Fractional concentration
$\delta^{13}C$ (‰$_{VPDB}$)
Reaction rates (mol m^{-3}s^{-1}mol CO$_2^{-1}$)
KIF – $\varepsilon^{13}C$ (‰$_{VPDB}$)
pH (Total scale), T = 15°C
Ph in cytosol
pH in CV
pH in chloroplast
pH in seawater
HCO_3^-
CO_2
DIC
Total C−B ([CA] = 0.1mM)
CA−catalysed hydration
Total C−B ([CA] = 5nM)
Total C−B (no CA)
Hydration
Hydroxylation
KIF CB ([CA] = 0.1mM)
KIF CB ([CA] = 5nM)
KIF CB (no CA)
KIF BC ([CA] = 0.1mM)
KIF BC ([CA] = 5nM)
KIF BC (no CA)
At Equilibrium
Kinetic Effects

3.3.1.1 Membrane permeabilities

Bach *et al.* (2013) observed an up-regulation of a putative bicarbonate anion exchanger at low CO_2. Here the results of Bach *et al.* (2013) are interpreted as consistent with an approximately linear increase in transcript abundance with the degree of carbon utilisation (Fig.3.5). This physiological result is assumed to reflect an increase in synthesis of anion exchanger proteins. Although HCO_3^- passage through membranes facilitated by anion exchange proteins may be driven by inverse gradients of other ions, it is here assumed that the movement of HCO_3^- through a membrane in either direction is proportional to its concentration on the proximal side of the membrane. This assumption is justified if the gradient of the co-ported ion across the membrane is relatively small. The up-regulation of anion exchanger proteins therefore increases the gradient-following movement of HCO_3^- ions across the membrane, and in this implementation is parameterised as the effective permeability of the membranes to HCO_3^-. This assumption is more coherent with the current biological literature than equivalent assumptions of previous models, including concentration-independent implicitly ATP-driven active uptake of HCO_3^-, assumed by Keller & Morel (1999) to scale with growth rate, or by Bolton & Stoll (2013) to be independent of all other parameters.

In this model, the permeability of membranes to CO_2 (P_{Ccell}) is assumed to be constant. The permeability of membranes to HCO_3^- (P_{Bcell}) is assumed to increase linearly with utilisation of background (i.e. before up regulation of anion exchange proteins) carbon supply (U_0), which is defined as:

$$U_0 = \frac{F_{FIX} + F_{CAL}}{C_{in0}}. \tag{3.5}$$

where C_{in0} is the net carbon supply when membrane permeabilities to CO_2 and to HCO_3^- are at their background values, and $F_{FIX} + F_{CAL}$ is the rate of fixation of

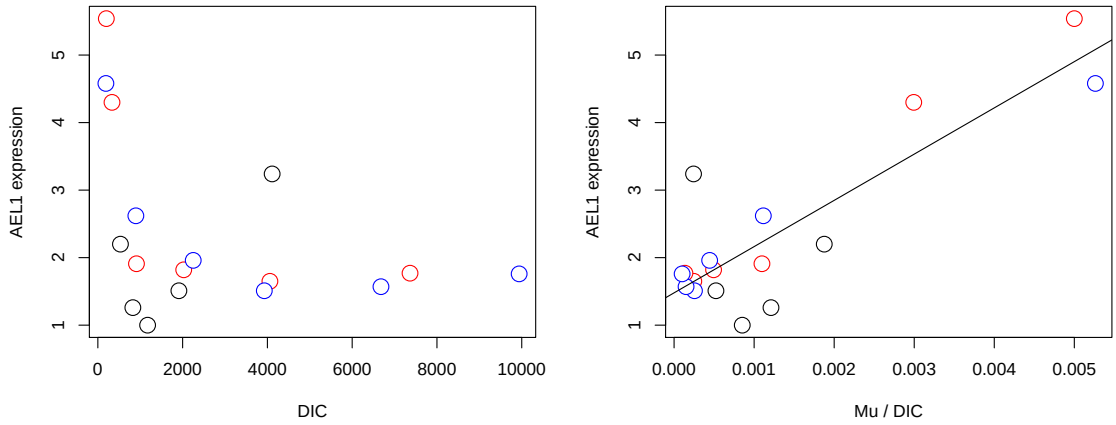

Figure 3.5: Interpretation of the data of Bach *et al.* (2013). **Left:** Transcript abundance of the AEL1 facilitative bicarbonate anion exchanger protein against [DIC]. **Right:** As left but plotted against (growth rate / [DIC]) which at constant cell size, carbon density and membrane permeability is approximately proportional to utilisation.

carbon into organic and inorganic matter. The membrane permeability to bicarbonate is therefore:

$$P_{Bcell} = T_0 + T_U U_0 \tag{3.6}$$

$$= T_0 + T_U \frac{F_{FIX} + F_{CAL}}{([CO_2]_{ex} P_{Ccell} + [HCO_3^-]_{ex} T_0) SA_{cell}}, \tag{3.7}$$

where T_0 is the base-level membrane permeability to HCO_3^- and T_U is the gradient of the increase in membrane permeability to HCO_3^- with increasing utilisation; F_{FIX} and F_{CAL} are the rates of carbon fixation and calcification respectively, $[CO_2]_{ex}$ and $[HCO_3^-]_{ex}$ are the concentrations of CO_2 and HCO_3^- in the ambient medium respectively, and SA_{cell} is the surface area of the cell. This line of reasoning is an assumption factored into the model via three universal constants describing the membrane permeability to CO_2 and to HCO_3^- (P_{Ccell}, T_0 and T_U). These three constants will be constrained by the data, explicitly leaving open the option of non-upregulated HCO_3^- transport (through $T_U = 0$), and complete impermeability of membranes to HCO_3^- (through $T_0 = T_U = 0$).

3.3.1.2 A note on external CA and the cellular boundary layer

Although DIC will never be a biomass limiting nutrient for phytoplankton in the ocean, it has been suggested that those relying on the passive diffusive supply of CO_2 alone (in the absence of CA) may be growth rate limited by the rate of CO_2 supply to the surface of the cell (Gavis & Ferguson, 1975; Riebesell *et al.*, 1993, Fig.3.6A). If the assimilation rate of carbon by a cell exceeds the reacto-diffusive supply rate, some mechanism of enhancing the supply to the cell must exist. The carbon supply rate to the cell in the absence of such a mechanism is the sum of HCO_3^- conversion to CO_2 within the boundary layer (reactive component), and the diffusion of CO_2 from the bulk medium into the boundary layer (diffusive component). Calculations given in Reinfelder (2011) based on a cellular organic carbon density of 20 fmol μm^{-3}(Fig.3.6B) suggest that under conditions typical of the modern ocean, cells with a radius of about 10 μm can sustain a maximum division rate of $\sim$1.0 per day (Fig.3.6C). This estimate is also based on the assumption that the concentration of CO_2 at the surface of the cell is 1/3rd the concentration of the bulk medium, which is reasonable; complete depletion of CO_2 in the boundary layer is not possible because cells that rely on the diffusive supply of CO_2 alone will leak CO_2 from their cells back into the boundary layer.

The numbers presented by Reinfelder (2011) are not quite representative of coccolithophores however. Although the results from the current study show that the cellular organic carbon density is very close to 20 fmolμm^{-3} in the species studied here

Figure 3.6 (following page): Considerations of the diffusive boundary layer around the cell. **A:** Schematic representation of cellular boundary layer, **B:** Estimates of organic and total carbon density per unit cellular volume, **C & D:** Maximum possible division rate sustainable given different assumed cellular carbon densities, **E:** Carbon usage by coccolithophores in each experiment; fill of points corresponds to experimental [DIC] condition. The four thick lines correspond to the four experiments, **F:** Theoretical [CO_2] depletion at the surface of coccolithophores in each experiment. See text of section 3.3.1.2 for details.

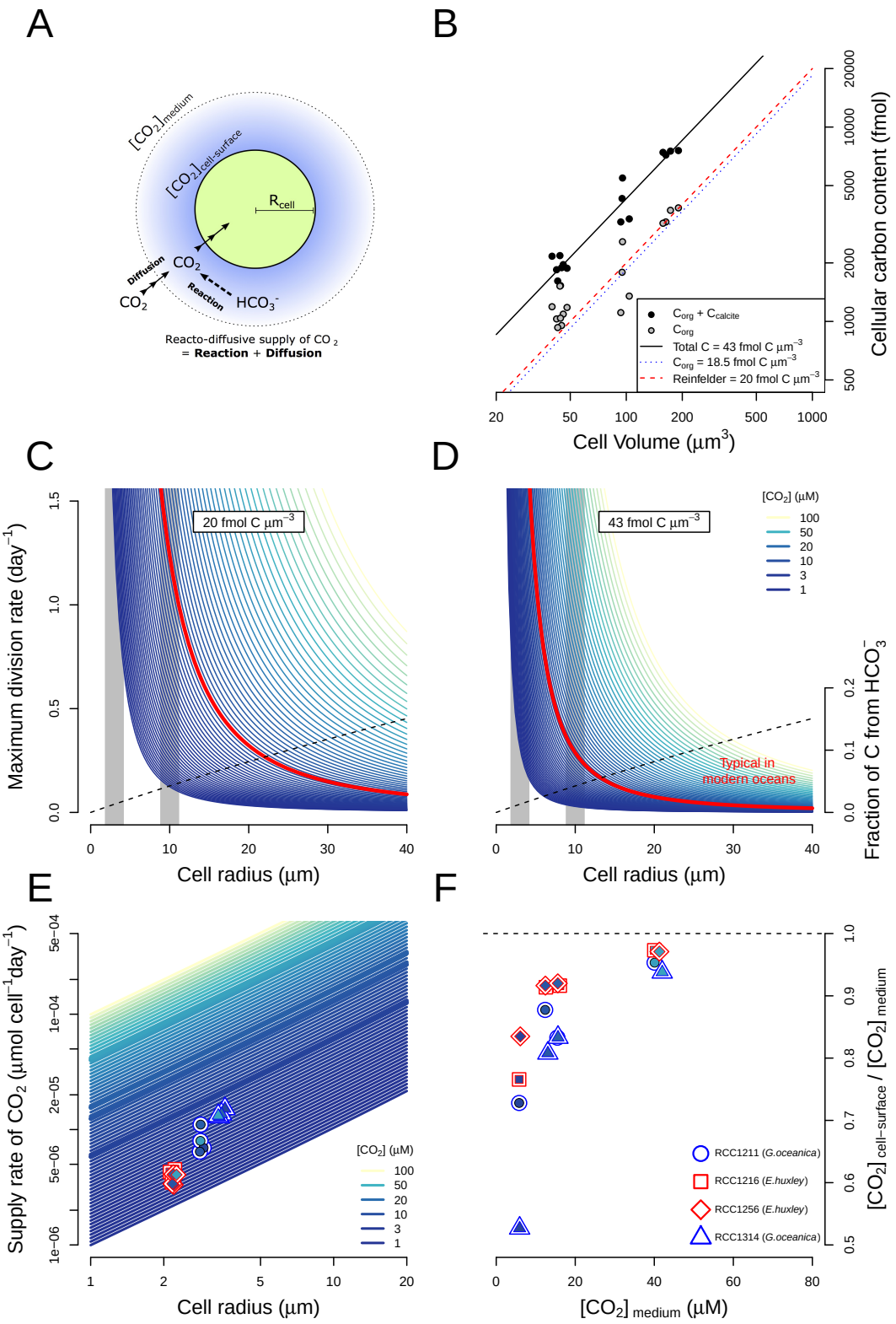
A
[CO2]medium
[CO2]cell-surface
Rcell
Diffusion
CO2
CO2
Reaction
HCO3-
Reacto-diffusive supply of CO2
= Reaction + Diffusion
B
Corg + Ccalcite
Corg
Total C = 43 fmol C µm-3
Corg = 18.5 fmol C µm-3
Reinfelder = 20 fmol C µm-3
Cellular carbon content (fmol)
Cell Volume (µm3)
C
20 fmol C µm-3
Maximum division rate (day-1)
Cell radius (µm)
D
43 fmol C µm-3
[CO2] (µM)
100
50
20
10
3
1
Typical in
modern oceans
Fraction of C from HCO3-
Cell radius (µm)
E
Supply rate of CO2 (µmol cell-1day-1)
[CO2] (µM)
Cell radius (µm)
F
RCC1211 (G.oceanica)
RCC1216 (E.huxley)
RCC1256 (E.huxley)
RCC1314 (G.oceanica)
[CO2] cell−surface / [CO2] medium
[CO2] medium (µM)

(Fig.3.6B), calcification also occurs intracellularly, so carbon used for calcification is additionally taken up across the same cellular membrane. The total cellular carbon density (organic plus inorganic carbon per unit cellular volume) in coccolithophores is $\sim$43 fmolμm^{-3} (Fig.3.6B), which is approximately double that for non-calcifiers. Additionally, the vast majority of calcification and photosynthesis in coccolithophores occurs in the light (Müller *et al.*, 2008), which means that the instantaneous carbon assimilation rate (which is relevant for comparing with the reacto-diffusive supply rate of CO_2) is approximately double that estimated through the cellular carbon content and division rate. Given these assumptions, the maximum division rate of a coccolithophore cell with a radius of 10 μm in the modern ocean would be more like 0.25 per day - a quarter of that predicted by Reinfelder (2011) (Fig.3.6D).

In the experiments conducted in this study, no carbon assimilation rates exceeded the maximum reacto-diffusive supply rate of CO_2, assuming that the minimum CO_2 concentration at the surface of the cell could be as low as 1/3rd that of the bulk medium (Fig.3.6E). The actual theoretical concentration of CO_2 at the surface of the cell, calculated from the observed assimilation rate, can however become highly depleted, reaching values as low as 50% that of the bulk medium (Fig.3.6F). Depletion such as this has implications for the rate of diffusion of CO_2 across the cellular membrane, and therefore for proxies such as the Alkenone CO_2 proxy, which assumes that DIC is supplied to the cell solely as a passive-diffusive supply of CO_2.

In this model, it is explicitly assumed that CA_e is present and active in all species, and that the concentration of CO_2 at the cell's surface can be assumed to equal that of the bulk medium. This is most likely true for *E. huxleyi* (Bach *et al.*, 2013; Richier *et al.*, 2009, 2011), but is less clear for other species such as *G. oceanica* and *C. pelagicus* (Nimer *et al.*, 1997). In these other species, it may therefore be possible that the microenvironment at the surface of the cell is depleted in CO_2, which would simply be manifest as a greater sensitivity to [CO_2].

3.3.2 Assumptions of the model

The assumptions on which this model is based, are:

- Cells are in steady-state growth. The concentration of every carbon pool (i.e. each carbon species in each intracellular compartment) is constant, which implies that all fluxes associated with that pool sum to zero.
- The cell and compartments are assumed to be of constant size and shape.
- CO_2 and HCO_3^- ions move across membranes via passive diffusion and facilitated diffusion respectively. Both chemical species are assumed to move across membranes with a flux proportional to surface area of the membrane and the concentration of the carbon species on the proximal side of the membrane. There is no concentration-independent active uptake of bicarbonate or carbon dioxide. Membranes are impermeable to carbonate ions. There is no other source of carbon to the cell.
- Loss of carbon from the cell is via carbon fixation, calcification, and passive and facilitated diffusion of CO_2 and HCO_3^- respectively.
- The membrane permeability to CO_2 is constant.
- The membrane permeability to HCO_3^- is a linear function of background carbon utilization (U_0; defined in Eq. 3.5). The special cases whereby HCO_3^- permeability is non-adaptive, or is zero are explicitly allowed.
- Membrane permeabilities to CO_2 and to HCO_3^- are identical for all compartments and across all species
- pH in each compartment is constant, and is prescribed *a priori*, according to the values measured by Anning *et al.* (1996).

- Organic matter is not remobilised from the organic pool to the cytosol via mitochondrial respiration.
- Movement of carbon across membranes does not impart a kinetic isotopic fractionation.
- All cells are assumed to exhibit active external carbonic anhydrase (see section 3.3.1.2).
- The chloroplast is assumed to consist of a single compartment with no pyrenoid. The large isotopic fractionation of carbon that occurs during fixation catalysed by the enzyme RuBisCO (ϵ_f), is here factored into the model as an effective pyrenoid/RuBisCO black box fractionation (ϵ_{fe}).

3.3.3 Cellular carbon fluxes

3.3.3.1 Carbon fluxes through membranes

Fluxes of CO_2 through membranes are the product of membrane surface area (SA), CO_2 concentration on the source side of the membrane, and membrane permeability to the specific carbon species. From Fig. 3.3, expressions for trans-membrane CO_2 fluxes are:

$$\begin{aligned} FC_{ei} &= C_e P_{Ccell} SA_{cell} \\ FC_{ie} &= C_i P_{Ccell} SA_{cell} \\ FC_{ix} &= C_i P_{Cx} SA_x \\ FC_{xi} &= C_x P_{Cx} SA_x \\ FC_{iv} &= C_i P_{Cv} SA_v \\ FC_{vi} &= C_v P_{Cv} SA_v, \end{aligned} \tag{3.8}$$

and likewise for HCO_3^- fluxes:

$$\begin{aligned} FB_{ei} &= B_e P_{Bcell} SA_{cell} \\ FB_{ie} &= B_i P_{Bcell} SA_{cell} \\ FB_{ix} &= B_i P_{Bx} SA_x \\ FB_{xi} &= B_x P_{Bx} SA_x \\ FB_{iv} &= B_i P_{Bv} SA_v \\ FB_{vi} &= B_v P_{Bv} SA_v, \end{aligned} \tag{3.9}$$

where all symbols are defined in Table 3.2, and refer to fluxes depicted in Fig. 3.3.

3.3.3.2 Intracompartmental interconversion of CO_2 and HCO_3^-

In each compartment, carbon dioxide and bicarbonate ions are interconverted by the reversible hydration and hydroxylation reactions, and by hydration in the presence

of carbonic anhydrase (CA):

$$\begin{aligned}
&\mathrm{CO_2 + H_2O} \underset{k_{m1}}{\overset{k_{p1}}{\rightleftharpoons}} \mathrm{H^+ + HCO_3^-} && (\textit{hydration}) \\
&\mathrm{CO_2 + OH^-} \underset{k_{m4}}{\overset{k_{p4}}{\rightleftharpoons}} \mathrm{HCO_3^-} && (\textit{hydroxylation}) \\
&\mathrm{CO_2 + H_2O} \underset{k_{mCA}}{\overset{k_{pCA}}{\rightleftharpoons}} \mathrm{H^+ + HCO_3^-} && (\textit{CA catalysed hydration}). \qquad (3.10)
\end{aligned}$$

where arrow annotations denote rate constants (see section 3.3.3.4 for CA rate constants). Combining the rate constants of Eq.s (3.10) at constant pH and [CA] in a generic compartment, a, gives:

$$k_{CBa} = OH_a.k_{p4} + k_{p1} + k_{pCA}.CA_a \qquad (3.11)$$

$$k_{BCa} = k_{m4} + H_a.(k_{m1} + k_{mCA}.CA_a) \qquad (3.12)$$

where k_{CBa} denotes the reaction rate constant for the conversion of $\mathrm{CO_2}$ to $\mathrm{HCO_3^-}$, and k_{BCa} denotes the rate constant for the reverse reaction. H_a, OH_a and CA_a refer to the concentrations of $\mathrm{H^+}$ ions, $\mathrm{OH^-}$ ions, and carbonic anhydrase in compartment, a. As compartment specific pH and [CA] are defined *apriori*, k_{CBa} and k_{BCa} can be treated as pH and [CA] dependent compound rate constants. The rates of the reactions described by Eq.s (3.10) in each compartment are therefore:

$$\begin{aligned}
FCB_i &= V_i C_i k_{CBi} \\
FBC_i &= V_i B_i k_{BCi} \\
FCB_x &= V_x C_x k_{CBx} \\
FBC_x &= V_x B_x k_{BCx} \\
FCB_v &= V_v C_v k_{CBv} \\
FBC_v &= V_v B_v k_{BCv} \qquad (3.13)
\end{aligned}$$

3.3.3.3 Compartment shapes and sizes

Each intracellular compartment is assumed to be an oblate spheroid. The equatorial axis of the spheroid, a, is assumed to have a constant ratio with the cell radius. This is referred to as the scaling factor ($sf_c \times r = a_c$). The polar axis, c, is assumed to have a constant ratio with the equatorial axis. This ratio is referred to as the aspect ratio factor ($af_c \times a_c = c_c$). Isometry is assumed across species, and in this way, two constants are used to describe the relative size and shape of each compartment, and therefore their volumes and surface areas. The surface area of an oblate spheroid is given by:

$$S_{\text{oblate}} = 2\pi a^2 \left(1 + \frac{1-e^2}{e} \tanh^{-1} e\right) \quad \text{where} \quad e^2 = 1 - \frac{c^2}{a^2}.$$

The volume of a spheroid is given by:

$$V = (4\pi/3)a^2 c$$

3.3.3.4 Intracellular Carbonic Anhydrase

The carbonic anhydrases (CAs) are a family of zinc-containing metalloenzymes responsible for catalysing the hydration and dehydration of CO_2 and HCO_3^- respectively. Their behaviour is well described by Michaelis Menten kinetics (Uchikawa & Zeebe, 2012). Given the general form of an enzymatically catalysed reaction:

$$E + S \underset{k_r}{\overset{k_f}{\rightleftharpoons}} ES \xrightarrow{k_{\text{cat}}} E + P \tag{3.14}$$

where E, S, ES and P denote enzyme, substrate, enzyme-substrate complex and product concentrations respectively. k_f, k_r, and k_{cat} are rate constants respectively for the binding and unbinding of substrate to the enzyme, and for the maximum catalytic throughput of the reaction.

According to the Michaelis Menten equations, the velocity of a reaction such as Eq. 3.14 is given by:

$$v = \frac{d[P]}{dt} = V_{\max} \frac{[S]}{K_m + [S]} = k_{\text{cat}}[E] \frac{[S]}{K_m + [S]}, \tag{3.15}$$

where K_m is the Michaelis constant, or half-saturation constant ($K_m = \frac{k_r + k_{\text{cat}}}{k_f}$), and describes the substrate concentration when $v = \frac{V_{\max}}{2}$. When $[S] \ll K_m$, Eq.3.15 becomes:

$$v \approx \frac{k_{\text{cat}}}{K_m}[E].[S], \tag{3.16}$$

and $\frac{K_m}{k_{cat}\,CA}$ is the specific activity of the carbonic anhydrase enzyme in units of $M^{-1}s^{-1}$. This is analogous to a rate constant (k_{pCA}), or activity, when multiplied by the concentration of the enzyme. As enzymes catalyse reactions but do not alter the position of equilibrium, the rate constant for the reverse reaction, CA-catalysed dehydration of HCO_3^-, is given by the hydration rate constant divided by the equilibrium constant:

$$k_{pCA} = \frac{k_{\text{cat}}}{K_{m\,CA}}[E], \qquad\qquad k_{mCA} = \frac{k_{pCA}}{K_1^*}. \tag{3.17}$$

A value of $2.7 \times 10^7 M^{-1}s^{-1}$ was determined by Uchikawa & Zeebe (2012) for the $\frac{k_{\text{cat}}}{K_m}$ of the hydration reaction catalysed by bovine erythrocyte CA.

3.3.3.5 Carbon flux balance

Carbon fluxes throughout the cell can be fully described with Eq.s (3.8), (3.9) and (3.13), and with two additional output fluxes; the rate of calcification (F_{CAL}) and the rate of photosynthetic carbon fixation (F_{FIX}) (Fig. 3.3). Assuming steady state, the rate of change of the amount of each carbon species in each compartment is zero, giving:

$$\begin{aligned}
V_i\frac{dC_i}{dt} &= 0 = FC_{ei} + FC_{vi} + FC_{xi} + FBC_i - FC_{ie} - FC_{iv} - FC_{ix} - FCB_i \\
V_i\frac{dB_i}{dt} &= 0 = FB_{ei} + FB_{vi} + FB_{xi} + FCB_i - FB_{ie} - FB_{iv} - FB_{ix} - FBC_i \\
V_x\frac{dC_x}{dt} &= 0 = FC_{ix} + FBC_x - FCB_x - FC_{xi} - F_{FIX} \\
V_x\frac{dB_x}{dt} &= 0 = FB_{ix} + FCB_x - FBC_x - FB_{xi} \\
V_v\frac{dC_v}{dt} &= 0 = FC_{iv} + FBC_v - FCB_v - FC_{vi} \\
V_v\frac{dB_v}{dt} &= 0 = FB_{iv} + FCB_v - FBC_v - FB_{vi} - F_{CAL}
\end{aligned} \tag{3.18}$$

At steady state these differential equations become linear functions of the concentration of the different inorganic carbon species. Substituting in Eq.s (3.8), (3.9) and (3.13):

$$\begin{aligned}
-C_e P_{Ccell} SA_{cell} &= C_v P_{Cv} SA_v + C_x P_{Cx} SA_x + B_i V_i k_{BCi} \\
&\quad + C_i(-P_{Ccell} SA_{cell} - P_{Cv} SA_v - P_{Cx} SA_x - V_i k_{CBi}) \\
-B_e P_{Bcell} SA_{cell} &= B_v P_{Bv} SA_v + B_x P_{Bx} SA_x + C_i V_i k_{CBi} \\
&\quad + B_i(-P_{Bcell} SA_{cell} - P_{Bv} SA_v - P_{Bx} SA_x - V_i k_{BCi}) \\
F_{FIX} &= C_i P_{Cx} SA_x + B_x V_x k_{BCx} + C_x(-V_x k_{CBx} - P_{Cx} SA_x) \\
0 &= B_i P_{Bx} SA_x + C_x V_x k_{CBx} + B_x(-V_x k_{BCx} - P_{Bx} SA_x) \\
0 &= C_i P_{Cv} SA_v + B_v V_v k_{BCv} + C_v(-V_v k_{CBv} - P_{Cv} SA_v) \\
F_{CAL} &= B_i P_{Bv} SA_v + C_v V_v k_{CBv} + B_v(-V_v k_{BCv} - P_{Bv} SA_v). \qquad (3.19)
\end{aligned}$$

This set of interdependent equations can be written as a linear system of the form:

$$A \cdot \Phi = N, \qquad (3.20)$$

where A is the coefficient matrix of the linear system, N is the nonhomogeneous term and Φ is the unknown vector containing the carbon species concentrations in each compartment. (3.20) can be solved for Φ, where A and N, defined by the dynamic carbon species concentration equations, are as follows:

$$A = \begin{pmatrix} \begin{matrix} -P_{Ccell}SA_{cell} \\ -P_{Cv}SA_v \\ -P_{Cx}SA_x \\ -V_i k_{CBi} \end{matrix} & V_i k_{BCi} & P_{Cx}SA_x & 0 & P_{Cv}SA_v & 0 \\ V_i k_{CBi} & \begin{matrix} -P_{Bcell}SA_{cell} \\ -P_{Bv}SA_v \\ -P_{Bx}SA_x \\ -V_i k_{BCi} \end{matrix} & 0 & P_{Bx}SA_x & 0 & P_{Bv}SA_v \\ P_{Cx}SA_x & 0 & \begin{matrix} -V_x k_{CBx} \\ -P_{Cx}SA_x \end{matrix} & V_x k_{BCx} & 0 & 0 \\ 0 & P_{Bx}SA_x & V_x k_{CBx} & \begin{matrix} -V_x k_{BCx} \\ -P_{Bx}SA_x \end{matrix} & 0 & 0 \\ P_{Cv}SA_v & 0 & 0 & 0 & \begin{matrix} -V_v k_{CBv} \\ -P_{Cv}SA_v \end{matrix} & V_v k_{BCv} \\ 0 & P_{Bv}SA_v & 0 & 0 & V_v k_{CBv} & \begin{matrix} -V_v k_{BCv} \\ -P_{Bv}SA_v \end{matrix} \end{pmatrix} \tag{3.21}$$

$$N = \begin{pmatrix} -C_e P_{Ccell} SA_{cell} \\ -B_e P_{Bcell} SA_{cell} \\ F_{FIX} \\ 0 \\ 0 \\ F_{CAL} \end{pmatrix} \tag{3.22}$$

$$\Phi = \begin{pmatrix} C_i \\ B_i \\ C_x \\ B_x \\ C_v \\ B_v \end{pmatrix} \tag{3.23}$$

3.3.4 Carbon Isotopes

As [^{13}C] is very low compared to [^{12}C], carbon fluxes are assumed to represent ^{12}C. ^{13}C dynamics are therefore determined by prefixing each C flux with corresponding R, where:

$$R = \frac{[^{13}C]}{[^{12}C]}.$$

If the definition of δ^{13}C given in Box 3.1 on p.53, is rearranged to give:

$$R = R_{standard}\left(\frac{\delta^{13}C}{1000}+1\right),$$

the assumption of balanced growth allows both offset $R_{standard}$ and scale factor $\frac{R_{standard}}{1000}$ to be eliminated while preserving the same system of equations. Effectively, we can thus prefix each flux directly with the associated δ^{13}C value. For fractionation fluxes, this leads to a prefix with the sum of the δ^{13}C of the source pool and the process-specific fractionation factor (ϵ). In the following, $\delta_{\Theta a}$ refers to the δ^{13}C of carbon species, Θ, in compartment, a.

3.3.4.1 Interconversion of CO_2 and HCO_3^-

The following fractionation factors (in ‰ as defined in Box 3.1) are taken from Zeebe & Wolf-Gladrow (2001), and assumed constant:

$$\begin{aligned}
\epsilon_{p1} &= -13 \\
\epsilon_{p4} &= -11 \\
\epsilon_{m1} &= -22 \\
\epsilon_{m4} &= -20 \\
\epsilon_{pCA} &= -1 \\
\epsilon_{mCA} &= -10,
\end{aligned} \tag{3.24}$$

where the subscripts are consistent with those from Eq.s (3.10). Analogous to the compound rate constants of Eq.s (3.11) and (3.12), the interconversion of carbon dioxide and bicarbonate has a pH and [CA] dependent, compartment-specific, compound isotopic fractionation factor.

$$\epsilon_{CBa} = \frac{\epsilon_{cb4}.OH_a.k_{p4} + \epsilon_{cb1}.k_{p1} + \epsilon_{cbCA}.k_{pCA}.CA_a}{OH_a.k_{p4} + k_{p1} + k_{pCA}.CA_a} \tag{3.25}$$

$$\epsilon_{BCa} = \frac{\epsilon_{bc4}.k_{m4} + \epsilon_{bc1}.H_a.k_{m1} + \epsilon_{bcCA}.k_{pCA}.CA_a}{k_{m4} + \epsilon_{bc1}.H_a.(k_{m1} + k_{mCA}.CA_a)}. \tag{3.26}$$

3.3.4.2 Carbon isotope mass balance

When the linear system described in section 3.3.3 is solved, all carbon species concentrations in all compartments are known. Dynamic equations for the isotopic composition of each compartment, assuming balanced growth, and expressed in terms of carbon dioxide, and bicarbonate fluxes, and fractionation factors are thus:

$$V_i \frac{d\delta_{Ci}.C_i}{dt} = 0 = \delta_{Ce}.FC_{ei} + \delta_{Cv}.FC_{vi} + \delta_{Cx}.FC_{xi} + (\delta_{Bi} + \epsilon_{BCi}).FBC_i + \delta_{Ci}.(-FC_{ie} - FC_{iv} - FC_{ix}) - (\delta_{Ci} + \epsilon_{CBi}).FCB_i \quad (3.27)$$

$$V_i \frac{d\delta_{Bi}.B_i}{dt} = 0 = \delta_{Be}.FB_{ei} + \delta_{Bv}.FB_{vi} + \delta_{Bx}.FB_{xi} + (\delta_{Ci} + \epsilon_{CBi}).FCB_i + \delta_{Bi}.(-FB_{ie} - FB_{iv} - FB_{ix}) - (\delta_{Bi} + \epsilon_{BCi}).FBC_i \quad (3.28)$$

$$V_x \frac{d\delta_{Cx}.C_x}{dt} = 0 = \delta_{Ci}.FC_{ix} + (\delta_{Bx} + \epsilon_{BCx}).FBC_x - (\delta_{Cx} + \epsilon_{CBx}).FCB_x - \delta_{Cx}.FC_{xi} - (\delta_{Cx} + \epsilon_{FIX}).F_{FIX} \quad (3.29)$$

$$V_x \frac{d\delta_{Bx}.B_x}{dt} = 0 = \delta_{Bi}.FB_{ix} + (\delta_{Cx} + \epsilon_{CBx}).FCB_x - (\delta_{Bx} + \epsilon_{BCx}).FBC_x - \delta_{Bx}.FB_{xi} \quad (3.30)$$

$$V_v \frac{d\delta_{Cv}.C_v}{dt} = 0 = \delta_{Ci}.FC_{iv} + (\delta_{Bv} + \epsilon_{BCv}).FBC_v - (\delta_{Cv} + \epsilon_{CBv}).FCB_v - \delta_{Cv}.FC_{vi} \quad (3.31)$$

$$V_v \frac{d\delta_{Bv}.B_v}{dt} = 0 = \delta_{Bi}.FB_{iv} + (\delta_{Cv} + \epsilon_{CBv}).FCB_v - (\delta_{Bv} + \epsilon_{BCv}).FBC_v - \delta_{Bv}.FB_{vi} - (\delta_{Bv} + \epsilon_{CAL}).F_{CAL} \quad (3.32)$$

At steady state the differential equations become linear functions of δ^{13}C of the different carbon species in the different compartments. Substituting in Eq.s (3.8), (3.9) and (3.13):

$$\begin{aligned}
&\epsilon_{CBi}.V_iC_ik_{CBi} - \delta_{Ce}.C_eP_{Ccell}SA_{cell} - \epsilon_{BCi}.V_iB_ik_{BCi} \\
&\quad = \quad \delta_{Cv}.C_vP_{Cv}SA_v + \delta_{Cx}.C_xP_{Cx}SA_x + \delta_{Bi}.V_iB_ik_{BCi} \\
&\qquad + \delta_{Ci}.(-C_iP_{Ccell}SA_{cell} - C_iP_{Cv}SA_v - C_iP_{Cx}SA_x - V_iC_ik_{CBi})
\end{aligned} \tag{3.33}$$

$$\begin{aligned}
&\epsilon_{BCi}.V_iB_ik_{BCi} - \delta_{Be}.B_eP_{Bcell}SA_{cell} - \epsilon_{CBi}.V_iC_ik_{CBi} \\
&\quad = \quad \delta_{Bv}.B_vP_{Bv}SA_v + \delta_{Bx}.B_xP_{Bx}SA_x + \delta_{Ci}.V_iC_ik_{CBi} \\
&\qquad + \delta_{Bi}.(-B_iP_{Bcell}SA_{cell} - B_iP_{Bv}SA_v - B_iP_{Bx}SA_x - V_iB_ik_{BCi})
\end{aligned} \tag{3.34}$$

$$\begin{aligned}
&\epsilon_{CBx}.V_xC_xk_{CBx} - \epsilon_{BCx}.V_xB_xk_{BCx} + \epsilon_{FIX}.F_{FIX} \\
&\quad = \quad \delta_{Ci}.C_iP_{Cx}SA_x + \delta_{Bx}.V_xB_xk_{BCx} \\
&\qquad + \delta_{Cx}.(-V_xC_xk_{CBx} - C_xP_{Cx}SA_x - F_{FIX})
\end{aligned} \tag{3.35}$$

$$\begin{aligned}
&\epsilon_{BCx}.V_xB_xk_{BCx} - \epsilon_{CBx}.V_xC_xk_{CBx} \\
&\quad = \quad \delta_{Bi}.B_iP_{Bx}SA_x + \delta_{Cx}.V_xC_xk_{CBx} \\
&\qquad + \delta_{Bx}.(-V_xB_xk_{BCx} - B_xP_{Bx}SA_x)
\end{aligned} \tag{3.36}$$

$$\begin{aligned}
&\epsilon_{CBv}.V_vC_vk_{CBv} - \epsilon_{BCv}.V_vB_vk_{BCv} \\
&\quad = \quad \delta_{Ci}.C_iP_{Cv}SA_v + \delta_{Bv}.V_vB_vk_{BCv} \\
&\qquad + \delta_{Cv}(-V_vC_vk_{CBv} - C_vP_{Cv}SA_v)
\end{aligned} \tag{3.37}$$

$$\begin{aligned}
&\epsilon_{BCv}.V_vB_vk_{BCv} - \epsilon_{CBv}.V_vC_vk_{CBv} + \epsilon_{CAL}.F_{CAL} \\
&\quad = \quad \delta_{Bi}.B_iP_{Bv}SA_v + \delta_{Cv}.V_vC_vk_{CBv} \\
&\qquad + \delta_{Bv}.(-V_vB_vk_{BCv} - B_vP_{Bv}SA_v - F_{CAL})
\end{aligned} \tag{3.38}$$

This set of interdependent equations can also be written as a linear system of the form:

$$A \cdot \Phi = N, \tag{3.39}$$

where A is the coefficient matrix of the linear system, N is the nonhomogeneous term and Φ is the unknown vector containing the carbon isotopic compositions of each carbon species in each compartment. (3.39) can be solved for Φ, where A and N, defined by the dynamic carbon species concentration equations, are as follows:

$$A = \begin{pmatrix} \begin{matrix}-C_iP_{Ccell}SA_{cell}\\-C_iP_{Cv}SA_v\\-C_iP_{Cx}SA_x\\-V_iC_ik_{CBi}\end{matrix} & V_iB_ik_{BCi} & C_xP_{Cx}SA_x & 0 & C_vP_{Cv}SA_v & 0 \\ V_iC_ik_{CBi} & \begin{matrix}-B_iP_{Bcell}SA_{cell}\\-B_iP_{Bv}SA_v\\-B_iP_{Bx}SA_x\\-V_iB_ik_{BCi}\end{matrix} & 0 & B_xP_{Bx}SA_x & 0 & B_vP_{Bv}SA_v \\ C_iP_{Cx}SA_x & 0 & \begin{matrix}-V_xC_xk_{CBx}\\-C_xP_{Cx}SA_x\\-F_{FIX}\end{matrix} & V_xB_xk_{BCx} & 0 & 0 \\ 0 & B_iP_{Bx}SA_x & V_xC_xk_{CBx} & \begin{matrix}-V_xB_xk_{BCx}\\-B_xP_{Bx}SA_x\end{matrix} & 0 & 0 \\ C_iP_{Cv}SA_v & 0 & 0 & 0 & \begin{matrix}-V_vC_vk_{CBv}\\-C_vP_{Cv}SA_v\end{matrix} & V_vB_vk_{BCv} \\ 0 & B_iP_{Bv}SA_v & 0 & 0 & V_vC_vk_{CBv} & \begin{matrix}-B_vP_{Bv}SA_v\\-V_vB_vk_{BCv}\\-F_{CAL}\end{matrix} \end{pmatrix} \tag{3.40}$$

$$N = \begin{pmatrix} \epsilon_{CBi}.V_iC_ik_{CBi} - \delta_{Ce}.C_eP_{Ccell}SA_{cell} - \epsilon_{BCi}.V_iB_ik_{BCi} \\ \epsilon_{BCi}.V_iB_ik_{BCi} - \delta_{Be}.B_eP_{Bcell}SA_{cell} - \epsilon_{CBi}.V_iC_ik_{CBi} \\ \epsilon_{CBx}.V_xC_xk_{CBx} - \epsilon_{BCx}.V_xB_xk_{BCx} + \epsilon_{FIX}.F_{FIX} \\ \epsilon_{BCx}.V_xB_xk_{BCx} - \epsilon_{CBx}.V_xC_xk_{CBx} \\ \epsilon_{CBv}.V_vC_vk_{CBv} - \epsilon_{BCv}.V_vB_vk_{BCv} \\ \epsilon_{BCv}.V_vB_vk_{BCv} - \epsilon_{CBv}.V_vC_vk_{CBv} + \epsilon_{CAL}.F_{CAL} \end{pmatrix} \tag{3.41}$$

$$\Phi = \begin{pmatrix} \delta_{Ci} \\ \delta_{Bi} \\ \delta_{Cx} \\ \delta_{Bx} \\ \delta_{Cv} \\ \delta_{Bv} \end{pmatrix} \tag{3.42}$$

Table 3.3: Parameters

Symbol	Definition	Derivation	Quantity	Units
		Measured Parameters		
C_e, B_e	External CO_2 and HCO_3^- concentration	Measured [DIC] and pH	Independent variable	$mol\,C\,m^{-3}$
δC_e, δB_e	$\delta^{13}C$ of external CO_2 & HCO_3^-	Calculated from $\delta^{13}C$ of DIC and pH	Independent variable	$‰_{PDB}$
	$\delta^{13}C$ of external HCO_3^-	$\delta^{13}C$ of DIC and pH	Independent variable	$‰_{PDB}$
F_{FIX}	Average carbon fixation rate	Division rate, mol C_{org} per cell	Measured variable	$mol\,C\,s^{-1}$
F_{CAL}	Average calcification rate	Division rate, mol calcite per cell	Measured variable	$mol\,C\,s^{-1}$
$PIC:POC$	Particulate inorganic to particulate organic carbon ratio of biomass	F_{CAL}/F_{FIX}	Measured variable	Molar ratio
TCR	Total carbon assimilation rate	$F_{CAL}+F_{FIX}$	Measured variable	$mol\,C\,s^{-1}$
δC_{org}	$\delta^{13}C$ of organic material	Measured directly	Measured variable	$‰_{PDB}$
δC_{cal}	$\delta^{13}C$ of calcite	Measured directly	Measured variable	$‰_{PDB}$
r_{cell}	Cell radius	Measured directly	Measured variable	m
SA_{cell}&V_{cell}	Cell surface area and volume	Functions of r_{cell}	Measured variable	m^2&m^3
rho	Cellular organic carbon density	This study, consistent with Reinfelder (2011)	20×10^{-15}	$mol\,C\,m^{-3}$
		Parameters from Literature		
ϵ_{cal}	Carbon isotopic fractionation during calcification	(Zeebe & Wolf-Gladrow, 2001)	+1 (from HCO_3^-)	$‰_{PDB}$
ϵ_{cb1}, ϵ_{bc1}, ϵ_{cb4}, ϵ_{bc1}, ϵ_{cbCA}, ϵ_{bcCA}	Kinetic carbon isotopic fractionation factors	(Zeebe & Wolf-Gladrow, 2001)	- 13, -22, -11, -20, -1, -10	$‰_{PDB}$
k_{p1}, k_{m1}, k_{p4}, k_{m4},	Kinetic rate constants	Calculated from (Zeebe & Wolf-Gladrow, 2001)	T and S dependent.	various - dependent on reaction
K_W^*,	Ion product of water	Calculated from (Dickson & Goyet, 1994)	T and S dependent.	$mol^2\,kg^{-2}$
K_1^*,	1st acidity constant of carbonic acid	Calculated from (Lueker *et al.*, 2000)	T and S dependent.	$mol\,kg^{-1}$
$\frac{K_{cat}}{K_m}_{CA}$	Specific activity of CA for hydration reaction	Inferred from bovine erythrocyte CA (Uchikawa & Zeebe, 2012)	2.7×10^7	$M^{-1}s^{-1}$
pH_i, pH_x&pH_v	pH in compartments i, x & v.	(Anning *et al.*, 1996) (but see Section 3.4.3)	7.0, 7.9 & 7.1 .	
f_x, f_v	Scale factor for compartments x & v	TEM images (Bendif & Young, 2014; Taylor *et al.*, 2007a)	1.1 & 0.6	
S_x, S_v	Shape factor for compartments x & y	TEM images (Bendif & Young, 2014; Taylor *et al.*, 2007a)	6 & 4	
		Fitted Parameters		
ϵ_{fe}	Effective carbon isotopic fractionation during C-fixation by Rubisco	Fitted parameter	-15	$‰_{PDB}$
P_{Cei}	Cell membrane permeability to CO_2	Fitted parameter	5×10^{-4}	$m\,s^{-1}$
P_{Bei} (T_0, T_U)	Cell membrane permeability to HCO_3^-	Fitted parameter	4.2×10^{-7}, 6×10^{-6}	$m\,s^{-1}$
$[CA]_i$, $[CA]_x$ & $[CA]_v$	[CA] in compartments i, x & v.	Inferred	0.1 - 1	$mol\,m^{-3}$

3.3.5 Parameter fitting

The results from culture were used to constrain P_{Ccell} (the permeability of membranes to CO_2), T_0, T_U (the constants required to define the linear dependence of membrane permeability to HCO_3^- on utilisation (see Eq.3.7)) and ϵ_{fe} (the effective enzymatic isotopic fractionation associated with carbon fixation by RuBisCO). Universal constants were fitted to the data by minimisation of a misfit function, which quantified the sum of squared deviations of the modelled results from the measured data. Minimisation of the misfit function was achieved using an R implementation (Steven G. Johnson, 2014) of the constrained DIRECT_L algorithm (Gablonsky & Kelley, 2001) within a defined parameter space. Final parameter values were checked with an alternative implementation of the model in Python, using a combination of a broad search with the Differential Evolution algorithm (Storn & Price, 1997), followed by refinement of its result with the Nelder-Mead Simplex algorithm (Nelder & Mead, 1965). Only complete data sets were used to computationally constrain the universal parameters of the model. The required parameters are: Cell size, PIC:POC, growth rate, medium pH and [DIC], $\delta^{13}C_{DIC}$, $\delta^{13}C_{cal}$ and $\delta^{13}C_{org}$. The model was fitted to these data multiple times with pseudo-replicate datasets generated by resampling each value from an assumed gaussian distribution defined by the expected value and uncertainty associated with each measurement. All input parameters were resampled in this way. Each of the parameters do not individually have an associated uncertainty as all parameters within a fitted set are interdependent. The fitted value of P_{Ccell} is $\sim 6.6 \times 10^{-4}$ ms^{-1}, which is at the high end of the range suggested by Hopkinson *et al.* (2011) for diatoms. T_0 is $\sim 1.2 \times 10^{-7}$ ms^{-1}; also consistent with values given by Hopkinson *et al.* (2011). Based on these results, at high DIC, the membrane is less than 1‰ as permeable to HCO_3^- as to CO_2. The constant T_U describing the increase in membrane permeability to HCO_3^- with increased utilisation is $\sim 1.1 \times 10^{-5}$ ms^{-1} per unit utilisation. When utilisation is low, either at high DIC or in small

cells, $\sim$ 10% of carbon enters the cell in the form of HCO_3^-. When cells experience high utilization, at low DIC or in larger cells, the contribution of HCO_3^- to total DIC supply can be as high as 50% (Fig. 3.7). ϵ_{fe} is $\sim$ -14.3‰, which is far smaller than that used in the literature to date (Bolton & Stoll, 2013; Cassar *et al.*, 2006; Keller & Morel, 1999; Laws *et al.*, 1995, 1997) but is closer to the *in vitro* measured value of ϵ_f given for *E. huxleyi* (-11‰ Boller *et al.*, 2011) and for the diatom *Skeletonema costatum*(-19‰ Boller *et al.*, 2015).

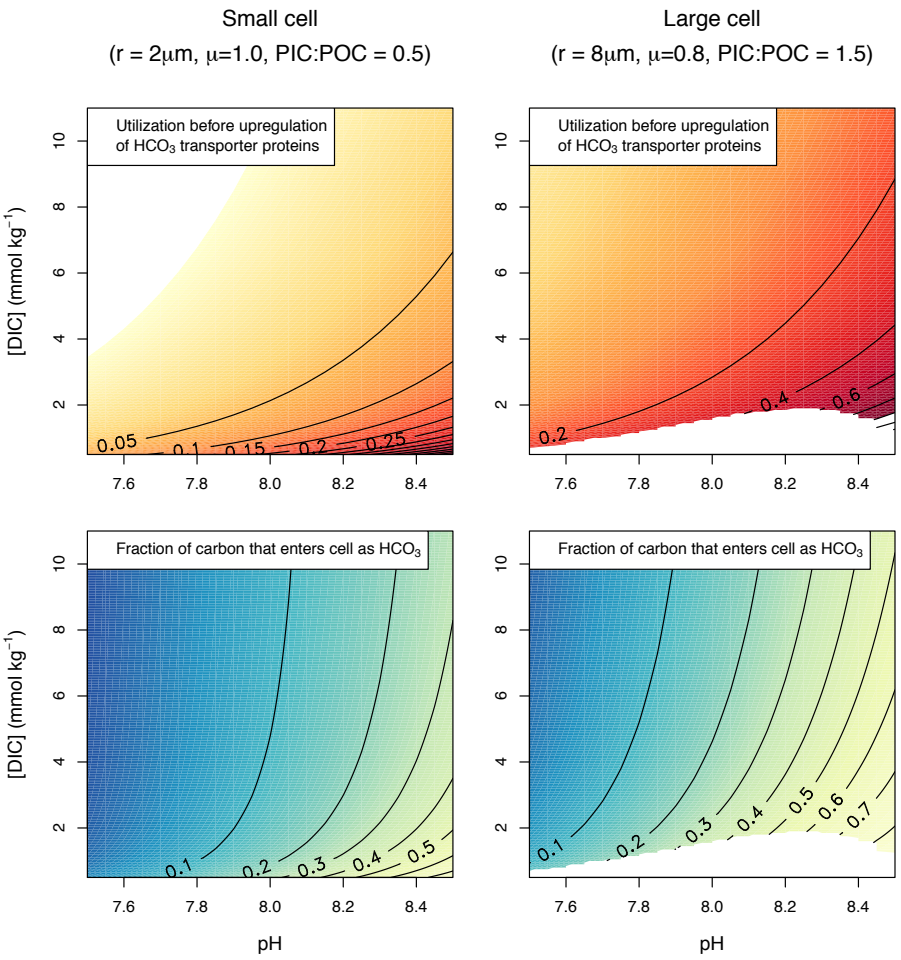

Figure 3.7: Top: Utilisation of background carbon supply (before up regulation of HCO_3^- transporters) of carbon across a theoretical carbonate chemistry parameter space for a typical small (left) and large (right) coccolithophore. **Bottom:** Isotopic composition of carbon entering the cell, changing due to the up regulation of HCO_3^- transporters at high utilisation, and the relative concentrations of CO_2 and HCO_3^- at different pH.

3.3.6 Results and mechanistic interpretation

The model successfully describes the observed trends towards isotopically heavier organic carbon with decreasing DIC, with the effect being greater in large cells. It also successfully describes the divergent behaviour of the carbon isotopic composition of the calcite. Large differences in vital effects are seen at low DIC, with vital effects disappearing at high DIC. Repeated refitting of the model parameters with pseudo-replicate datasets, perturbed according to the uncertainty associated with each measurement, shows that the stability of the result is good (Fig. 3.8).

3.3.6.1 Concepts for interpretation

The isotopic composition of each intracellular compartment is usefully interpreted in terms of the isotopic composition of the carbon source to the compartment, and compartmental utilisation ($U_{compartment}$). This is analogous to the description given in early work for the whole cell (e.g. Berry, 1989). The isotopic composition of carbon entering a compartment is a weighted sum of the isotopic compositions of the CO_2 and the HCO_3^- composing this flux. $U_{compartment}$ is defined as the fraction of DIC that enters a compartment that does not leave as DIC (i.e. is fixed). As utilisation increases, the isotopic fractionation associated with the compartment-specific carbon removal process causes a Rayleigh-type fractionation of the residual pool. When the supply of each carbon species is proportional to their respective concentrations in ambient medium alone, for a given growth rate, utilisation is greater in larger cells because the volume ($\propto$ carbon assimilation rate) to surface area ($\propto$ carbon supply rate) ratio decreases with increasing cell size. An additional layer of complexity arises when reactions internal to the carbonate system operate at a comparable (or slower) rate to carbon fluxes between compartments. When this is the case, the compartment may be in a state of isotopic, or even chemical, disequilibrium. Furthermore, differences in pH between compartments mean that the equilibrium state of the carbonate system in each compartment is different.

Figure 3.8 (following page): Model output plotted underneath data. Parameter values are constrained by measured data resampled according to its associated uncertainty, with 10 pseudo-replicate datasets here constraining 10 parameter sets. Curves are model outputs for a typical set of parameters for each species - held constant with varying [DIC]. Notice that *E. huxleyi* $\delta^{13}C_{cal}$ increases towards low DIC before sharply decreasing at very low values of DIC. All species curves are a similar shape controlled by a number of trade-offs, and with the point of inflexion and maximum $\delta^{13}C_{cal}$ determined by varying combinations of cell size, PIC:POC and growth rate (discussed in the text). Compartmental pH is prescribed to be the same as those empirically measured by Anning *et al.* (1996).

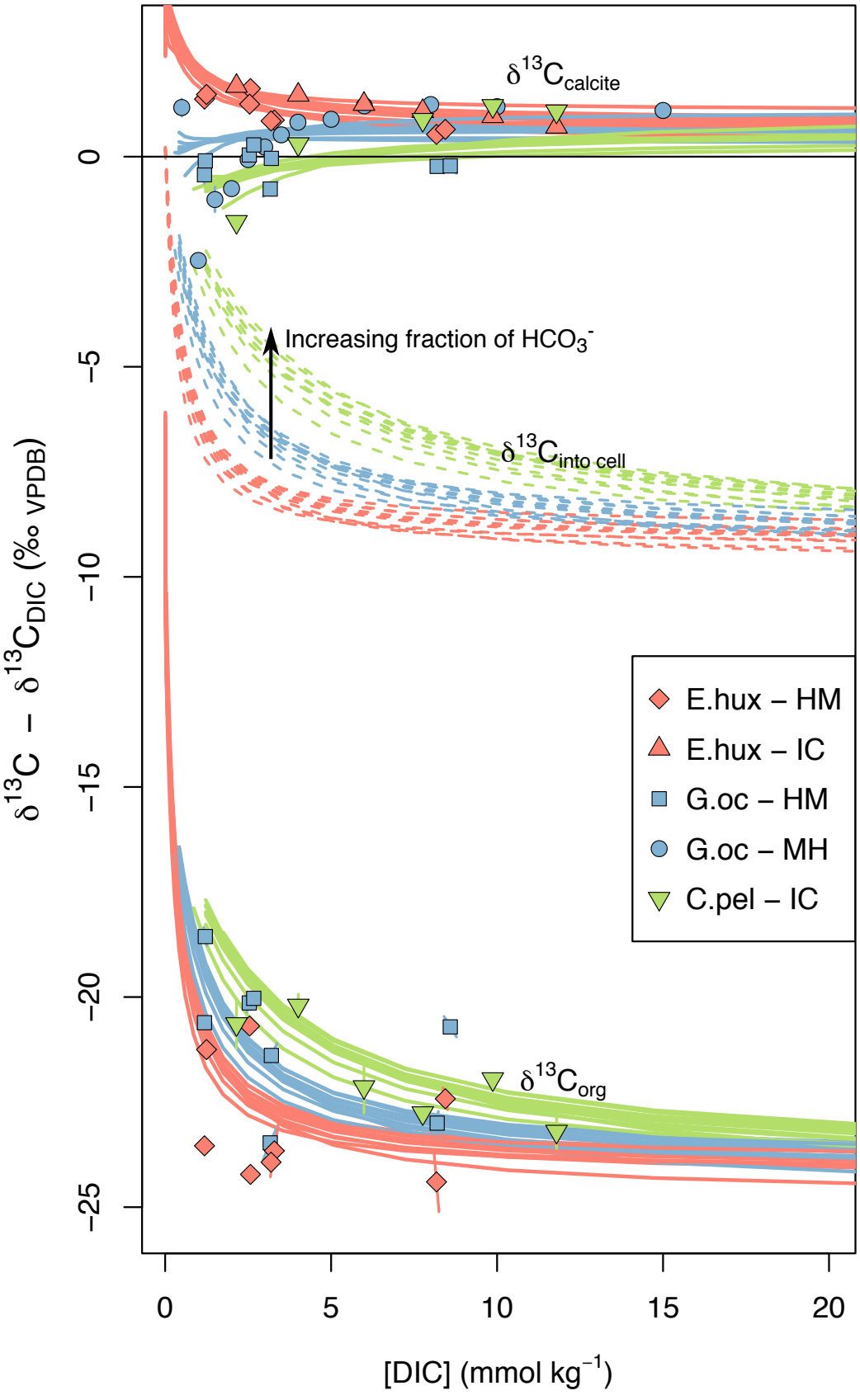
δ13Ccalcite
Increasing fraction of HCO3-
δ13Cinto cell
δ13Corg
E.hux – HM
E.hux – IC
G.oc – HM
G.oc – MH
C.pel – IC
δ13C – δ13CDIC (‰ VPDB)
0
−5
−10
−15
−20
−25
0
5
10
15
20
[DIC] (mmol kg−1)

3.3.6.2 Photosynthesis (chloroplast)

Carbon fixation into organic matter uses CO_2 as a substrate, and RuBisCO, the enzymatic catalyst responsible, imparts a strong negative isotopic fractionation (ϵ_{fe}) from this substrate. As CO_2 is depleted in the heavy isotope of carbon relative to HCO_3^-, these isotopic effects are additive, and within the chloroplast (CP), as U_{CP} increases, carbon fixation drives the intracompartmental pool of CO_2 to isotopically heavier values. The resultant Rayleigh-type fractionation is seen in the $\delta^{13}C_{org}$ trends (Fig. 3.8), and has been widely reported in the literature across other groups of algae (Table 3.1). The consequence of this depletion for the rest of the cell, and thus $\delta^{13}C_{cal}$ is communicated via the flux of carbon leaving the CP. Increasing U_{CP} results in a greater isotopic drift of the pool inside the CP, but a decrease in concentration, which is manifest as an isotopically enriched but volumetrically decreased flux leaving the pool. The maximum influence of photosynthesis on the isotopic composition of the cytosolic pool is therefore at intermediate values of U_{CP}. Taken to either limit; zero; and complete utilisation, photosynthesis in the CP has no effects on the rest of the cell. Photosynthesis causes an increase in $\delta^{13}C_{cal}$, which is greatest when ϵ_{fe} is large, when the product of isotopic enrichment and flux leaving the CP is highest at intermediate values of U_{CP}, and when the rate of photosynthesis is high relative to calcification (reflected in the PIC:POC ratio).

3.3.6.3 Calcification (coccolith vesicle)

Calcification uses HCO_3^-, the heavy species of carbon, and imposes a somewhat modest, positive isotopic fractionation (+1‰; Zeebe & Wolf-Gladrow, 2001). The tendency of the coccolith vesicle (CV) carbon pool is therefore to drift to light values at high U_{CV}. Similarly to the leakage from the CP, the leakage from the CV contributes to the isotopic composition of the cytosolic carbon pool, but this has very little effect on $\delta^{13}C_{org}$ in the CP as it is obscured by the strong fractionation by RuBisCO.

3.3.6.4 Membrane permeabilities and pH

According to the fitted values, membranes are around 3 orders of magnitude more permeable to CO_2 than to HCO_3^-, so the isotopic composition of a passive flux across a membrane is always skewed towards $\delta^{13}C_{\ CO_2}$ from $\delta^{13}C_{\ DIC}$. This effect influences the flux of carbon into the cell as well as the leakage of carbon from the cytosolic pool, following partial or complete reequilibration inside the cell. The compartment-specific pH values moderate this effect. With the pH values given by Anning *et al.* (1996), the cytosol and CV are a whole pH unit lower than the ambient medium, so at equilibrium the concentration ratio of CO_2 to HCO_3^- is an order of magnitude higher inside the CV and the cytosol than in the ambient medium. This model is formulated such that membrane permeabilities are equal for transport in either direction, so the flux of carbon leaving the cell is an order of magnitude more enriched in CO_2 relative to HCO_3^-, and therefore isotopically lighter relative to the internal pool, than that which enters the cell relative the the external pool. As a result, carbon in the cytosol and the CV is isotopically heavy compared with the flux entering the cell. These effects are independent of those that arise at high cellular utilisation, and thus explains why $\delta^{13}C_{cal}$ across species appear to converge to "equilibrium" values, when the carbon entering the cell is significantly lighter than DIC (Fig. 3.8).

3.3.6.5 HCO_3^- up-regulation

The up-regulation of anion exchange proteins facilitating greater influx of HCO_3^- to the cell at high utilisation increases $\delta^{13}C_{\ in}$, but also increases the supply of carbon. For $\delta^{13}C_{org}$, these effects constitute a trade-off (Keller & Morel, 1999); the effect is a subtle dampening of the response to decreasing DIC. For $\delta^{13}C_{cal}$, the effect of bicarbonate up-regulation is a dampening of the response to carbon limitation, and an increasingly important shift towards heavier values with increasing utilisation. Additionally, this up regulation of bicarbonate transport is consistent with the vital effects observed in oxygen isotopes (see section 3.3.7).

3.3.6.6 Presence of CA

In the absence of CA, the interconversion of CO_2 and HCO_3^-, and therefore the time required to achieve equilibrium at a given pH, is extremely sluggish (Fig. 3.4). For the current model assumptions, CA is required to be present in the CP and in the CV at a concentration of at least 0.1 mM to sustain the observed growth rates. This inferred localisation is consistent with the literature (Mackinder *et al.*, 2010; Soto *et al.*, 2006), and the inferred value is consistent with observations of Hopkinson *et al.* (2011) for the chloroplast of diatoms. The model output is highly insensitive to cytosolic [CA], which can be as low as 0. CA concentrations in the cytosol and the coccolith vesicle cannot be so high as to obliterate vital effects in the oxygen isotopic composition of calcite however (see section 3.3.7).

3.3.6.7 Fractionation by RuBisCO

The isotopic fractionation of carbon by the enzyme RuBisCO is the foundation of this area of research. The fractionation itself is thought to be due to increasing substrate specificity (Tcherkez *et al.*, 2006). Although isotopic fractionation by RuBisCO has been extensively studied in plants, only two studies to date have estimated the *in vitro* isotopic fractionation of carbon associated with carbon fixation catalysed by form ID RuBisCO as is found in the "red-lineage algae" such as the coccolithophores and the diatoms (Boller *et al.*, 2015, 2011). Form ID RuBisCOs measured *in vitro* exhibit a slightly lower associated isotopic discrimination factor (11 & 19 ‰; Boller *et al.*, 2015, 2011) than form II RuBisCOs (19.5‰; Robinson & Scott, 2003), and significantly lower isotopic discrimination than form IA and IB RuBisCOs (22 - 30‰; Guy *et al.*, 1993; Scott *et al.*, 2007). Despite this, recent modelling work has continued to use the markedly larger fractionation factors associated with plants and cyanobacteria (e.g. 27, 29‰ Bolton & Stoll, 2013; Schulz *et al.*, 2007). The fitted value for ϵ_{fe} output by our model is $\sim$ 14 - 15‰, which lies more in line with recent work on closely related taxa.

The model described here does not have treatment of the pyrenoid; a compartment of low pH nested within the relatively alkaline chloroplast where CO_2 and RuBisCO are thought to be highly concentrated, which may have profound implications for how reflective the model inferred value of ϵ_{fe} is of the actual enzymatic fractionation, ϵ_f. The introduction of another CO_2-permeable membrane between the ambient medium and the site of carbon fixation, may allow a further iterative isotopic discrimination to take place by the preferential uptake of CO_2 over HCO_3^-, which would allow the value of ϵ_f to be even smaller than the value of ϵ_{fe} predicted by our model. However, conversely, if compartmental utilisation of the pyrenoid were very high, ϵ_f may be far higher than the value of ϵ_{fe} predicted by the model. ϵ_{fe} constrained by the model is an effective pyrenoid/RuBisCO black-box fractionation for the given set-up.

3.3.7 Oxygen Isotopes

The oxygen kinetic isotopic fractionation factors (KIFs) for the hydration and dehydration of CO_2 and HCO_3^- respectively are not known, and theoretical predictions vary widely (Guo, 2009; Zeebe, 2014), so this model cannot be fully resolved with respect to oxygen isotopes. Although a definitive conclusion is not possible, some arguments can be made regarding the possible implications for oxygen isotopes of calcite ($\delta^{18}O_{cal}$) from *in silico* concentrations and fluxes of DIC. An additional complication over carbon isotopes that arises when considering oxygen isotopes in the DIC system is the interaction with water, which is through the hydration of CO_2 (Watkins *et al.*, 2013, 2014; Zeebe & Wolf-Gladrow, 2001). Over time, the DIC system equilibrates with water with respect to oxygen isotopes, with the rate of equilibration and the residence time of carbon in a compartment critical to the preservation of vital effects in calcite. However, the lack of a strong isotopic fractionation of oxygen by RuBisCO removes a level of complexity, and to an extent decouples these isotopic systems.

3.3.7.1 δ^{18}O of DIC entering CV

As with carbon, the oxygen isotopic composition of the calcite is heaviest is *E. huxleyi*, and lightest in *C. pelagicus*, with the difference greatest at low DIC, and the difference decreasing at high DIC (Fig. 3.9A). At first, these observations are problematic because HCO_3^- is isotopically heavier than CO_2 in carbon, but is lighter than CO_2 in oxygen, so the observed trends in carbon and oxygen isotopes cannot be simultaneously explained solely by a shift in carbon source from dominantly HCO_3^- to CO_2 or vice versa. However, although isotopic disequilibrium signatures seen in $\delta^{18}O_{cal}$ are likely to be influenced by that of DIC entering the cell, the model suggests that various intracellular processes obscure its influence on $\delta^{13}C_{cal}$. The modelled shift in the fraction of DIC entering the cell in the form of HCO_3^- increases at high cellular utilisation, so this is consistent with oxygen isotopic composition of calcite being lighter in larger cells, and with the differences between size fractions disappearing at high DIC (Fig. 3.9B). This process does not however explain why coccolith calcite becomes isotopically heavier in oxygen at low DIC.

3.3.7.2 Rayleigh-type fractionation of HCO_3^- pool

Calcite is precipitated from the CO_3^{2-} ion, but can be assumed to be precipitated from a combination of the CO_3^{2-} and HCO_3^- ions, due to the rapid interconversion of these species, and the dominating concentration of HCO_3^-. A typical approximate calcification rate in the cultures studied here is 1×10^{-17} mol s^{-1} $cell^{-1}$, and the surface area of a coccolith is on the order of $10^{-11}m^2$. This gives a "per unit area" calcification rate of 10^{-6} mol m^{-2} s^{-1}, which according to Watkins *et al.* (2014), corresponds to an isotopic fractionation from the bicarbonate ion of approximately -2‰. The isotopic fractionation factor changes with calcification rate, but is always negative. Therefore, unless the rate of hydration were far higher than the rate of calcification, it may be expected that the HCO_3^- pool would become enriched in

$\delta^{18}O$ with increasing utilisation of this carbon-species, in a Rayleigh fractionation-type scenario. Such a process would result in heavier calcite at low DIC for a given calcification rate, inline with the observed trend.

3.3.7.3 CA-catalysed hydration

In a compartment with greater than nano-molar concentrations of CA, the interconversion of CO_2 and HCO_3^- is dominated by CA-catalysed hydration and dehydration (Fig. 3.4). The model presented here requires CA concentrations of at least 0.1 mM in the CP and CV to sustain the observed carbon fixation rates. Increasing [CA] causes the rate of hydration to increase; if it is high enough that the rate of hydration is much higher than the rate of calcification, the system approaches equilibrium with respect to oxygen isotopes and vital effects are diminished. As we do observe vital effects in oxygen isotopes, [CA] cannot be infinitely high. Rates of hydration are strongly controlled by [CA], but all strongly decrease at low [DIC] (Fig. 3.9C). The decrease in relative hydration rate with decreasing DIC may also partially explain heavier oxygen isotopic compositions at low DIC, due to greater preservation of the signature of the heavy (CO_2-enriched relative to equilibrium) flux entering the cell.

3.3.7.4 Summary of possible sources of VEs in oxygen

The increased difference in oxygen isotopic vital effects between large and small cells at low [CO_2] is probably due a residual difference in the oxygen isotopic composition of DIC entering the cell following the up regulation of bicarbonate transport at high utilisation. It is here hypothesised that this signal may be superimposed on a Rayleigh type fractionation, which drives bicarbonate in the coccolith vesicle to heavy values at high utilisation, and by CA-catalysed hydration and dehydration which pushes the system further towards equilibrium at high DIC (Fig. 3.9).

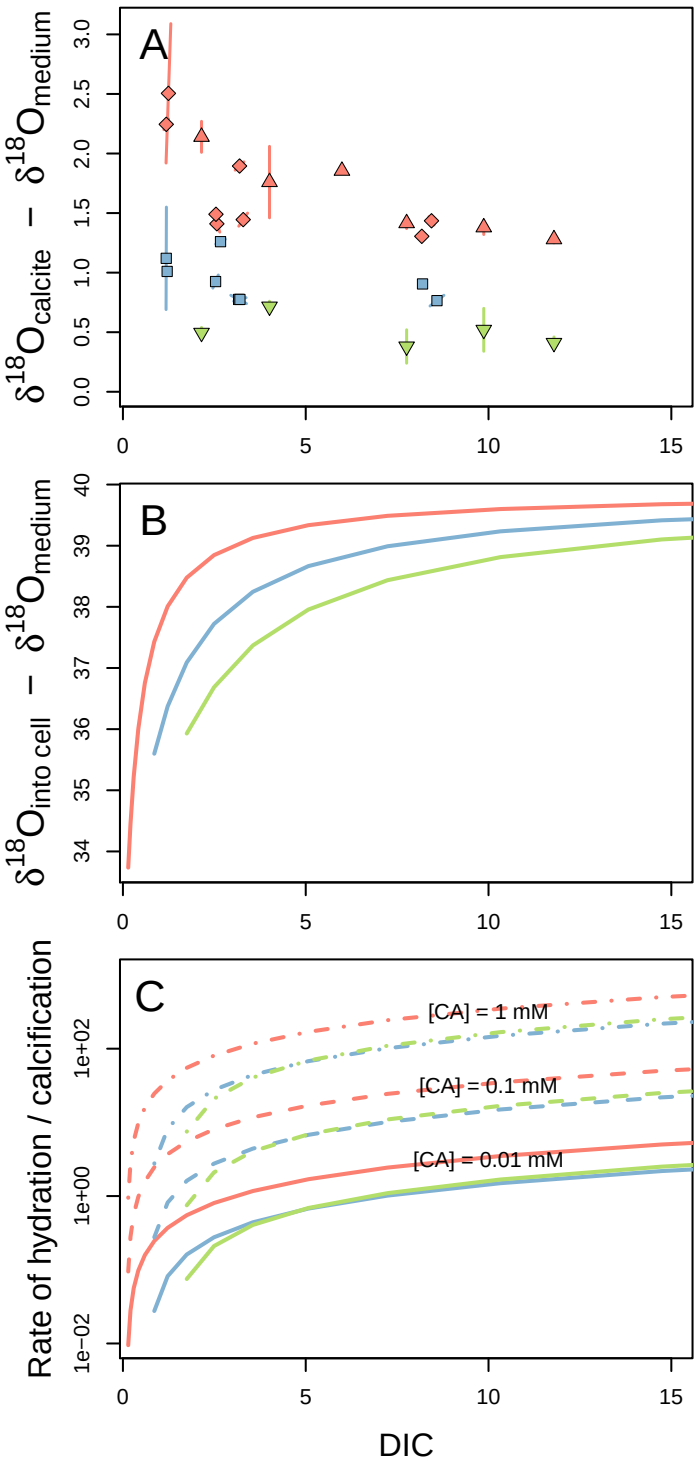

Figure 3.9: Implications for oxygen isotopes according to the model output. **A:** Oxygen isotopic composition of coccolith calcite. **B:**Oxygen isotopic composition of the DIC entering the cell. **C:** Hydration rate / calcification rate inside coccolith vesicle for different values of [CA]. The higher the value, the closer to equilibrium - i.e. at equilibrium, any effects caused by Rayleigh-type fractionation of the HCO_3^- pool and differences in $\delta^{18}O$ entering the cell are lost.

3.4 Discussion

This isotopic flux model presented here simultaneously explains the trends in $\delta^{13}C_{org}$ and in $\delta^{13}C_{cal}$ across different species in response to changing $[CO_2]$. As cells experience higher cellular utilisation, the trend in $\delta^{13}C_{org}$ is dominated by a Rayleigh-type fractionation within the chloroplast driving organic matter to isotopically heavier values, consistent with the vast majority of the existing literature (Cassar *et al.*, 2006; Keller & Morel, 1999; Laws *et al.*, 1995, 1997; Sharkey & Berry, 1985). $\delta^{13}C_{cal}$ is controlled by a number of more subtle superimposed processes; broadly, the direction of the vital effect is dictated by the PIC:POC, and the magnitude increases with utilisation.

For the special case where the CA concentration in all compartments is infinitely high, and thus all compartments can be assumed to be in chemical and isotopic equilibrium, the system is much simpler (see Appendix C). At equilibrium, when the pH of each intracellular compartment is prescribed *a priori*, the entire system can be described in terms of constants and two variables,

$$PIC : POC \;\; and \;\; \tau = \frac{r\rho\mu}{3P_C C_e}. \tag{3.43}$$

where all parameters are defined in Table 3.3. Here I name τ the utilisation parameter because it approximates cellular carbon utilisation (the fraction of carbon that enters the cell that is fixed as organic or inorganic carbon) and increases with increasing cell size, increasing growth rate, and decreasing external $[CO_2]$ (Fig. 3.10). τ is dimensionless, and takes an identical form to the early studies of isotopic fractionation in cellular algae (Cassar *et al.*, 2006; Farquhar, 1983; Farquhar *et al.*, 1982; Keller & Morel, 1999; Laws *et al.*, 1995, 1997; Popp *et al.*, 1998; Rau, 1996, 1997; Sharkey & Berry, 1985). The disequilibrium model collapses to a state completely consistent with these earlier works when equilibrium is assumed and PIC:POC = 0. When the cell is close to chemical and isotopic equilibrium with respect to carbon therefore, changes in cell size, growth rate and extracellular $[CO_2]$ cannot be decoupled.

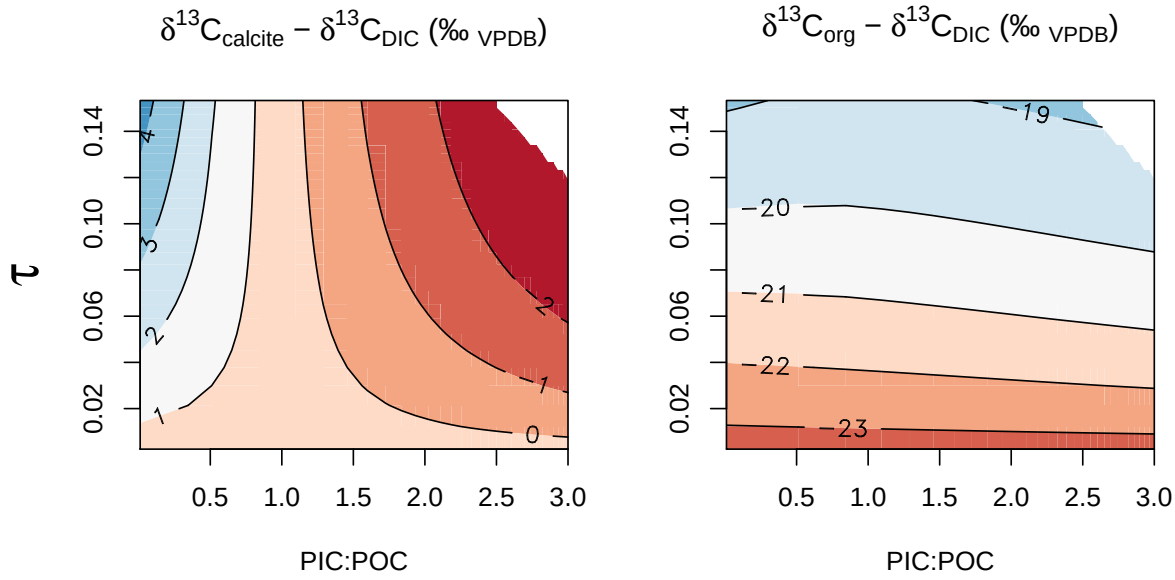

Figure 3.10: Summary of model output - isotopic compositions as a function of PIC:POC and of the utilisation parameter, τ. τ approximates utilisation, and is a dimensionless linear function of growth rate, cell size [DIC], as defined in Eq.3.43. **Left:** Carbon isotopic compositions depend strongly on PIC:POC - if PIC:POC is high, calcite becomes isotopically light as utilisation increases, if PIC:POC is low, calcite becomes isotopically heavy as utilisation increases. **Right:** The carbon isotopic composition of organic matter is largely independent of PIC:POC, and is a strong function of the utilisation parameter.

3.4.1 Synthesis - carbon isotopic vital effects

When utilisation is low (at high CO_2) and the flux of carbon into the cell exceeds that of any fractionating processes, $\delta^{13}C_{cal}$ of different species converge at the same value and appear to reflect "equilibrium" (abiogenic) calcite (Fig. 3.11.I). This observation is misleading however; it does not imply that the isotopic composition of the carbon entering the cell is the same as that of the medium, it simply implies that isotopic offset of carbon leaving the cell from the internal carbon reservoir is approximately the same as the isotopic offset between the flux into the cell and the external reservoir. The isotopic composition of the flux in either direction is a function of the ratio of membrane permeabilities to CO_2 and to HCO_3^-, the ratio $[CO_2]$: $[HCO_3^-]$ on the proximal side of the membrane, and the isotopic compositions of each of these substrates. If, as assumed here, carbon is acquired via down-gradient passive or facilitated diffusion, and if membranes are equally permeable in both directions, when utilisation is low and the intracellular environment is close to equilibrium, the flux of carbon leaving the cell is only different to that entering it when the intracellular pH differs to the extracellular pH. The value of the intracellular $\delta^{13}C$, and therefore $\delta^{13}C_{cal}$ at the plateau is higher than that of the carbon entering the cell because disproportionately more of the isotopically light carbon species, CO_2, is lost back into the surrounding medium (Fig. 3.8; $\delta^{13}C_{\ into\,cell}$). Vital effects arise when cellular carbon utilisation increases, such that the rate of carbon supply into the cell is not far in excess of intracellular fluxes. At very high utilisation, and as the flux of carbon leaving the cell tends towards zero, by a simple consideration of mass balance, the bulk isotopic composition of the cell must tend towards that of the carbon entering the cell. The effect of a number of other intracellular processes are superimposed on this drift.

In a cell with a low PIC:POC, $\delta^{13}C_{cal}$ becomes heavier as utilisation increases (Fig. 3.11.I-II). The increase in $\delta^{13}C_{cal}$ is dominantly due to the influence of heavy carbon

leaked from the CP (having been depleted by RuBisCO-catalysed carbon fixation), but also due to isotopically heavier carbon entering the cell as bicarbonate transport is upregulated. As utilisation becomes higher still (Fig. 3.11.II-III), although the isotopic composition of the flux from the chloroplast is heavier, the magnitude of the flux is lower, causing the overall effect on the cytosol and thus $\delta^{13}C_{cal}$ to diminish. This influence is superimposed on increased effect of Rayleigh-type fractionation within the coccolith vesicle driving the pool to lower values, and also the increasingly heavy isotopic composition of the carbon entering the cell. The value of intracellular CA dictates the extent to which the isotopic composition of carbon entering the cell affects $\delta^{13}C_{cal}$. However, the trends towards light isotopic values in cells with a low PIC:POC are usually not seen because cells become carbon limited. In a cell with a high PIC:POC, $\delta^{13}C_{cal}$ becomes light as utilisation increases (Fig.3.11.I-IV) and the effect of leakage from the chloroplast is obscured. This trend is due to isotopic depletion of the coccolith vesicle carbon pool by calcification, but the gradient with

Figure 3.11 (following page): Summary of causes of carbon isotope vital effects in coccolith calcite. **A:** Coccolithophore cell with isotopically depleted POC produced in the chloroplast and isotopically enriched PIC produced in the coccolith vesicle. **B:** Schematic representation of the effect of three dominant processes affecting $\delta^{13}C_{cal}$ (see text for detailed discussion). **Bottom:** Net result of carbon isotopic vital effects in coccolith calcite. At low τ (i.e. high CO_2, low cell size or low growth rate), the flux of carbon into the cell far exceeds intracellular processes, and all species plateau at the same value (**I**). The value of this plateau is heavier than that of the carbon entering the cell due to intracellular interconversion of carbon species and preferential loss of light carbon dioxide. **Low PIC:POC:** For a cell of low PIC:POC, as τ increases (**I-II**), the flux of isotopically heavy carbon leaving the chloroplast (depleted in light carbon by carbon fixation catalysed by RuBisCO) influences the isotopic composition of the coccolith vesicle. As τ increases further (**II-III**), the flux of carbon from the chloroplast, although isotopically increasingly heavy, tends towards zero, and Rayleigh-type fractionation within the coccolith vesicle itself (which removes isotopically heavy carbon) takes over, driving the pool to light values. **High PIC:POC:** For a cell of high PIC:POC, as τ increases (**I-IV**) the Rayleigh-type fractionation due to calcite precipitation drives the isotopic composition of the coccolith vesicle to light values. The effect of heavy carbon leaking from the chloroplast is obscured. Across all cells of all PIC:POC values, the trends in vital effects are moderated by the increased flux and isotopic composition of carbon entering the cell with increasing τ, which dampens the Rayleigh fractionation-type effects when τ is high.

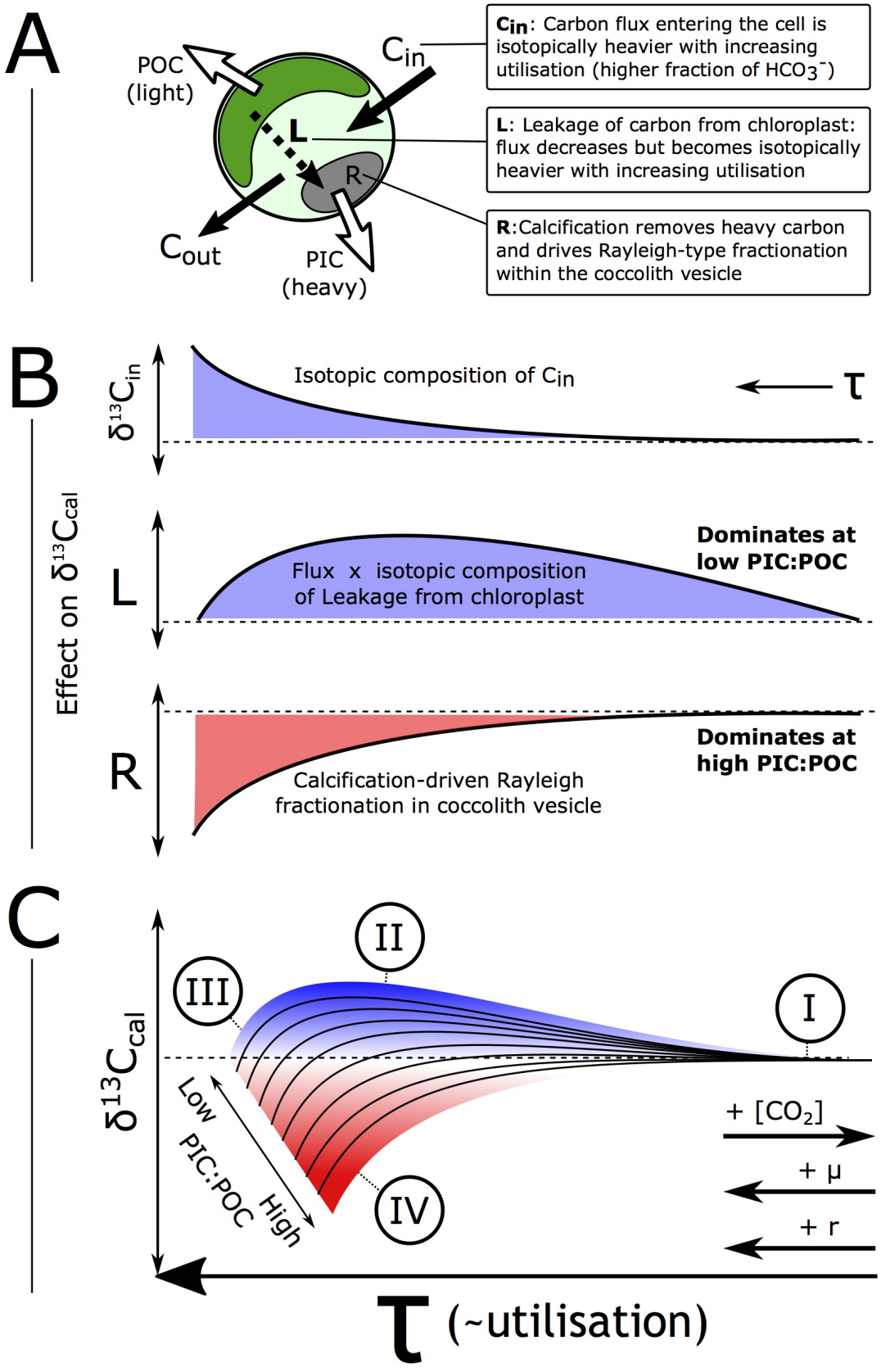
A
POC
(light)
Cin
L
R
Cout
PIC
(heavy)
Cin: Carbon flux entering the cell is isotopically heavier with increasing utilisation (higher fraction of HCO3-)
L: Leakage of carbon from chloroplast: flux decreases but becomes isotopically heavier with increasing utilisation
R:Calcification removes heavy carbon and drives Rayleigh-type fractionation within the coccolith vesicle
B
Effect on δ13Ccal
δ13Cin
Isotopic composition of Cin
τ
L
Flux x isotopic composition of Leakage from chloroplast
Dominates at low PIC:POC
R
Calcification-driven Rayleigh fractionation in coccolith vesicle
Dominates at high PIC:POC
C
δ13Ccal
II
III
I
IV
Low PIC:POC High
+ [CO2]
+ μ
+ r
τ (~utilisation)

decreasing CO_2 is dampened by the increased isotopic composition and flux of carbon entering the cell due to increased membrane permeability to bicarbonate. This synthesis is an alternative to the only other relevant modelling study of carbon isotopes in coccolith calcite (Bolton & Stoll, 2013), which suggests that the cell (and thus calcite) becomes isotopically lighter with increased active transport of isotopically heavy HCO_3^- to the chloroplast.

3.4.2 Bicarbonate fluxes

The role of HCO_3^- in fulfilling the substantial carbon requirements of coccolithophores is poorly understood (Herfort *et al.*, 2002; Kottmeier *et al.*, 2014; Mackinder *et al.*, 2011), and HCO_3^- fluxes have been treated very differently in isotopic models across the literature (Bolton & Stoll, 2013; Holtz *et al.*, 2014, 2015; Keller & Morel, 1999, see also Table.3.1). The model presented here assumes that HCO_3^- moves across membranes at a rate proportional to its concentration on the proximal side of the membrane; effectively parameterising HCO_3^- transport as analogous to passive diffusion. The formulation used here also allows membrane permeability to HCO_3^- to change in response to cellular carbon utilisation, but within the model, this response is not obligatory. Constraining the universal parameters that describe these membrane permeabilities with data, leaves open the possibility of membranes being non-adaptive (in response to increased utilisation) in their permeability to HCO_3^-, or even entirely impermeable to HCO_3^-. However, the model parameters that the data constrains are consistent with the most recent literature in describing approximately the same base-level permeability to HCO_3^- (Hopkinson *et al.*, 2011) and a significantly increased contribution of bicarbonate to the cell at low $[CO_2]$ (Bach *et al.*, 2013; Kottmeier *et al.*, 2014; Rost *et al.*, 2003, 2002). If cellular membranes are prescribed to be impermeable to HCO_3^- *a priori*, or do not allow increased permeability at high utilisation, the model does not fit the data satisfactorily.

HCO_3^- is thought to move across membranes in coccolithophores facilitated by anion exchange proteins (Herfort *et al.*, 2002; Mackinder *et al.*, 2011; von Dassow *et al.*, 2009), so HCO_3^- transport can be driven by a strong gradient in other ions such as Na^+ or Cl^- (Romero *et al.*, 2013). For the assumption used here of HCO_3^- concentration-driven HCO_3^- transport to be valid, the trans-membrane gradient in the co-ported ion must be close to zero, however there is a dearth of evidence regarding intracellular ionic concentrations in the literature. The next step in formulating a more exhaustive formulation of this model would be to explicitly consider all ionic species moving in and out of the cell assuming a steady state charge balance, which would give an independent means of calculating HCO_3^- fluxes, and would still accommodate the possibility of an up-regulation of anion exchange proteins at low CO_2. However, such an extension would require effective membrane permeabilities and transport mechanisms to all ionic species that traverse membranes (e.g. Na^+, Cl^-, Ca^{2+}, OH^-, H^+, HCO_3^-, etc...) to be known, thus introducing a number of unconstrained, or poorly constrained, parameters.

The assumption of HCO_3^- transport used in the model presented here requires its concentration in all intracellular compartments to be known, which in turn requires compartmental pH to be known. Intracellular pH in coccolithophores is not well understood however (Anning *et al.*, 1996; Suffrian *et al.*, 2011; Taylor *et al.*, 2011, 2012). In one of the very few studies making direct measurements Anning *et al.* (1996) reports intracellular compartmental pH values as being approximately the same in *E. huxleyi* and in *C. pelagicus*. These empirical measurements suggest that the pH of the CP is relatively high ($\sim$ pH 8) and that the pH of the CV is relatively low ($\sim$ 7.1).

3.4.3 Intracellular pH and $\Omega_{cal\,CV}$

Due to the fairly small dataset available, it was preferable to minimise the number of parameters constrained by the data. The model was therefore fitted with the only

multi-species, compartment-specific empirically measured pH values available in the literature (Anning *et al.*, 1996). With these pH values, and the described model set-up, relying on two-way concentration-driven movement of CO_2 and HCO_3^-, the calcite saturation state in the coccolith vesicle ($\Omega_{cal\,CV}$) is significantly below unity (Fig.3.12.iv). Calcite precipitation is thermodynamically unfavourable when $\Omega_{cal\,CV}$ is below unity (Zeebe & Wolf-Gladrow, 2001), so it is important to test the robustness of the model conclusions presented here with significantly higher, more realistic values of $\Omega_{cal\,CV}$.

$\Omega_{cal\,CV}$ is controlled by $[CO_3^{2-}]$ and $[Ca^{2+}]$, and by the solubility product of calcite in seawater (K_{SP}), which is a function of salinity, temperature and pressure (Mucci, 1983; Zeebe & Wolf-Gladrow, 2001). Many studies have invoked high pH in the CV, such that a larger proportion of DIC is in the form CO_3^{2-} (e.g. Raven & Crawfurd, 2012; Stoll *et al.*, 2011). Holtz *et al.* (2014) hypothesised an H^+ ATPase-coupled HCO_3^- and Ca^{2+} pump directing a flux from the cytosol into the coccolith vesicle, with no prescribed mechanism for loss of HCO_3^- from the CV other than via calcification, or via uncatalysed dehydration and leakage of CO_2. In this model, CO_3^{2-} and Ca^{2+} accumulate so that values of $\Omega_{cal\,CV}$ exceeding 10 are generated (Holtz *et al.*, 2014).

Calcification may be possible at lower pH or DIC by locally altering the value of K_{SP} or $[Ca^{2+}]$. Values of $[Ca^{2+}]$ in the CV have not been measured directly with much success (Anning *et al.*, 1996; Langer *et al.*, 2007), but hypothetical estimates vary across an order of magnitude (0.5 mM - 4 mM; Gussone *et al.*, 2006; Holtz *et al.*, 2014; Langer *et al.*, 2006). K_{SP} is two orders of magnitude higher (i.e. $\Omega_{cal\,CV}$ is lower and calcite precipitation is less likely to occur) in water with a salinity typical of seawater compared with distilled water (calculated from Mucci, 1983). The salinity of the CV, however, is likely to be close to that of seawater due to the osmotic pressure that is associated with large salinity differences (Kirst, 1990). Additionally, calcification in coccolithophores occurs in the presence of acidic polysaccharides,

which are embedded within, and distributed throughout, the whole coccolith calcite lattice (Marsh, 2003; Westbroek *et al.*, 1973; Young & Henriksen, 2003). These macromolecules bind to Ca^{2+} ions (Jong *et al.*, 1976) and create a microenvironment at the surface of the polysaccharide that probably has an anomalously high saturation state. The localised calcite precipitation-inducing effect on carbonate chemistry may even allow coccoliths to be built in a mostly calcite under-saturated vesicle. Little work has been undertaken to understand the localised influences of polysaccharides on carbonate chemistry however.

A number of scenarios were used to test the model-derived conclusions presented here regarding the origin of VEs (see Appendix D). Firstly, pH was allowed to vary and be constrained by the model in all compartments in addition to the three membrane permeability parameters and ϵ_{fe} (scenario iii; Fig.D.2 and Fig.D.5B). Secondly, in addition to constraining all pHs with the model, $\Omega_{cal\,CV}$ was artificially elevated by suppressing bicarbonate efflux from the CV (scenario ii; Fig.D.3 and Fig.D.6A). This scenario is similar to the model described by Holtz *et al.* (2014) except that bicarbonate uptake into the CV was here maintained as a facilitated, down-gradient flux, rather than active pumping. Lastly, in addition to suppressing HCO_3^- efflux from the CV, to further increase the saturation state of the CV, the pH was set to be a minimum of 8.3 (scenario i; Fig.D.4 and Fig.D.6B. The latter is the only scenario whereby the coccolith vesicle has a saturation state of greater than 1 across all DIC values at the salinity of seawater (Fig.3.12A.i). In all the described scenarios, the model reproduces fundamentally similar results to those described in Section 3.4.1 (see Appendix D). Following parameter fitting to the isotopic data (see Table D.1 for constrained parameter values), PIC:POC of greater or less than a value close to 1 determines the direction of VE, and the magnitude of the VE and of the fractionation of carbon into organic matter, is moderated by τ.

The $[CO_2]$ of the chloroplast was also inferred for each of the scenarios described above. Under present day ambient $[CO_2]$, $[CO_2]$ of the chloroplast was never seen to

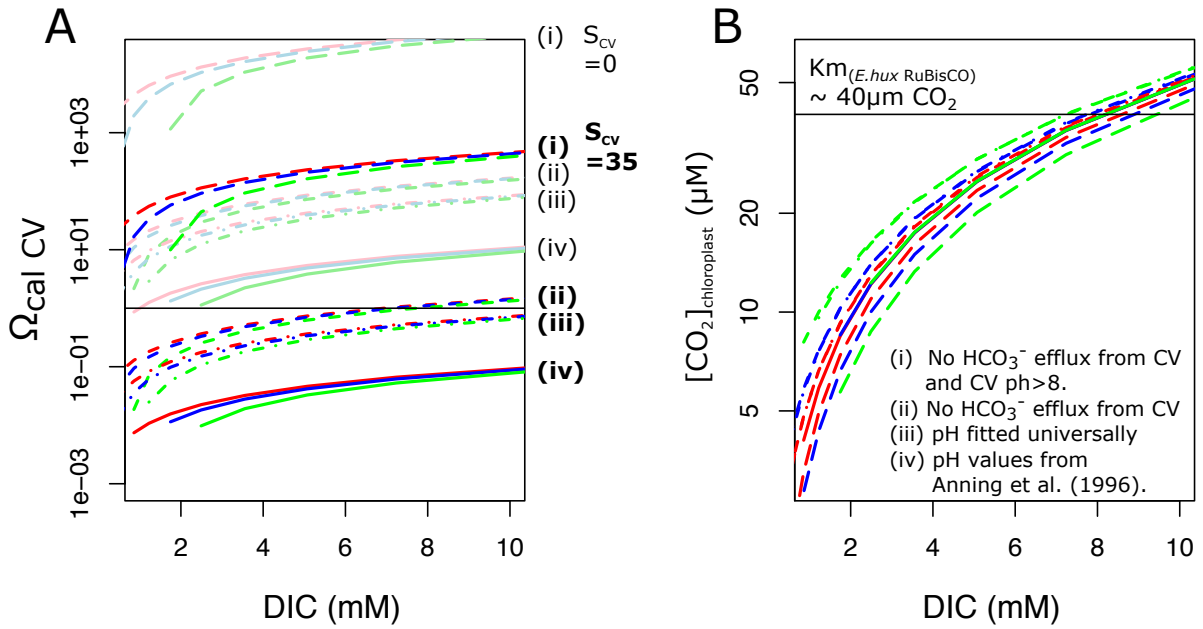

Figure 3.12: $\Omega_{cal\,CV}$ and $[CO_2]_{CP}$ for a range of different scenarios: **(i)** No HCO3- efflux from CV and CV pH >8. pH fitted elsewhere. **(ii)** No HCO3- efflux from CV and pH fitted in all compartments. **(iii)** All membranes 2-way permeable to HCO3-. pH fitted in all compartments. **(iv)** All membranes 2-way permeable to HCO3-. pH values prescribed *a priori* (Anning *et al.*, 1996). All of the described scenarios produce the same model behaviour (see Appendix D). **A:** $\Omega_{cal} = [Ca^{2+}][CO_3^{2-}]$ / K_{sp}, where K_{sp} is a strong function of salinity (S; Mucci, 1983). Values of Ω_{cal} are calculated for distilled water (light colours) and for seawater (bold colours) salinities; representing end-member salinities for the coccolith vesicle. $[Ca^{2+}]$ is assumed to be 3-4 mM, as inferred by Holtz *et al.* (2014). **B:** $[CO_2]_{CP}$ increases with DIC, and is always below the Km of a typical coccolithophore RuBisCO, but is likely to exceed this value in the low pH medium of the pyrenoid.

reach a level comparable with the Michaelis-Menten half-saturation constant of RuBisCO typical for a coccolithophore ($\sim$40 μM CO_2; Boller *et al.*, 2011, Fig.3.12B), as would be expected for maximum photosynthetic efficiency. However, the pyrenoid/thylakoid complex is a small region of very low pH where RuBisCO and CO_2 are in far higher concentration than in the rest of the chloroplast (Badger & Andrews, 1998; Hopkinson, 2014). Locally therefore, the low $[CO_2]$ inferred here for the chloroplast is unlikely to be reflective of the environment immediately in the vicinity of the RuBisCO enzyme.

3.5 Conclusions

In this chapter I have described a viable hypothesis for the source of vital effects in coccolith calcite, which is consistent with traditional isotope models for phytoplankton and the current biological literature concerning how coccolithophores acquire carbon. This is an alternative to the only other relevant model to date (Bolton & Stoll, 2013). The hypothesis presented here is based on a novel set of results from culture manipulation experiments, with a large number of variables, interpreted with a new isotopic flux model. The direction of the calcite vital effect is controlled dominantly by the photosynthesis to calcification ratio, whilst the magnitude of the vital effect increases with increased cellular carbon utilisation. Utilisation can be approximated with the compound dimensionless utilisation parameter τ, which is a linear product of cell size and growth rate, and the inverse of $[CO_2]$. At the intracellular equilibrium limit, τ and PIC:POC describe the isotopic system in its entirety. $\delta^{13}C_{org}$ is lightest at low utilisation and heaviest at high utilisation, and is relatively insensitive to PIC:POC. Although the pattern and mechanisms are robust, the absolute magnitude of carbon isotopic fractionation into organic and inorganic carbon depends on initial assumptions, which would be improved with refined estimates of parameters such as compartment-specific pH. The model, although incapable of explicitly describing oxygen due to the absence of kinetic fractionation factors of carbonate chemistry reactions, is qualitatively consistent with oxygen isotopes in calcite. In the next chapter, the understanding gained from these culture data and model are applied to the geological record.

Chapter 4

Calcite time-capsules preserve a molecule-specific record of pCO_2: development of a new paleobarometer.

4.1 Introduction

Quantifying the partial pressure of carbon dioxide in the atmosphere (pCO_{2atm}) during periods of climatic upheaval in the past is essential for accurately predicting the climatic response to anthropogenic CO_2 emissions over the coming decades to centuries (Alverson *et al.*, 2003). The most ambitious goal of reconstructing ancient pCO_{2atm} in this regard is through studying catastrophic events in Earth's past that may be considered to be analogous to anthropogenic emissions (Bains *et al.*, 2000; Ridgwell & Schmidt, 2010). Such events are extremely rare however, and there appears to be no perfect analogues for the modern situation, primarily because the current rate of pCO_{2atm} change seems to be unprecedented (IPCC, 2014). Beyond being an interesting scientific question in its own right, a more modest goal of understanding pCO_{2atm} in the geological past is in testing the very biogeochemical and climate models that are used for predicting future climate (Ridgwell & Zeebe, 2005; Ridgwell & Schmidt, 2010; Zeebe & Westbroek, 2003).

The longest continuous direct record of atmospheric pCO_2 is the Keeling curve, representing the partial pressure of CO_2 in dry air, which has been measured on

Mauna Loa since 1958 (`http://www.esrl.noaa.gov/gmd/ccgg/trends`; Fig. 4.1). Before direct measurements, pCO_{2atm} over the past 800 ky has been reconstructed from bubbles preserved in ice-cores (Lüthi *et al.*, 2008), with age corrections accounting for compaction of ice and diffusion of air (Fig. 4.1). There are no known samples of reliably untainted air more ancient than that trapped in the ice at the bottom of the deepest Antarctic ice core (Elderfield *et al.*, 2012). To infer pCO_2 in the very distant past therefore, we must use proxies. Paleoclimate proxies are models that constitute a means of indirectly inferring an environmental parameter from a time in the past, through the measurement of one or more physical characteristics, preserved in contemporaneous material. All proxy estimates of pCO_{2atm} are heavily caveatted, and consistency and reproducibility of reconstructions beyond 1 Ma is poor (Beerling & Royer, 2011). A reliable means of measuring pCO_{2atm} in the geological past is currently an urgent requirement for paleoclimate research. Proxies that have been used to reconstruct pCO_{2atm} over the last 300 Ma (Fig. 4.1; see caption for references) include: stomatal indices, boron isotopes and B/Ca ratios in biogenic calcite (via pH), carbon isotopic isotopic composition of fossil soils (paleosols), rare abiotic sodium carbonate minerals (the stability of these minerals are strongly dependent on $[CO_2]$), and a range of proxies that take advantage of the strong isotopic fractionation of carbon during photosynthetic carbon fixation catalysed by the enzyme RuBisCO. For a recent review of proxies for pCO_{2atm}, the reader is referred to Royer (2014), although novel proxies are continually emerging (e.g. Austin & Schroeder, 2014; Bottini *et al.*, 2014; Franks *et al.*, 2013, 2014; Pauly *et al.*, 2015).

Here I present and test a new approach for inferring $[CO_2]$ of ancient seawater. This approach uses a state-of-the-art technique for extracting and isotopically analysing nannogram-scale samples of a specific organic molecule from within fossil coccolith calcite, in combination with established techniques for taxonomic separation of coccoliths by size, and isotopic analysis of calcite. These results are analysed using the model described in Chapter 3.

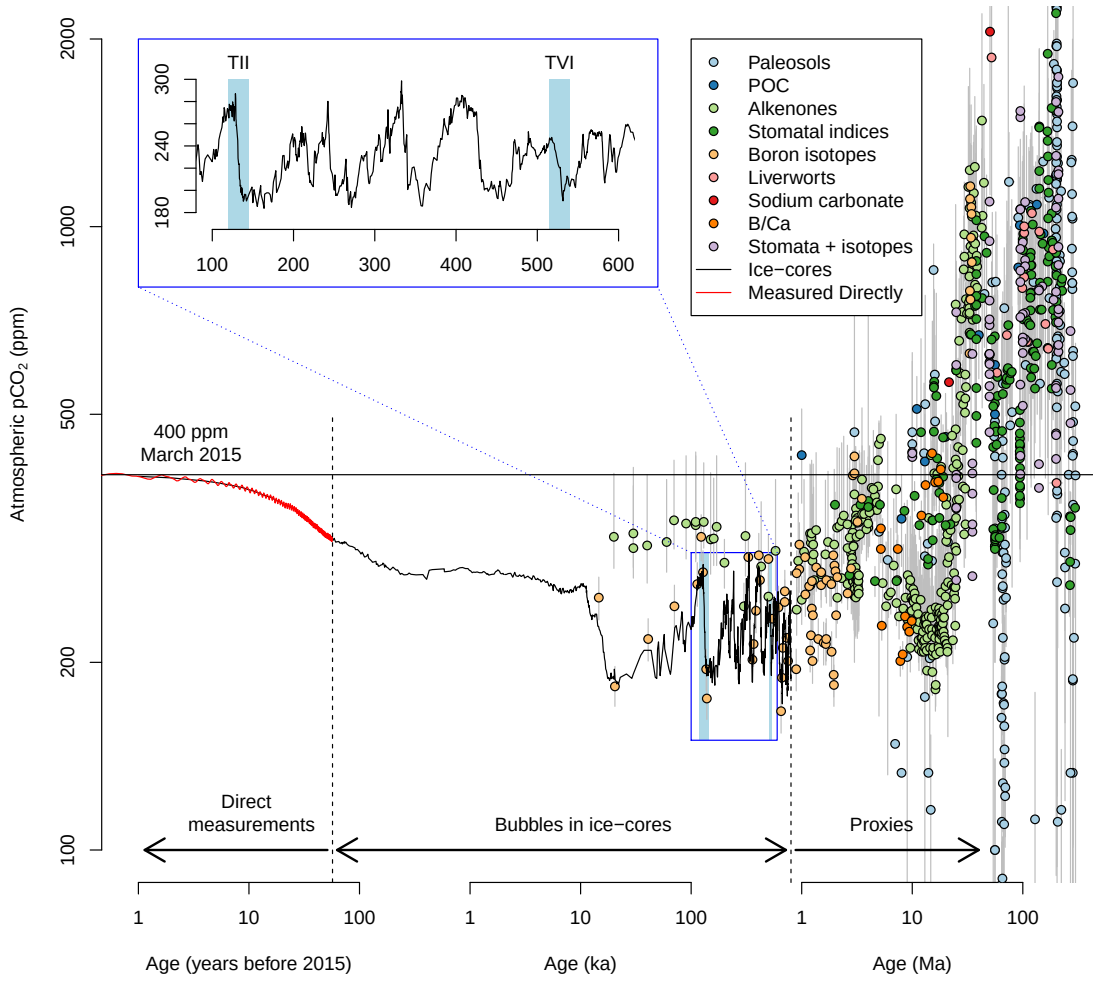

Figure 4.1: Geological history of pCO_{2atm} inferred over a range of timescales, and with a range of methods. From most to least accurate, pCO_{2atm} reconstructions are based on: **Red curve;** Daily pCO_{2atm} measurements from Mauna Loa (`http://www.esrl.noaa.gov/gmd/ccgg/trends`); **Black curve:** pCO_{2atm} reconstructed from gas trapped in ice (Bauska *et al.*, 2015; Lüthi *et al.*, 2008; Marcott *et al.*, 2014), and **Coloured points:** various deep-time pCO_{2atm} proxies (Badger *et al.*, 2013b; Beerling & Royer, 2011; Franks *et al.*, 2014; Hönisch *et al.*, 2009; Zhang *et al.*, 2013). See Beerling & Royer (2011) for the comprehensive list of earlier references.

4.1.1 pCO_{2atm} proxies based on biogenic $\delta^{13}C$

During photosynthetic carbon fixation by the enzyme Ribulose-1,5-bisphosphate carboxylase/oxygenase (RuBisCO), a strong isotopic kinetic fractionation occurs, with the light isotope of carbon (^{12}C) preferentially incorporated into organic matter over the heavy isotope (^{13}C) (Berry, 1989; Boller *et al.*, 2015, 2011; Guy *et al.*, 1993; Laws *et al.*, 1995). The basal premise of this group of proxies is that the ambient concentration of CO_2 determines the passive diffusive supply of carbon to the cell, and therefore the isotopic drift in the intracellular carbon pool in a Rayleigh fractionation-type scenario (Laws *et al.*, 1997; Popp *et al.*, 1998). Although details differ between approaches, generally the fractionation between organic matter and the external carbon source is considered to be a function of cell size, growth rate, and the relative ratio of bicarbonate to CO_2 taken into the cell (see Table 3.1 for summary of models to date). This approach has been applied to terrestrial plants, including Liverworts (Fletcher *et al.*, 2007), and recently in combination with an analysis of stomatal density (Franks *et al.*, 2014), but by far the dominant subject matter has been single-celled marine phytoplankton. This approach began as a fairly primitive empirical tool, using isotopic analysis of bulk sedimentary marine particulate organic matter (POC) as representative of phytoplankton organic matter, and sedimentary carbonate as indicative of the isotopic composition of DIC, with the difference correlating to the apparent fractionation (Freeman & Hayes, 1992; Hollander & McKenzie, 1991). Isotopic analysis of bulk organic matter is vulnerable to biases introduced by changes in the taxonomic make-up of the assemblage contributing to organic matter in sediment however (Burkhardt *et al.*, 1999). A significant step forward in terms of reproducibility occurred when specific compounds called alkenones were analysed as representative of organic matter (Jasper & Hayes, 1990; Pagani, 2002). Alkenones are a group of ketones; highly durable, and degradation resistant membrane lipids produced by only a single known family of open-ocean coccolithophore,

the Noëlaerhabdaceae (Laws *et al.*, 2001). An aspect of their molecular construction (the undersaturation ratio) is widely used as a deep time paleothermometer (Ho *et al.*, 2013; Sachs *et al.*, 2000). Not only does carbon isotopic analysis of alkenones limit any biological vital effect to a single taxon, but temperature reconstruction from the same molecule is a highly elegant means of accounting for the temperature effect on CO_2 dissolution (Pagani *et al.*, 2011). The influence of cell size has been considered by reconstructing cell size from fossil coccolithophores using the established relationship discussed in Chapter 2 (Henderiks, 2008; Henderiks & Pagani, 2007, 2008), but because alkenones are found in sediment and are not associated with a single size fraction, size cannot, with confidence, be explicitly factored in to any calculation. To account for the effects of growth rate, cell size and shape, the somewhat spurious all-encompassing parameter "b", is used (Bidigare & Fluegge, 1997; Jasper *et al.*, 1994; Pagani, 2002), which correlates linearly with phosphate concentration, and is incorporated into the estimate of pCO_{2atm} by inputting a range of realistic phosphate concentrations (Pagani *et al.*, 2005, 2011). The most recent innovation in this avenue of research took a parallel path when Rickaby *et al.* (2010a) considered the effect of cellular size on the isotopic composition of calcite *in vivo*. Vital effects (VEs); the isotopic deviation of biologically precipitated calcite from abiogenically precipitated calcite in identical conditions, were seen to be systematically related to size, and the difference between size fractions greatest at low $[CO_2]$. A contrasting but comparable dataset is presented in Chapter 3 of this thesis. Bolton & Stoll (2013) constructed a model to explain the cell size and $[CO_2]$ control on VEs, inferring that the observations could be explained by an up-regulation of active bicarbonate transport to the chloroplast at low CO_2, with the effect being greater in larger cells. They used this model to explain the pattern in vital effects from the Miocene to Recent as a result of decreasing pCO_{2atm}. Their model cannot however be used to make quantitative estimates of pCO_{2atm}, and the arguments made for carbon isotopes are not consistent with the trends observed in oxygen isotopes down-core or *in vivo*. The model

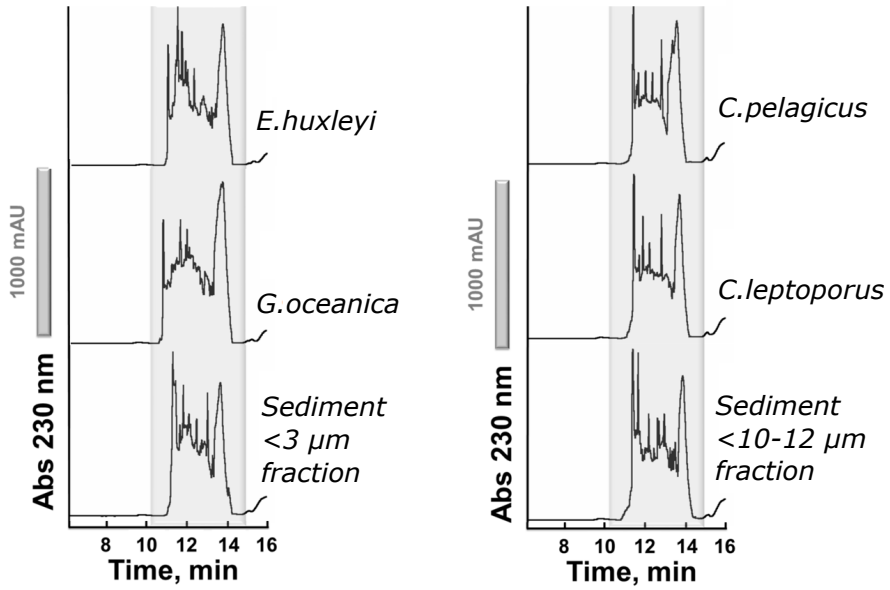

Figure 4.2: Results from HPLC analysis of polysaccharide extracted from cultures coccolithophores and from sediments, demonstrating the structural similarity of CAPs in all species here studied. The 0-3 μm sediment fraction contains *E. huxleyi* and *G. oceanica* coccoliths; both from the family Noëlaerhabdaceae. The 10-12 μm fraction contains a high purity of *C. pelagicus*. The results from *Calcidiscus leptoporus* are also shown.

described in Chapter 3 of this thesis is a further step forward, addressing unknown parameters explicitly. In order for the potential of this work to be realised, a means of obtaining size-specific organic carbon isotopic compositions in ancient samples is required. Fortunately, encased within the calcite crystals of coccoliths are organic molecules called polysaccharides, which can be extracted and analysed.

4.1.2 Coccolith-associated polysaccharides

Mineral-associated polyanions control biomineralisation in a wide range of organisms. In bivalve mollusc shells and in vertebrate dentin, the responsible macromolecules are proteins, but in coccolithophores, these are acidic polysaccharides (Marsh, 1994; Marsh *et al.*, 1992, 2002a). The carboxyl groups of galacturonic acid residues contained within coccolith-associated polysaccharides (CAPs) are thought to play the

dominant role in calcite precipitation (Wiedmer & Cassely, 2000). The CAP of *E. huxleyi* and the structurally homologous CAP of another highly studied coccolithophore, *Pleurochrysis carterae*, were found to be localized at the interface of growing crystals and the membrane of the mineralizing vesicle (Marsh *et al.*, 2002a; Westbroek *et al.*, 1984). *P.carterae* mutants lacking this CAP produce only proto-coccolith rings that do not develop into fully formed coccoliths (Marsh *et al.*, 2002a). Polysaccarides are actually preserved within the coccoliths that they aid in constructing, and as long as the calcite resists dissolution, the CAPs avoid degradation through geological time. The potential of these highly preserved molecules to temporally penetrate the geological record of coccolithophore organic carbon is seemingly limited only by the evolutionary emergence of coccoliths in the Late Triassic; CAPs have been found preserved in chalk from the Maastrichtian (65-70 Ma; Sand *et al.*, 2014), still with the quintessential properties of CAPs extracted from extant coccolithophores, and in our study we found CAPs in sediments from the Late Cenomanian (∼94Ma) and the Early Toarcian (∼184 Ma; Lee *et al.*, 2014)[1]. CAPs extracted from fossils from the last glacial inception (∼ 107ka) were found to be structurally identical to CAPs extracted from similar species grown in the laboratory (4.2; Lee *et al.*, 2014), suggesting that the integrity of these molecules is highly resistant to degradation.

4.2 Proxy concept

In coccolithophores, carbon enters the cell where it is used to form calcite and organic matter. Organic CAPs are encased within the calcite lattice, with the potential to be preserved alongside coccolith calcite in the fossil record (Fig. 4.3). The ability to extract and purify CAPs from fossil coccoliths in sediment presents an exciting new

[1]This work (Lee *et al.*, 2014) concerned the characterisation and uronic acid content of acidic polysaccharides extracted from coccoliths grown in culture and from the fossil record. This study was led by Renee Lee of the Oxford Earth Sciences department, and has been written up and submitted to *PNAS*. My role in this work was in size-separation of and polysaccharide extraction from the fossil samples, aiding with interpretation and with writing the paper.

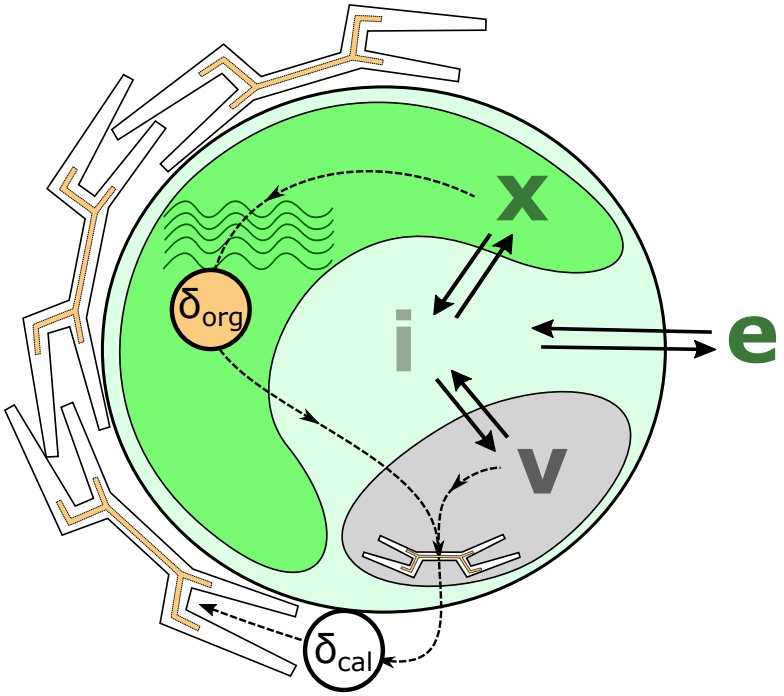

Figure 4.3: Carbon enters a coccolithophore cell in the form of CO_2 and HCO_3^-, and is reallocated to forming calcite in the coccolith vesicle and sugars through photosynthetic carbon fixation in the chloroplast; some of which become coccolith-associated acidic polysaccharides (CAPs). In the coccolith vesicle, calcite is precipitated onto a precursor organic base-plate scale, in the presence and under the influence of CAPs, which are trapped inside the crystal lattice. Following ejection from the cell, the coccolith preserves both organic and inorganic isotopic compositions, as well as containing morphometric information about cell size (see Chapter 2)

opportunity to measure the isotopic composition of organic coccolithophore biomass deep into the geological past. Unlike alkenones, which are putative storage lipids (Conte & Thompson, 1995), and following death of the cell are found disaffiliated from coccoliths in the organic component of sediment (Laws *et al.*, 2001; Sachs *et al.*, 2000), CAPs are preserved inside coccolith calcite, which in turn can be analysed morphometrically to infer cellular size (Chapter 2; Henderiks, 2008), and isotopically for $\delta^{13}C_{cal}$ (e.g. Bolton *et al.*, 2012; Dudley *et al.*, 1986). Additionally, in the modern open ocean alkenones are produced by only one family of extant coccolithophores, the Noëlaerhabdaceae (Marlowe *et al.*, 1990), and are not found in sediments older than 120Ma (Brassell & Dumitrescu, 2004); CAPs, by contrast, are preserved within coccoliths of a diverse range of taxa (Fig. 4.2), with a larger associated spatial and temporal range. The carbon isotopic composition of CAPs extracted from fossils can be determined using high-precision mass spectroscopy, and, as products of photosynthetic carbon fixation, must directly or indirectly reflect $\delta^{13}C_{org}$. $\delta^{13}C_{cal}$ of the calcite from which the CAPs were extracted can be straightforwardly obtained through traditional stable isotope mass spectroscopy.

As described in Chapter 3 of this thesis, both $\delta^{13}C_{org}$- $\delta^{13}C_{DIC}$ (ϵ_O) and $\delta^{13}C_{cal}$-$\delta^{13}C_{DIC}$ (ϵ_C) are predictable functions of cellular radius (r), growth rate (μ), PIC:POC and the external carbonate chemistry (e.g.[CO_2] and pH). Our approach is to invert the forward model to estimate [CO_2] from isotopic compositions. To do this, other influential parameters must be constrained by independent evidence, or, depending on the extent of covariance between parameters, may be constrained simultaneously by the model. To first order, the factors influencing ϵ_O are growth-rate, [CO_2] and cell size (Fig. 4.4), whereas ϵ_C is also very strongly influenced by PIC:POC. Without knowledge of PIC:POC for a given sediment size fraction, the relationship between [CO_2] and ϵ_C alone is obscure (Fig. 4.4). Dissecting τ, coccolith length scales linearly with coccolithophore cell radius (Chapter 2; Henderiks, 2008), so isotopic analysis of a narrow size fraction of sedimentary coccoliths is representative of a narrow size

range of r, and can be assumed to be approximately constant. The remaining variables, μ and $[CO_2]$, cannot be decoupled. Therefore, the value of τ constrained by the model can be interpreted as a value of $[CO_2]$, for a given value of μ, which must be prescribed.

At the intracellular equilibrium limit, for a given model parameterisation, the modelled system can be described in its entirety by three variables: PIC:POC, external pH and the compound variable τ (Appendix C):

$$\tau = \frac{\mu \rho r}{3 P_C [CO_2]} \tag{4.1}$$

where τ is analogous to the ratios traditionally used to describe cellular carbon utilisation, and to explain isotopic fractionation in phytoplankton. Cellular carbon density (ρ) and cellular membrane permeability to CO_2 (P_C) are assumed constant, and their values are calibrated *in vivo* together with membrane permeability to HCO_3^- (and the dependence of this permeability on utilisation) and the effective isotopic fractionation by RuBisCO. The consequence of μ, $[CO_2]$ and r being combined in a single compound variable at the equilibrium limit is that they cannot be decoupled without an independent estimate of any particular variable. The intracellular carbonate system is not in perfect chemical and isotopic equilibrium (because if it were, vital effects in oxygen would disappear). However, given the probable localisation of [CA] (Chapter 3) the degree to which it is in disequilibrium is unlikely to decouple the effects of μ and of $[CO_2]$ to a large enough extent to enable these variables to be resolved simultaneously. To first order therefore, the cell will be considered in terms of τ and PIC:POC alone.

Calculating absolute isotopic fractionation factors requires knowledge of $\delta^{13}C_{DIC}$ of surface seawater, which is usually reconstructed using proxies based on planktonic foraminifera or fish teeth, but which are associated with additional uncertainty, and may introduce artefacts. It is therefore useful to bypass $\delta^{13}C_{DIC}$, and apply understanding gained from our isotopic flux model to the differential effect of $[CO_2]$ on

$\delta^{13}C_{org}$ and $\delta^{13}C_{cal}$ in a single sample, and between different size fractions exhibiting contrasting cellular parameters such as radius and PIC:POC. At constant μ and r, the difference between the $\delta^{13}C_{cal}$ of coccoliths produced by cells of contrasting PIC:POC (ΔC) decreases at high [CO_2] (Fig. 4.4). When all but [CO_2] is held constant, ΔC can therefore be used to estimate [CO_2]. The difference between $\delta^{13}C_{org}$ and $\delta^{13}C_{cal}$ (ΔB and ΔD) always increases with increasing [CO_2] at constant r and μ, with the magnitude of the effect being controlled by PIC:POC (Fig. 4.4). The difference between the isotopic compositions of organic matter of different fractions (ΔA) is potentially useful due to the independence from PIC:POC, but if ΔB, ΔC and ΔD are known, provides no more information.

As a test of the sensitivity of this proxy approach to [CO_2] in nature, and across geological time, we investigated a period of known pCO_{2atm} change. Samples spanning the penultimate glacial termination (TII), from ODP site 1123 in the southernmost Pacific Ocean, were analysed. Details of the site are provided in Section 2.2.2.1 of Chapter 2. First these data are interpreted qualitatively based on the relationships predicted by the isotopic flux model (Fig. 4.4). As [CO_2] and μ cannot be decoupled, inferred changes in either parameter should be considered as a relative change - i.e. a doubling of growth rate is equivalent to a halving of [CO_2]. Secondly, the model will be used to quantitatively interpret these data directly using the model parameterisation for the *a priori* prescribed compartment-specific pH values of Anning *et al.* (1996).

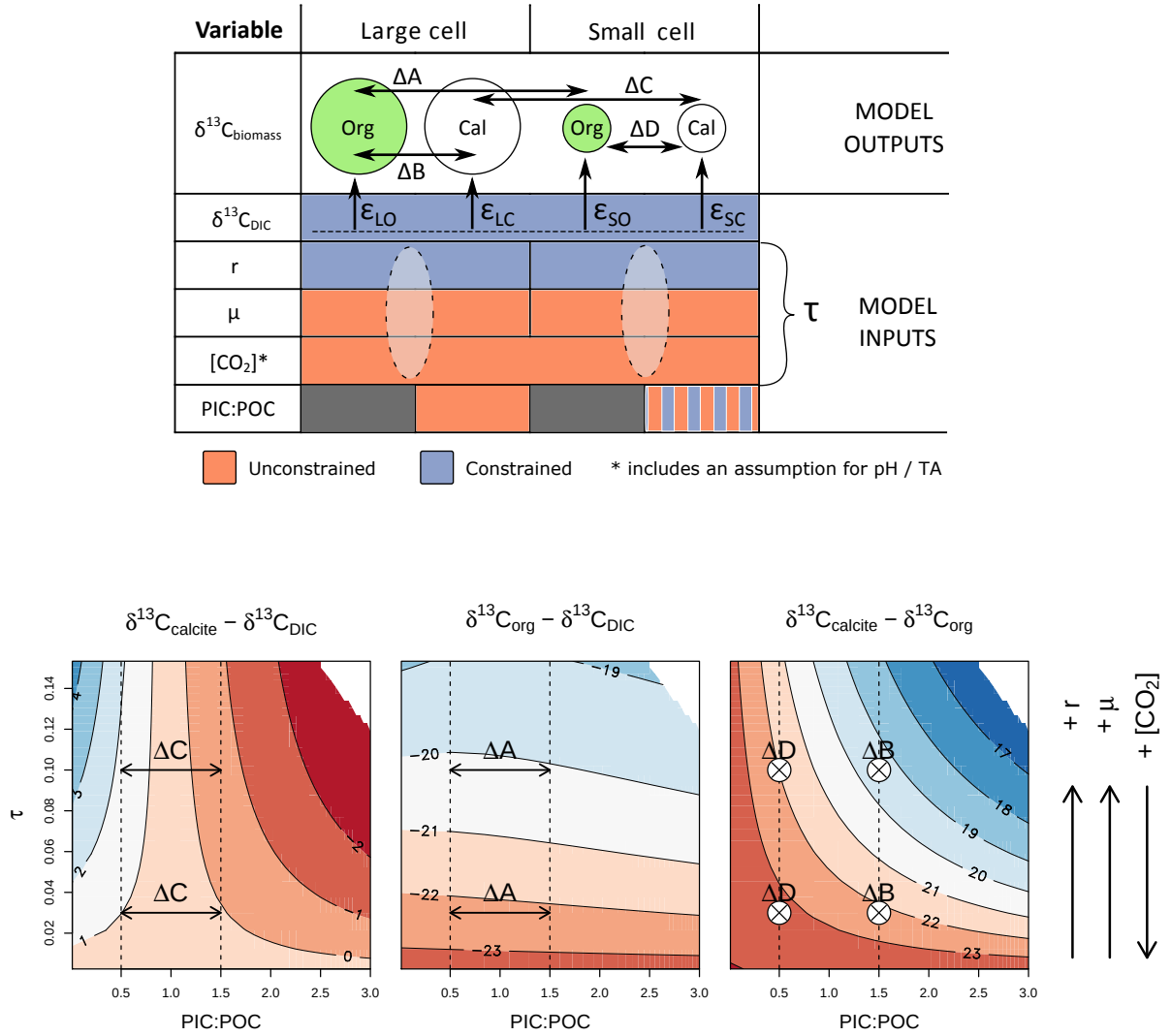

Figure 4.4: Top: parameters influencing $\delta^{13}C_{org}$ and $\delta^{13}C_{cal}$ in large and small size fractions. Boxes without a division denote a shared variable. r, μ and $[CO_2]$ all contribute to the value of τ (Eq. 4.1) and cannot be decoupled. PIC:POC in small cells may be loosely constrained using equations from Chapter 2. **Bottom:** Model output (Chapter 3) describing theoretical carbon isotopic compositions of inorganic (*left*) and organic (*middle*) material relative to $\delta^{13}C_{DIC}$, and $\delta^{13}C_{cal}$- $\delta^{13}C_{org}$ (right) over a range of PIC:POC and τ. The double headed arrows point to the difference between a cell with a PIC:POC typical of *E. huxleyi* (left) and a typical *C. pelagicus* (right); the number of $\delta^{13}C_{cal}$ contours crossed decreases with decreasing τ.

4.3 Methods

4.3.1 Size-separation

Twenty samples from ODP site 1123 were chosen to document changes over the penultimate glacial cycle (MIS 7-5), including ten samples spaced at higher resolution across the termination (TII). For each sample, approximately 5 g of sediment fine fraction (dry weight following wet-sieving at <63 μm), were separated by size according to the protocol of Minoletti *et al.* (2008). With this protocol, gentle ultrasonication was used to enable separation of micron-scale particles suspended in neutralised and buffered water with lazer-etched polycarbonate membranes. Following light-microscope taxonomic and morphometric assessment of sample smear slides, membrane pore-sizes were critically chosen to obtain two size fractions each approximately containing a single taxon. The resultant <3μm fraction was typically 2-3 g dry weight, containing members of the Noëlaerhabdaceae, *E. huxleyi* and *G. oceanica* (monophyletic at family level), and the 8 - 12 μm fraction was typically 0.2 - 0.5 g dry weight, containing *C. pelagicus* alone. The 3 - 8 μm fraction could not be further divided without obtaining a fraction containing multiple distantly related taxa, whilst the >12 μm fraction contained only very large coccoliths, and some foraminiferal debris.

4.3.2 Polysaccharide extraction

From the size separated samples, ∼1.0 g (dry weight) of the <3 μm fraction (hereafter referred to as the small fraction), and ∼0.1 g (dry weight) of the 8 - 12 μm fraction (hereafter referred to as the large fraction) were taken for the following analyses. The polysaccharide extraction protocol used here was adapted by Renee Lee of the Oxford Earth Sciences department from established protocols (Jong *et al.*, 1976; Marsh *et al.*, 1992; Ramus, 1977). The present study constitutes the first down-core application of this CAP extraction protocol. The process behind this protocol contains the following

steps: 1. Cleaning of size-separated coccolith fractions to remove any residual external organic matter. 2. Decalcification of cleaned coccoliths to break open the calcite. 3. Purification of acidic polysaccharides from within the coccolith.

1. **Cleaning:** Samples were suspended in 10 ml 1% (by volume) TritonX-100 and 4.5% (by volume) NaOCl in 0.05 M $NaHCO_3$, and gently shaken for 30 minutes. Samples were rinsed thoroughly three times by resuspension in MilliQ and centrifugation. Following suspension in 0.05 M NH_4HCO_3, further cleaning entailed repeated (4×) centrifugation through a gradient of Ludox TM-50 colloidal silica layered with a 0.2 g/mL sucrose solution, at 23,000 g for 20 min, before resuspension of clean coccoliths in 0.05 M NH_4HCO_3.

2. **PS extraction:** The cleaned coccoliths were decalcified with 0.5M EDTA (pH 8.0) at 4°C for 12 hours, before strong ultrasonication to fully break apart any remaining solid calcite. Following centrifugation at 31,000 g, the insoluble residue, consisting mostly of clays, was discarded.

3. **PS purification:** The largest organic macromolecules in the suspension were collected through diafiltration with 12 -14 kDa Amicon Ultracel membranes, and repeatedly rinsed with 20 mM Tris-HCl (pH 8.0). The filtrate was discarded, and organic residue was resuspended in 20 mM Tris-HCl, before anion exchange liquid chromatography. Using a HiTrap DEAE FF anion change column according to the manufacturers instructions, the large acidic organic molecules were separated from the large neutral organic molecules. The largest acidic molecules left in the column constituted a high purity sample of coccolith-associated polysaccharides (CAP). The CAP sample was eluted using 0.5 M NaCl, and diafiltered against MilliQ.

4.3.2.1 HPLC analysis of CAP

The fine-fraction of a very large IODP sample (∼30g) from site 1123 in the southern Pacific Ocean, from the last glacial inception (∼ 107 ka), was separated into size-delimited, approximately single-taxon fractions following the protocol of Minoletti *et al.* (2008) giving a *C. pelagicus* fraction (10-12 μm) and a Noëlaerhabdaceae fraction (0-3 μm). Extant species corresponding to those contained within the sediment samples were grown to high density in batch cultures in natural seawater. CAPs extracted from the size-separated fossil coccoliths and the coccoliths from cultures were biochemically characterised using reverse-phase high performance liquid chromatography (RP-HPLC), revealing that the CAPs preserved in sediments are almost structurally identical to those extracted from the cultured organisms (Fig. 4.2).

4.3.3 Inorganic carbon isotopes

Aliquots of all four size-separated sediment fractions, and an aliquot of bulk sediment for all 20 samples were taken for in-house isotopic analysis. Carbon and oxygen isotopic compositions of calcite were measured using a VG Isogas Prism II mass spectrometer with an on-line VG Isocarb common acid bath preparation system. Samples were dosed with acetone and dried at 60°C for at least 30 minutes. In the instrument they were reacted with purified phosphoric acid at 90°C. Calibration to PDB standard was via the international standard NBS-19 using the Oxford in-house (NOCZ) Carrara marble standard. Reproducibility of replicated standards was better than 0.1‰ for δ^{13}C and δ^{18}O (1σ) expressed relative to the V-PDB standard.

4.3.4 Organic carbon isotopes

The purified CAP samples were measured on a Thermo Delta Plus Advantage stable isotope mass spectrometer, with moving-wire interface, in collaboration with the Pearson Laboratory at Harvard University, MA, USA. The moving wire interface allows measurement of ng scale samples, and works as follows. A nickel moving wire is

passed through a cleaning oven, which is maintained at 950°C. This process oxidizes any organic carbon on the wire, removing it, and oxidizes the surface of the nickel wire, to form nickel oxide, which catalyzes the ensuing reaction. A syringe connected to an autosampler samples 4 μL of sample, and places a 0.8 μL droplet of the sample on the moving wire. The droplet moves through a second cooler oven ($\sim$150°C) where the solvent evaporates and the organic material clings to the wire. The wire then passes through a third, hot oven, where the organic material is combusted in the presence of a copper and platinum catalyst in a thin quartz tube to form CO_2. A known fraction of this CO_2 is dehydrated and passed through a capillary tube to a continuous-flow isotope ratio mass spectrometer. A more detailed description of the equipment and protocol is given in Sessions *et al.* (2005). Organic carbon measurements made in Harvard were calibrated for consistency with measurements made in Oxford, using a pectin standard in a dilution series.

4.3.4.1 Blanks

Blanks were created to test whether contamination is accrued at various points of the CAP extraction and purification protocol, and include:

1. Samples of laboratory-grade calcium carbonate, roasted at $\sim$600°C. These samples should contain no organic matter. These blanks test whether organic matter contamination occurs after decalcification with EDTA.

2. Samples where the calcium carbonate has been dissolved with acid, and then neutralised and washed. These samples contain organic matter, but no calcium carbonate. These blanks test the quality of the cleaning steps prior to decalcification with EDTA.

3. Picked, cleaned and crushed foraminifera. These blanks test whether foraminiferal debris (and the organic matter locked inside them) has the potential to contaminate the CAP sample via the extraction and purification protocol described above.

There was no systematic difference between the amount and isotopic composition of carbon detected across the different blanks, which suggests that the protocol introduces negligible contamination. The analysed properties of the blanks were used to estimate the isotopic composition and volume of carbon that must be accounted for in each sample.

4.3.4.2 Uncertainty in $\delta^{13}C_{org}$

For the isotopic analysis of CAP samples, a mass-balance correction was applied to account for the size and isotopic composition of the blank. The size of the sample relative to the size of the blank strongly influences the uncertainty in the estimate. If the sizes of sample and blank are similar, the actual estimate is also strongly affected. Across all blanks, the isotopic composition was -27±1‰. The average size of the blanks was taken as the size to be accounted for, with an uncertainty of 25%. This uncertainty is a conservative guess, which is larger than the standard deviation of blank size, and is reasonable from experience (Ann Pearson pers. comm). Propagating these uncertainties (Eq. 5.19 of Hayes, 1983), gives the errors shown in Fig. 4.5.

4.4 Results

Down-core evaluation of $\delta^{13}C_{cal}$ and $\delta^{18}O_{cal}$ of size-separated coccoliths, and of $\delta^{13}C_{org}$ represented by CAPs extracted from those same samples, reveals that carbon and oxygen isotopic VEs in coccolithophores, and the fractionation of carbon into organic matter, changes across TII. Isotopic results are compared with estimated values of $[CO_2]$ assumed to be in equilibrium with an assumed well mixed atmosphere ($[CO_2]_{eq.}$), calculated from pCO_{2atm} values from ice-cores (Lüthi *et al.*, 2008), and sea surface temperatures (SSTs) from Mg/Ca ratios in planktonic foraminifera (Fig. 4.5A; Section 2.2.2.2 for methods). As reported by previous studies (Bolton & Stoll, 2013; Bolton *et al.*, 2012; Hermoso, 2014), the smallest size fraction, consisting of members

of the family Noëlaerhabdaceae, contains the isotopically heaviest calcite in both carbon and oxygen, and the largest fraction, consisting of *C. pelagicus*, the lightest. A $\delta^{13}C_{DIC}$ reconstruction based on planktonic foraminiferal calcite, with a size and species-specific constant correction (+1.1‰ for *G. bulloides* 300 μm fraction; Spero & Lea, 1996) compared with the coccolith calcite results shows that although *C. pelagicus* is always lighter than $\delta^{13}C_{DIC}$, the Noëlaerhabdaceae fraction can be lighter or heavier than $\delta^{13}C_{DIC}$- although this depends heavily on the exact foraminiferal calcite to DIC correction. When $[CO_2]_{eq.}$ is low, the VE offset between the large and the small fraction is at a maximum in both carbon (3.1‰; Fig. 4.5B; ΔC) and oxygen (1.5‰; Fig. 4.5C), with the VE offset being driven to smaller values (1.8‰ in carbon and 0.5‰ in oxygen) with increasing $[CO_2]_{eq.}$ across the termination. These results in carbon isotopic vital effects are qualitatively consistent with the model prediction (Fig. 4.4; ΔC), and with results from the laboratory (Fig. 3.8; Rickaby *et al.*, 2010b). Quantitatively, the change in the isotopic difference between calcite carbon isotopes of the two size fractions over the glacial termination (a decrease of 1.3‰) is around the same as that observed in the laboratory for the same change in $[CO_2]$ (Fig. 3.8; $\sim$8 - 12 μM).

$\delta^{13}C_{org}$ reconstructions based on the isotopic composition of CAPs extracted from size-separated samples, are associated with somewhat larger uncertainties than $\delta^{13}C_{cal}$ measurements ($1\sigma \geq \sim$1‰; see section 4.3.4.2 for details). The largest (*C. pelagicus*) size fraction, constituted the smallest volume of calcite; the molar amount of CAP that this yielded was approximately the same size of the measurement blank, which led to large uncertainties. Nonetheless, the $\delta^{13}C_{DIC}$-corrected and $\delta^{13}C_{cal}$-referenced time-series appear to show a slight increase in the magnitude of fractionation under higher $[CO_2]_{eq.}$ (ϵ_{LO} & ΔB; Fig. 4.5D), which is as expected (Fig. 4.4). Uncertainties associated with isotopic compositions of CAPs extracted from the smaller size fraction were smaller due to a greater yield of CAP from the calcite fraction. These data show a clear increase in the magnitude of carbon isotopic fractionation into organic matter

(ϵ_{SO}; Fig. 4.5E) of $\sim$ 4‰ in response to a 3-4 μM increase in $[CO_2]_{eq.}$ across the glacial termination. This response is the same direction as expected, and is a similar magnitude to that observed across a similar $[CO_2]$ gradient in natural ocean samples in alkenones (Pagani *et al.*, 2002), but is around double the change expected based on laboratory experiments (Fig. 3.8). The difference between $\delta^{13}C_{org}$ and $\delta^{13}C_{cal}$ in this fraction (ΔD) also clearly increases under increasing $[CO_2]_{eq.}$ (Fig. 4.5E). Surprisingly, the larger size fraction exhibits lighter organic carbon isotopic compositions than the smaller fraction. If these cells lived contemporaneously in seawater that has the same isotopic composition and carbonate chemistry, the most parsimonious explanation of this observation is that the larger cells grew significantly more slowly. The difference between $\delta^{13}C_{org}$ of the different size fractions (ΔA) has too large an associated uncertainty to decipher any significant response to changing $[CO_2]_{eq.}$ (Fig. 4.5F).

4.5 Discussion

Where sample yield was sufficient to generate data with small uncertainties, the observed trends in the data are qualitatively as expected, with the isotopic offset between the calcite of small and large size fractions (ΔC) decreasing, and ϵ_{SO} increasing with increasing $[CO_2]_{eq.}$. The magnitude of isotopic change observed down-core is approximately the same as expected for ΔC and approximately double that expected for ϵ_{SO} compared with data from cultures. However, the model of Chapter 3 showed that besides $[CO_2]$ there are other influential parameters; PIC:POC, growth rate and cell size, which must be explicitly considered. An inverse modelling approach was therefore adapted to explore these data.

4.5.1 Inverse modelling of down-core data

Here, with the model presented in Chapter 3, an inverse approach is used to iteratively search parameter space for the combination of values of unconstrained variables that minimises the disagreement with the input data. In the surface ocean, $[CO_2]$ is

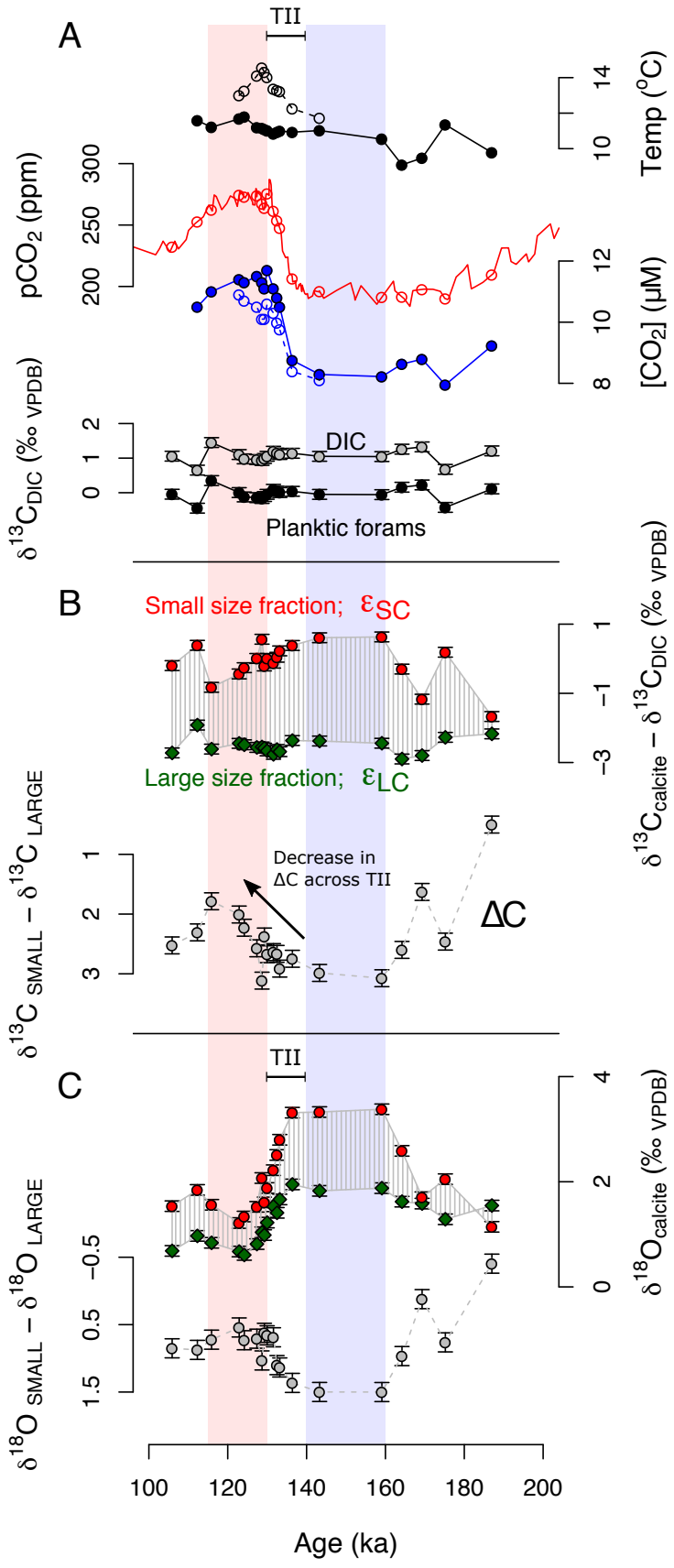

Figure 4.5: Down-core results - see Fig 4.4 for plots to aid interpretation, and for notation. **A:** Sea surface temperatures, pCO_{2atm}, $[CO_2]_{eq.}$ and $\delta^{13}C_{DIC}$ based on proxy reconstructions. Details of temperature and $[CO_2]_{eq.}$ reconstruction are given in section 2.2.2.1. $\delta^{13}C_{DIC}$ values are reconstructed from planktonic foraminifera $\delta^{13}C$, with a published size and species-specific correction (Spero & Lea, 1996). **B:** $\delta^{13}C_{DIC}$-corrected $\delta^{13}C_{cal}$ values for large (ϵ_{LC}; green diamonds) and small (ϵ_{SC};red circles) size fractions, and with the isotopic difference between these fractions (ΔC; grey circles). **C:** $\delta^{18}O_{\ calcite}$ values for large and small size fractions, and with the isotopic difference between these fractions.

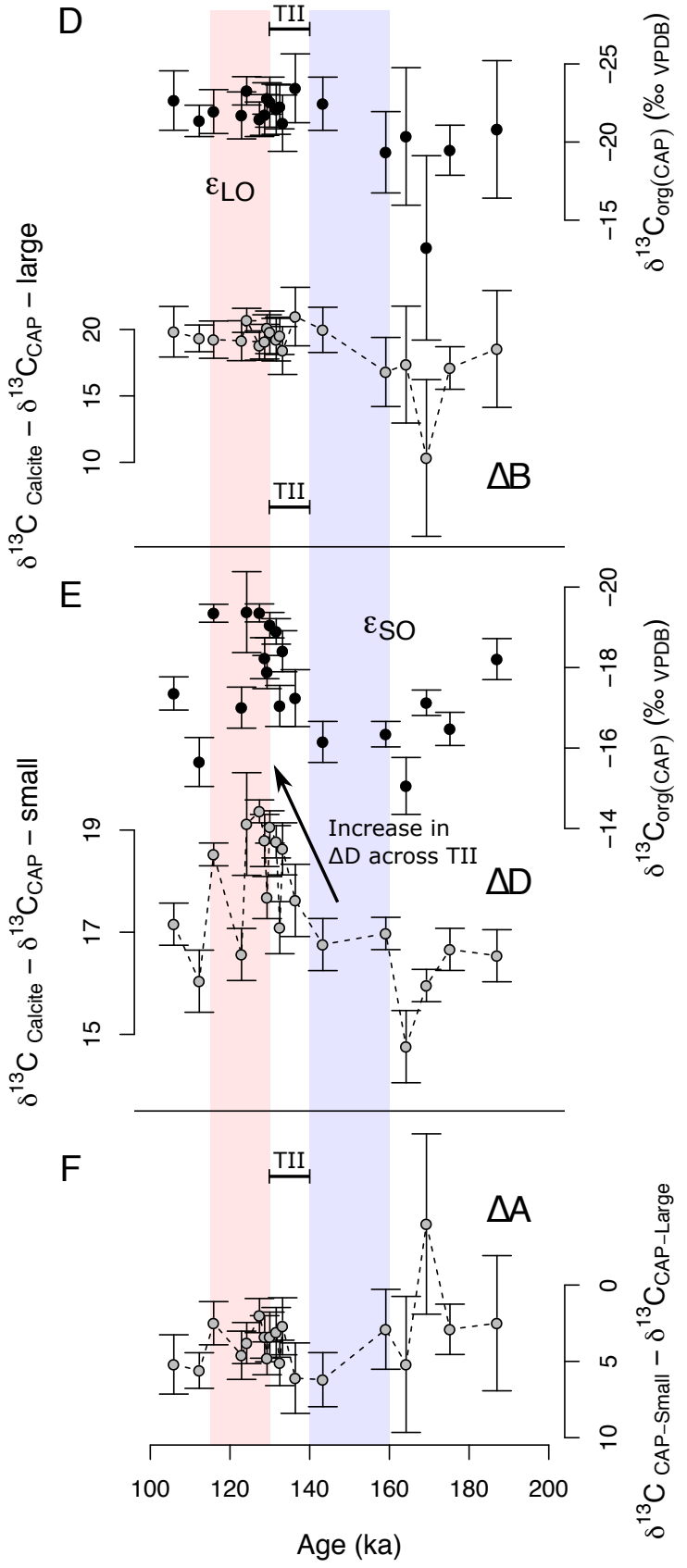

D: $\delta^{13}C_{DIC}$-corrected $\delta^{13}C_{\ CAP}$ values for the large size fraction (filled circles; ϵ_{LO}), and the isotopic difference between calcite and CAPs (hollow circles; ΔB); **E:** $\delta^{13}C_{DIC}$-corrected $\delta^{13}C_{\ CAP}$ values for the small size fraction (filled circles; ϵ_{SO}), and the isotopic difference between calcite and CAPs (hollow circles; ΔD); **F:** Difference between isotopic compositions of CAPs of the large and small size fractions. Error bars represent 1σ error.

unlikely to deviate far from $[CO_2]_{eq.}$ due to the relatively fast exchange of carbon between the surface ocean and atmosphere relative to the other processes that affect $[CO_2]$ and pCO_{2atm} (Zeebe & Wolf-Gladrow, 2001). Therefore, model-predicted $[CO_2]$ should not deviate far from $[CO_2]_{eq.}$. Due to the large uncertainty associated with $\delta^{13}C_{org}$ of the large size fraction, differences between size fractions cannot be used to constrain the model with confidence, so the absolute fractionation factors for $\delta^{13}C_{org}$ and $\delta^{13}C_{cal}$ are used, based on $\delta^{13}C_{DIC}$ reconstructed from foraminifera (Spero & Lea, 1996). $\delta^{13}C_{CAP}$ is initially assumed to be representative of $\delta^{13}C_{org}$ (but see section 4.5.1.3). Both the large and small size fractions were analysed to explore the propagated effect on uncertainty in $[CO_2]$ estimates of different degrees of uncertainty associated with isotopic data.

To fully constrain the forward model, once calibrated (Chapter 3), the external carbonate chemistry, r, PIC:POC, μ and $\delta^{13}C_{DIC}$ must be known. In this implementation, model parameters were fitted assuming pH values of Anning *et al.* (1996, scenario iv, Appendix D). It is important to note that the forward model estimates isotopic compositions when physiological parameters are prescribed, regardless of how realistic they are, as long as the *in silico* concentration of any carbon species is never required to be negative. There are therefore regions of parameter space that are reported as valid, but which do not exist in reality, so the onus is on the input values being realistic, for a meaningful interpretation. Here, the known variables are isotopic compositions, and $[CO_2]$, r, μ and PIC:POC are all desired outputs. An iterative approach is therefore adopted, minimising the disagreement between modelled isotope output and isotope data. As r, μ and $[CO_2]$ cannot be decoupled and constitute the compound parameter τ (section 4.2), it is τ and PIC:POC that the isotopic information constrains when parameter space is iteratively searched. Additional knowledge is required to extract $[CO_2]$ from τ by filling in the unknown values and rearranging Equation 4.1.

Cell radii (r) were estimated for each sediment size-fraction using the relationship established in Chapter 2. For the small (< 3 μm) Noëlaerhabdaceae fraction, the typical coccolithophore cell radius was taken to be 2.5 μm, and for the large (8 - 12 μm) *C. pelagicus* fraction it was taken to be 10μm. In the absence of a reliable proxy for growth rate, a range of realistic growth rates were pre-specified for both size fractions. Due to the large uncertainty associated with the isotopic values for each sample, pseudo-replicate datasets were generated based on a random resampling of assumed gaussian probability distributions defined by the expected value and the 1σ uncertainty calculated for each value. Ten pseudo replicate datasets for each of five prescribed growth rates were generated for every sample, for each size fraction. A misfit function was defined on the basis of the sum of squared differences between modelled and measured $\delta^{13}C_{org}$ and $\delta^{13}C_{cal}$ with equal weighting. This misfit function was minimised by searching the parameter space defined by PIC:POC and $[CO_2]$ for each pseudo-replicate dataset using an R implementation (Steven G. Johnson, 2014) of the constrained DIRECT_L algorithm (Gablonsky & Kelley, 2001). This analysis was carried out twice - firstly, $[CO_2]$ was varied along a vector in carbonate chemistry space assuming a constant seawater pH of 8.2, and secondly assuming a constant seawater total alkalinity (TA) of 2.35 mmol kg^{-1}. The assumptions of constant pH and of constant TA constitute end-member scenarios of respectively complete or negligible buffering of seawater pH by carbonate dissolution or precipitation following changes in $[CO_2]$ (Zeebe & Wolf-Gladrow, 2001).

4.5.1.1 Model results

The uncertainty associated with model-fitted values for τ and PIC:POC are mostly dictated by the uncertainties associated with values of $\delta^{13}C_{org}$. The large uncertainty in $\delta^{13}C_{org}$ leads to a poorly constrained output in the large size fraction highlighting the need for larger organic carbon samples and smaller associated uncertainties in isotopic compositions. The relatively small isotopic uncertainties in the small size

fraction, however, lead to a well-constrained output (Fig. 4.6). The large size fraction will not be discussed further. Estimates of τ in the small size fraction show a clear response to carbonate chemistry. Under the low $[CO_2]_{eq.}$ of the glacial (Fig. 4.6A), τ is high and decreases significantly across the glacial termination, before a rise to higher values following the interglacial (Fig. 4.6C). Across the range of prescribed growth rates, the trend in model-predicted $[CO_2]$ is consistent with $[CO_2]_{eq.}$ inferred from ice-core data (Fig. 4.6B). The magnitude of $[CO_2]$ predicted by the model however is approximately an order of magnitude lower than $[CO_2]_{eq.}$. PIC:POC is inferred to be at a minimum during the peak glacial, and increase in the interglacial (Fig. 4.6D), which is similar to the result described in Chapter 2. Whether constant pH or constant TA is assumed, the trends and magnitudes are almost identical.

4.5.1.2 Interpreting τ

τ shows a clear response to the environmental changes that occurred through the glacial cycle. As a compound variable consisting of $[CO_2]$, μ and r, with the latter two being poorly understood functions of other environmental parameters such as temperature, interpretation of τ is not straight forward. Despite having a relatively tight constraint on r through size-separation of coccoliths and the established relationship between coccoliths and cell size (Chapter 2; Henderiks, 2008), a cell-size shift within the isolated sediment fraction is possible. The small size fraction approximately corresponds to the Noëlaerhabdaceae of Chapter 2, which show an increase in size across termination II (Fig. 2.3). Laboratory experiments show that increases in $[CO_2]$ over the reconstructed $[CO_2]$ and temperature range for the species represented

Figure 4.6 (following page): Isotopically constrained model output for a range of representative growth rates. **A:** $[CO_2]_{eq.}$ based on pCO_{2atm} from ice-cores and SSTs from planktonic foraminifera, **B:** Modelled $[CO_2]$ for a range of possible growth rates, **C:** Model-constrained τ (Eq. 4.1), **D:** Model-constrained PIC:POC. Notice how τ and PIC:POC are well constrained, and are independent of μ, whereas $[CO_2]$ is a strong function of μ. $\delta^{13}C_{org}$ for the large size fraction has a large uncertainty, and so the model is too poorly constrained to resolve a clear response to changes in carbonate chemistry.

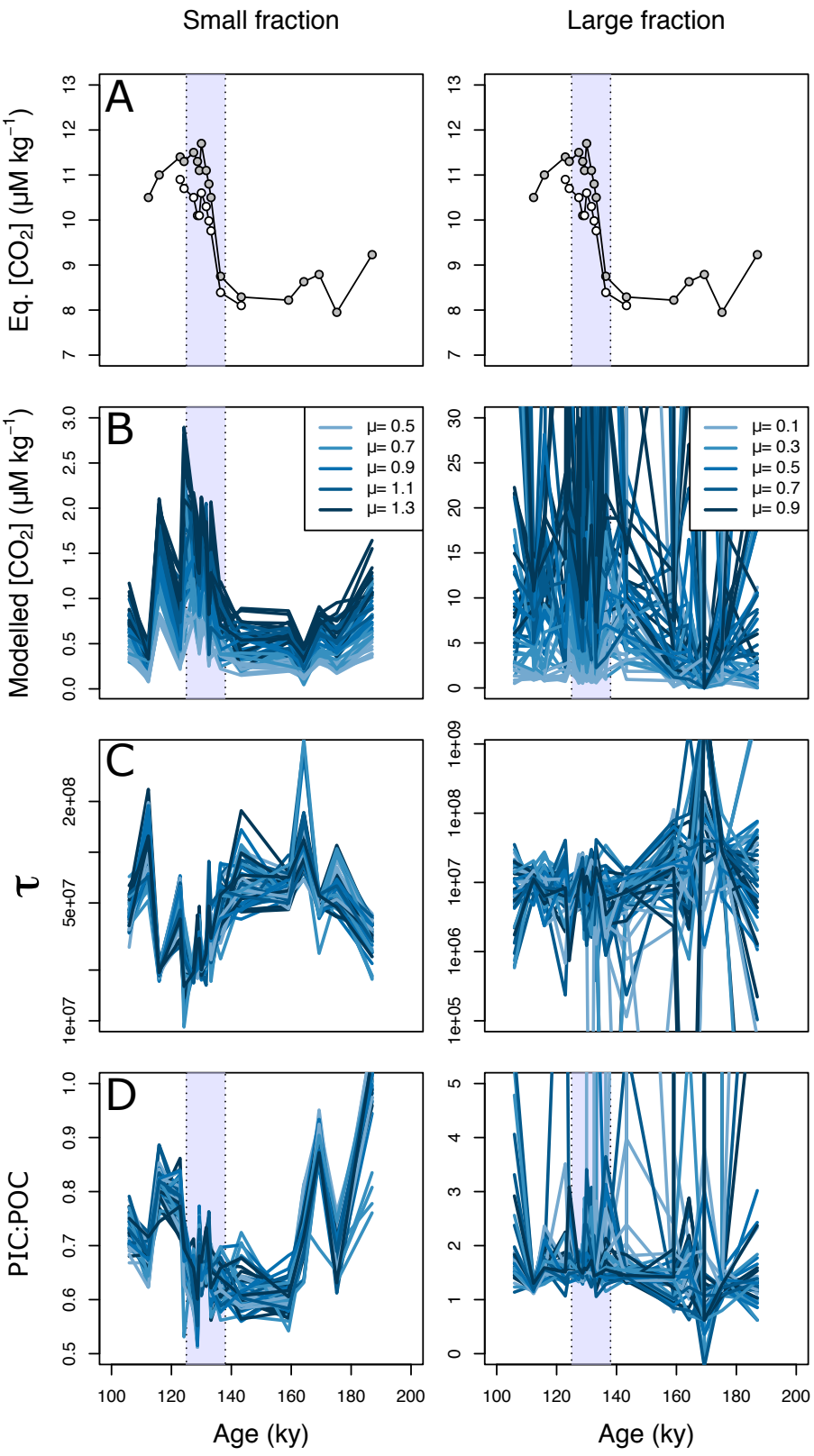
Small fraction
Large fraction
A
B
C
D
Eq. [CO2] (µM kg−1)
Modelled [CO2] (µM kg−1)
τ
PIC:POC
µ= 0.5
µ= 0.7
µ= 0.9
µ= 1.1
µ= 1.3
µ= 0.1
µ= 0.3
µ= 0.5
µ= 0.7
µ= 0.9
Age (ky)
Age (ky)

are most likely to lead to an increase in μ (Bach *et al.*, 2011; Sett *et al.*, 2014). Increases in μ and in r correspond to an increase in τ, which strongly suggests that the decrease in τ inferred from isotopic compositions is driven by the increase in $[CO_2]$.

Despite coherence in the trends, there is an order of magnitude discrepancy in the absolute predicted values of $[CO_2]$ and $[CO_2]_{eq.}$ for the given inputs. If $[CO_2]$ is assumed to be equal to $[CO_2]_{eq.}$, and prescribed as an input parameter, the growth-rate necessary to satisfy the isotopic compositions at the given cellular size is around 10 divisions per day, which is highly unrealistic (Sett *et al.*, 2014; Taylor *et al.*, 2007a). The boundary layer effect described in section 3.3.1.2 may account for up to half of this apparent discrepancy, if coccolithophores represented in this fraction do not produce external CA. In the absence of external CA, the $[CO_2]$ at the surface of the cell, and thus that recorded in the isotopic composition of the biomass, may be depleted when the rate of CO_2 uptake exceeds the reacto-diffusive supply rate to the surface of the cell.

4.5.1.3 Isotopic offset between CAP and bulk organic carbon

The low model $[CO_2]$ estimates are mostly caused by the magnitude of ϵ_{SO} ($\delta^{13}C_{org}$-$\delta^{13}C_{DIC}$ in small size fraction represented by CAPs) being smaller (i.e. less negative) than values observed in the laboratory for the same $[CO_2]$ range. The most likely explanation for this is a systematic offset between the isotopic composition of CAPs and bulk organic matter. The carbon isotopic composition of carbohydrates has been widely reported to be heavier than bulk organic matter by around 4 - 6 ‰ in bacteria (Benthien *et al.*, 2007; Teece & Fogel, 2007; van Dongen, 2002). This offset is due to kinetic fractionation processes that cause more derived organic molecules such as lipids and proteins to be depleted in the heavy isotope of carbon (Fiorini *et al.*, 2010), leaving molecules that have undergone less biochemical processing since the initial fixation of carbon, such as carbohydrates, relatively isotopically enriched (Teece & Fogel, 2007). CAPs are large, somewhat derived carbohydrates, and so although

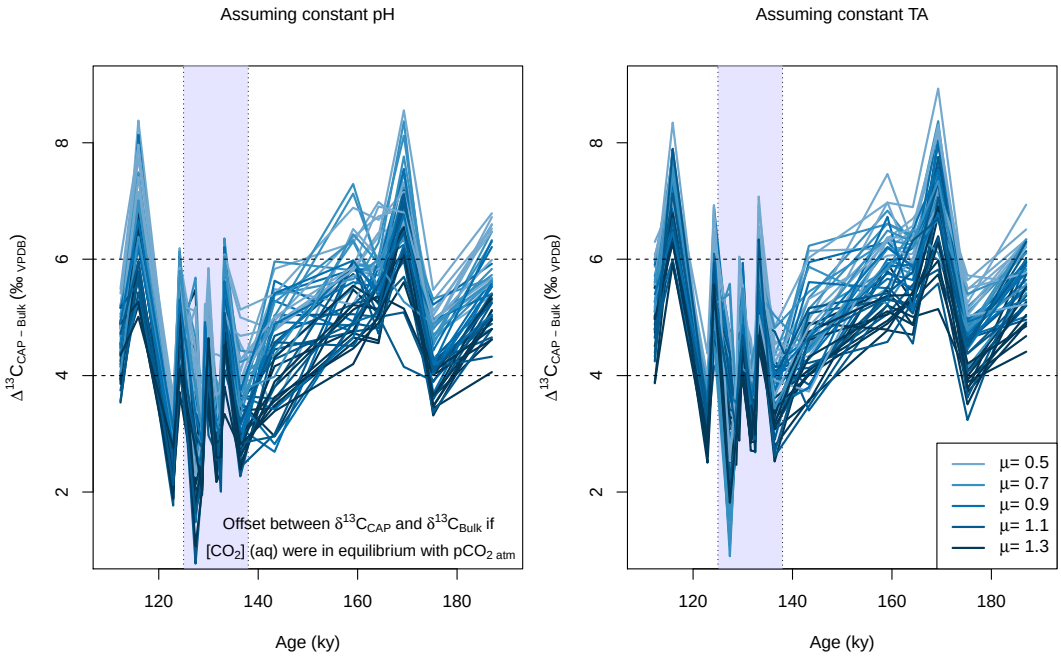

Figure 4.7: Required isotopic offset between CAP and bulk of the small size fraction for the following criteria to be met: model-$[CO_2] = [CO_2]_{eq.}$. Offsets calculated for a range of growth rates. Shaded region highlights the glacial termination. Horizontal dashed lines denote the range of isotopic offsets between polysaccharides and bulk organic carbon reported in the literature.

they are likely to be heavier than bulk organic matter (Benthien *et al.*, 2007), without direct measurement, the relative magnitude of the isotopic enrichment is not obvious. To my knowledge there are no existing paired measurements of bulk organic carbon and CAPs reported in the literature[2].

If $[CO_2]$ of the surface ocean was in equilibrium with the atmosphere, the isotopic offset between bulk organic carbon and CAPs required to satisfy the model given the set of calibration parameters employed here, is 2 - 8 ‰ (Fig. 4.7). The required offset varies through the glacial cycle, being lowest during the glacial termination (Fig. 4.7). If, in reality, the offset between $\delta^{13}C_{org}$ and $\delta^{13}C_{\ CAP}$ is actually approximately constant, as is widely assumed for alkenones, or remains within the range of values reported in the literature for other organisms and shorter chain carbohydrates, the difference in the offset required for equilibrium suggests that $[CO_2]$ is higher than equilibrium during the glacial termination, and lower than equilibrium during the glacial period. This circumstantial evidence is qualitatively consistent with recent findings (Martínez-Botí *et al.*, 2015). When a constant offset of greater than 4‰ is applied, the model predicts infinitely high values of CO_2 when $[CO_2]_{eq.}$ is high, because predicted values of CO_2 are highly sensitive to small changes in ϵ_{SO}, when the magnitude of fractionation is close to its maximum value. If an isotopic offset between bulk organic matter and CAPs of 6‰ is assumed (Teece & Fogel, 2007; van Dongen, 2002), the magnitude of $[CO_2]$ is approximately equal to $[CO_2]_{eq.}$ in the time period 180-140 ka, but in the period 140-110 ka the record is very noisy, thanks to noise increasing at higher $[CO_2]$ (Fig. 4.8).

4.5.1.4 Sensitivity of $[CO_2]$ estimates

Estimates of τ are determined by a combination of ϵ_{SO} and ϵ_{SC}. ϵ_{SO} has a maximum value which occurs when τ is zero; that is, when $[CO_2]$ is infinitely high, or when μ or r

[2]As of writing, I am awaiting results from the Pearson Laboratory at Harvard, for the isotopic composition of CAPs extracted from cultures, where the bulk organic matter has already been measured. This will provide an independent and coccolithophore-specific estimate of the required correction.

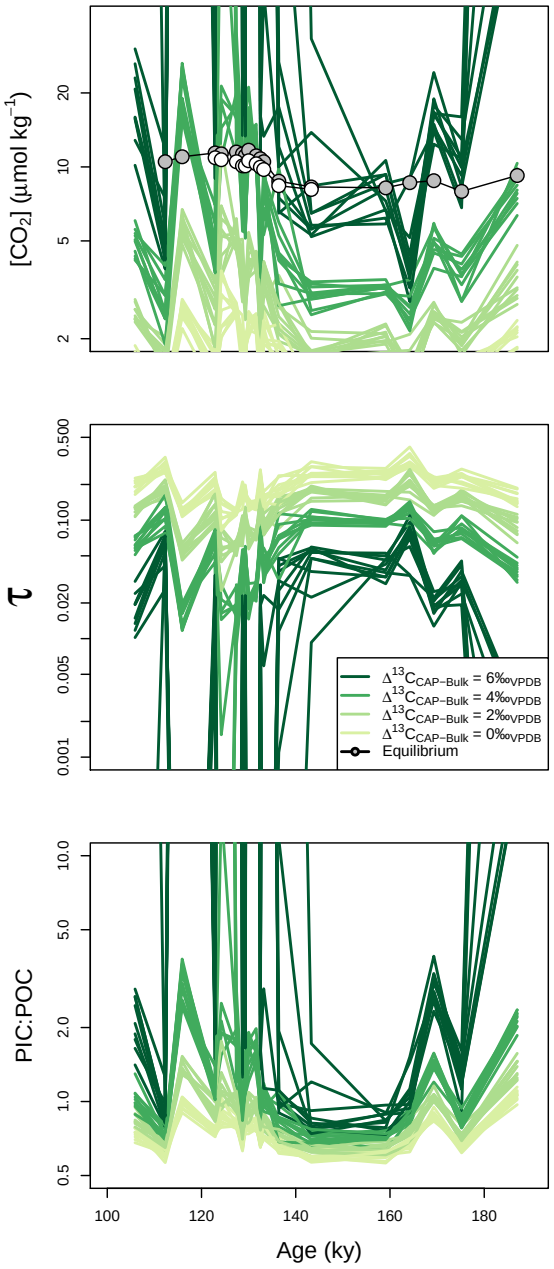

Figure 4.8: Reconstructed parameters, given different isotopic offsets between CAPs and bulk organics. Lines are plotted for cells of $r = 2.5$ μm, at a constant μ of 0.8 div day^{-1} and at a constant pH of 8.2. These results are consistent with the literature which suggests that polysaccharides should be ~6‰ heavier than bulk organic carbon, but due to the highly non-linear relationship between ϵ_p and [CO_2], uncertainty in [CO_2] is very high when [CO_2] is greater than ~10μM.

is zero. As the relationships between μ, r and $[CO_2]$ with ϵ_{SO} are all individually non linear, but the uncertainty in ϵ_{SO} is constant, the uncertainty in the inferred variables is not constant. The uncertainty in ϵ_{SO} is fairly large ($\sim$1‰) so when values of ϵ_{SO} approach its asymptotic limit, inferred $[CO_2]$ values become unrealistically high. Once a correction for the isotopic offset between CAPs and bulk organic matter is factored into calculations and is perturbed according to the associated uncertainty, many of the pseudo replicate down-core reconstructed ϵ_{SO} datasets exceed the maximum value. When the maximum value of ϵ_{SO} is exceeded, τ is inferred to be zero; consequently $[CO_2]$ is inferred to be unfeasibly high (Fig. 4.8). These observations suggest that the *in vivo*-calibration (see Chapter 3) may benefit from some refinement, because the relationship is currently too sensitive to changes in $[CO_2]$ at higher values. With the current calibration, for estimates of ancient $[CO_2]$ at higher than $\sim$10 μM, a sediment fraction representing larger or faster growing cells is required.

4.5.2 Caveats and potential pitfalls

The universal constants: membrane permeabilities to CO_2 and to HCO_3^-; the carbon isotopic fractionation associated with carboxylation by RuBisCO; and compartment-specific pH, can be easily recalibrated as more data becomes available, and more parameter space is explored. Membrane permeabilities have not been measured for coccolithophores, and in the absence of this information we must assume that membrane permeabilities are constant across species, and through evolutionary time. Equally, this is true of compartment-specific pH. The values used here were those of Anning *et al.* (1996), and although when a different parameterisation is used, the trends in the data area qualitatively the same, there are quantitative differences (e.g. Fig.D.5 and Fig.D.6). Any quantitative estimates of $[CO_2]$ in the past must therefore be presented with the caveat that they are for a specific model parameterisation.

The isotopic fractionation associated with enzymatically catalysed carbon fixation by RuBisCO (ϵ_f) measured *in vitro* has been shown to be higher in RuBisCO enzymes

that have a higher specificity for CO_2, over its competitor substrate, O_2 (Tcherkez *et al.*, 2006). RuBisCOs with a higher specificity also have a lower maximum catalytic throughput (Tcherkez *et al.*, 2006), which establishes a trade off whereby ambient, and therefore intracellular, CO_2 to O_2 ratios may constitute a selective pressure that has an indirect effect on the enzymatic isotopic fractionation associated with RuBisCO. As only a single *in vitro* measurement of ϵ_f has been made for a coccolithophore (Boller *et al.*, 2011), and this being the cosmopolitan but evolutionarily recent, *E. huxleyi*, it is impossible to predict the degree to which ϵ_f may have the capacity to change within closely related taxa. Another potential pitfall concerns trophy; the assumption made by all isotopic studies of phytoplankton to date, including the present study, is universal photolithoautotrophy. Although modern coccolithophores appear to be mostly lithotrophic (Thierstein & Young, 2004), the haptophytes are descended from a heterotrophic eukaryotic ancestor (Gould *et al.*, 2008), and there is some evidence of residual mixotrophy in modern taxa (de Vargas & Aubry, 2007). The implications of putative mixotrophy is in the unknown fractional contribution of an unknown external organic carbon source to organic matter (including CAPs) produced by coccolithophores. Lastly, fundamental to the reliability of the approach described here is whether coccolithophore physiology can be assumed to be uniformitarian at the level of biological detail that we have pursued; that is, with respect to cellular compartmentation and the universal constants constrained *in vivo*. It may be argued that the assumptions presented here are preferable to the black box type approach used thus far for alkenones (Badger *et al.*, 2013a; Pagani, 2002; Pagani *et al.*, 2005), but it is known that coccolithophores are fast-evolving (Lohbeck *et al.*, 2012; Schlüter *et al.*, 2014), and there is evidence of infraspecific physiological variation that exceeds the range of phenotypic plasticity in the geological record (Chapter 2).

4.6 Conclusions

The isotopic composition of coccolith calcite and of the CAPs preserved within have been shown to be sensitive to environmental changes across a glacial termination. Interpreted quantitatively, assuming that CAPs reflect bulk organic carbon, using data from the small size fraction and the isotopic flux model from Chapter 3, across a range of growth rates, the system is well constrained in terms of τ and PIC:POC. τ is shown to decrease across the termination, which is most likely a direct record of the influence of $[CO_2]$, rather than due to changes in physiology. PIC:POC appears to be higher during the interglacial, approximately consistent with the results from Chapter 2. Absolute $[CO_2]$ inferred from isotopes is consistent with reconstructed equilibrium values of $[CO_2]_{eq.}$, if a correction for $\delta^{13}C_{\ CAP}$ - $\delta^{13}C_{org\ \ Bulk}$ of around 6‰ is employed. However, the uncertainty of $[CO_2]$ estimates based on analysis of the small size fraction is too large to be informative when $[CO_2]$ is greater than $\sim$10 μM, because isotopic fractionation is close to its *in vivo*-inferred maximum, and any noise in the isotopic data is amplified. Under high $[CO_2]$ conditions, faster growing or larger cells are required for estimating changes in $[CO_2]$, as estimates have a smaller uncertainty when carbon utilisation is higher due to the non-linear relationship between isotopic fractionation and $[CO_2]$.

The best measurements of $[CO_2]$ of the surface ocean waters on glacial-interglacial timescales are from boron isotopes, which are used to reconstruct pH (Foster, 2008; Martínez-Botí *et al.*, 2015). As $[CO_2]$ is only a unique function of pH when another parameter of the carbonate system is held constant, estimating $[CO_2]$ directly would be a significant improvement. Alkenones have thus far failed to capture $[CO_2]$ change on a glacial-interglacial scale (Zhang *et al.*, 2013), suggesting that the approach presented here may be the most sensitive direct $[CO_2]$ proxy currently available for studying glacial cycles. Further work is however required for more accurate absolute $[CO_2]$ values. The next steps required for the development of this proxy approach are: Firstly,

quantification of the offset between $\delta^{13}C_{\ CAP}$ and $\delta^{13}C_{org\ -bulk}$. Secondly, obtaining larger samples for extraction and analysis of CAPs, especially for the large size fractions, for smaller analytical errors and reduced uncertainty in $\delta^{13}C_{org}$ and therefore $[CO_2]$ estimates. If $\delta^{13}C_{org}$ and $\delta^{13}C_{cal}$ of all size fractions can be constrained with small errors, differences between size fractions can bypass the need to infer $\delta^{13}C_{DIC}$ from foraminifera. Thirdly, constrain the model more thoroughly *in vivo*, through exploring a wider range of parameter space, and where possible, through making measurements of the universal constants currently constrained by the model. There is clearly great potential for this approach, with the possibility of probing further into the geological past than with any other phytoplankton carbon isotope-based $[CO_2]$ proxy.

Chapter 5

Conclusions and future directions

Coccoliths in sediment have been shown to contain information about the physiology of ancient coccolithophores, and the carbonate chemistry of the seawater in which they lived. Chapter 2 described a new rationale for size normalising coccolith mass, and showed that calcification to net photosynthesis (PIC:POC) ratios in ancient coccolithophores can be estimated using a geometric approach based on fossil coccoliths. In Chapters 3 and 4 it was shown that PIC:POC ratios can also be reconstructed using an isotopic analysis of fossils in sediment. In Chapter 3 a hypothesis for the origin of carbon isotopic "vital effects" was presented, following the construction of a model of intracellular carbon fluxes. In Chapter 4 a new method for the extraction of coccolith associated acidic polysaccharides (CAPs) from fossil coccoliths was used in parallel with the isotopic analysis of the encasing calcite, to assess how the isotopic fractionation of carbon into organic matter changes through a glacial-interglacial cycle. A new approach for inferring $[CO_2]$ in past oceans from isotopic data was presented in Chapter 4, and may lead to a better understanding of phytoplankton-based paleo-pCO_{2atm} barometers. These methods all constitute new means of overcoming current limitations in the fields of paleoclimate and coccolithophore evolutionary biology.

5.1 PIC:POC

Coccolith mass is a biologically abstract quantity. Coccolithophores of any size can be heavily or lightly calcifying. However, bigger coccolithophores produce bigger

coccoliths, yet mass alone has been widely used to describe a coccolithophore's tendency to calcify. The PIC:POC ratio is a biologically relevant quantity, being the integrated rate of calcification normalised to that of net carbon fixation. In Chapter 2 it was shown, via a theoretical geometric argument and an empirical relationship, that in the Noëlaerhabdaceae, the world's most abundant family of coccolithophores, the aspect ratio (size-normalised thickness) of a coccolith is linearly related to the PIC:POC ratio of the organism. The geometric relationships derived in Chapter 2 for the Noëlaerhabdaceae are remarkably consistent with the only available data for this family of coccolithophores (Henderiks, 2008). Firstly, this relationship was taken as an indication and justification of how it is most sensible to normalise coccolith mass. The resultant metric is similar to the uncalibrated method of size-normalising mass recently used to observe changes in coccolith-calcification across the Paleocene-Eocene thermal maximum (O'Dea *et al.*, 2014). Secondly, this relationship was used to infer the likely change in PIC:POC across a glacial termination. In Chapter 4 the strong dependence of $\delta^{13}C_{cal}$ on PIC:POC, also in the Noëlaerhabdaceae, provided an additional, independent estimate of PIC:POC from isotopic data, using the model described in Chapter 3.

The geometric and isotopic approaches were applied to sedimentary material from the penultimate glacial termination, and the geometric approach was additionally applied to material from Termination VI. In all time series, PIC:POC was found to be higher under periods of high $[CO_2]$ following changes on a millennial timescale. This result is opposite to that expected based on laboratory experiments alone, and introduces a temporal dimension to the prevailing view. The changes documented here constitute the first estimates in the literature of PIC:POC compositions of coccolithophores based on proxy derived evidence from the geological record.

Phytoplankton in the surface ocean are generally biomass limited by light or nutrients. Biogeochemically PIC:POC is interesting because it describes how much calcite is produced per unit organic biomass. Calcite production is a relatively greater sink

of alkalinity than of carbon, and so decreases the buffering capacity of seawater for CO_2. The observed increase in community coccolithophore PIC:POC with increasing [CO_2] therefore constitutes a positive climatic feedback.

PIC:POC links biological experiments and the fossil record. The possibility of inferring a quantitative trait from fossils that is so biologically meaningful, will allow broader questions about evolutionary trends within the coccolithophores to be addressed. If PIC:POC can be determined across the entire range of extant and extinct taxa, PIC:POC can be quantitatively mapped onto an established phylogenetic tree. Such an approach would elucidate where phylogenetic clustering of heavily and lightly calcifying species of coccolithophore species occurs. Correlation with reconstructed environmental parameters would potentially suggest what external factors promote divergences between highly and lightly calcifying groups, and perhaps even provide more fundamental insight into why coccolithophores calcify. The limitation to this approach may be that relatively large samples of coccolith calcite are required, and to gain the taxonomic purity required for phylogenetic insight, very large bulk sediment samples will be required.

5.2 Vital Effects

Calcite precipitated by organisms that live in the surface ocean records the isotopic composition of the ambient seawater, but is often isotopically offset from abiogenically precipitated calcite. The offset is referred to as the "vital effect" because it is mediated by living processes. In coccolithophores, vital effects are particularly enigmatic because they are not constant, being a function of external parameters such as [CO_2]. Coccolithophore calcite has therefore been of limited use in paleoenvironmental studies where proxies require the isotopic composition of seawater to be known. Chapter 3 provides an explanation for vital effects in coccolith calcite that reconciles the taxonomically delimited "light" and "heavy" groups with a single isotopic flux

model, calibrated with *in vivo* data. It is shown that the heavy and light groups exist as a result of differing calcification to photosynthesis ratios; the carbon isotopic composition of coccolith calcite is heavier than abiogenically precipitated calcite when PIC:POC is low, and is lighter when PIC:POC is high. Vital effects are greatest at high utilisation (low $[CO_2]$, high growth rate or large cell size) and are negligible at low utilisation. From a practical perspective, the greatest benefits of understanding vital effects in coccolithophores is in exploiting them as proxies in their own right, as shown in Chapter 4. If knowledge of the isotopic composition of seawater were desired however, and was otherwise unattainable, such as in the absence or poor preservation of foraminifera in sediment, correction for vital effects would be possible using the work described here, but may introduce large errors. To remove vital effects, cellular utilisation must be inferred from organic matter isotopic compositions (through isotopic analysis of coccolith-associated acidic polysaccharides), and PIC:POC must be independently inferred using the geometric approach. The system would then be fully constrained, and the carbon isotopic vital effect could be estimated.

5.3 pCO_{2atm}

For the first time, both organic and inorganic isotopes in multiple sizes of coexsting coccolithophores can place simultaneous constraints on a model system representing coccolithophores living in ancient seawaters. However, even with this unprecedented degree of constraint, to gain a reliable estimate of $[CO_2]$, growth rate must be known. Growth rate has been estimated from Sr/Ca ratios in coccolith calcite (Bolton & Stoll, 2013), temperature (Rosenthal *et al.*, 2000), or through empirically established relationships with nutrient availability (Heureux & Rickaby, 2015; Pagani, 2002; Pagani *et al.*, 2005). A more satisfactory avenue however would be in coupling the isotopic model to a separate physiological model. The great advantage of the approach presented here is that the system is biologically meaningful, but requires only a few

universal parameters to be fully constrained. Models of increased complexity such as that of Holtz *et al.* (2014, 2015) require many constants, and although exceptionally useful for understanding processes *in vivo* may compromise the potential predictive power of this approach, if applied to the fossil record.

Knowledge of the offset in isotopic compositions between coccolith associated acidic polysaccharides ($\delta^{13}C_{CAP}$) and bulk organic matter ($\delta^{13}C_{org}$), and whether this value is constant, is essential to the progression of this approach. In Chapter 4 it is shown that if the value of this offset is around 6‰ ($\delta^{13}C_{CAP}$ - $\delta^{13}C_{org}$), then $[CO_2]$ inferred from the isotopic composition of $\delta^{13}C_{org}$ is of the same magnitude as $[CO_2]$ in equilibrium with the atmosphere independently inferred from ice-core data. However, given this offset, the uncertainty in $[CO_2]$ estimates based on analysis of the small size fraction is too large to be informative when $[CO_2]$ is greater than $\sim$10 μM. $\delta^{13}C_{org}$ of larger cells is required for estimating changes in $[CO_2]$ at higher concentration, as estimates have a smaller uncertainty when utilisation is higher. Additionally, if $\delta^{13}C_{org}$ and the carbon isotopic composition of calcite of all size fractions can be constrained with small errors, differences between size fractions can circumvent the need to infer the isotopic composition of carbon dissolved in seawater from foraminifera. To measure the $\delta^{13}C_{org}$ of larger cells reliably, more calcite is required from large coccolith size fractions, for the extraction and analysis of acidic polysaccharides. The next step in refining this proxy is through more thorough *in vivo* parameter calibration; particularly with more data collected at the extremes of $[CO_2]$, and with carbonate chemistry manipulated in different ways. Some experimental data exist in the literature, but none, other than those presented here, contain all parameters required for calibration. Lastly, one of the largest sources of uncertainty in this model are the values of intracellular pH. A reproduction of the work of Anning *et al.* (1996) across many species of coccolithophore, and determination of the degree of intracellular pH homeostasis across variable external pH, would be invaluable.

The sedimentary record of alkenones may extend back to 120Ma, but the first fossil occurrence of the only known extant open ocean coccolithophores that produce alkenones was at around 4.15 Ma (`http://ina.tmsoc.org/Nannotax3`). It is therefore difficult to ascertain from which species alkenones came in sediment older than this. As acidic polysaccharides have been found inside coccoliths preserved in sediments as old as 184Ma, and probably exist in coccoliths of any age, the potential to istopically analyse organic matter produced coccolithophores of known size and taxonomic affiliation has been pushed back 200 million years to the time when coccolithophores first appeared. Beyond the ∼800 ka temporal extent of ice-cores, very little is known for certain about pCO_{2atm} in Earth's past, and this proxy may contribute in the future in addressing big questions in paleoclimate research such as: Was the 65 million year long cooling trend of the Cenozoic driven by pCO_{2atm}? and: What was the role of pCO_{2atm} in the massive ocean anoxic events of the Mesozoic, and during the Paleocene-Eocene thermal maximum?

Even before further calibration, however, in its current state this proxy can be used to infer the direction of changes in $[CO_2]$, as is demonstrably sensitive to $[CO_2]$ changes across glacial cycles. The role of CO_2 in glacial cycles prior to ice core records is currently unknown, and this proxy may be ideally suited to address such a problem. The time shortly prior to the start of ice-core records is specifically of interest because prior to the mid-Pleistocene transition (∼600-800 ka), glacial cycles occurred with a frequency of $\sim$ 40 ky rather than $\sim$ 100 ky. A high resolution continuous record from the period $\sim$ 1.4 Ma - 700 ka (approximately 300 samples), would elucidate whether or not CO_2 also drove these higher frequency glacial cycles.

The work documented in this thesis has drawn together aspects of paleoclimate, experimental biology, biogeochemistry and modelling to probe the relationship between coccolithophore physiology and carbon dioxide. New tools have been developed,

and it is anticipated that this work will form the foundation for new projects seeking to understand coccolithophore physiology, evolution and paleoclimate by studying the sedimentary fossil record.

Appendix A

Histograms

This appendix shows the raw coccolith morphometry data on which Fig. 2.2 in Chapter 2 is based. To account for noise in the spectra, each log-normal distribution was fitted with a gaussian curve and visually inspected.

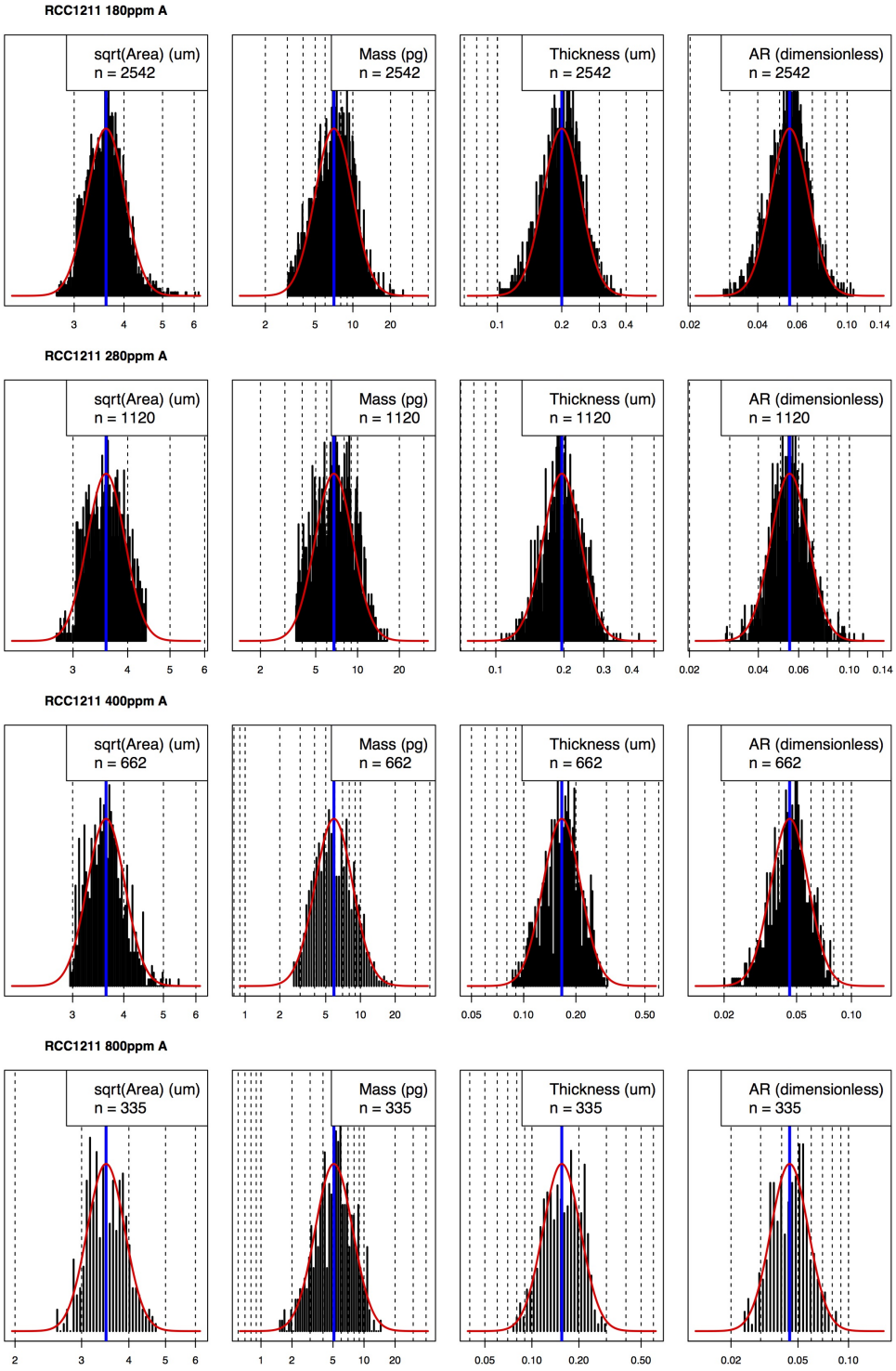

Figure A.1: Histograms (1)

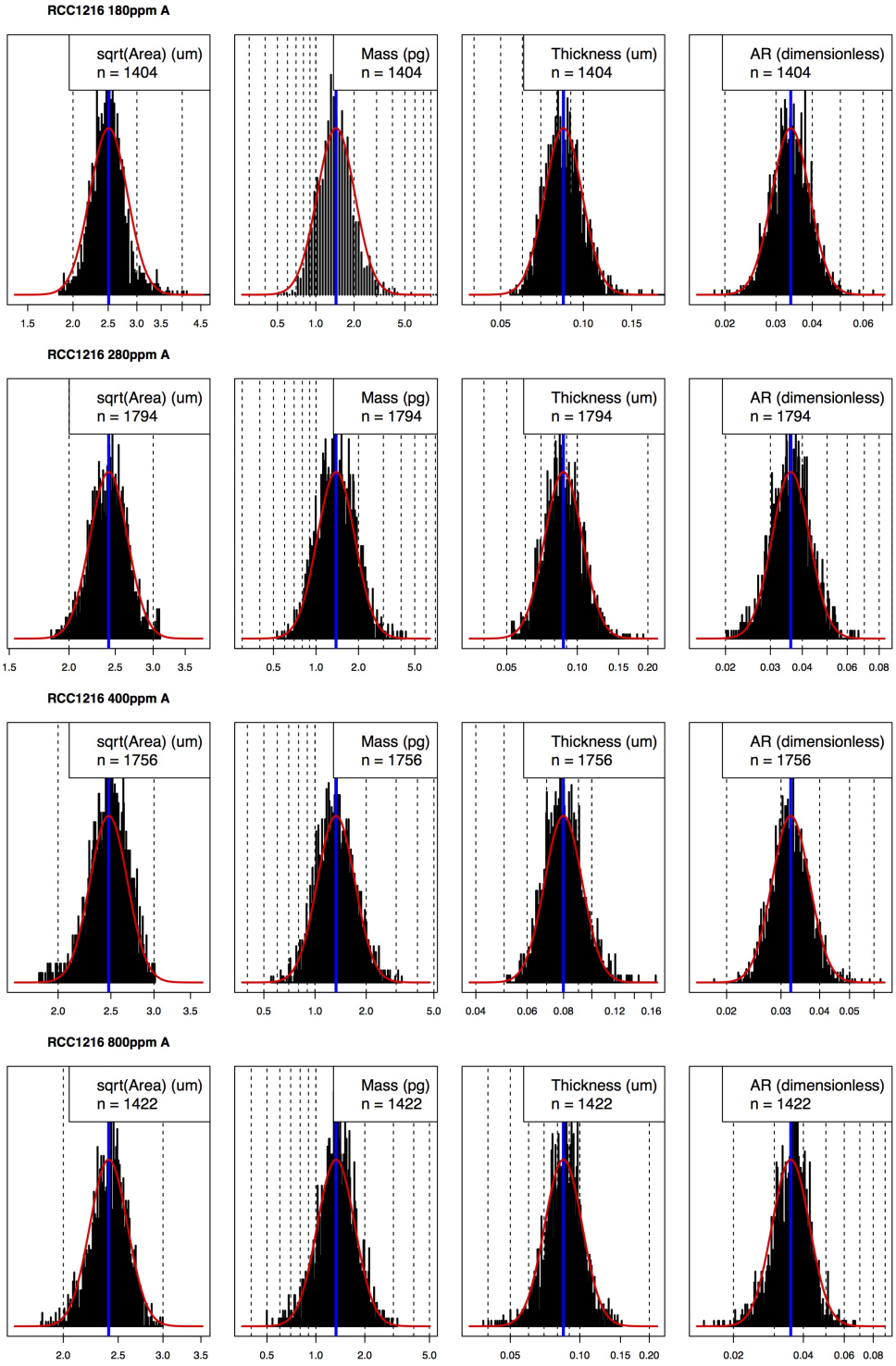

Figure A.2: Histograms (2)

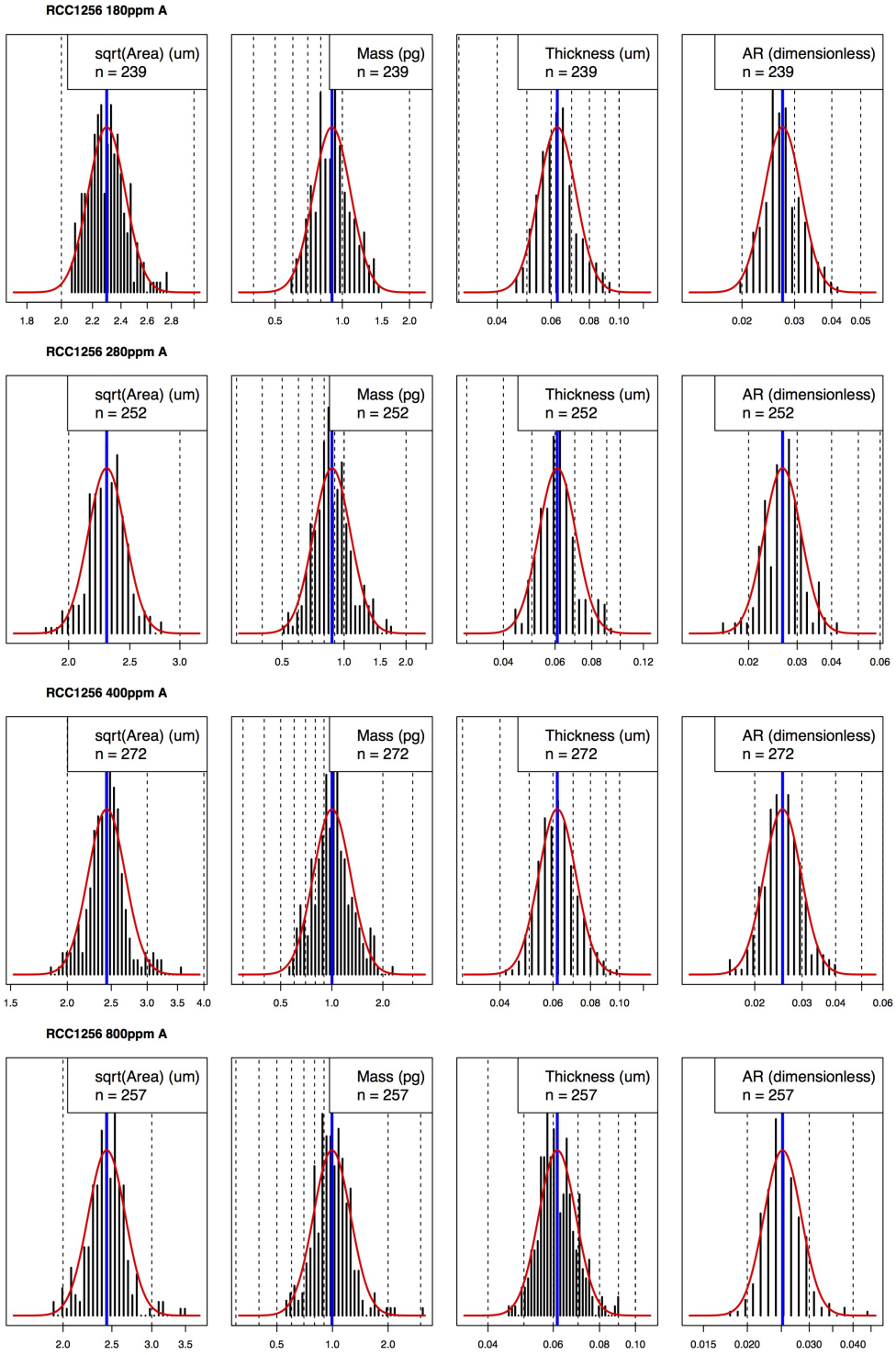

Figure A.3: Histograms (3)

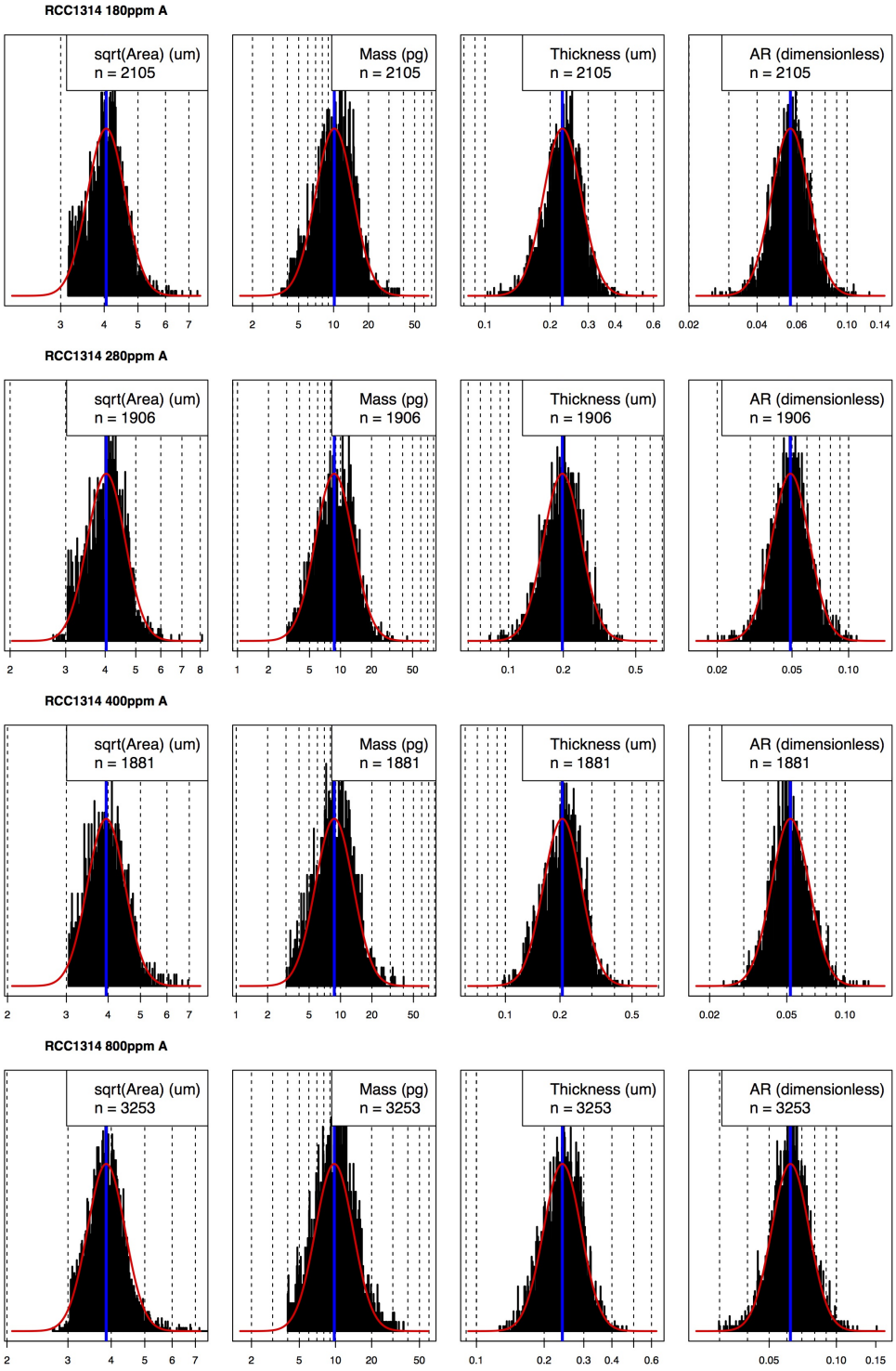

Figure A.4: Histograms (4)

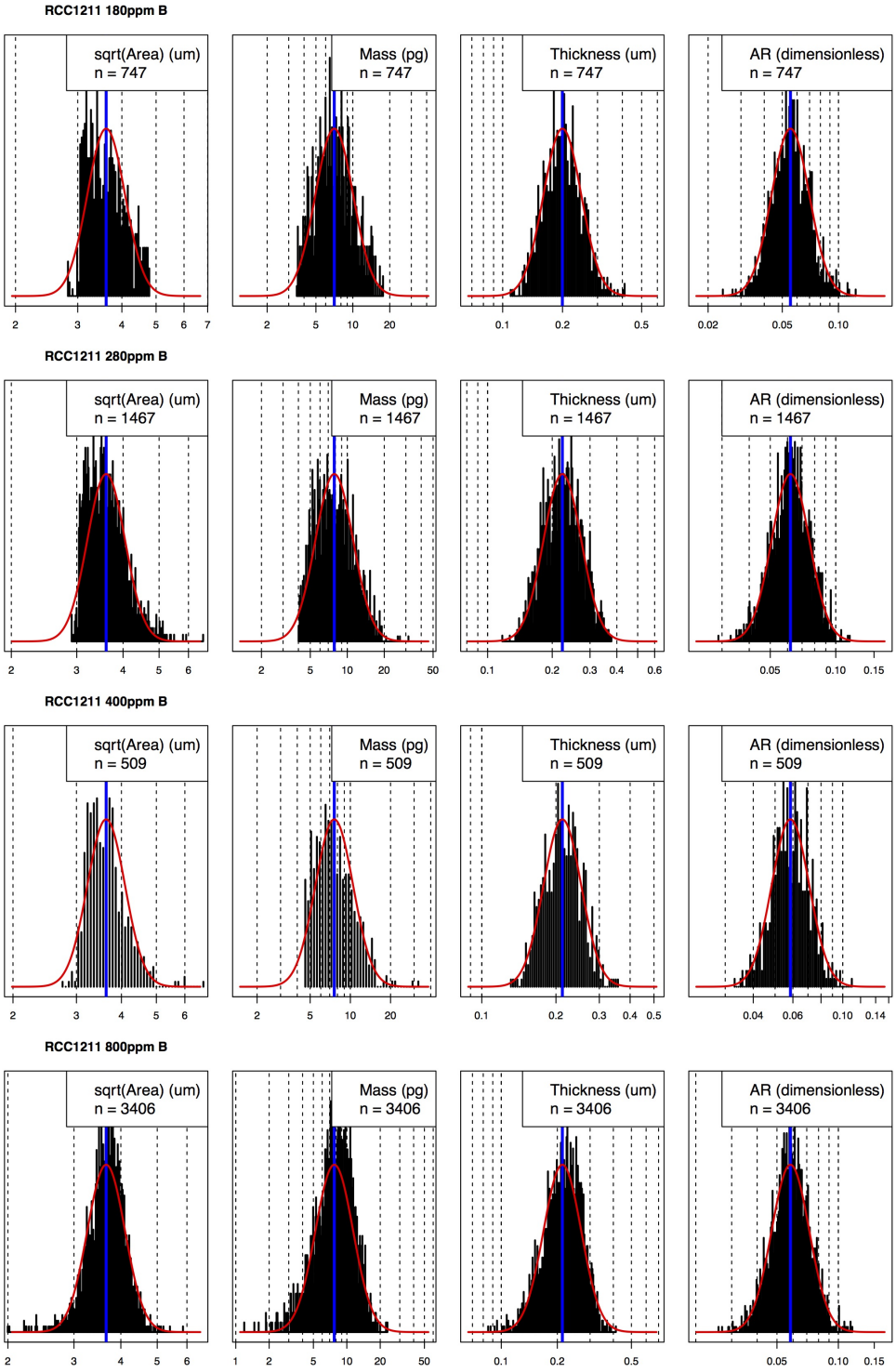

Figure A.5: Histograms (5)

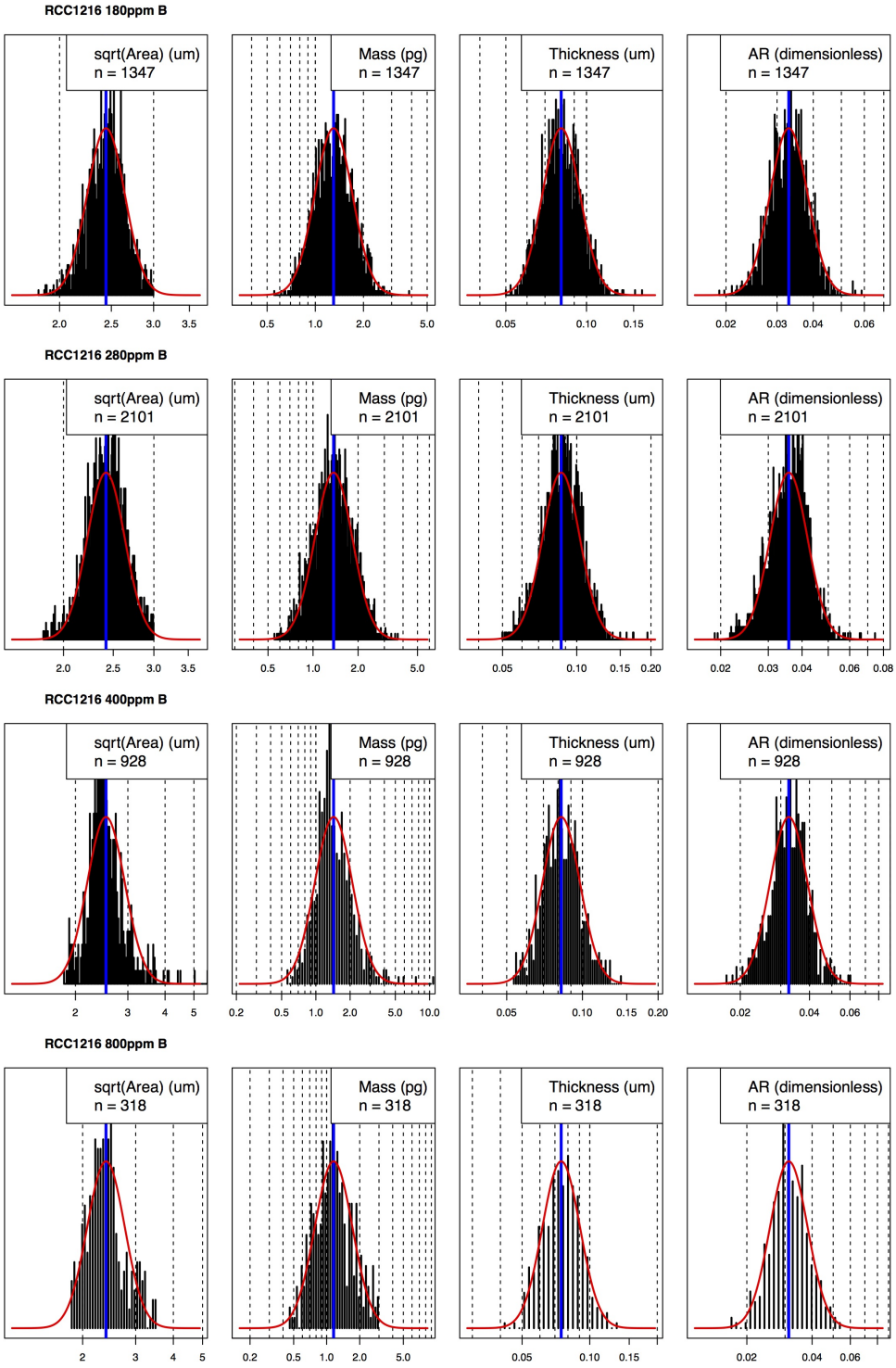

Figure A.6: Histograms (6)

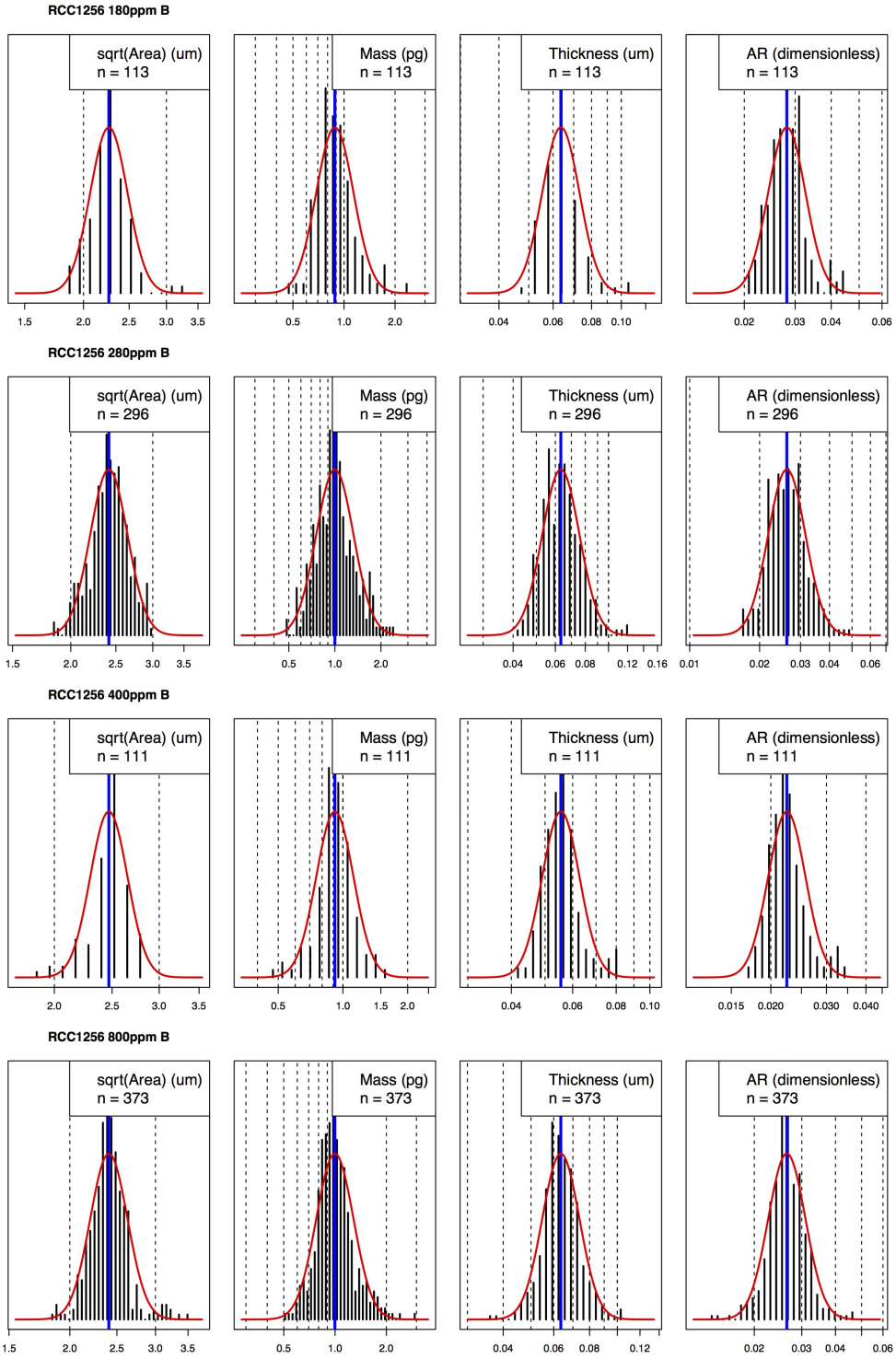

Figure A.7: Histograms (7)

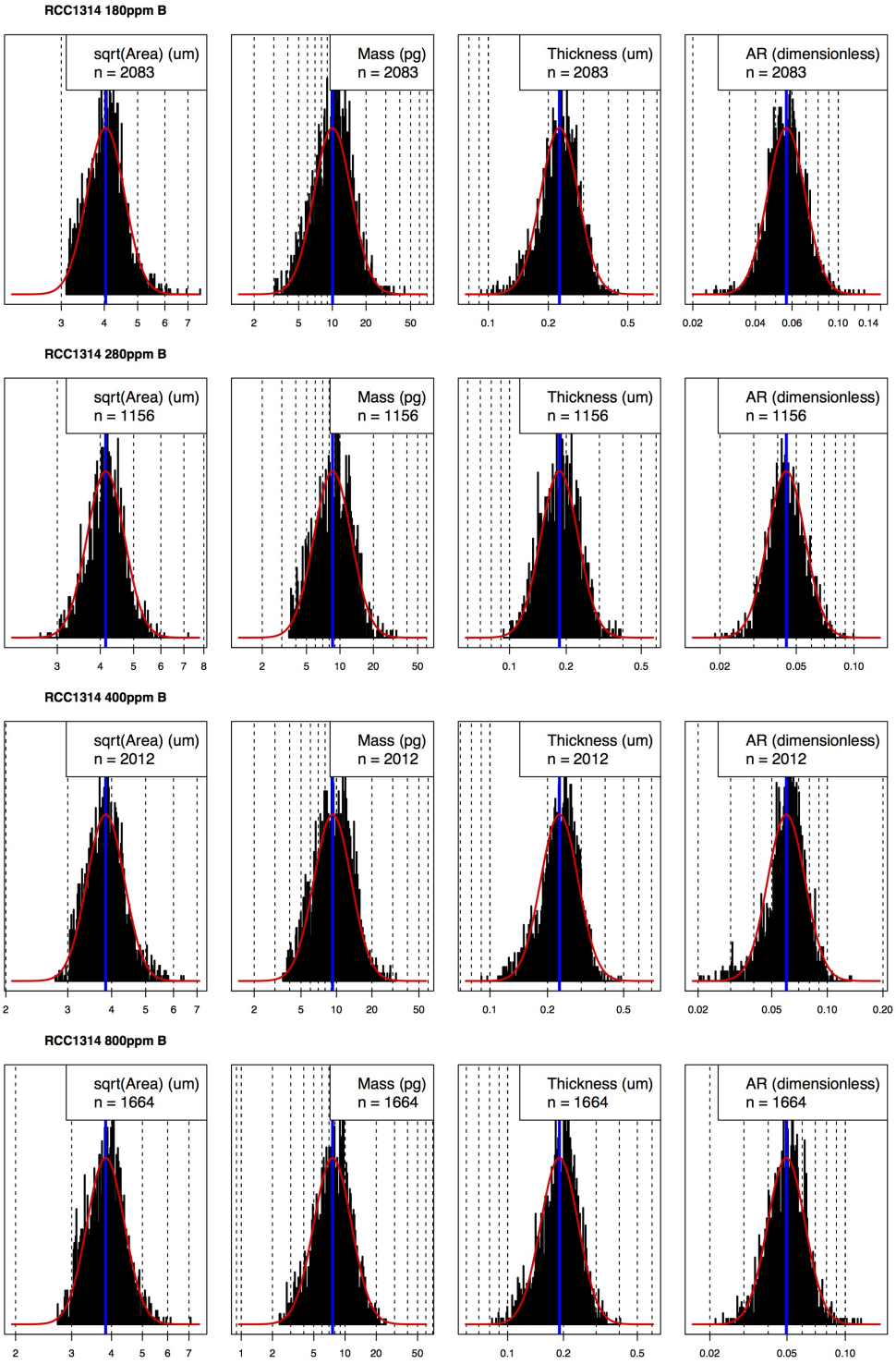

Figure A.8: Histograms (8)

Appendix B

Data

The tables in this appendix contain all of the final data presented in figures in this thesis.

Table B.1: Culture data from Chapter 2 - see table B.3 for isotopic data.

Species	Strain	Exp no.	Duplicate	$\sqrt{(A)}$	R_s	T	$R_s - R_c$	log(AR)	ARcv	Count	PIC:POC
goc	1211	1	A	3.60742784	3.738727584	0.200105182	0.809454611	-2.891907151	0.192833667	2542	1.242382271
goc	1211	2	A	3.570784442	3.735819559	0.195665394	0.929022039	-2.904134554	0.189219073	1120	2.355319149
goc	1211	3	A	3.620839334	3.582157738	0.165822711	0.747090774	-3.083541926	0.237764573	662	0.84592145
goc	1211	4	A	3.481550107	3.7027026	0.155397237	0.863620031	-3.109248247	0.257559393	335	1.381974249
ehux	1216	1	A	2.507681002	2.63512502	0.084583616	0.41342471	-3.389373119	0.148900323	1404	0.795305164
ehux	1216	2	A	2.420996593	2.619410519	0.087233961	0.419255465	-3.323340831	0.169313502	1794	0.849315068
ehux	1216	3	A	2.476825507	2.570574348	0.079898802	0.445525018	-3.433972122	0.139882839	1756	0.779081134
ehux	1216	4	A	2.404969811	NA	0.084869003	NA	-3.344183709	0.186115147	1422	0.819219791
ehux	1256	1	A	2.297223928	2.463713768	0.062846553	0.263094807	-3.598760588	0.143510338	239	0.422193878
ehux	1256	2	A	2.297530537	2.486266473	0.061040876	0.310003433	-3.62804641	0.15522095	252	0.684254606
ehux	1256	3	A	2.442814825	2.51808182	0.0620211	0.333277407	-3.673431623	0.159276497	272	0.487357775
ehux	1256	4	A	2.441535478	2.55861767	0.061519428	0.298493907	-3.681029387	0.121908663	257	0.526610644
goc	1314	1	A	4.05390645	4.317564672	0.227735552	0.754321723	-2.879251155	0.191735689	2105	1.005707763
goc	1314	2	A	4.03019479	4.23412164	0.197566488	0.824817877	-3.015494811	0.230597599	1906	1.363636364
goc	1314	3	A	3.948556591	4.233461669	0.206192876	0.761677691	-2.952293347	0.22359442	1881	0.990960452
goc	1314	4	A	3.869230818	4.247272728	0.240876285	0.887272728	-2.776527549	0.193997215	3253	1.385964912
goc	1211	1	B	3.611192086	3.723233696	0.199672654	0.825973732	-2.895113921	0.232505468	747	1.831858407
goc	1211	2	B	3.601546815	3.77107438	0.222965682	0.951253444	-2.782100835	0.199360551	1467	1.595744681
goc	1211	3	B	3.628122999	3.650131867	0.212335681	0.823922717	-2.838302291	0.192794621	509	1.752362949
goc	1211	4	B	3.655724651	3.679064466	0.212907659	0.863089623	-2.84319107	0.212505762	1703	1.427098675
ehux	1216	1	B	2.443181556	2.626975633	0.080460977	0.406163402	-3.413284077	0.149144443	1347	0.806054872
ehux	1216	2	B	2.420222721	2.621626722	0.08646041	0.413615703	-3.331928222	0.159981306	2101	1.165876777
ehux	1216	3	B	2.533004491	2.547016592	0.08233226	0.437822776	-3.42639841	0.188147688	464	0.872636816
ehux	1216	4	B	2.39102619	2.523706851	0.074636541	0.362343215	-3.466847709	0.199427157	318	0.766329347
ehux	1256	1	B	2.264036322	2.469147382	0.063579461	0.28221073	-3.572613997	0.148787472	113	0.52027972
ehux	1256	2	B	2.414582893	2.475812842	0.063258001	0.310819672	-3.642060221	0.184960915	296	0.786713287
ehux	1256	3	B	2.469310101	2.525867294	0.055492106	0.328223616	-3.795453302	0.135871642	111	0.388023952
ehux	1256	4	B	2.406191448	2.563658533	0.063537251	0.308862615	-3.634174099	0.159232511	373	0.665869219
goc	1314	1	B	4.036990606	4.340680697	0.227328393	0.761076935	-2.876859156	0.207282079	2083	0.942702703
goc	1314	2	B	4.146859677	4.131315188	0.184058918	0.765320565	-3.114850707	0.224815635	1156	1.093902439
goc	1314	3	B	3.846225783	4.205482821	0.230846016	0.761025928	-2.813096737	0.233264794	2012	1.044083527
goc	1314	4	B	3.834027089	NA	0.190314329	NA	-3.002993922	0.22257069	1664	1.230566535

Table B.2: Down-core data from Chapter 2

Age (ka)	SST (°C)	pCO_2 (ppm)	CO_2aq (M)	M_N	$M_N$cv	A_N	$A_N$cv	AR_N	AR_Ncv	$M_E.hux$	$A_E.hux$	$AR_E.hux$	$M_G.oc$	$A_G.oc$	$AR_G.oc$
117.5	11.82406768	267.5833333	1.10E-05	1.685277521	1.698839901	5.369597634	1.328945432	0.049979226	1.263998093	1.407096233	4.8489327	0.048627873	3.178758964	7.647344396	0.055465424
122.5	11.67651802	272.1	1.13E-05	1.919257787	1.926277308	5.908326192	1.41115202	0.04931367	1.312336235	1.343108591	4.940195424	0.045136267	4.681703739	9.195380093	0.061955535
127.5	11.43114259	270.75	1.13E-05	2.578633385	2.243450694	6.939984533	1.537936092	0.052026702	1.335916045	1.343112738	4.928866916	0.045287598	5.334321169	9.782416933	0.064353025
132.5	10.83760055	260.6384615	1.11E-05	2.111479307	1.73582615	6.105314969	1.356713793	0.051668469	1.289606923	1.500058537	5.034662997	0.048986074	3.310593093	7.703701899	0.05701882
137.5	10.87585738	203.60625	8.65E-06	1.923410734	1.562183037	5.929442088	1.26587024	0.049146277	1.258707003	1.486391373	5.153496722	0.046879363	2.69450485	7.130830196	0.052157256
142.5	11.46893934	193.6571429	8.07E-06	1.87311846	1.554780798	5.902760469	1.277692924	0.048196246	1.250246737	1.459175052	5.11587544	0.04653269	2.629179936	7.116033912	0.051108602
147.5	11.449893	196.9	8.21E-06	1.812225358	1.537865785	5.760343147	1.262096593	0.048364518	1.252440071	1.452927576	5.081228182	0.046810188	2.605987336	7.047701921	0.051398691
152.5	12.02756695	196.1	8.03E-06	1.751332256	1.520950772	5.617925825	1.246500262	0.04853279	1.254633404	1.4466801	5.046580923	0.047087687	2.582794736	6.97936993	0.051688779
157.5	11.13190786	187.3333333	7.89E-06	1.678472717	1.549938103	5.483656399	1.249536587	0.04820217	1.254079572	1.375527431	4.945354589	0.04614513	2.623829915	6.974769824	0.05255978
162.5	10.40355701	195.625	8.44E-06	1.52580821	1.581338147	5.453111233	1.281361045	0.044204512	1.281439921	1.265831367	4.933036843	0.042631638	3.087381973	7.722854881	0.052834047
167.5	9.546407447	191.225	8.48E-06	1.438057329	1.614183515	5.224998995	1.291221186	0.044455846	1.276430544	1.21759391	4.837675574	0.042249318	3.009275662	7.383419856	0.055266072
482.5	12.75749795	229.5571429	9.18E-06	2.390911938	1.580772774	5.893734936	1.28852497	0.061667737	1.246146744	1.901159035	5.133843359	0.060317416	3.65155	7.371112362	0.067332613
487.5	12.30873409	228.94	9.29E-06	2.177774916	1.559013167	5.59051746	1.285911751	0.060783678	1.242992018	1.831930383	5.021146495	0.060070543	3.469468521	7.286075196	0.065105006
492.5	11.91090942	240.2111111	9.87E-06	2.055116512	1.604460774	5.597348499	1.311917218	0.057301247	1.272681946	1.707859337	4.978274934	0.056748533	3.365472072	7.309964253	0.062815347
497.5	12.08079616	241.8	9.88E-06	2.169273086	1.626485769	5.793716349	1.311456138	0.057417254	1.278092454	1.722459084	5.018152232	0.05652975	3.563963446	7.532953087	0.063593699
502.5	13.32221809	234.7428571	9.22E-06	2.198804517	1.643995172	5.942787186	1.32841292	0.056037674	1.247532956	1.671434426	5.025028505	0.054720926	3.421960952	7.527950073	0.061152501
507.5	13.88341355	231.4166667	8.94E-06	2.527339008	1.606299033	6.241775157	1.302881388	0.059826261	1.267265844	1.861574572	5.174516979	0.058366596	3.669430262	7.548614352	0.065264603
512.5	13.82137906	236.3285714	9.14E-06	2.442561205	1.641827151	6.267212132	1.33658638	0.057443484	1.271165315	1.785271961	5.139480105	0.056544053	3.643798877	7.625731633	0.063849957
517.5	14.07924733	238.75	9.16E-06	2.315014194	1.660245714	5.94752834	1.315386128	0.05889586	1.244693203	1.770912527	5.073162699	0.057185386	3.670529493	7.556990419	0.065204094
522.5	14.68533324	245.4875	9.25E-06	2.545679428	1.662540943	6.099474035	1.336328799	0.062358526	1.249824622	1.897090318	5.102096382	0.060742929	3.831295676	7.527408501	0.068455469
527.5	15.47016598	235.7	8.67E-06	2.677582257	1.687596911	6.60495972	1.358339192	0.058200307	1.267011476	1.780665423	5.122561616	0.056677345	3.891353564	7.943701113	0.064132679
532.5	13.90856609	221.7	8.56E-06	2.794419672	1.691383647	6.96538206	1.342155725	0.056410142	1.259057104	1.689110819	5.168726786	0.053000897	3.850806416	8.064747682	0.062184292
537.5	11.73950931	199.9333333	8.26E-06	2.620328413	1.756996275	6.991482963	1.390252512	0.052303708	1.26855487	1.513723752	5.037196373	0.049407629	3.612938648	8.151030724	0.057289166
542.5	11.83521059	208.875	8.60E-06	2.69231175	1.776939402	7.301164588	1.377684748	0.050357927	1.271215597	1.4056701	5.10242915	0.045003744	3.697291803	8.211966012	0.057975396
547.5	12.3105709	208.26	8.45E-06	2.112502514	1.753507773	6.460699978	1.374812973	0.047468836	1.260478176	1.411942824	5.175836344	0.044246306	3.165306377	7.692083953	0.054749535
552.5	11.77496136	212.3285714	8.76E-06	2.18457376	1.611196503	5.935359004	1.307799349	0.055747597	1.246760584	1.684303853	5.044316567	0.05486906	3.226903465	7.385027993	0.059280624
557.5	11.70567283	231.3833333	9.57E-06	1.952280287	1.610396487	5.923948356	1.319220319	0.04996386	1.262548394	1.520815018	5.077847567	0.049044195	2.840552027	7.097277769	0.055436494
562.5	12.58975361	235.3692308	9.46E-06	2.057080575	1.602667583	5.981109809	1.290637091	0.051893068	1.271324252	1.57313959	5.134998574	0.04988701	3.113099906	7.470629837	0.056258473
567.5	12.61978669	249.9214286	1.00E-05	2.335174874	1.859887522	6.223988571	1.428105002	0.055494116	1.276013899	1.552932774	4.923871735	0.052447316	3.53553384	7.872386021	0.059064446
572.5	13.28267266	250.8285714	9.87E-06	2.135538097	1.989551695	5.831256099	1.494900048	0.05596221	1.296980325	1.483780651	4.743384147	0.052999035	3.875042013	7.918194399	0.064175297
577.5	15.33045571	251.0636364	9.28E-06	2.201419015	2.1166172	6.222578877	1.563740725	0.052333262	1.27465564	1.391577842	4.751336052	0.049580921	3.65472188	7.942086559	0.060253616
582.5	13.4805772	230.3923077	9.01E-06	2.116260464	1.981706885	5.728242693	1.487108814	0.056971172	1.283649007	1.531631448	4.743676093	0.054705583	4.042998206	7.873476494	0.067578563

Table B.3: Culture data from Chapter 3 - see table B.1 for geometric data.

Species	Strain	Exp no.	Duplicate	DIC (mM)	CO_2 (μM)	TA	pH	T	C_{inorg} / cell (mol)
goc	1211	1	A	1.18	5.8	1303.1	8.2	15	1.50E-12
goc	1211	2	A	2.46	12.02	2703.82	8.2	15	9.65E-13
goc	1211	3	A	2.95	14.44	3246.74	8.2	15	3.53E-12
goc	1211	4	A	8.16	39.91	8974.49	8.2	15	1.84E-12
ehux	1216	1	A	1.25	6.11	1373.68	8.2	15	1.10E-12
ehux	1216	2	A	2.49	12.17	2736.4	8.2	15	1.08E-12
ehux	1216	3	A	3.17	15.53	3491.05	8.2	15	1.32E-12
ehux	1216	4	A	8.25	40.35	9072.22	8.2	15	9.85E-13
ehux	1256	1	A	1.31	6.42	1444.26	8.2	15	1.08E-12
ehux	1256	2	A	2.54	12.41	2790.69	8.2	15	9.29E-13
ehux	1256	3	A	3.31	16.18	3637.64	8.2	15	1.50E-12
ehux	1256	4	A	8.37	40.95	9207.95	8.2	15	1.27E-12
goc	1314	1	A	1.26	6.16	1384.54	8.2	15	3.65E-12
goc	1314	2	A	2.8	13.69	3078.43	8.2	15	2.80E-12
goc	1314	3	A	3.37	16.47	3702.79	8.2	15	4.17E-12
goc	1314	4	A	8.4	41.07	9235.09	8.2	15	3.47E-12
goc	1211	1	B	1.19	5.82	1308.53	8.2	15	1.19E-12
goc	1211	2	B	2.61	12.75	2866.7	8.2	15	1.26E-12
goc	1211	3	B	3.38	16.52	3713.65	8.2	15	1.60E-12
goc	1211	4	B	8.23	40.25	9050.5	8.2	15	1.73E-12
ehux	1216	1	B	1.12	5.48	1232.52	8.2	15	1.07E-12
ehux	1216	2	B	2.65	12.97	2915.56	8.2	15	8.25E-13
ehux	1216	3	B	3.41	16.66	3746.22	8.2	15	1.05E-12
ehux	1216	4	B	8.1	39.65	8914.77	8.2	15	1.07E-12
ehux	1256	1	B	1.18	5.77	1297.67	8.2	15	1.00E-12
ehux	1256	2	B	2.55	12.48	2806.98	8.2	15	9.30E-13
ehux	1256	3	B	3.07	14.99	3371.61	8.2	15	1.53E-12
ehux	1256	4	B	8.51	41.63	9359.96	8.2	15	1.09E-12
goc	1314	1	B	1.16	5.7	1281.38	8.2	15	4.02E-12
goc	1314	2	B	2.54	12.44	2796.12	8.2	15	3.69E-12
goc	1314	3	B	3.03	14.8	3328.18	8.2	15	3.29E-12
goc	1314	4	B	8.78	42.96	9658.57	8.2	15	2.93E-12

C_{org} / cell (mol)	PIC	POC	Div. rate	Growth rate	R_s	R_c	$\delta^{18}O_{cal}$	$\delta^{18}O_{water}$	$\Delta\delta^{13}C_{cal}$	$\Delta\delta^{13}C_{org}$
1.86E-12	1.24	1.03	0.72	3.74	2.93	-5.51	-6.2	-0.64	-20.57	
2.27E-12	2.36	1	0.69	3.74	2.81	-5.33	-6.2	0.02	-20.36	
2.99E-12	0.85	NA	NA	3.58	2.84	-5.39	-6.2	-0.95	-23.87	
2.54E-12	1.38	0.99	0.69	3.7	2.84	-5.28	-6.2	-0.18	-23.28	
8.77E-13	1.83	1.15	0.79	2.64	2.22	-3.91	-6.2	1.35	-23.54	
9.13E-13	1.6	0.89	0.61	2.62	2.2	-4.72	-6.2	1.64	-24.24	
1.03E-12	1.75	1.05	0.73	2.57	2.13	-4.81	-6.2	0.72	-24.28	
8.07E-13	1.43	0.99	0.69	2.52	NA	-4.9	-6.2	0.53	-25.11	
4.56E-13	0.8	1.04	0.72	2.46	2.2	-3.11	-6.2	1.68	-21.33	
6.36E-13	0.85	1.04	0.72	2.49	2.18	-4.71	-6.2	1.32	-20.5	
7.29E-13	0.78	0.93	0.65	2.52	2.18	-4.27	-6.2	0.84	-23.91	
6.68E-13	0.82	1.05	0.73	2.56	2.26	-4.73	-6.2	0.75	-22.16	
3.67E-12	0.81	0.97	0.67	4.32	3.56	-5.18	-6.2	-0.07	-18.77	
3.82E-12	1.17	0.96	0.66	4.23	3.41	-4.92	-6.2	0.27	-19.88	
4.13E-12	0.87	0.9	0.62	4.23	3.47	-5.41	-6.2	-0.11	-21.11	
4.82E-12	0.77	0.77	0.54	4.25	3.36	-5.48	-6.2	-0.04	-20.46	
2.18E-12	0.42	1.03	0.71	3.72	2.9	-4.65	-6.2	-0.21	-20.65	
2.01E-12	0.68	0.98	0.68	3.77	2.82	-5.22	-6.2	0.07	-19.92	
2.80E-12	0.49	1.01	0.7	3.65	2.83	-5.46	-6.2	-0.59	-23.07	
2.46E-12	0.53	0.87	0.6	3.68	2.82	-5.31	-6.2	-0.28	-22.72	
8.62E-13	0.52	1.16	0.8	2.63	2.22	-4	-6.2	1.39	NA	
9.61E-13	0.79	1.01	0.7	2.62	2.21	-4.86	-6.2	1.6	-24.19	
9.19E-13	0.39	0.93	0.65	2.55	2.11	-4.7	-6.2	1.01	-23.03	
8.23E-13	0.67	0.9	0.62	2.52	2.16	-4.89	-6.2	0.52	-23.68	
5.22E-13	1.01	1.13	0.78	2.47	2.19	-4.28	-6.2	1.28	-21.17	
7.32E-13	1.36	1.06	0.74	2.48	2.16	-4.71	-6.2	1.18	-20.87	
5.92E-13	0.99	0.95	0.66	2.53	2.2	-4.34	-6.2	0.86	-23.95	
7.27E-13	1.39	1.11	0.77	2.56	2.25	-4.8	-6.2	0.55	-22.68	
3.79E-12	0.94	1.03	0.72	4.34	3.58	-5.2	-6.2	-0.12	-18.34	
4.04E-12	1.09	0.83	0.58	4.13	3.37	-4.96	-6.2	0.29	-20.18	
3.44E-12	1.04	0.91	0.63	4.21	3.44	-5.44	-6.2	0.03	-21.67	
3.60E-12	1.23	1.01	0.7	NA	3.34	-5.39	-6.2	-0.4	-20.95	

Table B.4: Down-core data from Chapter 4

Age (ka)	pCO_2	F < 3 $\delta^{13}C_{cal}$	F 3-8 $\delta^{13}C_{cal}$	F 8-12 $\delta^{13}C_{cal}$	F > 12 $\delta^{13}C_{cal}$	Bulk $\delta^{13}C_{cal}$	F <3 $\delta^{18}O_{cal}$	F 3-8 $\delta^{18}O_{cal}$	F 8-12 $\delta^{18}O_{cal}$
105.9	232.2127	0.857476736	-1.385105776	-1.666716633	-1.538722474	0.363	1.535858974	0.213390301	0.684707891
112.3	252.726	1.041015171	-1.044936486	-1.265346063	-1.256004464	0.142	1.844458264	0.531041867	0.970042719
115.9	262.3531	0.623551471	-1.151020325	-1.162252721	-0.958143846	0.026	1.561553856	0.534672479	0.838805523
122.9	274.4097	0.664183398	-1.215480299	-1.342857517	-1.379883289	0.256	1.21468644	-0.093619434	0.672761004
124.2	272.9507	0.718766977	-1.215271931	-1.509929605	-1.517714931	0.142	1.338443035	0.058729388	0.607432304
127.4	273.9559	0.966441421	-1.076011168	-1.606414331	-1.899245187	0.07	1.52302538	0.232368162	0.814704994
128.7	267.3836	1.496030428	-0.993039042	-1.617929201	-1.774384503	0.156	2.070327781	0.103142835	1.03914789
129.3	263.853	0.778401493	-1.380013764	-1.59692003	-1.885956369	0.055	1.60748984	0.353885095	0.986021095
130	275.5635	1.060790639	-1.045434214	-1.611370055	-1.836424788	0.136	1.881201812	0.50954191	1.222941904
131.6	261.3898	1.070620283	-0.816691394	-1.565980132	-1.859510096	0.103	2.219656015	0.868282963	1.532225045
132.5	253.6546	1.18889544	-1.005378611	-1.477582645	-1.985422483	0.335	2.509251826	0.946267928	1.408866842
133.2	247.5683	1.331983252	-0.966966198	-1.580991595	-1.804732507	0.306	2.798254021	0.959544282	1.663260576
133.8	233.0116	-0.527349519	-1.054017404	-1.528710974	-1.761484722	0.344	2.075779071	0.94705177	1.835577757
136.4	206.3685	1.522871325	-0.8723635	-1.225277741	-1.601651668	0.508	3.313703282	1.230546253	1.949237494
143.3	196.0191	1.658273914	0.025087247	-1.326886508	-1.387629848	0.965	3.32556821	1.180382408	1.826827193
159.1	191.3057	1.675392763	-0.937964604	-1.398309439	-1.604884618	0.711	3.378498115	1.41817696	1.878326156
164.2	191.5202	0.959475788	-1.075769052	-1.639914706	-1.398	0.371	2.587186185	1.209387344	1.621075122
169.3	197.6125	0.155846813	-1.05895039	-1.473656517	-1.133	0.421	1.705989371	1.254084072	1.584369247
175.2	190.0976	0.863537325	-0.906471188	-1.597472525	-1.485	0.106	2.049255795	2.070302343	1.286165093
187	209.5426	-0.460443573	-1.071886343	-0.962431474	-0.604	-0.396	1.142358092	1.154208766	1.546968304

F >12 $\delta^{18}O_{cal}$	Bulk $\delta^{18}O_{cal}$	F < 3$\delta^{13}C_{org}$	σ	F 8 - 12 $\delta^{13}C_{org}$	σ	SST A	SST B	F < 3$\delta^{13}C_{foram}$	CO_2(aq) A	CO_2(aq) B
0.706143659	1.675	-16.3	0.4	-21.5	1.9	NA	NA	-0.043836124	NA	NA
0.872568369	1.84	-15	0.6	-20.6	1	11.58233568	NA	-0.447070119	1.05E-05	NA
0.952255569	1.103	-17.9	0.2	-20.4	1.4	11.20844492	NA	0.350051943	1.10E-05	NA
0.495838936	1.18	-15.9	0.5	-20.5	1.5	11.68108957	12.99884864	0.003781144	1.14E-05	1.09E-05
0.493268191	1.155	-18.4	1	-22.2	0.9	11.78992421	13.25015888	-0.122437072	1.13E-05	1.07E-05
0.446490822	1.344	-18.4	0.2	-20.4	1.1	11.19483947	14.10204452	-0.142640001	1.15E-05	1.05E-05
0.74584252	1.497	-17.3	0.5	-20.7	1.3	11.15491447	14.55580433	-0.167369867	1.13E-05	1.01E-05
0.214129314	1.472	-16.9	0.4	-21.7	1	11.08891982	14.308225	-0.111917837	1.11E-05	1.01E-05
0.863085826	1.651	-18	0.3	-21.4	1.6	11.01192605	14.01938244	-0.047223803	1.17E-05	1.06E-05
1.132437479	2.083	-17.7	0.3	-20.8	1.6	10.83907219	13.36406853	0.098372791	1.11E-05	1.03E-05
0.808373639	2.259	-15.9	0.5	-21	1.4	10.92681921	13.28472175	0.045874696	1.08E-05	9.98E-06
1.410821858	2.404	-17.3	0.5	-20	1.8	10.99506689	13.22300759	0.005042843	1.05E-05	9.76E-06
1.232029382	2.478	-17.9	0.3	-21.2	1.3	11.0535649	13.17010973	-0.029955887	9.84E-06	9.20E-06
1.329902026	2.914	-16.1	0.7	-22.2	2.2	10.92773159	12.25543428	0.039893754	8.75E-06	8.39E-06
1.544216554	3.281	-15.1	0.5	-21.3	1.7	11.02155143	11.72791536	-0.048514323	8.29E-06	8.10E-06
1.719307476	3.07	-15.3	0.3	-18.2	2.6	10.5381545	NA	-0.055562262	8.22E-06	NA
1.556	2.552	-13.8	0.7	-19	4.4	9.09035402	NA	0.15845155	8.63E-06	NA
1.693	2.596	-15.8	0.3	-11.8	5.9	9.473867542	NA	0.224895062	8.79E-06	NA
1.36	2.137	-15.8	0.4	-18.7	1.6	11.35255979	NA	-0.424926818	7.95E-06	NA
1.805	2.147	-17	0.5	-19.5	4.4	9.778484918	NA	0.109735876	9.23E-06	NA

Appendix C

Special case: CA = ∞ in all compartments

At the limit where carbonic anhydrase (CA) activity is infinitely high in all compartments, complete chemical and isotopic equilibrium with respect to carbon can be assumed. In this scenario, the total [DIC] (D) in each compartment and its isotopic composition, along with (prescribed) pH, completely specifies the concentrations and isotopic compositions of the different inorganic carbon species in each compartment. In the following, notation is the same as described in Chapter 3.

C.1 Carbon fluxes

The dynamic equations for total DIC (D) in the three different compartments are:

$$\begin{aligned} V_i\frac{dD_i}{dt} = 0 = {} & FC_{ei} - FC_{ie} + FB_{ei} - FB_{ie} - FC_{ix} + FC_{xi} \\ & - FB_{ix} + FB_{xi} - FC_{iv} + FC_{vi} - FB_{iv} + FB_{vi} \end{aligned} \tag{C.1}$$

$$V_x\frac{dD_x}{dt} = 0 = FC_{ix} - FC_{xi} + FB_{ix} - FB_{xi} - F_{FIX} \tag{C.2}$$

$$V_v\frac{dD_v}{dt} = 0 = FC_{iv} - FC_{vi} + FB_{iv} - FB_{vi} - F_{CAL} \tag{C.3}$$

In steady state all three equations must equal 0, which implies:

$$F_{FIX} = FC_{ix} - FC_{xi} + FB_{ix} - FB_{xi} \tag{C.4}$$

$$F_{CAL} = FC_{iv} - FC_{vi} + FB_{iv} - FB_{vi} \tag{C.5}$$

Cytosol

Inserting these into Eq.(C.1), the expression for cytoplasm total DIC, gives:

$$V_i \frac{dD_i}{dt} = FC_{ei} - FC_{ie} + FB_{ei} - FB_{ie} - F_{FIX} - F_{CAL} = 0. \tag{C.6}$$

The four fluxes across the cell membrane equal:

$$FC_{ei} = P_C C_e SA \tag{C.7}$$

$$FC_{ie} = P_C C_i SA \tag{C.8}$$

$$FB_{ei} = P_B B_e SA \tag{C.9}$$

$$FB_{ie} = P_B B_i SA \tag{C.10}$$

where the permeability for HCO_3^- relates to the permeability for CO_2 through background utilisation:

$$P_B = P_C(T_0 + T_U U_0). \tag{C.11}$$

As a result, all cross-membrane fluxes are proportional to $P_C SA$ and Eq. (C.6) can be divided through by this factor. With chemical equilibrium and prescribed pH_c in the cytoplasm, B_c is proportional to C_c for any compartment $c \in \{e, i, x, v\}$:

$$B_c = \frac{K^*_{H_2CO_3}}{H_c} C_c \tag{C.12}$$

where $K^*_{H_2CO_3}$ is the temperature and salinity dependent chemical equilibrium constant, and H_c the H^+ concentration ($H_c = 10^{-pH_c}$). Thus Eq. (C.6) can be rewritten as:

$$V_i \frac{dD_i}{dt} = C_e \left(1 + \frac{K^*_{H_2CO_3}}{H_e}(T_0 + T_U U_0)\right) - C_i \left(1 + \frac{K^*_{H_2CO_3}}{H_i}(T_0 + T_U U_0)\right) - \frac{F_{FIX}}{P_C SA} - \frac{F_{CAL}}{P_C SA} = 0. \tag{C.13}$$

Isolating C_i and divine through by C_e gives:

$$\frac{C_i}{C_e} = \frac{\left(1 + \frac{K^*_{H_2CO_3}}{H_e}(T_0 + T_U U_0)\right) - \frac{F_{FIX}}{C_e P_C SA} - \frac{F_{CAL}}{C_e P_C SA}}{1 + \frac{K^*_{H_2CO_3}}{H_i}(T_0 + T_U U_0)} \tag{C.14}$$

Thus, concentrations and fluxes of carbon species in all compartments are known.

Chloroplast

Following the same process, two additional fluxes across the chloroplast membrane equal:

$$FC_{ix} = f_x P_C C_i SA \tag{C.15}$$

$$FC_{xi} = f_x P_C C_x SA \tag{C.16}$$

where f_x is the ratio of the product of cellular membrane permeability and surface area to that of the chloroplast. Equation (C.4) can therefore be rewritten:

$$\frac{F_{FIX}}{f_x P_C SAC_e} = \frac{C_i}{C_e}\left(1 + \frac{K^*_{H_2CO_3}}{H_i}(T_0 + T_U U_0)\right) - \frac{C_x}{C_e}\left(1 + \frac{K^*_{H_2CO_3}}{H_x}(T_0 + T_U U_0)\right), \tag{C.17}$$

and inserting Eq. (C.14) becomes:

$$\frac{C_x}{C_e} = \frac{\left[\frac{\left(1+\frac{K^*_{H_2CO_3}}{H_e}(T_0+T_U U_0)\right) - \frac{F_{FIX}}{C_e P_C SA} - \frac{F_{CAL}}{C_e P_C SA}}{1+\frac{K^*_{H_2CO_3}}{H_i}(T_0+T_U U_0)}\right]\left(1 + \frac{K^*_{H_2CO_3}}{H_i}(T_0 + T_U U_0)\right) - \frac{F_{FIX}}{f_x P_C SAC_e}}{1 + \frac{K^*_{H_2CO_3}}{H_x}(T_0 + T_U U_0)}. \tag{C.18}$$

Coccolith vesicle

Similarly, two additional fluxes across the coccolith vesicle membrane equal:

$$FC_{iv} = f_v P_C C_i SA \tag{C.19}$$

$$FC_{vi} = f_v P_C C_v SA \tag{C.20}$$

where f_v is the ratio of the product of cellular membrane permeability and surface area to that of the coccolith vesicle. Equation (C.5) can therefore be rewritten:

$$\frac{F_{CAL}}{f_v P_C SAC_e} = \frac{C_i}{C_e}\left(1 + \frac{K^*_{H_2CO_3}}{H_i}(T_0 + T_U U_0)\right) - \frac{C_v}{C_e}\left(1 + \frac{K^*_{H_2CO_3}}{H_v}(T_0 + T_U U_0)\right), \tag{C.21}$$

and inserting Eq. (C.14) likewise becomes:

$$\frac{C_v}{C_e} = \frac{\left[\frac{\left(1+\frac{K^*_{H_2CO_3}}{H_e}(T_0+T_UU_0)\right)-\frac{F_{FIX}}{C_eP_CSA}-\frac{F_{CAL}}{C_eP_CSA}}{1+\frac{K^*_{H_2CO_3}}{H_i}(T_0+T_UU_0)}\right]\left(1+\frac{K^*_{H_2CO_3}}{H_i}(T_0+T_UU_0)\right)-\frac{F_{FIX}}{f_vP_CSAC_e}}{1+\frac{K^*_{H_2CO_3}}{H_v}(T_0+T_UU_0)}. \tag{C.22}$$

The values f_x and f_v are constants when all membranes are assumed to have the same permeability, and isometry is assumed.

Utilisation

Membrane permeability to bicarbonate is reliant on the background utilisation of carbon, U_0. The value of U_0 is given by:

$$U_0 = \frac{F_{FIX}+F_{CAL}}{P_CSA(C_e+T_0B_e)} = \frac{\frac{F_{FIX}}{P_CSA}+\frac{F_{CAL}}{P_CSA}}{C_e+T_0B_e} = \frac{\frac{F_{FIX}}{P_CSAC_e}+\frac{F_{CAL}}{P_CSAC_e}}{1+T_0\frac{K^*_{H_2CO_3}}{H_e}} \tag{C.23}$$

C.2 Isotopes

At equilibrium, HCO_3^- has a constant isotopic offset from CO_2, denoted here as E. As both HCO_3^- and CO_2 in each compartment are known if one is known, the whole system can be described by CO_2 alone. The dynamic equations for isotopic fluxes are:

$$\begin{aligned}\frac{d\delta C_i}{dt} = 0 =& \delta C_eFC_{ei} - \delta C_iFC_{ie} + \delta C_xFC_{xi} - \delta C_iFC_{ix} + \delta C_vFC_{vi} \\ & - \delta C_iFC_{iv} - (\delta C_i+E)FB_{ie} + (\delta C_e+E)FB_{ei} + (\delta C_x+E)FB_{xi} - (\delta C_i+E)FB_{ix} \\ & + (\delta C_v+E)FB_{vi} - (\delta C_i+E)FB_{iv}\end{aligned} \tag{C.24}$$

$$\frac{d\delta C_x}{dt} = 0 = \delta C_iFC_{ix} - \delta C_xFC_{xi} + (\delta C_i+E)FB_{ix} - (\delta C_x+E)FB_{xi} - (\delta C_x+\epsilon_f)F_{FIX} \tag{C.25}$$

$$\frac{d\delta C_v}{dt} = 0 = \delta C_iFC_{iv} - \delta C_vFC_{vi} + (\delta C_i+E)FB_{iv} - (\delta C_v+E)FB_{vi} - (\delta C_v+E+\epsilon_{cal})F_{CAL} \tag{C.26}$$

As with chemical fluxes, substituting in expressions for concentration driven diffusion, membrane permeability to HCO_3^- in terms of background utilisation, HCO_3^- concentration in terms of CO_2 and H^+, and rearranging gives:

$$\delta C_v = \frac{\delta C_i \frac{C_i}{C_e}\left(1+(1+E)\frac{K^*_{H_2CO_3}}{H_i}(T_0+T_U U_0)\right) - \frac{(E+\epsilon_{cal})F_{CAL}}{f_v P_C SAC_e}}{\frac{-F_{CAL}}{f_v P_C SAC_e} + \frac{C_v}{C_e}\left(1+(1+E)\frac{K^*_{H_2CO_3}}{H_v}(T_0+T_U U_0)\right)} \tag{C.27}$$

$$\delta C_x = \frac{\delta C_i \frac{C_i}{C_e}\left(1+(1+E)\frac{K^*_{H_2CO_3}}{H_i}(T_0+T_U U_0)\right) - \frac{\epsilon_f F_{FIX}}{f_x P_C SAC_e}}{\frac{-F_{FIX}}{f_x P_C SAC_e} + \frac{C_x}{C_e}\left(1+(1+E)\frac{K^*_{H_2CO_3}}{H_x}(T_0+T_U U_0)\right)} \tag{C.28}$$

$$\delta C_i = \frac{\delta C_e\left(1+(1+E)\frac{K^*_{H_2CO_3}}{H_e}(T_0+T_U U_0)\right) - \frac{(\delta C_x+\epsilon_f)F_FIX}{P_C SAC_e} - \frac{(\delta C_v+E+\epsilon_{cal})F_C AL}{P_C SAC_e}}{\frac{C_i}{C_e}\left(1+(1+E)\frac{K^*_{H_2CO_3}}{H_i}(T_0+T_U U_0)\right)} \tag{C.29}$$

C.3 Summary

The chemical carbon flux equations (C.22), (C.18) and (C.14) can be solved simultaneously. Further, the carbon isotope flux equations, (C.27), (C.28) and (C.29) can also be solved simultaneously, using the chemical carbon flux equations. In these expressions, including U_0, the rates of fixation and calcification always occur divided by $P_C SAC_e$, and this is also the only appearance of these parameters. Thus,

$$\frac{F_{CAL}}{P_C SAC_e} \;\; and \;\; \frac{F_{FIX}}{P_C SAC_e} \tag{C.30}$$

are compound varibles that describe the entire system when constant and intracellular pH is assumed and known *a priori*. In this model, the fixation rate is related to cell size via the equation,

$$F_{FIX} = \rho V \mu \tag{C.31}$$

where ρ is the cellular carbon density and V and μ are the volume and division rate of a cell respectively. As PIC:POC is equal to $\frac{F_{CAL}}{F_{FIX}}$, the compound parameters become:

$$\frac{F_{FIX}}{P_C SAC_e} = \frac{\rho V \mu}{P_C SAC_e} = \frac{r\rho\mu}{3P_C C_e} \tag{C.32}$$

and:

$$\frac{F_{CAL}}{P_C SAC_e} = \frac{PIC:POC\rho V\mu}{P_C SAC_e} = \frac{PIC:POCr\rho\mu}{3P_C C_e}. \tag{C.33}$$

Therefore, at the limit, where intracellular CA is infinitely high such that all compartments are in chemical and isotopic equilibrium, the orthogonal variables that describe the entire system are:

$$PIC:POC \;\; and \;\; \tau = \frac{r\rho\mu}{3P_C C_e}. \tag{C.34}$$

τ is a parameter that is similar to the ratios that evolved through early work describing carbon fluxes in phytoplankton (Cassar *et al.*, 2006; Farquhar, 1983; Farquhar *et al.*, 1982; Keller & Morel, 1999; Laws *et al.*, 1995, 1997; Popp *et al.*, 1998; Sharkey & Berry, 1985). The more complicated disequilibrium model collapses to a state completely consistent with these earlier work when equilibrium is assumed and PIC:POC = 0. When the cell is close to chemical and isotopic equilibrium with respect to carbon therefore, changes in cell size, growth rate and extracellular [CO_2] cannot be decoupled.

Appendix D

Alternative intracellular pH

In this appendix, the model outputs for the alternative scenarios described in Section 3.4.3 are presented. The model-constrained parameter values for each of these alternative scenarios are given in Table D.1. The parameters are: membrane permeability to CO_2 (P_C), background membrane permeability to HCO_3^- (T_0), increased permeability of membranes to HCO_3^- per unit utilisation (T_U), isotopic fractionation of carbon my the enzyme RuBisCO during carbon fixation ϵ_f, and pHs in all compartments (chloroplast - pH_x, coccolith vesicle - pH_v, cytosol - pH_i). Note how the form of the model output is consistent across different scenarios, even when rather contrived adjustments are made to enhance the saturation state of the coccolith vesicle (CV).

Table D.1: Model-constrained parameters for alternative scenarios.

Scenario	P_C	T_0	T_U	ϵ_f	$\mathbf{pH}_x$	$\mathbf{pH}_v$	$\mathbf{pH}_i$
(iv) pH of Anning *et al.* (1996)	5.12×10^{-04}	9.16×10^{-8}	7.88×10^{-6}	-14.6	7.90	7.10	7.00
(iii) pH constrained by model	8.30×10^{-04}	1.20×10^{-7}	1.34×10^{-7}	-14.5	7.14	7.55	7.05
(ii) pH constrained by model and HCO_3^- efflux from CV = 0	8.61×10^{-4}	6.30×10^{-8}	1.35×10^{-5}	-14.3	6.78	7.71	8.20
(i) pH constrained by model, HCO_3^- efflux from CV = 0 and pH_v specified as being >8.3	5.08×10^{-04}	7.72×10^{-8}	7.26×10^{-6}	-13.4	8.20	8.95	7.95

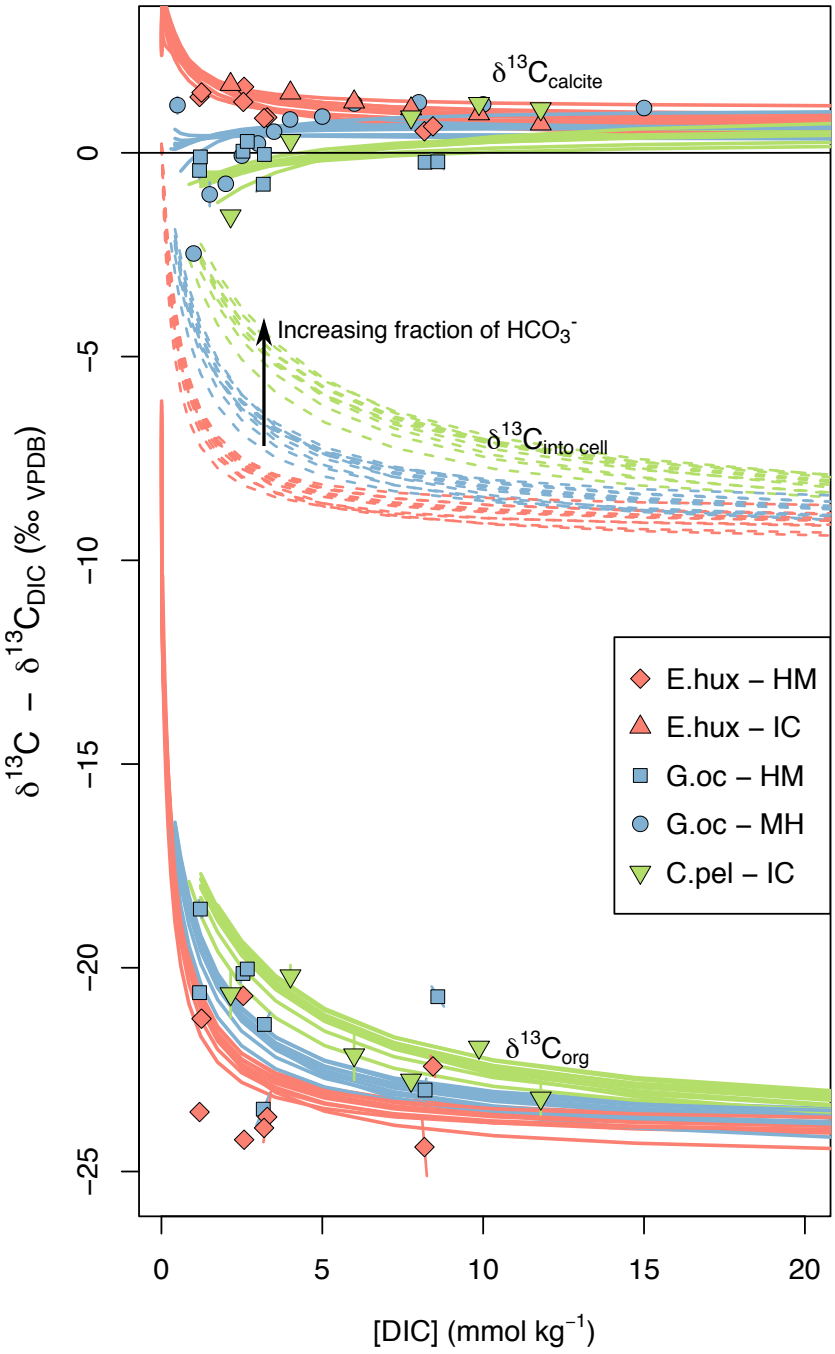

Figure D.1: Culture data with modelled output **(iv)**, for three sets of typical species-specific variables, held constant with DIC. Four free parameters constrained by the model: P_C, T_0, T_U and ϵ_f, with pH values for each compartment pre-specified according to the values of Anning *et al.* (1996)

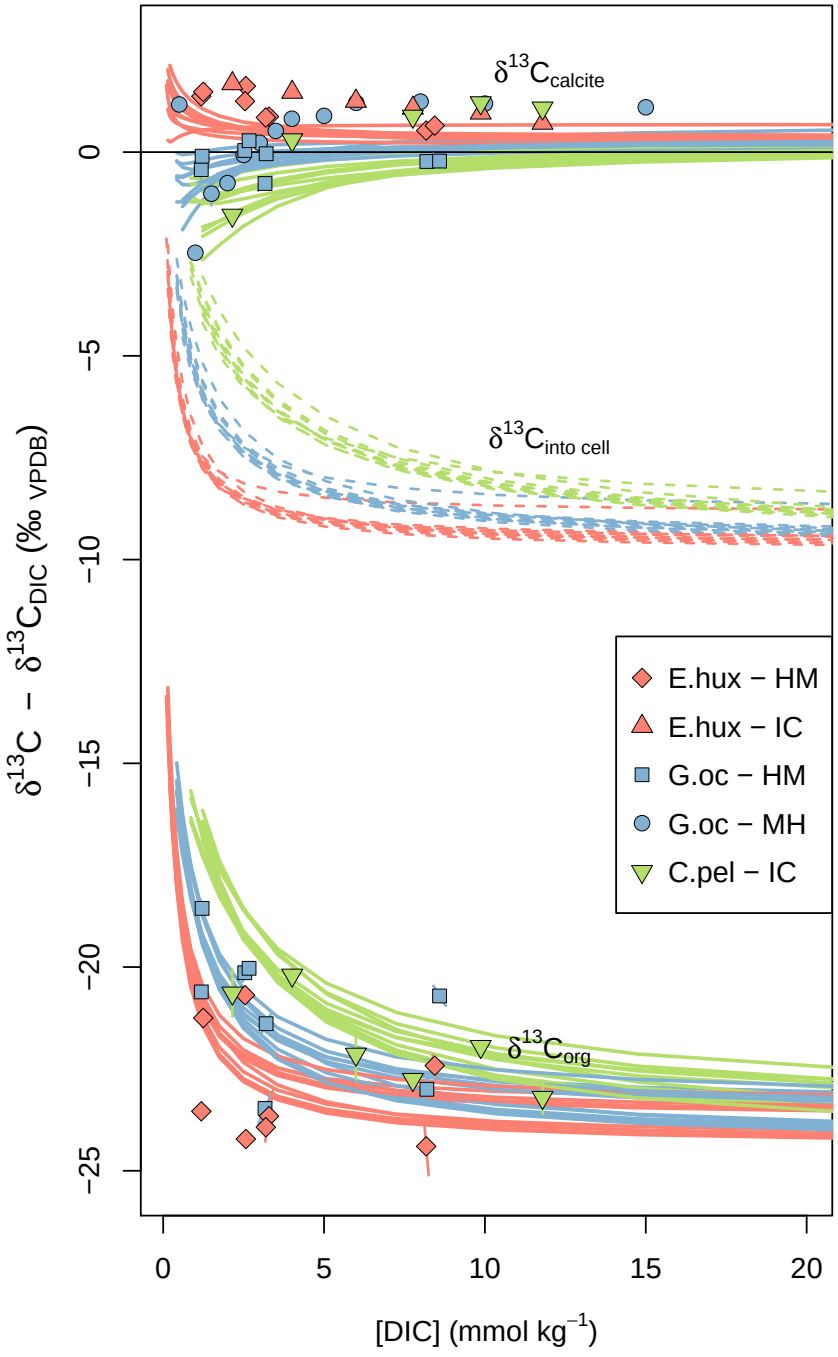

Figure D.2: Culture data with modelled output **(iii)**, for three sets of typical species-specific variables, held constant with DIC. Seven free parameters constrained by the model: P_C, T_0, T_U, ϵ_f, and pH in all compartments.

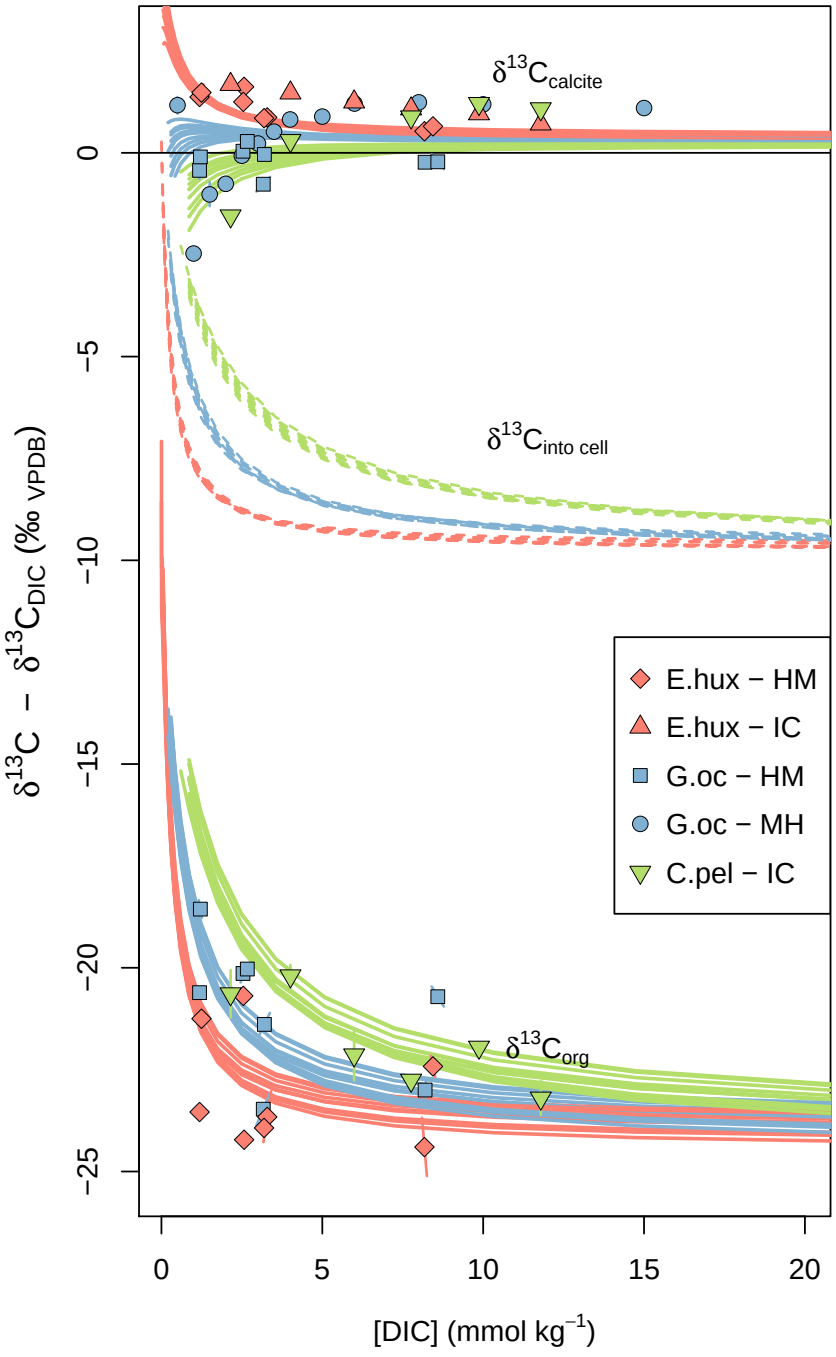

Figure D.3: Culture data with modelled output **(ii)**, for three sets of typical species-specific variables, held constant with DIC. Seven free parameters constrained by the model: P_C, T_0, T_U, ϵ_f, and pH in all compartments. Bicarbonate efflux from the CV is suppressed, all other fluxes are passive or facilitated diffusion as described previously.

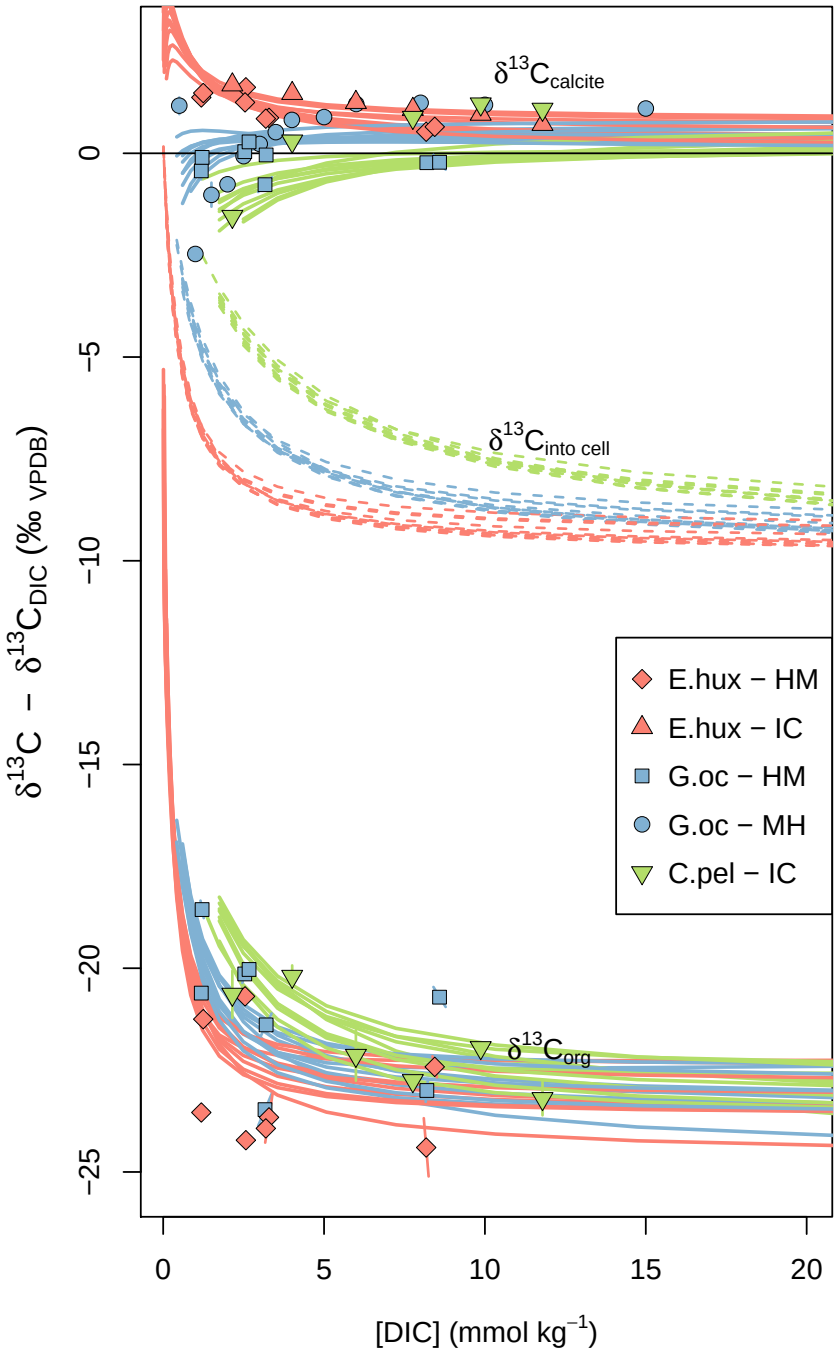

Figure D.4: Culture data with modelled output **(i)**, for three sets of typical species-specific variables, held constant with DIC. Seven free parameters constrained by the model: P_C, T_0, T_U, ϵ_f, and pH in all compartments, but also with the additional constraint that pH in the CV must be above 8.3 (results of Holtz *et al.*, 2014). Bicarbonate efflux from the CV is suppressed, all other fluxes are passive or facilitated diffusion as described previously.

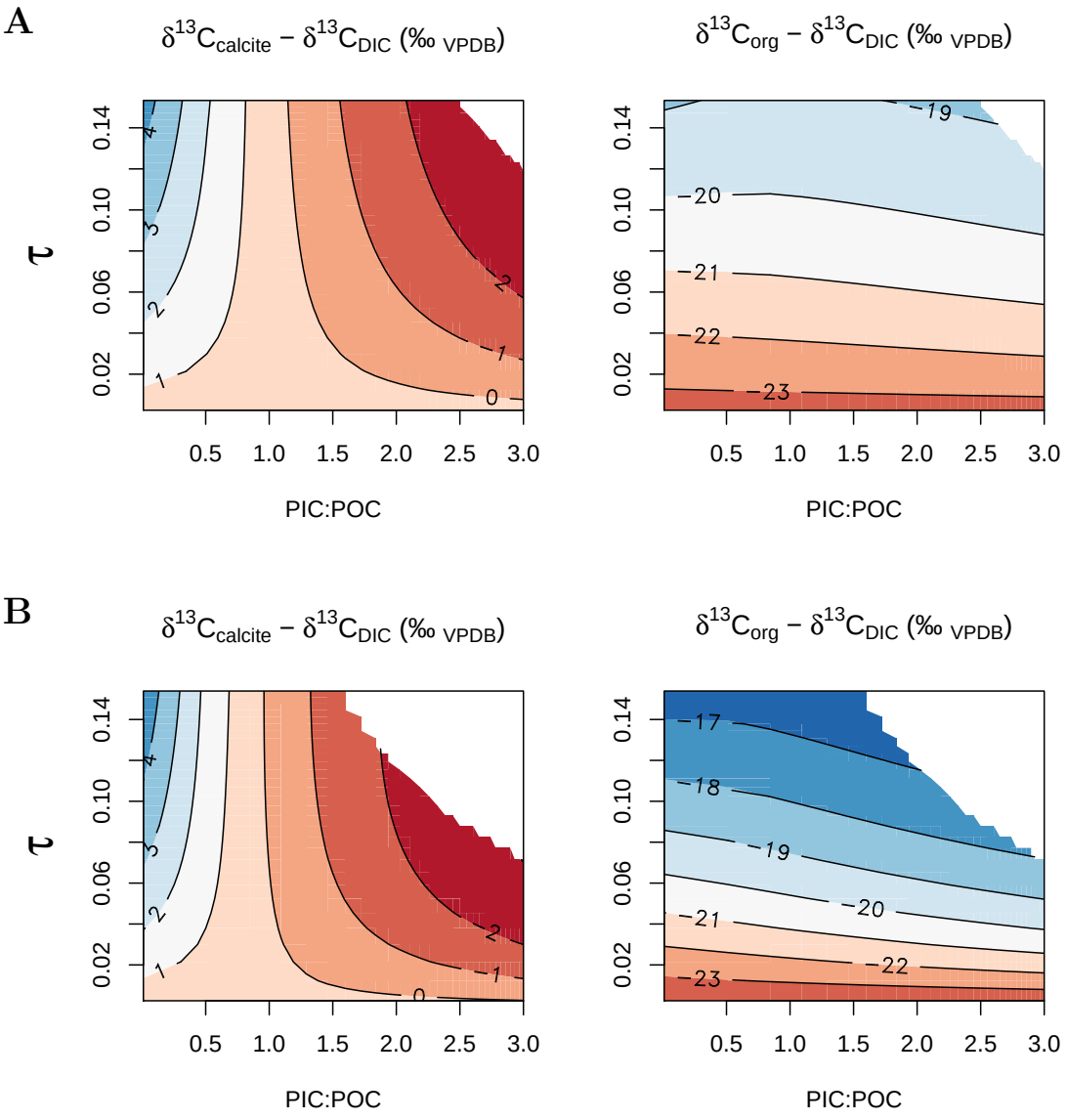

Figure D.5: Model output in PIC:POC / τ space. **A:** Results for scenario **iv** - pH specified by Anning *et al.* (1996). **B:** Results for scenario **iii** - pH fitted by the model. Note how the aspect of model behaviour whereby PIC:POC controls the divergence in vital effects is robust, but that the PIC:POC value at which the divergence occurs differs slightly between scenarios.

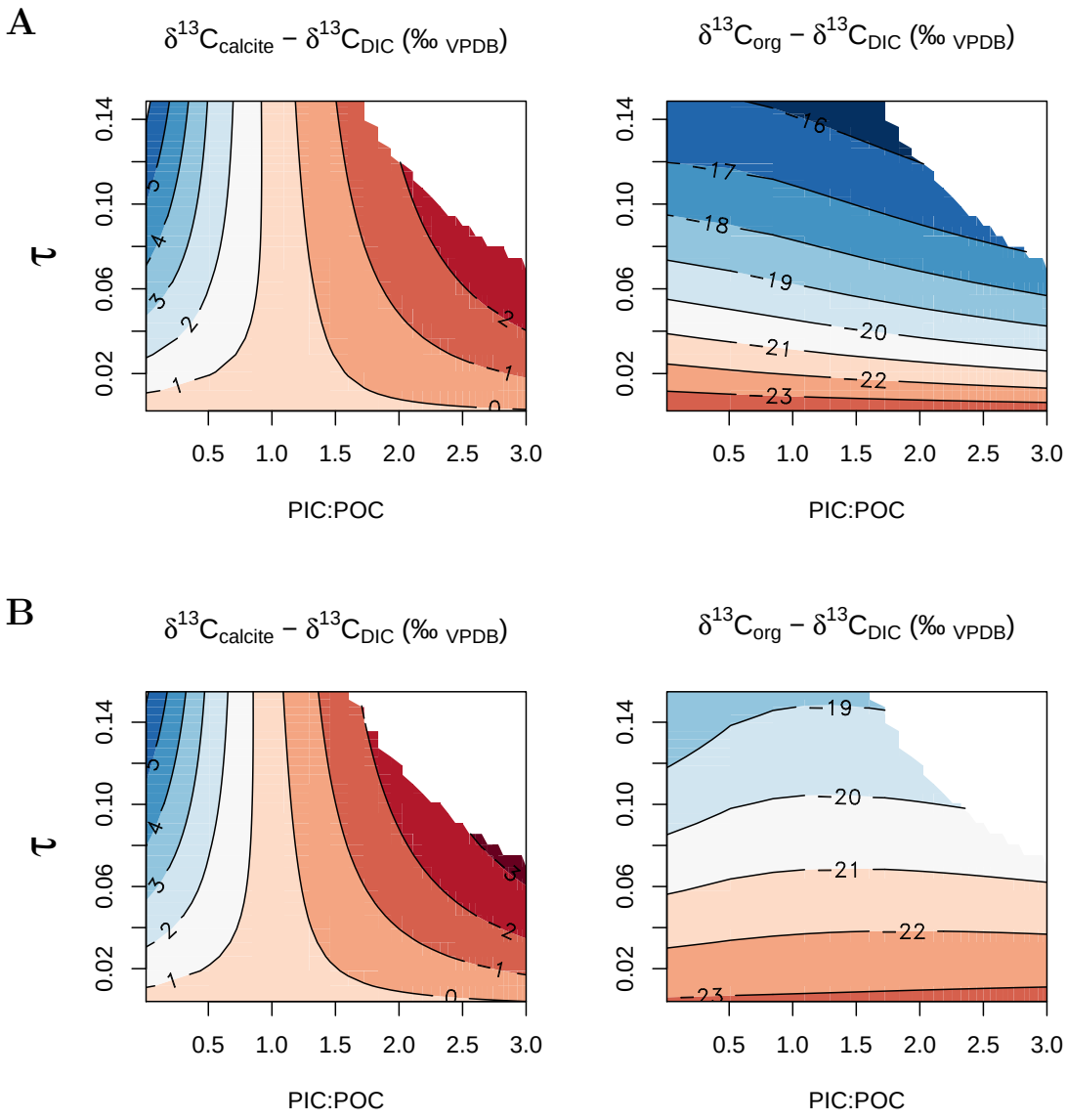

Figure D.6: Model output in PIC:POC / τ space. **A:** Results for scenario **ii** - pH fitted by the model, and carbon is not allowed to leave the CV. **B:** Results for scenario **i** - pH fitted by the model, and carbon is not allowed to leave the CV, additional constraint of high pH (>8.3) in CV. Note how the aspect of model behaviour whereby PIC:POC controls the divergence in vital effects is robust, but that the PIC:POC value at which the divergence occurs differs slightly between scenarios.

References

Alverson, KD, Bradley, RS, & Pedersen, TF. 2003. *Paleoclimate, global change and the future*, Springer-Verlag Berlin Heidelberg.

Anand, Pallavi, Elderfield, Henry, & Conte, MH. 2003. Calibration of Mg/Ca thermometry in planktonic foraminifera from a sediment trap time series. *Paleoceanography*, **28**(2), 1–15.

Anning, T, Nimer, N, Merrett, MJ, & Brownlee, C. 1996. Costs and benefits of calcification in coccolithophorids. *Journal of marine systems*, **9**, 45–56.

Archer, & Maier-Reimer. 1994. Effect of deep-sea sedimentary calcite preservation on atmospheric CO_2 concentration. *Nature*, **367**, 260–263.

Archer, D., Kheshgi, H., & Maier-Reimer, E. 1997. Multiple timescales for neutralization of fossil fuel CO_2. *Geophysical research letters*, **24**(4), 405–408.

Archer, David. 1991. Modelling the calcite lysocline. *Journal of geophysical research*, **96**(C9), 17037–17050.

Austin, JC, & Schroeder, PA. 2014. Assessment of Pedogenic Gibbsite as a Paleo-pCO_2 Proxy Using a Modern Ultisol. *Clays and clay minerals*, **62**(4), 253 – 266.

Bach, Lennart Thomas, Riebesell, Ulf, & Georg Schulz, Kai. 2011. Distinguishing between the effects of ocean acidification and ocean carbonation in the coccolithophore *Emiliania huxleyi*. *Limnology and oceanography*, **56**(6), 2040–2050.

Bach, Lennart Thomas, Riebesell, Ulf, Gutowska, Magdalena, Federwisch, Luisa, & Schulz, Kai Georg. 2015. A unifying concept of coccolithophore sensitivity to changing carbonate chemistry embedded in an ecological framework. *Progress in oceanography*, **135**, 125–138.

Bach, LT, Mackinder, L, & Schulz, KG. 2013. Dissecting the impact of CO_2 and pH on the mechanisms of photosynthesis and calcification in the coccolithophore *Emiliania huxleyi*. *New phytologist*, **199**, 121–134.

Badger, Marcus P. S., Lear, Caroline H., Pancost, Richard D., Foster, Gavin L., Bailey, Trevor R., Leng, Melanie J., & Abels, Hemmo,. 2013a. CO_2 drawdown following the middle Miocene expansion of the Antarctic Ice Sheet. *Paleoceanography*, **28**(1), 42–53.

Badger, Marcus P S, Schmidt, Daniela N, Mackensen, Andreas, & Pancost, Richard D. 2013b. High-resolution alkenone palaeobarometry indicates relatively stable pCO_2 during the Pliocene (3.3-2.8 Ma). *Philosophical transactions. Series A, mathematical, physical, and engineering sciences*, **371**(2001)

Badger, MR, & Andrews, TJ. 1998. The diversity and coevolution of Rubisco, plastids, pyrenoids, and chloroplast-based CO_2-concentrating mechanisms in algae. *Canadian journal of botany*, **76**(6), 1052–1071.

Bains, Santo, Norris, RD, Corfield, RM, & Faul, KL. 2000. Termination of global warmth at the Palaeocene/Eocene boundary through productivity feedback. *Nature*, **407**, 171–174.

Barker, S., Greaves, M., & Elderfield, H. 2003a. A study of cleaning procedures used for foraminiferal Mg/Ca paleothermometry. *Geochemistry, geophysics, geosystems*, **4**(9).

Barker, S, Higgins, J, & Elderfield, H. 2003b. The future of the carbon cycle: review, calcification response, ballast and feedback on atmospheric CO_2. *Philosophical transactions. Series A, mathematical, physical, and engineering sciences*, **361**(1810), 1977–98; discussion 1998–9.

Baumann, Gregory F., Isenberg, Henry D., & Gennaro, Joseph Jr. 1978. The Inverse Relationship Between Nutrient Nitrogen Concentration and Coccolith Calcification in Cultures of the Coccolithophorid *Hymenomonas sp. Journal of protozoology*, **25**(2), 253–256.

Bauska, Thomas K., Joos, Fortunat, Mix, Alan C., Roth, Raphael, Ahn, Jinho, & Brook, Edward J. 2015. Links between atmospheric carbon dioxide, theland carbon reservoir and climate over thepast millennium. *Nature geoscience*, **8**(5), 383–387.

Beaufort, L, & Dollfus, D. 2004. Automatic recognition of coccoliths by dynamical neural networks. *Marine micropaleontology*, **51**(1-2), 57–73.

Beaufort, L., Probert, I., de Garidel-Thoron, T., Bendif, E. M., Ruiz-Pino, D., Metzl, N., Goyet, C., Buchet, N., Coupel, P., Grelaud, M., Rost, B., Rickaby, R. E. M., & de Vargas, C. 2011. Sensitivity of coccolithophores to carbonate chemistry and ocean acidification. *Nature*, **476**(7358), 80–83.

Beaufort, Luc. 2005. Weight estimates of coccoliths using the optical properties (birefringence) of calcite. *Micropaleontology*, **51**(4), 289–297.

Beaufort, Luc, Barbarin, Nicolas, & Gally, Yves. 2014. Optical measurements to determine the thickness of calcite crystals and the mass of thin carbonate particles such as coccoliths. *Nature protocols*, **9**(3), 633–42.

Beckmann Coulter. *The Coulter Principle.* www.beckmancoulter.com.

Beerling, David J., & Royer, Dana L. 2011. Convergent Cenozoic CO_2 history. *Nature geoscience*, **4**(7), 418–420.

Bendif, El Mahdi, & Young, Jeremy. 2014. On the Ultrastructure of *Gephyrocapsa oceanica* (Haptophyta) Life Stages. *Cryptogamie, algologie*, **35**(4), 379–388.

Bendif, El Mahdi, Probert, Ian, Carmichael, Margaux, Romac, Sarah, Hagino, Kyoko, & de Vargas, Colomban. 2014. Genetic delineation between and within the widespread coccolithophore morpho-species *Emiliania huxleyi* and *Gephyrocapsa oceanica* (Haptophyta). *Journal of phycology*, **50**(1), 140–148.

Benthien, Albert, Zondervan, Ingrid, Engel, Anja, Hefter, Jens, Terbrüggen, Anja, & Riebesell, Ulf. 2007. Carbon isotopic fractionation during a mesocosm bloom experiment dominated by *Emiliania huxleyi*: Effects of CO_2 concentration and primary production. *Geochimica et cosmochimica acta*, **71**(6), 1528–1541.

Berger, A. 1988. Milankovitch theory and climate. *Reviews of geophysics*, **26**(4), 624–657.

Berges, John., Franklin, Daniel J., & Harrison, Paul J. 2001. Evolution of an Artificial Seawater Medium: Improvements in Enriched Seawater, Artificial Water Over the Last Two Decades. *Journal of phycology*, **37**(6), 1138–1145.

Berner, RA, Lasaga, AC, & Garrels, RM. 1983. The carbonate-silicate geochemical cycle and its effect on atmospheric carbon dioxide over the past 100 million years. *American journal of science*, **283**(7), 641–683.

Berry, JA. 1989. Studies of mechanisms affecting the fractionation of carbon isotopes in photosynthesis. *Stable isotopes in ecological research*, **6**, 82–94.

Bidigare, RR, & Fluegge, A. 1997. Consistent fractionation of ^{13}C in nature and in the laboratory: Growth-rate effects in some haptophyte algae. *Global biogeochemical cycles*, **11**(2), 279–292.

Boller, AJ, Thomas, PJ, Cavanaugh, CM, & Scott, KM. 2015. Isotopic discrimination and kinetic parameters of RubisCO from the marine bloom–forming diatom, *Skeletonema costatum*. *Geobiology*, **13**(1), 33–43.

Boller, Amanda J., Thomas, Phaedra J., Cavanaugh, Colleen M., & Scott, Kathleen M. 2011. Low stable carbon isotope fractionation by coccolithophore RuBisCO. *Geochimica et cosmochimica acta*, **75**(22), 7200–7207.

Bollmann, J. 2014. Technical Note: Weight approximation of coccoliths using a circular polarizer and interference colour derived retardation estimates (The CPR Method). *Biogeosciences*, **11**(7), 1899–1910.

Bolton, Clara T, & Stoll, Heather M. 2013. Late Miocene threshold response of marine algae to carbon dioxide limitation. *Nature*, **500**(7464), 558–62.

Bolton, Clara T., Stoll, Heather M., & Mendez-Vicente, Ana. 2012. Vital effects in coccolith calcite: Cenozoic climate–pCO_2 drove the diversity of carbon acquisition strategies in coccolithophores? *Paleoceanography*, **27**(4).

Bottini, Cinzia, Erba, Elisabetta, & Tiraboschi, Daniele. 2014. Calcareous nannofossil paleofluxes as proxy for pCO_2 during the Aptian. *EGU general assembly abstracts volume*, **16**, 5411.

Bown, Paul. 1998. *Calcareous nannofossil biostratigraphy.* Springer.

Boyd, Philip W, & Doney, Scott C. 2003. The Impact of Climate Change and Feedback Processes on the Ocean Carbon Cycle. *In:* Fasham, Michael J.R. (ed), *Ocean biogeochemistry.* Springer.

Brassell, Simon C., & Dumitrescu, Mirela. 2004. Recognition of alkenones in a lower Aptian porcellanite from the west-central Pacific. *Organic geochemistry*, **35**(2), 181–188.

Broecker, Wallace S. 1975. Climatic Change: Are we on the brink of a pronounced global warming? *Science*, **189**, 460–463.

Broecker, WS. 1966. Absolute Dating and the Astronomical Theory of Glaciation. *Science*, **151**(3708), 299–304.

Buitenhuis, Erik T., de Baar, Hein J. W., & Veldhuis, Marcel J. W. 1999. Photosynthesis and Calcification By *Emiliania huxleyi* (Prymnesiophyceae) As a Function of Inorganic Carbon Species. *Journal of phycology*, **35**(5), 949–959.

Burkhardt, S, Riebesell, U, & Zondervan, I. 1999. Stable carbon isotope fractionation by marine phytoplankton in response to daylength, growth rate, and CO_2 availability. *Marine ecology progress series*, **184**, 31–41.

Burki, Fabien, Okamoto, Noriko, Pombert, Jean-François, & Keeling, Patrick J. 2012. The evolutionary history of haptophytes and cryptophytes: phylogenomic evidence for separate origins. *Proceedings. biological sciences / the royal society*, **279**(1736), 2246–54.

Cassar, Nicolas, Laws, Edward., & Popp, Brian N. 2006. Carbon isotopic fractionation by the marine diatom *Phaeodactylum tricornutum* under nutrient- and light-limited growth conditions. *Geochimica et cosmochimica acta*, **70**(21), 5323–5335.

Cavalier-Smith, T. 2002. The phagotrophic origin of eukaryotes and phylogenetic classification of Protozoa. *International journal of systematic and evolutionary microbiology*, **52**(2), 297–354.

Cavalier-Smith, Tom. 1999. Principles of Protein and Lipid Targeting in Secondary Symbiogenesis: Euglenoid, Dinoflagellate, and Sporozoan Plastid Origins and the Eukaryote Family Tree, 2. *The journal of eukaryotic microbiology*, **46**(4), 347–366.

Collins, S. 2010. Comment on "Effects of long-term high CO_2 exposure on two species of coccolithophore" by Müller et al. (2010). *Biogeosciences*, **7**(7), 2199–2202.

Conte, Maureen H., Sicre, Marie-Alexandrine, Rühlemann, Carsten, Weber, John C., Schulte, Sonja, Schulz-Bull, Detlef, & Blanz, Thomas. 2006. Global temperature calibration of the alkenone unsaturation index (U^K_{37}) in surface waters and comparison with surface sediments. *Geochemistry, geophysics, geosystems*, **7**(2).

Conte, MH, & Thompson, Anthony. 1995. Lipid biomarker diversity in the coccolithophorid *Emiliania huxleyi* (Prymnesiophycae) and the related species *Gephyrocapsa oceanica*. *Journal of phycology*, **31**, 272–281.

Coplen, TB. 1995. Reporting of stable hydrogen, carbon, and oxygen isotopic abundances. *Geothermics*, **66**(2), 273–276.

Corstjens, PLAM, van der Kooij, A, Linschooten, C, Brouwers, G, Westbroek, P, & Vrind-de Jong, E. 1998. GPA, a calcium-binding protein in the coccolithophorid *Emiliania huxleyi* (Prymnesiophyceae). *Journal of phycology*, **630**, 622–630.

Crundwell, Martin, Scott, George, Naish, Tim, & Carter, Lionel. 2008. Glacial–interglacial ocean climate variability from planktonic foraminifera during the Mid-Pleistocene transition in the temperate Southwest Pacific, ODP Site 1123. *Palaeogeography, palaeoclimatology, palaeoecology*, **260**(1-2), 202–229.

Darwin, C. 1859. *On the origin of species by means of natural selection*. London: Murray.

de Vargas, Colomban, & Aubry, MP. 2007. Origin and evolution of coccolithophores: From coastal hunters to oceanic farmers. *In:* Falkowski, P. & Knoll, A.H. (eds), *Evolution of primary producers in the sea*. Elsevier.

de Vargas, Colomban, Sáez, AG, Medlin, LK, & Thierstein, HR. 2004. Super-species in the calcareous plankton. *In:* Thierstein, HR. & Young, J. (eds), *Coccolithophores: From molecular processes to global impacts*. Springer.

de Villiers, S, Greaves, M. J., & Elderfield, H. 2002. An intensity ratio calibration method for the accurate determination of Mg/Ca and Sr/Ca of marine carbonates by ICP–AES. *Geochemistry, geophysics, geosystems*, **3**(1).

der Wal, P Van, & Jong, EW De. 1983. Ultrastructural polysaccharide localization in calcifying and naked cells of the coccolithophorid *Emiliania huxleyi*. *Protoplasma*, **168**, 157–168.

Dickson, AG. 1981. An exact definition of total alkalinity and a procedure for the estimation of alkalinity and total inorganic carbon from titration data. *Deep sea research part a. oceanographic research papers*, **28**(6), 609–623.

DOE. 1994. Handbook of Methods for the Analysis of the Various Parameters of the Carbon Dioxide System in Sea Water, *version 2.* Dickson, AG, & Goyet, C.(eds)

Doney, Scott C., Fabry, Victoria J., Feely, Richard, & Kleypas, Joan. 2009. Ocean Acidification: The Other CO_2 Problem. *Annual review of marine science*, **1**(1), 169–192.

Duarte, CM, & Cebrian, J. 1996. The fate of marine autotrophic production. *Limnology and oceanography*, **41**(8), 1758–1766.

Dudley, W.C., Blackwelder, P., Brand, L., & Duplessy, J.C. 1986. Stable isotopic composition of coccoliths. *Marine micropaleontology*, **10**(1-3), 1–8.

Elderfield, H, & Ganssen, G. 2000. Past temperature and δ^{18}O of surface ocean waters inferred from foraminiferal Mg/Ca ratios. *Nature*, **405**(6785), 442–5.

Elderfield, H, Ferretti, P, & Greaves, M. 2012. Evolution of Ocean Temperature and Ice Volume Through the Mid-Pleistocene Climate Transition. *Science*, **704**(2012).

Emiliani, C. 1966. Isotopic Paleotemperatures. *Science*, **154**(3751), 851–857.

Falkowski, P, Scholes, RJ, & Boyle, E., Canadell, J., Canfield, D., Elser, J., Gruber, N., Hibbard, K., Högberg, P., Linder, S., Mackenzie, F. T., Moore B., Pedersen, T., Rosenthal, Y., Seitzinger, S., Smetacek, V., & Steffen, W. 2000. The global carbon cycle: a test of our knowledge of earth as a system. *Science*, **290**, 291–297.

Falkowski, Paul G, Katz, Miriam E, Knoll, Andrew H, Quigg, Antonietta, Raven, John, Schofield, Oscar, & Taylor, F J R. 2004. The evolution of modern eukaryotic phytoplankton. *Science*, **305**(5682), 354–60.

Falkowski, PG, & Raven, JA. 2013. *Aquatic photosynthesis*. Princeton University Press.

Farquhar, GD. 1983. On the nature of carbon isotope discrimination in C4 species. *Australian journal of plant physiology*, **10**, 205–226.

Farquhar, GD, O'leary, MH, & Berry, JA. 1982. On the relationship between carbon isotope discrimination and the intercellular carbon dioxide concentration in leaves. *Australian journal of plant physiology*, **9**, 121–137.

Fink, Christina, Baumann, Karl-Heinz, Groeneveld, Jeroen, & Steinke, Stephan. 2010. Strontium/Calcium ratio, carbon and oxygen stable isotopes in coccolith carbonate from different grain-size fractions in South Atlantic surface sediments. *Geobios*, **43**(1), 151–164.

Fiorini, Sarah, Gattuso, Jean-Pierre, van Rijswijk, Pieter, & Middelburg, Jack. 2010. Coccolithophores lipid and carbon isotope composition and their variability related to changes in seawater carbonate chemistry. *Journal of experimental marine biology and ecology*, **394**(1-2), 74–85.

Fletcher, Benjamin J., Brentnall, Stuart J., Anderson, Clive W., Berner, Robert, & Beerling, David J. 2007. Atmospheric carbon dioxide linked with Mesozoic and early Cenozoic climate change. *Nature geoscience*, **1**(1), 43–48.

Foster, G.L. 2008. Seawater pH, pCO_2 and $[CO_3^{2-}]$ variations in the Caribbean Sea over the last 130 kyr: A boron isotope and B/Ca study of planktic foraminifera. *Earth and planetary science letters*, **271**(1-4), 254–266.

Frada, Miguel, Probert, Ian, Allen, Michael J, Wilson, William H, & de Vargas, Colomban. 2008. The "Cheshire Cat" escape strategy of the coccolithophore *Emiliania huxleyi* in response to viral infection. *Proceedings of the national academy of sciences of the united states of america*, **105**(41), 15944–15949.

Francois, R, & Altabet, MA., Goericke, R., McCorkle, D.C., Brunet, C., Poisson, A. 1993. Changes in the δ^{13}C of surface water particular organic matter across the subtropical convergence in the SW Indian Ocean. *Global Biogeochemical Cycles*, **7**(3), 627–644.

Frankignoulle, M, Canon, C, & Gattuso, JP. 1994. Marine calcification as a source of carbon dioxide: Positive feedback of increasing atmospheric CO_2. *Limnology and oceanography*, **39**(2) 458–462.

Franks, PJ, Adams, MA, & Amthor, JS. 2013. Sensitivity of plants to changing atmospheric CO_2 concentration: from the geological past to the next century. *New phytologist*, **197**(4) 1077–1094.

Franks, PJ, Royer, DL, Beerling, D., Van de Water, P., Cantrill, D., Barbour, M., & Berry, J. 2014. New constraints on atmospheric CO_2 concentration for the Phanerozoic. *Geophysical research letters*, 4685–4694.

Freeman, KH, & Hayes, JM. 1992. Fractionation of carbon isotopes by phytoplankton and estimates of ancient CO_2 levels. *Global biogeochemical cycles*, **6**(2), 185–198.

Gablonsky, JM, & Kelley, CT. 2001. A locally-biased form of the DIRECT algorithm. *Journal of global optimization*, **21**, 27–37.

Gattuso, J-P, Magnan, A, Billé, R, Cheung, W W L, Howes, E L, Joos, F, Allemand, D, Bopp, L, Cooley, S R, Eakin, C M, Hoegh-Guldberg, O, Kelly, R P, Pörtner, H-O, Rogers, a D, Baxter, J M, Laffoley, D, Osborn, D, Rankovic, A, Rochette, J, Sumaila, U R, Treyer, S, & Turley, C. 2015. Contrasting futures for ocean and society from different anthropogenic CO_2 emissions scenarios. *Science*, **349**(6243).

Gavis, J, & Ferguson, JF. 1975. Kinetics of carbon dioxide uptake by phytoplankton at high pH1. *Limnology and oceanography*, **20**(2), 211–221.

Gibbs, Samantha J., Poulton, Alex J., Bown, Paul R., Daniels, Chris J., Hopkins, Jason, Young, Jeremy R., Jones, Heather L., Thiemann, Geoff J., O'Dea, Sarah a., & Newsam, Cherry. 2013. Species-specific growth response of coccolithophores to Palaeocene–Eocene environmental change. *Nature geoscience*, **6**(3), 1–5.

Gould, Sven B., Waller, Ross F., & McFadden, Geoffrey I. 2008. Plastid Evolution. *Annual review of plant biology*, **59**(1), 491–517.

Greaves, M., & Caillon, N. 2008. Interlaboratory comparison study of calibration standards for foraminiferal Mg/Ca thermometry. *Geochemistry Geophysics Geosystems*, **9**(8).

Gregg, Watson W., & Casey, Nancy W. 2007. Modeling coccolithophores in the global oceans. *Deep sea research part ii: Topical studies in oceanography*, **54**(5-7), 447–477.

Guo, W. 2009. Carbonate clumped isotope thermometry: application to carbonaceous chondrites and effects of kinetic isotope fractionation. Dissertation (Ph.D.), California Institute of Technology.

Gussone, Nikolaus, Langer, Gerald, & Thoms, S. 2006. Cellular calcium pathways and isotope fractionation in *Emiliania huxleyi*. *Geology*, **34**(8), 625–628.

Guy, RD, Fogel, ML, & Berry, JA. 1993. Photosynthetic Fractionation of the Stable lsotopes of Oxygen and Carbon. *Plant physiology*, **101**(1), 37–47.

Halloran, P. R., Hall, I. R., Colmenero-Hidalgo, E., & Rickaby, R. E. M. 2008. Evidence for a multi-species coccolith volume change over the past two centuries: understanding a potential ocean acidification response. *Biogeosciences*, **5**(6), 1651–1655.

Hayes, JM. 1983. Practice and principles of isotopic measurements in organic geochemistry. *In:* W. G. Meinschein (ed.), *Organic Geochemistry of Contemporaneous and Ancient Sediments,*. Society of Economic Paleontologists and Mineralogists

Henderiks, Jorijntje. 2008. Coccolithophore size rules – Reconstructing ancient cell geometry and cellular calcite quota from fossil coccoliths. *Marine micropaleontology*, **67**(1-2), 143–154.

Henderiks, Jorijntje, & Pagani, Mark. 2007. Refining ancient carbon dioxide estimates: Significance of coccolithophore cell size for alkenone–based pCO_2 records. *Paleoceanography*, **22**(3)

Henderiks, Jorijntje, & Pagani, Mark. 2008. Coccolithophore cell size and the Paleogene decline in atmospheric CO_2. *Earth and planetary science letters*, **269**(3-4), 576–584.

Herbert, T D. 2003. *Treatise on Geochemistry*. Elsevier.

Herfort, Lydie, Thake, Brenda, & Roberts, James. 2002. Acquisition and use of bicarbonate by *Emiliania huxleyi*. *New phytologist*, **156**(3), 427–436.

Hermoso, Michaël. 2014. Coccolith-Derived Isotopic Proxies in Palaeoceanography: Where Geologists Need Biologists. *Cryptogamie, algologie*, **35**(4), 323–351.

Hermoso, Michaël, Horner, Tristan J., Minoletti, Fabrice, & Rickaby, Rosalind E.M. 2014. Constraints on the vital effect in coccolithophore and dinoflagellate calcite by oxygen isotopic modification of seawater. *Geochimica et cosmochimica acta*, **141**, 612–627.

Heureux, Ana M.C., & Rickaby, Rosalind E.M. 2015. Refining our estimate of atmospheric CO_2 across the Eocene–Oligocene climatic transition. *Earth and planetary science letters*, **409**, 329–338.

Ho, SL, Naafs, BDA, & Lamy, F. 2013. Alkenone Paleothermometry Based on the Haptophyte Algae. *The encyclopedia of quaternary science*, **2**, 755–764.

Hollander, DJ, & McKenzie, JA. 1991. CO_2 control on carbon-isotope fractionation during aqueous photosynthesis : A paleo-pCO_2 barometer. *Geology*, **19**(9), 929–932

Holtz, Lena-Maria, Wolf-Gladrow, Dieter, & Thoms, Silke. 2014. Numerical cell model investigating cellular carbon fluxes in *Emiliania huxleyi*. *Journal of theoretical biology*, **364**, 305–315.

Holtz, Lena-Maria, Wolf-Gladrow, Dieter, & Thoms, Silke. 2015. Simulating the effects of light intensity and carbonate system composition on particulate organic and inorganic carbon production in *Emiliania huxleyi*. *Journal of theoretical biology*, **372**, 192–204.

Hönisch, Bärbel, Hemming, N Gary, Archer, David, Siddall, Mark, & McManus, Jerry F. 2009. Atmospheric carbon dioxide concentration across the mid-Pleistocene transition. *Science* , **324**(5934), 1551–4.

Hopkinson, Brian M. 2014. A chloroplast pump model for the CO_2 concentrating mechanism in the diatom *Phaeodactylum tricornutum*. *Photosynthesis research*, **121**(2-3), 223–33.

Hopkinson, Brian M, Dupont, Christopher L, Allen, Andrew E, & Morel, François M M. 2011. Efficiency of the CO_2-concentrating mechanism of diatoms. *Proceedings of the national academy of sciences of the united states of america*, **108**(10), 3830–7.

Horigome, M. T., Ziveri, P., Grelaud, M., Baumann, K.-H., Marino, G., & Mortyn, P. G. 2014. Environmental controls on the *Emiliania huxleyi* calcite mass. *Biogeosciences*, **11**(8), 2295–2308.

Houdan, Aude, Billard, Chantal, Marie, Dominique, Not, Fabrice, Sáez, Alberto G., Young, Jeremy R., & Probert, Ian. 2004. Holococcolithophore / heterococcolithophore (Haptophyta) life cycles: Flow cytometric analysis of relative ploidy levels. *Systematics and biodiversity*, **1**(4), 453–465.

Hutchins, David. 2011. Forecasting the rain ratio. *Nature*, **476**, 41–42.

Iglesias-Rodriguez, M Debora, Halloran, Paul R, Rickaby, Rosalind E M, Hall, Ian R, Colmenero-Hidalgo, Elena, Gittins, John R, Green, Darryl R H, Tyrrell, Toby, Gibbs, Samantha J, von Dassow, Peter, Rehm, Eric, Armbrust, E Virginia, & Boessenkool, Karin P. 2008. Phytoplankton calcification in a high-CO_2 world. *Science*, **320**(5874), 336–40.

IPCC; P. Ciais, C. Sabine, G. Bala, L. Bopp, V. Brovkin. 2014. Carbon and other biogeochemical cycles. *In:* T. Stocker, D. Qin, G.-K. Plattner, M. Tignor, S.K. Allen, J. Boschung, A. Nauels, Y. Xia , V. Bex, & Midgley., P.M. (eds) *Climate change 2013: The physical science basis. contribution of working group i to the fifth assessment report of the intergovernmental panel on climate change*.

Irie, Takahiro, Bessho, Kazuhiro, Findlay, Helen S, & Calosi, Piero. 2010. Increasing costs due to ocean acidification drives phytoplankton to be more heavily calcified: optimal growth strategy of coccolithophores. *Plos one*, **5**(10).

Jasper, J.P., & Hayes, JM. 1990. A carbon isotope record of CO_2 levels during the late quaternary. *Nature*, **347**(6292), 462–464.

Jasper, JP, Hayes, JM, Mix, AC, & Prahl, FG. 1994. Photosynthetic fractionation of ^{13}C and concentrations of dissolved CO_2 in the central equatorial Pacific during the last 255,000 years. *Paleoceanography.***9** (6), 781–798

Jin, X., Gruber, N., Dunne, J. P., Sarmiento, J. L., & Armstrong, R. a. 2006. Diagnosing the contribution of phytoplankton functional groups to the production and export of particulate organic carbon, $CaCO_3$, and opal from global nutrient and alkalinity distributions. *Global biogeochemical cycles*, **20**(2), 1–17.

Jong, Elisabeth W., Bosch, Leendert, & Westbroek, Peter. 1976. Isolation and Characterization of a Ca^{2+}–Binding Polysaccharide Associated with Coccoliths of *Emiliania huxleyi* (Lohmann) Kamptner. *European journal of biochemistry*, **70**(2), 611–621.

Joos, Fortunat, Plattner, GK, & Stocker, TF. 1999. Global Warming and Marine Carbon Cycle Feedbacks on Future Atmospheric CO_2. *Science*, **284**, 464–468.

Jouzel, J, Masson-Delmotte, V, Cattani, O, Dreyfus, G, Falourd, S, Hoffmann, G, Minster, B, Nouet, J, Barnola, J M, Chappellaz, J, Fischer, H, Gallet, J C, Johnsen, S, Leuenberger, M, Loulergue, L, Luethi, D, Oerter, H, Parrenin, F, Raisbeck, G, Raynaud, D, Schilt, A, Schwander, J, Selmo, E, Souchez, R, Spahni, R, Stauffer, B, Steffensen, J P, Stenni, B, Stocker, T F, Tison, J L, Werner, M, & Wolff, E W. 2007. Orbital and millennial Antarctic climate variability over the past 800,000 years. *Science*, **317**(5839), 793–6.

Keller, K, & Morel, FMM. 1999. A model of carbon isotopic fractionation and active carbon uptake in phytoplankton. *Marine ecology progress series.* **182**, 295–298.

Keller, MD, Selvin, RC, Claus, W., & Guillard, R. R. L. 1987. Media for the culture of oceanic ultraphytoplankton. *Journal of phycology*, **23**, 633–638.

Kirst, GO. 1990. Salinity tolerance of eukaryotic marine algae. *Annual review of plant biology*, **40** 21–53.

Klaas, Christine, & Archer, D.E. 2002. Association of sinking organic matter with various types of mineral ballast in the deep sea: Implications for the rain ratio. *Global biogeochem. cycles*, **16**(4), 1116.

Kottmeier, Dorothee M, Rokitta, Sebastian D, Tortell, Philippe D, & Rost, Björn. 2014. Strong shift from HCO_3^- to CO_2 uptake in *Emiliania huxleyi* with acidification: new approach unravels acclimation versus short-term pH effects. *Photosynthesis research*, **121**(2-3), 265–75.

Langer, G., Nehrke, G., Probert, I., Ly, J., & Ziveri, P. 2009. Strain-specific responses of *Emiliania huxleyi* to changing seawater carbonate chemistry. *Biogeosciences*, **6**(11), 2637–2646.

Langer, Gerald, Gussone, Nikolaus, Nehrke, Gernot, Riebesell, Ulf, Eisenhauer, Anton, Kuhnert, Henning, Rost, Björn, Trimborn, Scarlett, & Thoms, Silke. 2006. Coccolith strontium to calcium ratios in *Emiliania huxleyi*: The dependence on seawater strontium and calcium concentrations. *Limnology and oceanography*, **51**(1), 310–320.

Langer, Gerald, Gussone, Nikolaus, Nehrke, Gernot, Riebesell, Ulf, Eisenhauer, Anton, & Thoms, Silke. 2007. Calcium isotope fractionation during coccolith formation in *Emiliania huxleyi*: Independence of growth and calcification rate. *Geochemistry, geophysics, geosystems*, **8**(5).

Laws, EA, Popp, BN., Bidigare, R., Riebesell, U., Burkhardt, S., Wakeham, S.G., 2001. Controls on the molecular distribution and carbon isotopic composition of alkenones in certain haptophyte algae. *Geochemistry Geophysics Geosystems*, **2**(2000).

Laws, EA, Popp, BN, & Bidigare, RR. 1995. Dependence of phytoplankton carbon isotopic composition on growth rate and [CO_2]aq: Theoretical considerations and experimental results. *Geochemica et cosmochimica acta*, **59**(6).

Laws, EA, Bidigare, RR, & Popp, BN. 1997. Effect of growth rate and CO_2 concentration on carbon isotopic fractionation by the marine diatom *Phaeodactylum tricornutum*. *Limnology and oceanography*, **42**(7), 1552–1560.

Lea, DW, Martin, PA, Pak, DK, & Spero, HJ. 2002. Reconstructing a 350ky history of sea level using planktonic Mg/Ca and oxygen isotope records from a Cocos Ridge core. *Quaternary science reviews*, **21**, 283–293.

Lee, R, Mavridou, D, McClelland, H.L.O., Anderson, C, & Rickaby, R.E.M. 2014. Coccolithophores put a CAP on calcification. *(submitted to PNAS)*.

Leonardos, Nikos, Read, Betsy, Thake, Brenda, & Young, Jeremy R. 2009. No Mechanistic Dependence of Photosynthesis on Calcification in the Coccolithophorid *Emiliania huxleyi* (Haptophyta). *Journal of phycology*, **45**(5), 1046–1051.

Lisiecki, L. E., & Raymo, M. E. 2005. A Pliocene-Pleistocene stack of 57 globally distributed benthic δ^{18}O records. *Paleoceanography*, **20**(1), 1–17.

Lohbeck, Kai T., Riebesell, Ulf, & Reusch, Thorsten B. H. 2012. Adaptive evolution of a key phytoplankton species to ocean acidification. *Nature geoscience*, **5**(5), 346–351.

Loubere, Paul, Siedlecki, Samantha., & Bradtmiller, Louisa I. 2007. Organic carbon and carbonate fluxes: Links to climate change. *Deep sea research part ii: Topical studies in oceanography*, **54**(5-7), 437–446.

Loutre, MF. 2003. Ice ages (Milankovitch theory). *In:* James R. Holton (Ed.) *Encyclopedia of atmospheric sciences.*, Elsevier.

Lueker, Timothy J, Dickson, Andrew G, & Keeling, Charles D. 2000. Ocean pCO_2 calculated from dissolved inorganic carbon, alkalinity, and equations for K1 and K2: validation based on laboratory measurements of CO_2 in gas and seawater at equilibrium. *Marine chemistry*, **70**(1-3), 105–119.

Lüthi, Dieter, Le Floch, Martine, Bereiter, Bernhard, Blunier, Thomas, Barnola, Jean-Marc, Siegenthaler, Urs, Raynaud, Dominique, Jouzel, Jean, Fischer, Hubertus, Kawamura, Kenji, & Stocker, Thomas F. 2008. High-resolution carbon dioxide concentration record 650,000-800,000 years before present. *Nature*, **453**(7193), 379–82.

Lynch–Stieglitz, J, Stocker, Thomas F., Fairbanks, Richard G., & Broecker Wallace S. 1995. The influence of air-sea exchange on the isotopic composition of oceanic carbon: Observations and modeling. *Global biogeochemical cycles*, **9**(4), 653–665.

Mackinder, Luke, Wheeler, Glen, Schroeder, Declan, Riebesell, Ulf, & Brownlee, Colin. 2010a. Molecular Mechanisms Underlying Calcification in Coccolithophores. *Geomicrobiology journal*, **27**(6-7), 585–595.

Mackinder, Luke, Wheeler, Glen, Schroeder, Declan, von Dassow, Peter, Riebesell, Ulf, & Brownlee, Colin. 2011. Expression of biomineralization-related ion transport genes in *Emiliania huxleyi*. *Environmental microbiology*, **13**(12), 3250–65.

Marcott, Shaun a., Bauska, Thomas K., Buizert, Christo, Steig, Eric J., Rosen, Julia L., Cuffey, Kurt M., Fudge, T. J., Severinghaus, Jeffery P., Ahn, Jinho, Kalk, Michael L., McConnell, Joseph R., Sowers, Todd, Taylor, Kendrick C., White, James W. C., & Brook, Edward J. 2014. Centennial-scale changes in the global carbon cycle during the last deglaciation. *Nature*, **514**(7524), 616–619.

Marlowe, I, Brassell, S, Eglinton, G, & Green, J. 1990. Long-chain alkenones and alkyl alkenoates and the fossil coccolith record of marine sediments. *Chemical geology*, **88**(3-4), 349–375.

Marsh, M. 2003. Regulation of $CaCO_3$ formation in coccolithophores. *Comparative biochemistry and physiology part b: Biochemistry and molecular biology*, **136**(4), 743–754.

Marsh, Mary E. 1994. Polyanion-mediated mineralization – assembly and reorganization of acidic polysaccharides in the Golgi system of a coccolithophorid alga during mineral deposition. *Protoplasma*, **177**(3-4), 108–122.

Marsh, ME, Chang, DK, & King, GC. 1992. Isolation and Characterization of a Novel Acidic Polysaccharide Containing Tartrate and Glyoxylate Residues from the Mineralized Scales of a Unicellular Coccolithophorid Alga Pleurochrysis curterue. *Journal of biological chemistry*, **267**, 20507–20512.

Marsh, M.E, Ridall, L., Azadi, P, & Duke, P.J. 2002a. Galacturonomannan and Golgi-derived membrane linked to growth and shaping of biogenic calcite. *Journal of structural biology*, **139**(1), 39–45.

Martínez-Botí, M. a., Marino, G., Foster, G. L., Ziveri, P., Henehan, M. J., Rae, J. W. B., Mortyn, P. G., & Vance, D. 2015. Boron isotope evidence for oceanic carbon dioxide leakage during the last deglaciation. *Nature*, **518**(7538), 219–222.

McCave, I N. 1975. Vertical flux of particles in the ocean. *Deep Sea Research and Oceanographic Abstracts*, **22**(7) 491–502.

McClelland, H.L.O., Taylor, PD, O'Dea, Aaron, & Okamura, Beth. 2014. Revising and refining the bryozoan zs-MART seasonality proxy. *Palaeogeography, palaeoclimatology, palaeoecology*, **410**, 412–420.

Meier, K. J. S., Beaufort, L., Heussner, S., & Ziveri, P. 2014a. The role of ocean acidification in *Emiliania huxleyi* coccolith thinning in the Mediterranean Sea. *Biogeosciences*, **11**(10), 2857–2869.

Meier, K.J.S., Berger, C., & Kinkel, H. 2014b. Increasing coccolith calcification during CO_2 rise of the penultimate deglaciation (Termination II). *Marine micropaleontology*, **112**, 1–12.

Milanković, M. 1930. Mathematische klimalehre und astronomische theorie der klimaschwankungen. *Borntraeger*.

Milliman, J. D., & Droxler, a. W. 1996. Neritic and pelagic carbonate sedimentation in the marine environment: ignorance is not bliss. *Geologische rundschau*, **85**(3), 496–504.

Milliman, JD. 1993. Production and accumulation of calcium carbonate in the ocean: budget of a nonsteady state. *Global biogeochemical cycles*, **7**(4), 927–957.

Milliman, J.D., Troy, P.J., Balch, W.M., a.K. Adams, Li, Y.-H., & Mackenzie, F.T. 1999. Biologically mediated dissolution of calcium carbonate above the chemical lysocline? *Deep sea research part i: Oceanographic research papers*, **46**(10), 1653–1669.

Minoletti, Fabrice, Hermoso, Michaël, & Gressier, Vincent. 2008. Separation of sedimentary micron-sized particles for palaeoceanography and calcareous nannoplankton biogeochemistry. *Nature protocols*, **4**(1), 14–24.

Moore, C. M., Mills, M. M., Arrigo, K. R., Berman-Frank, I., Bopp, L., Boyd, P. W., Galbraith, E. D., Geider, R. J., Guieu, C., Jaccard, S. L., Jickells, T. D., La Roche, J., Lenton, T. M., Mahowald, N. M., Marañón, E., Marinov, I., Moore, J. K., Nakatsuka, T., Oschlies, Saito, M, Thingstad, T. F., Tsuda, & Ulloa, O. 2013. Processes and patterns of oceanic nutrient limitation. *Nature geoscience*, **6**(9), 701–710.

Mucci, A. 1983. The solubility of calcite and aragonite in seawater at various salinities, temperatures and one atmosphere total pressure. *American journal of science*. **288**, 780–799

Müller, M, Antia, A, & LaRoche, J. 2008. Influence of cell cycle phase on calcification in the coccolithophore *Emiliania huxleyi*. *Limnology and oceanography*, **53**(2), 506–512.

Müller, M. N., Schulz, K. G., & Riebesell, U. 2010. Effects of long-term high CO_2 exposure on two species of coccolithophores. *Biogeosciences*, **7**(3), 1109–1116.

Munhoven, Guy. 2007. Glacial–interglacial rain ratio changes: Implications for atmospheric and ocean–sediment interaction. *Deep sea research part ii: Topical studies in oceanography*, **54**(5-7), 722–746.

Nelder, JA, & Mead, R. 1965. A simplex method for function minimization. *The computer journal*. **7**(4), 308–313.

Nimer, Nabil A, Iglesias-rodriguez, M Debora, & Merrett, M.J. 1997. Bicarbonate utilisation by marine phytoplankton species. *Journal of Phychology*, **33**(4), 625–631.

O'Brien, C. J., Peloquin, J. a., Vogt, M., Heinle, M., Gruber, N., Ajani, P., Andruleit, H., Arístegui, J., Beaufort, L., Estrada, M., Karentz, D., Kopczyska, E., Lee, R., Poulton, a. J., Pritchard, T., & Widdicombe, C. 2013. Global marine plankton functional type biomass distributions: coccolithophores. *Earth system science data*, **5**(2), 259–276.

O'Dea, Sarah a, Gibbs, Samantha J, Bown, Paul R, Young, Jeremy R, Poulton, Alex J, Newsam, Cherry, & Wilson, Paul a. 2014. Coccolithophore calcification response to past ocean acidification and climate change. *Nature communications*, **5**, 5363.

Omta, Anne Willem, Bruggeman, Jorn, Kooijman, Bas, & Dijkstra, Henk. 2009. The organic carbon pump in the Atlantic. *Journal of sea research*, **62**(2-3), 179–187.

Omta, Anne Willem, K. van Voorn, George a., M. Rickaby, Rosalind E., & Follows, Michael J. 2013. On the potential role of marine calcifiers in glacial-interglacial dynamics. *Global biogeochemical cycles*, **27**(July).

Orr, James C, Fabry, Victoria J, Aumont, Olivier, Bopp, Laurent, Doney, Scott C, Feely, Richard a, Gnanadesikan, Anand, Gruber, Nicolas, Ishida, Akio, Joos, Fortunat, Key, Robert M, Lindsay, Keith, Maier-Reimer, Ernst, Matear, Richard, Monfray, Patrick, Mouchet, Anne, Najjar, Raymond G, Plattner, Gian-Kasper, Rodgers, Keith B, Sabine, Christopher L, Sarmiento, Jorge L, Schlitzer, Reiner, Slater, Richard D, Totterdell, Ian J, Weirig, Marie-France, Yamanaka, Yasuhiro, & Yool, Andrew. 2005. Anthropogenic ocean acidification over the twenty-first century and its impact on calcifying organisms. *Nature*, **437**(7059), 681–6.

Paasche, E. 1963. The Adaptation of the Carbon14 Method for the Measurement of Coccolith Production in *Coccolithus huxleyi*. *Physiologia plantarum*. **16** (1), 186–200.

Pagani, Mark. 2002. The alkenone-CO_2 proxy and ancient atmospheric carbon dioxide. *Philosophical transactions. Series A, mathematical, physical, and engineering sciences*, **360**(1793), 609–32.

Pagani, Mark, Freeman, Katherine H., Ohkouchi, Nao, & Caldeira, Ken. 2002. Comparison of water column [CO_2aq] with sedimentary alkenone-based estimates: A test of the alkenone-CO_2 proxy. *Paleoceanography*, **17**(4), 1–21.

Pagani, Mark, Zachos, JC, Freeman, KH, Tipple, Brett, & Bohaty, Stephen. 2005. Marked decline in atmospheric carbon dioxide concentrations during the Paleogene. *Science*, 600–604.

Pagani, Mark, Huber, Matthew, Liu, Zhonghui, & Bohaty, SM. 2011. The role of carbon dioxide during the onset of Antarctic glaciation. *Science*, **334**, 1261–1265.

Parrenin, F, Barnola, J, Beer, J, Blunier, T, Castellano, E, Chappellaz, J, Dreyfus, G, Fischer, H, & Fujita, S. 2007. The EDC3 chronology for the EPICA Dome C ice core. *Climate of the past* **3** 485–497.

Pauly, M., Kamenos, N. a., Donohue, P., & LeDrew, E. 2015. Coralline algal Mg-O bond strength as a marine pCO_2 proxy. *Geology*, **43**(3), 267–270.

Pearson, P N, & Palmer, M R. 2000. Atmospheric carbon dioxide concentrations over the past 60 million years. *Nature*, **406**(6797), 695–9.

Pearson, Paul N, Foster, Gavin L, & Wade, Bridget S. 2009. Atmospheric carbon dioxide through the Eocene-Oligocene climate transition. *Nature*, **461**(7267), 1110–3.

Piotrowski, AM, & Goldstein, SL. 2005. Temporal relationships of carbon cycling and ocean circulation at glacial boundaries. *Science*. **307**(5717), 1933–1938

Popp, BN, Laws, EA, & Bidigare, RR. 1998. Effect of Phytoplankton Cell Geometry on Carbon Isotopic Fractionation. *Geochemica et cosmochimica acta*. **62**(1), 69–77

Prahl, FG, Lange, GJ De, Lyle, M, & Sparrow, MA. 1989. Post-depositional stability of long-chain alkenones under contrasting redox conditions. *Nature*. **341**, 434–437

Ramus, J. 1977. Alcian blue: A quantitative aqueous assay for algal acid and sulfated polysaccharides. *Journal of phycology*. **13**(4), 345–348

Rau, GH, Riebesell, Ulf & Wolf-Gladrow, Dieter. 1996. A model of photosynthetic ^{13}C fractionation by marine phytoplankton based on diffusive molecular CO_2 uptake.. *Marine ecology progress series*, **133**, 275–285.

Rau, GH, Riebesell, Ulf & Wolf-Gladrow, Dieter. 1997. CO_2aq-dependent photosynthetic ^{13}C fractionation in the ocean: A model versus measurements. *Global biogeochemical cycles*, **11**(2), 267–278.

Raven, John, & Crawfurd, K. 2012. Environmental controls on coccolithophore calcification. *Marine ecology progress series*, **470**, 137–166.

Raven, John, Beardall, John, & Giordano, Mario. 2014. Energy costs of carbon dioxide concentrating mechanisms in aquatic organisms. *Photosynthesis research*, **121**(2-3), 111–24.

Reinfelder, John R. 2011. Carbon Concentrating Mechanisms in Eukaryotic Marine Phytoplankton. *Annual review of marine science*, **3**(1), 291–315.

Revelle, R, & Suess, HE. 1957. Carbon Dioxide Exchange Between Atmosphere and Ocean and the Question of an Increase of Atmospheric CO_2 during the Past Decades. *Tellus*. **9**(1) 18–27

Richaud, Mathieu, Loubere, Paul, Pichat, Sylvain, & Francois, Roger. 2007. Changes in opal flux and the rain ratio during the last 50,000 years in the equatorial Pacific. *Deep sea research part ii: Topical studies in oceanography*, **54**(5-7), 762–771.

Richier, Sophie, Kerros, Marie-Emmanuelle, de Vargas, Colomban, Haramaty, Liti, Falkowski, Paul G, & Gattuso, Jean-Pierre. 2009. Light-dependent transcriptional regulation of genes of biogeochemical interest in the diploid and haploid life cycle stages of *Emiliania huxleyi*. *Applied and environmental microbiology*, **75**(10), 3366–9.

Richier, Sophie, Fiorini, Sarah, Kerros, Marie-Emmanuelle, von Dassow, Peter, & Gattuso, Jean-Pierre. 2011. Response of the calcifying coccolithophore *Emiliania huxleyi* to low pH/high pCO_2: from physiology to molecular level. *Marine biology*, **158**(3), 551–560.

Rickaby, R. E. M., Elderfield, H., Roberts, N., Hillenbrand, C.-D., & Mackensen, a. 2010a. Evidence for elevated alkalinity in the glacial Southern Ocean. *Paleoceanography*, **25**(1), 1–15.

Rickaby, R. E. M., Henderiks, J., & Young, J. N. 2010b. Perturbing phytoplankton: response and isotopic fractionation with changing carbonate chemistry in two coccolithophore species. *Climate of the past*, **6**(6), 771–785.

Ridgwell, A, & Zeebe, R. 2005. The role of the global carbonate cycle in the regulation and evolution of the Earth system. *Earth and planetary science letters*, **234**(3-4), 299–315.

Ridgwell, A., Schmidt, D. N., Turley, C., Brownlee, C., Maldonado, M. T., Tortell, P., & Young, J. R. 2009. From laboratory manipulations to Earth system models: scaling calcification impacts of ocean acidification. *Biogeosciences*, **6**(11), 2611–2623.

Ridgwell, A., Watson, A.J., & Archer, D.E. 2002. Modeling the response of the oceanic Si inventory to perturbation, and consequences for atmospheric CO_2. *Global biogeochem. cycles*, **16**(4), 1071.

Ridgwell, A., & Schmidt, Daniela N. 2010. Past constraints on the vulnerability of marine calcifiers to massive carbon dioxide release. *Nature geoscience*, **3**(3), 196–200.

Ridgwell, A., 2003. An end to the "rain ratio" reign? *Geochemistry geophysics geosystems*, **4**(6), 1–5.

Riebesell, U. 2004. Effects of CO_2 enrichment on marine phytoplankton. *Journal of oceanography*, **60**(4), 719–729.

Riebesell, U., Wolf-Gladrow, D. A., & Smetacek, V. 1993. Carbon dioxide limitation of marine phytoplankton growth rates. *Nature*, **361**(6409), 249–251.

Riebesell, Ulf, Zondervan, Ingrid, Rost, B.È., Tortell, P.D., Zeebe, R.E., & Morel, F.Ë.M.M. 2000a. Reduced calcification of marine plankton in response to increased atmospheric CO_2. *Nature*, **407**, 2–5.

Riebesell, Ulf, Revill, Andrew T., Holdsworth, Daniel G., & Volkman, John K. 2000b. The effects of varying CO_2 concentration on lipid composition and carbon isotope fractionation in *Emiliania huxleyi*. *Geochimica et cosmochimica acta*, **64**(24), 4179–4192.

Riebesell, Ulf, Körtzinger, Arne, & Oschlies, Andreas. 2009. Sensitivities of marine carbon fluxes to ocean change. *Proceedings of the national academy of sciences of the united states of america*, **106**(49), 20602–9.

Robinson, JJ, & Scott, KM. 2003. Kinetic isotope effect and characterization of form II RubisCO from the chemoautotrophic endosymbionts of the hydrothermal vent tubeworm Riftia pachyptila. *Limnology and oceanography*, **48**(1), 48–54.

Romero, Michael F, Chen, An-Ping, Parker, Mark D, & Boron, Walter F. 2013. The SLC4 family of bicarbonate (HCO_3^-) transporters. *Molecular aspects of medicine*, **34**(2-3), 159–82.

Rosenthal, Yair, Dahan, Maimon, & Shemesh, Aldo. 2000. Southern Ocean contributions to glacial-interglacial changes of atmospheric pCO_2: An assessment of carbon isotope records in diatoms. *Paleoceanography*, **15**(1), 65–75.

Rosenthal, Yair, Perron-Cashman, Suzanne, Lear, Caroline H., Bard, Edouard, Barker, Stephen, Billups, Katharina, Bryan, Martha, Delaney, Margaret L., DeMenocal, Peter B., Dwyer, Gary S., Elderfield, Henry, German, Chris R., Greaves, Mervyn, Lea, David W., Marchitto, Thomas M., Pak, Dorothy K., Paradis, Georges L., Russell, Ann D., Schneider, Ralph R., Scheiderich, Kathleen, Stott, Lowell, Tachikawa, Kazuyo, Tappa, Eric, Thunell, Robert, Wara, Michael, Weldeab, Syee, & Wilson, Paul. 2004. Interlaboratory comparison study of Mg/Ca

and Sr/Ca measurements in planktonic foraminifera for paleoceanographic research. *Geochemistry, geophysics, geosystems*, **5**(4).

Rost, B, Riebesell, Ulf, Burkhardt, Steffen, & Su, Dieter. 2003. Carbon acquisition of bloom–forming marine phytoplankton. *Limnology and oceanography*, **48**(1), 55–67.

Rost, Bjorn, & Riebesell, Ulf. 2004. Coccolithophores and the biological pump: responses to environmental changes. *In:* Theirstein, Hans, & Young, Jeremy (eds), *Coccolithophores: From molecular processes to global impacts*. Springer.

Rost, Bjorn, Zondervan, Ingrid, & Riebesell, Ulf. 2002. Light-dependent carbon isotope fractionation in the coccolithophorid *Emiliania huxleyi*. *Limnology and oceanography*, **47**(1), 120–128.

Royer, D L. 2014. *Treatise on Geochemistry*. 2 edn. Elsevier.

Sabine, Christopher L, Feely, Richard a, Gruber, Nicolas, Key, Robert M, Lee, Kitack, Bullister, John L, Wanninkhof, Rik, Wong, C S, Wallace, Douglas W R, Tilbrook, Bronte, Millero, Frank J, Peng, Tsung-Hung, Kozyr, Alexander, Ono, Tsueno, & Rios, Aida F. 2004. The oceanic sink for anthropogenic CO_2. *Science*, **305**(5682), 367–71.

Sachs, Julian P., Schneider, Ralph R., Eglinton, Timothy I., Freeman, Katherine H., Ganssen, Gerald, McManus, Jerry F., & Oppo, Delia W. 2000. Alkenones as paleoceanographic proxies. *Geochemistry, geophysics, geosystems*, **1**(11).

Sanchez-Puerta, M. Virginia, & Delwiche, Charles F. 2008. A Hypothesis for Plastid Evolution in Chromalveolates. *Journal of phycology*, **44**(5), 1097–1107.

Sand, K. K., Pedersen, C. S., Sjöberg, S., Nielsen, J. W., Makovicky, E., & Stipp, S. L. S. 2014. Biomineralization: Long-Term Effectiveness of Polysaccharides on the Growth and Dissolution of Calcite. *Crystal growth & design*, **14**(11), 5486–5494.

Sarmiento, J L, & Bender, M. 1994. Carbon biogeochemistry and climate change. *Photosynthesis research*, **39**(3), 209–34.

Sarmiento, JL, & Gruber, Nicolas. 2013. *Ocean biogeochemical dynamics*. Princeton University Press.

Sarnthein, M, & Winn, Kyaw. 1988. Global variations of surface ocean productivity in low and mid latitudes: influence on CO_2 reservoirs of the deep ocean and atmosphere during the last 21,000 years.. *Paleoceanography*, **3**(3), 361–399.

Schlüter, Lothar, Lohbeck, Kai T., Gutowska, Magdalena a., Gröger, Joachim P., Riebesell, Ulf, & Reusch, Thorsten B. H. 2014. Adaptation of a globally important coccolithophore to ocean warming and acidification. *Nature climate change*, **4**, 1024?1030

Schulz, K, Rost, B, Burkhardt, S, Riebesell, U, Thoms, S, & Wolfgladrow, D. 2007. The effect of iron availability on the regulation of inorganic carbon acquisition in the coccolithophore *Emiliania huxleyi* and the significance of cellular compartmentation for stable carbon isotope fractionation. *Geochimica et cosmochimica acta*, **71**(22), 5301–5312.

Scott, K. M., Henn-Sax, M., Harmer, T. L., Longo, D. L., Frame, C. H., & Cavanaugh, C. M. 2007. Kinetic isotope effect and biochemical characterization of form IA RubisCO from the marine cyanobacterium *Prochlorococcus marinus* MIT9313. *Limnology and oceanography*, **52**(5), 2199–2204.

Seki, Osamu, Foster, Gavin L., Schmidt, Daniela N., Mackensen, Andreas, Kawamura, Kimitaka, & Pancost, Richard D. 2010. Alkenone and boron-based Pliocene pCO_2 records. *Earth and planetary science letters*, **292**(1-2), 201–211.

Sekino, Keisuke, & Shiraiwa, Yoshihiro. 1994. Accumulation and Utilization of Dissolved Inorganic Carbon by a Marine Unicellular Coccolithophorid, *Emiliania huxleyi*. **35**(3), 353–361.

Sessions, Alex L, Sylva, Sean P, & Hayes, John M. 2005. Moving-wire device for carbon isotopic analyses of nanogram quantities of nonvolatile organic carbon. *Analytical chemistry*, **77**(20), 6519–27.

Sett, Scarlett, Bach, Lennart T, Schulz, Kai G, Koch-Klavsen, Signe, Lebrato, Mario, & Riebesell, Ulf. 2014. Temperature Modulates Coccolithophorid Sensitivity of Growth, Photosynthesis and Calcification to Increasing Seawater pCO_2. *Plos one*, **9**(2).

Sharkey, & Berry. 1985. Carbon isotope fractionation of algae as influenced by an inducible CO_2 concentrating mechanism. *In:* Lucas,W.J. and Berry, J.A, (eds), *Inorganic carbon uptake by aquatic photosynthetic organisms*, The American Society of Plant Physiologists

Siegenthaler, U., & Sarmiento, JL. 1993. Atmospheric carbon dioxide and the ocean. *Nature*, **365**(6442), 119–125.

Sigman, DM, & Boyle, EA. 2000. Glacial/Interglacial variations in atmospheric carbon dioxide. *Nature*, **407**, 859–869.

Sigman, DM, & Haug, GH. 2003. The biological pump in the past. *In:* Holland, Heinrich D. and Turekian, Karl K., (eds) *Treatise on geochemistry*. Elsevier.

Sikes, EL, Farrington, JW, & Keigwin, LD. 1991. Use of the alkenone unsaturation ratio U^K_{37} to determine past sea surface temperatures: core-top SST calibrations and methodology considerations. *Earth and planetary science letters*, **104**, 36–47.

Soto, Amelia R, Zheng, Hong, Shoemaker, Dorinda, Rodriguez, Jason, Read, Betsy, & Wahlund, Thomas M. 2006. Identification and preliminary characterization of two cDNAs encoding unique carbonic anhydrases from the marine alga *Emiliania huxleyi*. *Applied and environmental microbiology*, **72**(8), 5500–11.

Spero, Howard J., & Lea, David W. 1996. Experimental determination of stable isotope variability in *Globigerina bulloides*: implications for paleoceanographic reconstructions. *Marine micropaleontology*, **28**(3-4), 231–246.

Steven G. Johnson. 2014. *The NLopt nonlinear-optimization package*. ab-initio.mit.edu/nlopt

Stiller, John W, Schreiber, John, Yue, Jipei, Guo, Hui, Ding, Qin, & Huang, Jinling. 2014. The evolution of photosynthesis in chromist algae through serial endosymbioses. *Nature communications*, **5**, 5764.

Stoll, H., & Ziveri, P. 2004. Coccolithophorid-based geochemical proxies. *In:* Thierstein, H., & Young, J. R. (eds), *Coccolithophores: From molecular processes to global impacts*. Springer.

Stoll, Heather, Langer, Gerald, Shimizu, Nobumichi, & Kanamaru, Kinuyo. 2011. B/Ca in coccoliths and relationship to calcification vesicle pH and dissolved inorganic carbon concentrations. *Geochimica et cosmochimica acta*, **80**, 143–157.

Stoll, M H C, Bakker, K, Nobbe, G H, & Haese, R R. 2001. Continuous-Flow Analysis of Dissolved Inorganic Carbon Content in Seawater. **73**(17), 4111–4116.

Storn, Rainer, & Price, K. 1997. Differential evolution – a simple and efficient heuristic for global optimization over continuous spaces. *Journal of global optimization*, **11**, 341–359.

Suffrian, K, Schulz, K G, Gutowska, M, Riebesell, U, & Bleich, M. 2011. Cellular pH measurements in *Emiliania huxleyi* reveal pronounced membrane proton permeability. *The new phytologist*, **190**(3), 595–608.

Sültemeyer, D, & Rinast, Karl-albert. 1996. The CO_2 permeability of the plasma membrane of *Chlamydomonas reinhardtii*: mass- spectrometric ^{18}O-exchange measurements from $^{13}C^{18}O_2$ in suspensions of carbonic anhydrase-loaded plasma-membrane vesicles. *Planta*, **49**, 358–368.

Taylor, Alison R., Russell, Mark a., Harper, Glenn M., Collins, Toby F. T., & Brownlee, Colin. 2007a. Dynamics of formation and secretion of heterococcoliths by *Coccolithus pelagicus ssp. braarudii*. *European journal of phycology*, **42**(2), 125–136.

Taylor, Alison R, Chrachri, Abdul, Wheeler, Glen, Goddard, Helen, & Brownlee, Colin. 2011. A voltage-gated H^+ channel underlying pH homeostasis in calcifying coccolithophores. *Plos biology*, **9**(6).

Taylor, Alison R, Brownlee, Colin, & Wheeler, Glen L. 2012. Proton channels in algae: reasons to be excited. *Trends in plant science*, **17**(11), 675–84.

Tcherkez, Guillaume G B, Farquhar, Graham D, & Andrews, T John. 2006. Despite slow catalysis and confused substrate specificity, all ribulose bisphosphate carboxylases may be nearly perfectly optimized. *Proceedings of the national academy of sciences of the united states of america*, **103**(19), 7246–51.

Teece, Mark a., & Fogel, Marilyn L. 2007. Stable carbon isotope biogeochemistry of monosaccharides in aquatic organisms and terrestrial plants. *Organic geochemistry*, **38**(3), 458–473.

Thierstein, HR, & Young, JR. 2004. *Coccolithophores: from molecular processes to global impact*. Springer

Trenberth, KE. 1998. Atmospheric moisture residence times and cycling: Implications for rainfall rates and climate change. *Climatic change*. **39**(4) 667–694

Trimborn, Scarlett, Langer, Gerald, & Rost, Björn. 2007. Effect of varying calcium concentrations and light intensities on calcification and photosynthesis in *Emiliania huxleyi*. *Limnology and oceanography*, **52**(5), 2285–2293.

Uchikawa, Joji, & Zeebe, RE. 2012. The effect of carbonic anhydrase on the kinetics and equilibrium of the oxygen isotope exchange in the CO_2–H_2O system: Implications for $\delta^{18}O$ vital effects in biogenic carbonates. *Geochimica et cosmochimica acta*, **95**, 15–34.

Urey, HC. 1947. The thermodynamic properties of isotopic substances. *J. chem. soc.* 562–581

van Dongen, BE. 2002. Carbon isotope variability in monosaccharides and lipids of aquatic algae and terrestrial plants. *Marine ecology progress series*, **232**, 83–92.

von Dassow, Peter, Ogata, Hiroyuki, Probert, Ian, Wincker, Patrick, Da Silva, Corinne, Audic, Stéphane, Claverie, Jean-Michel, & de Vargas, Colomban. 2009. Transcriptome analysis of functional differentiation between haploid and diploid cells of *Emiliania huxleyi*, a globally significant photosynthetic calcifying cell. *Genome biology*, **10**(10).

von Dassow, Peter, John, Uwe, Ogata, Hiroyuki, Probert, Ian, Bendif, El Mahdi, Kegel, Jessica U, Audic, Stéphane, Wincker, Patrick, Da Silva, Corinne, Claverie, Jean-Michel, Doney, Scott, Glover, David M, Flores, Daniella Mella, Herrera, Yeritza, Lescot, Magali, Garet-Delmas, Marie-José, & de Vargas, Colomban. 2014. Life-cycle modification in open oceans accounts for genome variability in a cosmopolitan phytoplankton. *The ISME journal*. **9** 1365–1377.

Watkins, James M., Nielsen, Laura C., Ryerson, Frederick J., & DePaolo, Donald J. 2013. The influence of kinetics on the oxygen isotope composition of calcium carbonate. *Earth and planetary science letters*, **375**, 349–360.

Watkins, James M., Hunt, Jonathan D., Ryerson, Frederick J., & DePaolo, Donald J. 2014. The influence of temperature, pH, and growth rate on the $\delta^{18}O$ composition of inorganically precipitated calcite. *Earth and planetary science letters*, **404**, 332–343.

Westbroek, P, Jong, EW De, Dam, W, & Bosch, L. 1973. Soluble Intracrystalline Polysaccharides from Coccoliths of Coccolithus huxleyi (Lohmann) Kamptner. *Calcified tissue research*, **238**, 227–238.

Westbroek, P., Jong, EW De, Wal, Paul Van Der, Borman, A.H., de Vrind, J., Kok, D., de Bruijn, W.C., & Parker, S.B. 1984. Mechanism of calcification in the marine alga *Emiliania huxleyi*. *Philosophical transactions of the royal society of london. Series B, biological sciences*, **304**, 435–444.

Wiedmer, Susanne K, & Cassely, Aaron. 2000. Electrophoretic studies of polygalacturonate oligomers and their interactions with metal ions. **21** (15), 3212-9.

Wilson, J. D., Barker, S., & Ridgwell, A. 2012. Assessment of the spatial variability in particulate organic matter and mineral sinking fluxes in the ocean interior: Implications for the ballast hypothesis. *Global biogeochemical cycles*, **26**(4).

Yoon, Hwan Su, Hackett, Jeremiah D, Ciniglia, Claudia, Pinto, Gabriele, & Bhattacharya, Debashish. 2004. A molecular timeline for the origin of photosynthetic eukaryotes. *Molecular biology and evolution*, **21**(5), 809–18.

Young. 1998. Neogene. *In:* Bown, Paul R. (ed), *Calcareous nannofossil biostratigraphy*. Springer.

Young, J N, Rickaby, R E M, Kapralov, M V, & Filatov, D a. 2012. Adaptive signals in algal Rubisco reveal a history of ancient atmospheric carbon dioxide. *Philosophical transactions of the royal society of london. Series B, biological sciences*, **367**(1588), 483–92.

Young, J. R. 1994. Function of coccoliths. *In:* Winter, A., & Siesser, W. G. (eds), *Coccolithophores*. Cambridge University Press, Cambridge.

Young, Jeremy R., & Ziveri, Patrizia. 2000. Calculation of coccolith volume and it use in calibration of carbonate flux estimates. *Deep sea research part ii: Topical studies in oceanography*, **47**(9-11), 1679–1700.

Young, Jeremy R., Andruleit, Harald, & Probert, Ian. 2009. Coccolith Function and Morphogenesis: Insights From Appendage-Bearing Coccolithophores of the Family Syracosphaeraceae (Haptophyta). *Journal of phycology*, **45**(1), 213–226.

Young, JR, & Henriksen, Karen. 2003. Biomineralization within vesicles: the calcite of coccoliths. *Reviews in mineralogy and geochemistry*. **54**(1), 189–215

Young, JR, Didymus, JM, Brown, PR, Prins, B, & Mann, S. 1992. Crystal assembly and phylogenetic evolution in heterococcoliths. *Nature*. **356**, 516–518

Young, Jr, Davis, Sa, Bown, Pr, & Mann, S. 1999. Coccolith ultrastructure and biomineralisation. *Journal of structural biology*, **126**(3), 195–215.

Yu, Jimin, & Day, Jason. 2005. Determination of multiple element/calcium ratios in foraminiferal calcite by quadrupole ICP–MS. *Geochemistry, geophysics, geosystems*, **6**(8).

Zachos, J, Pagani, M, Sloan, L, Thomas, E, & Billups, K. 2001. Trends, rhythms, and aberrations in global climate 65 Ma to present. *Science*, **292**, 686–694.

Zeebe, RE. 2014. Kinetic fractionation of carbon and oxygen isotopes during hydration of carbon dioxide. *Geochimica et cosmochimica acta*, **139**, 540–552.

Zeebe, RE, & Westbroek, P. 2003. A simple model for the $CaCO_3$ saturation state of the ocean: The "Strangelove", the "Neritan", and the "Cretan" Ocean. *Geochemistry, geophysics, geosystems*, **4**(12).

Zeebe, R.E., & Wolf-Gladrow, Dieter. 2001. *CO_2 in Seawater: Equilibrium, Kinetics, Isotopes*. Elsevier.

Zhang, Yi Ge, Pagani, Mark, Liu, Zhonghui, Bohaty, Steven M, & Deconto, Robert. 2013. A 40-million-year history of atmospheric CO_2. *Philosophical transactions. Series A, mathematical, physical, and engineering sciences*, **371**.

Ziveri, P., Stoll, H., Probert, I., Klaas, C., Geisen, M., Ganssen, G., & Young, J. 2003. Stable isotope "vital effects" in coccolith calcite. *Earth and planetary science letters*, **210**(1-2), 137–149.

Ziveri, Patrizia, de Bernardi, Bianca, Baumann, Karl-Heinz, Stoll, Heather M., & Mortyn, P. Graham. 2007. Sinking of coccolith carbonate and potential contribution to organic carbon ballasting in the deep ocean. *Deep sea research part ii: Topical studies in oceanography*, **54**(5-7), 659–675.

Zondervan, I., Zeebe, R.E., Rost, B., & Riebesell, U. 2001. Decreasing marine biogenic calcification: A negative feedback. *Global biogeochemical cycles*, **15**(2), 507–516.